

Stone Stability  
Under Non-uniform Flow



# Stone Stability Under Non-uniform Flow

Proefschrift

ter verkrijging van de graad van doctor  
aan de Technische Universiteit Delft,  
op gezag van de Rector Magnificus prof.dr.ir. J.T. Fokkema,  
voorzitter van het College voor Promoties,  
in het openbaar te verdedigen

op maandag 3 november 2008 om 12.30 uur

door

Nguyen Thanh Hoan  
civiel ingenieur  
geboren te Nam Dinh, Vietnam

Dit manuscript is goedgekeurd door de promotor:  
Prof.dr.ir. M.J.F. Stive

Copromotor:  
Ir. H.J. Verhagen

Samenstelling promotiecommissie:

Rector Magnificus	voorzitter
Prof.dr.ir. M.J.F. Stive	Technische Universiteit Delft, promotor
Ir. H.J. Verhagen	Technische Universiteit Delft, copromotor
Prof.dr.ir. H.H.G. Savenije	Technische Universiteit Delft
Prof.dr.ir. J.A. Roelvink	UNESCO-IHE Institute for Water Education
Prof.dr.ir. J. de Rouck	Universiteit Gent
Dr.ir. W.S.J. Uijttewaal	Technische Universiteit Delft
Dr.ir. B. Hofland	Deltares
Prof.dr.ir. G.S. Stelling	Technische Universiteit Delft, reservelid

Drs. R. Booij has provided substantial guidance and support in the preparation of this thesis.

This research has been financially supported by the Ministry of Education and Training of Vietnam and Delft University of Technology.

Keywords: Stone stability, stone transport, stone entrainment, incipient motion, threshold condition, bed protection, bed damage, non-uniform flow, turbulent flow, decelerating flow.

This thesis should be referred to as: Hoan, N. T. (2008). *Stone stability under non-uniform flow*. Ph.D. thesis, Delft University of Technology.

ISBN 978-90-9023584-4

Copyright © 2008 by [Nguyen Thanh Hoan](#)

Printed by PrintPartners Ipskamp B.V., the Netherlands.

All rights reserved. No part of the material protected by this copyright notice may be reproduced or utilized in any form or by any means, electronic or mechanical, including photocopying, recording or by any information storage and retrieval system, without written permission of the author.

*To my family*



# Contents

<b>Summary</b>	<b>v</b>
<b>Samenvatting</b>	<b>ix</b>
<b>Tom tat</b>	<b>xiii</b>
<b>1 Introduction</b>	<b>1</b>
1.1 Background	1
1.2 Objectives of this study	2
1.3 Research methodology	3
1.4 Outline	3
<b>2 Literature review</b>	<b>7</b>
2.1 Introduction	7
2.2 Turbulence and flow properties	7
2.2.1 Uniform open-channel flow over a rough bed	7
2.2.2 Non-uniform open-channel flow	11
2.3 Hydrodynamic forces on a single stone	13
2.4 Stability parameters	16
2.4.1 Governing variables	16
2.4.2 The Shields stability parameter	18
2.4.3 The Jongeling et al. stability parameter	18
2.4.4 The Hofland stability parameter	19
2.5 Mobility parameters	20
2.6 Methods for stone stability assessment	21
2.6.1 The stability threshold concept	21
2.6.2 The stone transport concept	26
2.6.3 Comparison and selection of methods	29
2.7 Concluding remarks	30
<b>3 Experimental arrangement and data processing methods</b>	<b>33</b>
3.1 Introduction	33
3.2 Experimental configuration	34
3.2.1 Geometry	34

3.2.2	Instrumentation . . . . .	36
3.3	Stones . . . . .	38
3.4	Test program . . . . .	39
3.4.1	Hydraulic conditions . . . . .	39
3.4.2	Measurements . . . . .	42
3.5	Selected time series . . . . .	43
3.6	Data processing methods . . . . .	45
3.6.1	Velocity and turbulence data . . . . .	45
3.6.2	Stone entrainment rate data . . . . .	46
3.6.3	Correlation analysis . . . . .	47
<b>4</b>	<b>Flow characteristics</b>	<b>49</b>
4.1	Introduction . . . . .	49
4.2	Flow quantities . . . . .	50
4.3	Shear velocity . . . . .	52
4.4	Mean flow velocity . . . . .	53
4.5	The eddy viscosity and mixing length . . . . .	55
4.6	Turbulence intensity data . . . . .	59
4.7	Reynolds shear stress data . . . . .	63
4.8	Concluding remarks . . . . .	65
<b>5</b>	<b>Stone transport formulae</b>	<b>67</b>
5.1	Introduction . . . . .	67
5.2	The proposed stability parameter . . . . .	68
5.3	Final formulation of the proposed stability parameter . . . . .	70
5.4	Evaluation of the available stability parameters . . . . .	72
5.4.1	The Shields stability parameter . . . . .	72
5.4.2	The Jongeling et al. stability parameter . . . . .	73
5.4.3	The Hofland stability parameter . . . . .	75
5.5	Discussion . . . . .	76
5.5.1	Comparison of the stability parameters . . . . .	77
5.5.2	Sensitivity analysis of key parameters . . . . .	78
5.5.3	Entrainment correction . . . . .	80
5.5.4	Data comparison . . . . .	81
5.6	Conclusions . . . . .	84
<b>6</b>	<b>Estimation of stone entrainment using numerical flow modeling</b>	<b>87</b>
6.1	Introduction . . . . .	87
6.2	Flow conditions . . . . .	88
6.3	Numerical model set-up . . . . .	88
6.3.1	Grid . . . . .	89
6.3.2	Boundary condition . . . . .	91
6.3.3	Model validation . . . . .	92



6.3.4	Model calibration and verification . . . . .	94
6.4	Computation results . . . . .	95
6.5	Estimation of bed damage . . . . .	97
6.6	Conclusions and recommendations . . . . .	99
<b>7</b>	<b>Conclusions and recommendations</b>	<b>101</b>
7.1	General . . . . .	101
7.2	Conclusions . . . . .	102
7.3	Recommendations . . . . .	104
	<b>References</b>	<b>106</b>
<b>A</b>	<b>Stones</b>	<b>115</b>
A.1	Artificial stones . . . . .	115
A.2	Stone gradation . . . . .	116
<b>B</b>	<b>Data</b>	<b>117</b>
B.1	Introduction . . . . .	117
B.2	Velocity and turbulence data . . . . .	117
B.3	Governing variables . . . . .	124
<b>C</b>	<b>Numerical flow modeling</b>	<b>129</b>
C.1	Turbulence modeling . . . . .	129
C.1.1	Mean-flow equations . . . . .	129
C.1.2	The two-equation $k$ - $\epsilon$ model . . . . .	130
C.2	Deft input files . . . . .	132
C.2.1	Mesh description . . . . .	132
C.2.2	Problem description . . . . .	136
C.2.3	Typical sequence of an Deft session . . . . .	139
	<b>List of symbols</b>	<b>141</b>
	<b>List of figures</b>	<b>145</b>
	<b>List of tables</b>	<b>148</b>
	<b>Acknowledgements</b>	<b>151</b>
	<b>Curriculum Vitae</b>	<b>153</b>



# Summary

Despite the fact that many studies on the stability of stones in bed protections under flowing water have been conducted, our knowledge is still far from advanced and reliable. Issues like how to quantify the hydraulic loads exerted on the stones on a bed and how to assess the stability of the stones are central and most challenging in stone stability research.

Firstly, it is important that the hydraulic forces exerted on the stones in a bed are adequately quantified. A stability parameter - expressed as a dimensionless relationship between hydraulic loads and bed strength - is often used to quantify the influence of these forces on the bed. As the turbulence fluctuations of the flow are of importance for the stability of stones, their effect has to be taken into account, especially for non-uniform flow. In the few studies available, no stability parameters have proven to be adequate in quantifying the hydraulic loads exerted on the bed for non-uniform flow.

Secondly, the method with which the stability of stones is assessed also plays an important role. Available stability formulae used to determine the required stone sizes and weights are mainly based on the concept of incipient motion of bed material. Due to the stochastic nature of bed material movement, a robust flow condition at which the stones begin to move does not exist. Therefore, the threshold of movement is a rather subjective matter and the stone stability assessment method based on it often yields inconsistent design criteria. In contrast, the stability assessment method based on the stone transport concept leads to a result with a cause-and-effect relationship between flow parameters and the bed response. Such a relationship provides consistent and more reliable design criteria and allows an estimate of the cumulative damage over time which is important for making decisions regarding maintenance frequency and lifetime analysis of hydraulic structures. Surprisingly, most of the previous studies on stone stability are restricted to the stability threshold concept and few have attempted to derive stone transport formulae. As a result, no physical relationship between the hydraulic load and the bed response is available for non-uniform flow.

These two challenging issues are dealt with in this thesis. The objectives of the study are (i) to increase insight into the effect of hydraulic parameters, such as the velocity and the turbulence fluctuations, on the stability of stones in bed protections, (ii) to establish a physical relationship between the hydraulic param-

eters and the bed damage (i.e., stone transport formulae) for non-uniform flow to obtain a reliable estimate of bed damage, and (iii) to evaluate the use of the outputs of numerical flow modeling to predict bed damage.

Experimental work is central in this study. A detailed set of measurements was carried out in a laboratory flume. The program comprised the measurement of the flow in gradually expanding open-channels and of the induced damage to the bottom. This flow configuration was chosen because in such a flow the turbulence intensity is high. Three experimental configurations with different expansion rates were used to create different combinations of velocity and turbulence. The bed response (quantified by a dimensionless entrainment rate) and the flow field (quantified by velocity and turbulence intensity distributions) were measured. The subsequent analysis has been directed towards the understanding of the effect of hydraulic parameters on stone stability and the cause-and-effect relationship between the flow and its induced damage to the bottom.

Based on our data, the various ways of quantifying the hydraulic loads exerted on the stones on a bed have been extensively reviewed, verified and extended. The physical reasoning behind this is that if a stability parameter properly describes the hydraulic loads exerted on a bed, it should correlate well with the bed response (i.e., the dimensionless entrainment rate).

The correlation analysis has yielded quantitative confirmation of earlier findings on the inappropriateness of using the bed shear stress alone to represent the hydraulic loads exerted on a bed in non-uniform flow. An approach that uses a combination of velocity and turbulence distributions to quantify the flow forces has been verified for the first time since it was proposed by [Jongeling et al. \(2003\)](#). Inspired by this approach, a new stability parameter has been proposed to better quantify the hydraulic loads exerted on the stones. The formulation of the newly-proposed stability parameter has physically explained and quantitatively described the hydraulic loads exerted on the stones in bed protections. This provides valuable insight into the understanding of the influence of the different flow characteristics such as velocity and turbulence distributions on stone stability. Based on the physical analysis and practical considerations, a final expression for the new stability parameter was formulated.

For the first time, the physical relationship between flow parameters and the bed damage - expressed as stone transport formulae - has been established for non-uniform flow. Since a good collapse of the data is obtained for a variety of stone densities (varying from 1320 to 1970 kg/m<sup>3</sup>), the influence of stone density is well incorporated into the formulae. Therefore, the newly-developed stone transport formulae are likely to be valid for other bed materials with different densities, including natural stones.

The newly-developed stone transport formulae can be used together with the outputs of numerical flow modeling to estimate bed damage. This was evaluated by comparing the measured and the calculated damage using the outputs of numerical flow modeling. The analysis has shown a good agreement between the

measurements and calculations. Therefore, with the availability of the newly-developed stone transport formulae and more reliable turbulence models, the bed damage level can be more accurately computed for arbitrary flow conditions.



# Samenvatting

Ondanks het feit dat er veel studie is gedaan naar de stabiliteit van stenen in bodemverdedigingen in stromend water, is onze kennis nog onvoldoende. Aspecten zoals het kwantificeren van de hydraulische belasting op de stenen in de bodem en hoe de stabiliteit van de stenen te bepalen staan centraal en zijn vooral uitdagend in steenstabiliteitsonderzoek.

Ten eerste is het belangrijk dat de hydraulische krachten op de stenen op de bodem goed worden gekwantificeerd. Een stabiliteitsparameter - uitgedrukt als een dimensieloze relatie tussen hydraulische belasting en bodemsterkte - wordt vaak gebruikt om de invloed van deze krachten op de bodem te kwantificeren. Omdat de turbulente fluctuaties van de stroming van belang zijn voor de stabiliteit van de stenen, moet dat effect ook in beschouwing genomen worden, vooral bij niet-uniforme stroming. In de weinige beschikbare studies, heeft geen van de stabiliteitsparameters bewezen een adequate kwantificering van de hydraulische belastingen van niet-uniforme stroming op de bodem te kunnen geven.

Ten tweede, de methode waarmee de stabiliteit van stenen wordt beoordeeld speelt ook een belangrijke rol. Beschikbare stabiliteitsformules om benodigde steengrootte en gewicht te bepalen zijn vooral gebaseerd op het concept van beginnend bewegen van bodem materiaal. Door het stochastische karakter van bodem materiaal beweging bestaat er geen eenduidige stromingsconditie waarbij de stenen beginnen te bewegen. Daarom is de grens van bewegen tamelijk subjectief en steenstabiliteitbeoordeling hierop gebaseerd leidt vaak tot inconsistente ontwerpcriteria. De stabiliteit beoordelingsmethode gebaseerd op het steen transport concept, daarentegen, leidt tot een resultaat met een causaal verband tussen stromingsparameters en bodemrespons. Zo'n verband draagt bij aan consistente en betrouwbaardere ontwerp criteria en biedt de mogelijkheid cumulatieve schade in de tijd te schatten. Dit is belangrijk voor besluitvorming betreffende de onderhoudsfrequentie en levensduur analyse van waterbouwkundige constructies. Het is daarom opmerkelijk dat de meeste eerdere studies over steenstabiliteit, beperkt waren tot het stabiliteitsgrens concept en enkelen een poging tot het afleiden van een steen transport formule beschrijven. Daarom is er geen fysische relatie tussen de hydraulische belasting en de bodem respons beschikbaar voor niet-uniforme stroming.

Deze twee uitdagende aspecten komen aan de orde in dit proefschrift. De

doelen van de studie zijn (i) inzicht verbeteren in het effect van hydraulische parameters zoals de stroomsnelheid en turbulente fluctuaties, op de stabiliteit van stenen in bodem verdedigingen, (ii) vaststellen van een fysische relatie tussen de hydraulische parameters en de bodemschade (d.i., steentransportformules) voor niet-uniforme stroming voor het verkrijgen van een betrouwbare schatting van de bodemschade, en (iii) evaluatie van het gebruik van de resultaten van numerieke stromingsmodellering om bodemschade te voorspellen.

Experimenteel werk staat centraal in deze studie. Een gedetailleerde set van metingen is uitgevoerd in een laboratorium. Het programma behelsde metingen van vrije oppervlakte stroming in een geleidelijk breder wordende goot en van de veroorzaakte schade aan de bodem. Deze stromingsconfiguratie is gekozen omdat hierbij de turbulente intensiteit hoog is. Drie experimentele configuraties met verschillende mate van verbreding zijn toegepast om verschillende combinaties van snelheid en turbulentie te creëren. De bodem respons (gekwantificeerd door een dimensieloze mate van materiaal opname) en het stromingsveld (gekwantificeerd door snelheid en turbulente intensiteitsverdelingen) zijn gemeten. De bijhorende analyse was gericht op het begrijpen van het effect van hydraulische parameters op steen stabiliteit en het causaal verband tussen de stroming en de veroorzaakte schade aan de bodem.

Gebaseerd op de verkregen data zijn de verschillende manieren van kwantificering van de hydraulische belasting op de stenen op een bodem uitgebreid bekeken, geverifieerd en uitgebreid. De fysische redenering hierachter is dat als een stabiliteitsparameter de hydraulische belastingen op een bodem goed beschrijft, deze ook goed correleert met de bodem respons (d.i., de dimensieloze mate van materiaal opname).

De correlatie analyse heeft geleid tot kwantitatieve bevestiging van eerdere bevindingen over de ongeschiktheid van het gebruik van bodemschuifspanning alleen om hydraulische belastingen op een bodem in niet-uniforme stroming weer te geven. Een aanpak die gebruik maakt van een combinatie van snelheid en turbulentie verdelingen om de stromingskrachten te kwantificeren is voor het eerst nadat dit is voorgesteld door [Jongeling et al. \(2003\)](#) geverifieerd. Geïnspireerd door deze aanpak, is een nieuwe stabiliteitsparameter voorgesteld om de hydraulische krachten op de stenen beter te kwantificeren. De formulering van de nieuw-voorgestelde stabiliteitsparameter geeft een fysische onderbouwing en kwantitatieve beschrijving van de hydraulische belastingen op de stenen in bodemverdedigingen. Dit geeft waardevol inzicht in de invloed van verschillende stromingskarakteristieken zoals snelheid en turbulentie verdelingen op steen stabiliteit. Een definitieve uitdrukking voor een nieuwe stabiliteitsparameter is geformuleerd, gebaseerd op de fysische analyse en praktische beschouwingen.

Voor het eerst is er een fysische relatie tussen stromingsparameters en bodemschade - uitgedrukt als steen transport formules - vastgesteld voor niet-uniforme stroming. Aangezien er een goede correlatie van de data bereikt is voor een ver-



scheidenheid aan steendichtheden (variërend van 1320 tot 1970 kg/m<sup>3</sup>), is de invloed van steendichtheid goed inbegrepen in de formules. Het is daarom aanneemelijk dat de nieuw ontwikkelde steentransportformuleringen ook geldig zijn voor andere bodem materialen met andere dichtheden, inclusief natuurlijke stenen.

De nieuw ontwikkelde steentransportformules kunnen gebruikt worden in combinatie met de resultaten van numerieke stromingsmodellen om zo bodemschade te voorspellen. Dit is geëvalueerd door het vergelijken van gemeten schade en berekende schade op basis van de resultaten van een numeriek stromingsmodel. De analyse laat een goede overeenstemming tussen de metingen en de berekeningen zien. Met de beschikbaarheid van de nieuw ontwikkelde steentransport formules en de vele mogelijkheden van nieuwe numerieke modellen, is het daarom mogelijk het bodemschade niveau nauwkeuriger te berekenen voor willekeurige condities.



# Tóm tắt

Các lớp đá thường được sử dụng rộng rãi trong xây dựng công trình thủy để gia cố đáy, giữ ổn định cho công trình khỏi tác động xói lở do dòng chảy. Các viên đá, ngoài yêu cầu về chất lượng, cần đảm bảo kích thước sao cho không bị cuốn trôi dưới tác động của dòng chảy. Vì vậy, việc xác định trọng lượng viên đá có ý nghĩa đặc biệt quan trọng đến sự ổn định chung của công trình. Tuy nhiên, các công thức hiện có vẫn chỉ cho kết quả gần đúng do tính phức tạp của bài toán. Dù đã có rất nhiều nghiên cứu được tiến hành xong hiện vẫn còn nhiều vấn đề chưa được giải quyết một cách thỏa đáng. Vấn đề định lượng hóa tác động của dòng chảy lên lòng dẫn, việc đánh giá độ ổn định của viên đá vẫn là những vấn đề khó khăn và phức tạp trong việc nghiên cứu sự ổn định của các khối gia cố đáy dưới tác động của dòng chảy.

Trong hai vấn đề trên, việc định lượng tác động của dòng chảy lên các viên đá gia cố đáy có ý nghĩa đặc biệt quan trọng. Chỉ tiêu ổn định - một đại lượng không thứ nguyên được đo bằng tỷ số giữa lực tác động của dòng chảy và độ bền của đáy - thường được sử dụng để định lượng hóa tác động của dòng chảy lên lòng dẫn. Do tính rối động của dòng chảy có tác động lớn đến sự ổn định của đá gia cố đáy nên ảnh hưởng đó cần phải được xét đến, đặc biệt là đối với dòng chảy không đều. Trong số ít các nghiên cứu về vấn đề này, chưa có chỉ tiêu ổn định nào được chứng minh là đã mô tả đúng tác động của dòng chảy lên lòng dẫn trong điều kiện dòng chảy không đều.

Tiếp đến, các phương pháp dùng để đánh giá sự ổn định của khối đá gia cố đáy cũng đóng vai trò rất quan trọng. Các công thức hiện có dùng để xác định trọng lượng và kích thước đá gia cố đáy chủ yếu dựa trên khái niệm trạng thái khởi động (incipient motion concept) của vật liệu đáy. Do chuyển động của vật liệu đáy có tính chất ngẫu nhiên nên thực tế không thể tồn tại một trạng thái dòng chảy ổn định mà tại đó vật liệu đáy bắt đầu chuyển động. Vì vậy trạng thái khởi động là một khái niệm định tính và phương pháp đánh giá độ ổn định của viên đá gia cố đáy dựa vào khái niệm này sẽ dẫn đến các kết quả không thống nhất giữa các nghiên cứu. Ngược lại, phương pháp đánh giá độ ổn định của viên đá gia cố đáy dựa trên khái niệm sức vận chuyển vật liệu đáy (stone transport concept) sẽ dẫn đến mối quan hệ nhân quả giữa các yếu tố thủy lực (hydraulic parameters) và độ biến động lòng dẫn (bed response). Quan hệ dạng này sẽ cho phép tìm ra các tiêu chuẩn thiết kế có tính nhất quán và đáng tin cậy hơn, qua đó có thể tính toán được mức độ biến động của lòng dẫn theo thời

gian, một yếu tố rất quan trọng trong việc phân tích tuổi thọ và quyết định thời điểm duy tu công trình thủy. Tuy nhiên, hầu hết các nghiên cứu hiện nay về ổn định viên đá gia cố đáy đều giới hạn trong khái niệm trạng thái khởi động, trong khi rất ít nghiên cứu dựa vào khái niệm sức vận chuyển vật liệu đáy. Do đó, mối quan hệ giữa các yếu tố thủy lực và độ biến động lòng dẫn vẫn chưa được xác lập cho dòng chảy không đều.

Hai vấn đề phức tạp trên là đối tượng nghiên cứu chính của đề tài. Mục tiêu nghiên cứu là (i) tìm hiểu ảnh hưởng của các yếu tố thủy lực, như phân bố vận tốc và rối động, đến sự ổn định của viên đá gia cố đáy, (ii) thiết lập mối quan hệ giữa các yếu tố thủy lực và mức độ biến động của lòng dẫn (công thức về sức vận chuyển vật liệu đáy - stone transport formulae), và (iii) đánh giá khả năng sử dụng kết quả của mô hình toán về dòng chảy để tính toán mức độ biến động của lòng dẫn.

Trong nghiên cứu này, công cụ chính được sử dụng là các thí nghiệm trên mô hình vật lý. Nội dung thí nghiệm bao gồm đo đạc các đặc trưng dòng chảy trong kênh hở có mặt cắt biến đổi dần và độ biến động tương ứng của lòng dẫn. Thí nghiệm trên được lựa chọn vì với nó sẽ tạo ra được dòng chảy với lưu tốc mạch động cao. Ba máng thí nghiệm được thiết kế với kích thước phần mở rộng khác nhau để tạo ra nhiều tổ hợp về vận tốc và rối động. Mức độ biến động của đáy (được đặc trưng bằng đại lượng không thứ nguyên sức vận chuyển vật liệu đáy - dimensionless entrainment rate) và các yếu tố thủy lực (phân bố vận tốc và rối động) được đo đạc cho từng phương án thí nghiệm. Các phân tích tập trung vào nghiên cứu ảnh hưởng của các yếu tố thủy lực đối với sự ổn định của viên đá gia cố đáy và thiết lập công thức về lưu lượng vật liệu đáy (stone transport formulae).

Từ kết quả thí nghiệm, các chỉ tiêu ổn định khác nhau được vận dụng để định lượng tác động của dòng chảy đến lòng dẫn. Mức độ phù hợp của các chỉ tiêu này được kiểm tra, đánh giá dựa trên mức độ tương quan giữa chúng với độ biến động lòng dẫn thực đo. Cơ sở của các phân tích này là: một chỉ tiêu ổn định nếu mô tả đúng tác động của dòng chảy lên lòng dẫn sẽ có mối tương quan chặt chẽ với độ biến động lòng dẫn.

Kết quả thí nghiệm cho thấy việc chỉ sử dụng ứng suất tiếp đáy (hoặc vận tốc trung bình thủy trực) để đặc trưng cho tác động của dòng chảy lên lòng dẫn là bất hợp lý. Từ số liệu thí nghiệm, phương pháp sử dụng tổng hợp phân bố vận tốc và rối động để đặc trưng cho tác động của dòng chảy lên lòng dẫn đã được đánh giá, kiểm nghiệm lần đầu tiên kể từ khi được Jongeling et al. (2003) đề xuất. Dựa theo hướng nghiên cứu trên, tác giả đề tài đã đề xuất một chỉ tiêu ổn định mới để mô tả đúng hơn tác động của dòng chảy lên lòng dẫn. Quá trình xây dựng chỉ tiêu mới này cũng đã lý giải rõ hơn ảnh hưởng của các yếu tố thủy lực đối với độ biến động lòng dẫn.

Lần đầu tiên, mối quan hệ giữa các yếu tố thủy lực và độ biến động lòng dẫn đã được thiết lập cho dòng chảy không đều. Vì kết quả thí nghiệm thu được từ nhiều loại trọng lượng riêng của vật liệu đáy (từ 1320 đến 1970 kg/m<sup>3</sup>) nên công

thức đề xuất về sức vận chuyển vật liệu đáy (stone transport formulae) có thể áp dụng cho nhiều loại vật liệu khác nhau.

Công thức sức vận chuyển vật liệu đáy được thiết lập trong nghiên cứu này có thể được sử dụng cùng với kết quả của mô hình toán về dòng chảy để tính toán độ biến động lòng dẫn. Mức độ tin cậy được đánh giá thông qua việc so sánh giá trị đo đạc và giá trị tính toán của độ biến động lòng dẫn. Kết quả phân tích cho thấy hai giá trị này có sự tương đồng cao. Vì vậy, với sự ra đời của công thức sức vận chuyển vật liệu đáy và những thành tựu của mô hình toán về dòng chảy, độ biến động lòng dẫn có thể được tính toán chính xác hơn với những điều kiện dòng chảy khác nhau.



# Chapter 1

## Introduction

### 1.1 Background

Bed protections constructed of layers of stone or rock are often used to protect hydraulic structures such as groins, breakwaters, revetments, weirs etc., with the objective to prevent the sand bed from scouring. In flowing water these granular bed protections can be characterized by a hydraulically rough flow regime, low mobility transport, non-cohesive stones, narrow grading of sizes, angular stones and non-equilibrium transport (Hofland, 2005). The top layer of bed protections must be made of stones large enough to withstand the exerting hydraulic loads.

In the design of bed protections, stone sizes and weights are chosen in such a way that no or only little damage is allowed for. This is, however, complicated by the fact that the actual interaction between flow and stones on a bed is rather complex and that there is only limited knowledge of the mechanism of entrainment of bed material. Available stability formulae are mainly based on the concept of incipient motion of bed material (see Buffington and Montgomery, 1997, for a review). Due to the stochastic nature of bed material movement, a generic definition of the flow condition at which the stones begin to move does not exist. Therefore, the threshold of movement is subjectively dependent on the definition of incipient motion, making it difficult to compare among different investigations and more importantly, often yielding inconsistent design criteria (Paintal, 1971; Hofland, 2005; Bureau of Reclamation U.S. Department of the Interior, 2006).

In contrast, a generic stone transport approach will lead to a result with a cause-and-effect relationship between the flow parameters and the bed response. Such a relationship provides consistent and more reliable design criteria and allows an estimate of the cumulative damage over time which is important for making decisions regarding maintenance frequency and lifetime analysis of hydraulic structures. Stone transport formulae, if available, can be used together with the outputs of numerical flow modeling to estimate bed damage level for a given flow condition. This would make the use of expensive physical models obsolete. Surprisingly, most of the previous studies on stone stability are re-

stricted to the stability threshold concept and few have attempted to derive stone transport formulae. Examples of the investigations that use a stone transport approach are [Paintal \(1971\)](#), for uniform flow) and [Hofland \(2005\)](#), for non-uniform flow). However, still no generic physical relationship between the hydraulic load and the bed response is available for non-uniform flow.

In the author's opinion, the most challenging issue in stone stability research is how to quantify the hydraulic loads exerted on the stones on a bed. The bed shear stress is widely used as the only hydraulic quantity for this purpose ever since it was introduced by [Shields \(1936\)](#). The Shields stability parameter, however, does not explicitly take into account the influence of turbulence fluctuations in the flow, which has been proven to be of importance for the stability of stones. In uniform flow, the turbulence effect is implicitly incorporated through empirical constants. In non-uniform flow, correction factors are conventionally applied to account for the turbulence fluctuations. This approach, however, can only be used as a rule-of-thumb since the various correction factors are given rather arbitrary. Recently, [Jongeling et al. \(2003\)](#) and [Hofland \(2005\)](#) developed more generic approaches that utilize a combination of velocity and turbulence distributions over a water column to quantify the hydraulic loads. These promising approaches, however, have not been verified since the data that were used are highly scattered.

Despite the fact that much research on stone stability has been accumulated over the years, our knowledge is still far from advanced and reliable. The above discussion has focussed on the stability of stones in bed protections under flowing water, which is also central in this study. Aspects like the influence of turbulence fluctuations, the quantification of hydraulic loads exerted on the stones and stone transport formulae will be addressed in this thesis.

## 1.2 Objectives of this study

This study focuses on stability or damage formulations for granular bed protections under flowing water. An important investigated aspect is the effect of turbulence fluctuations of the flow on the stability of stones. The objectives of this study are: (i) to increase insight into the effect of hydraulic parameters, such as the velocity and the turbulence fluctuations, on the stability of stones in bed protections; (ii) to establish a physical relationship between the hydraulic parameters and the bed damage (i.e., stone transport formulae) for non-uniform flow to obtain a reliable estimation of bed damage and (iii) to evaluate the use of the outputs of numerical flow modeling to predict bed damage.



## 1.3 Research methodology

The aforementioned objectives are reached by the following steps (Figure 1.1). First, a literature study is carried out. It provides an overview on turbulent flow and stone stability. The existing information reveals that there are not many studies conducted for stone transport formulae and that it is not possible to develop stone transport formulae for non-uniform flow on the basis of the existing data. Also turbulent flows over a rough bed can not be fully resolved by numerical simulations. Therefore, experimental work is conducted.

The flow in gradually expanding open-channels and its influence on stone stability were focused on because under these conditions the turbulence intensity is high. In the experiments, both the bed damage and the flow quantities (velocity and turbulence intensity) are measured. A new stability parameter is formulated to better describe the impact of hydraulic parameters on stone stability. This new stability parameter together with those of Shields (1936), Jongeling et al. (2003) and Hofland (2005) are evaluated using the measured data. New stone transport formulae are suggested by correlating these stability parameters with the bed damage.

With the available data and newly-developed stone transport formulae, it is possible to evaluate the application of a numerical flow model to predict bed damage. This is done by using Reynolds averaged numerical simulations, using a  $k - \epsilon$  model, to reproduce the flows in the experiments. The simulated flows are used to calculate the bed damage using the newly-developed stone transport formulae. The evaluation is made by comparing the calculated bed damage with the measurements.

## 1.4 Outline

The thesis is structured as follows. Chapter 2 provides an overview on turbulent flow and stone stability. The overview is essential before proceeding into further studies. First, the flow and turbulence characteristics that are important to the present study are discussed. Then, the stability of a single stone and an entire bed under flowing water is presented and discussed. As a result, concluding remarks are derived. Next, in Chapter 3, a detailed description of the three experimental configurations is presented. There, the rationale for the choice of stones and flow conditions is discussed. In Chapter 4, an analysis of the flow quantities that are measured in the experiments is given, focusing on the difference in the characteristics between the studied flow and uniform flow. The idea behind this is that an understanding of the flow characteristics is required before a thorough analysis can be made of its influence on stone stability. Chapter 5 focuses on establishing the physical relationship between the flow forces and their induced damage to the bottom, i.e. stone transport formulae. These formulae could be used to-

gether with the outputs of numerical flow models to estimate the bed damage for a given flow condition. This is evaluated in Chapter 6. Finally, conclusions and recommendations from the present study are drawn in Chapter 7.

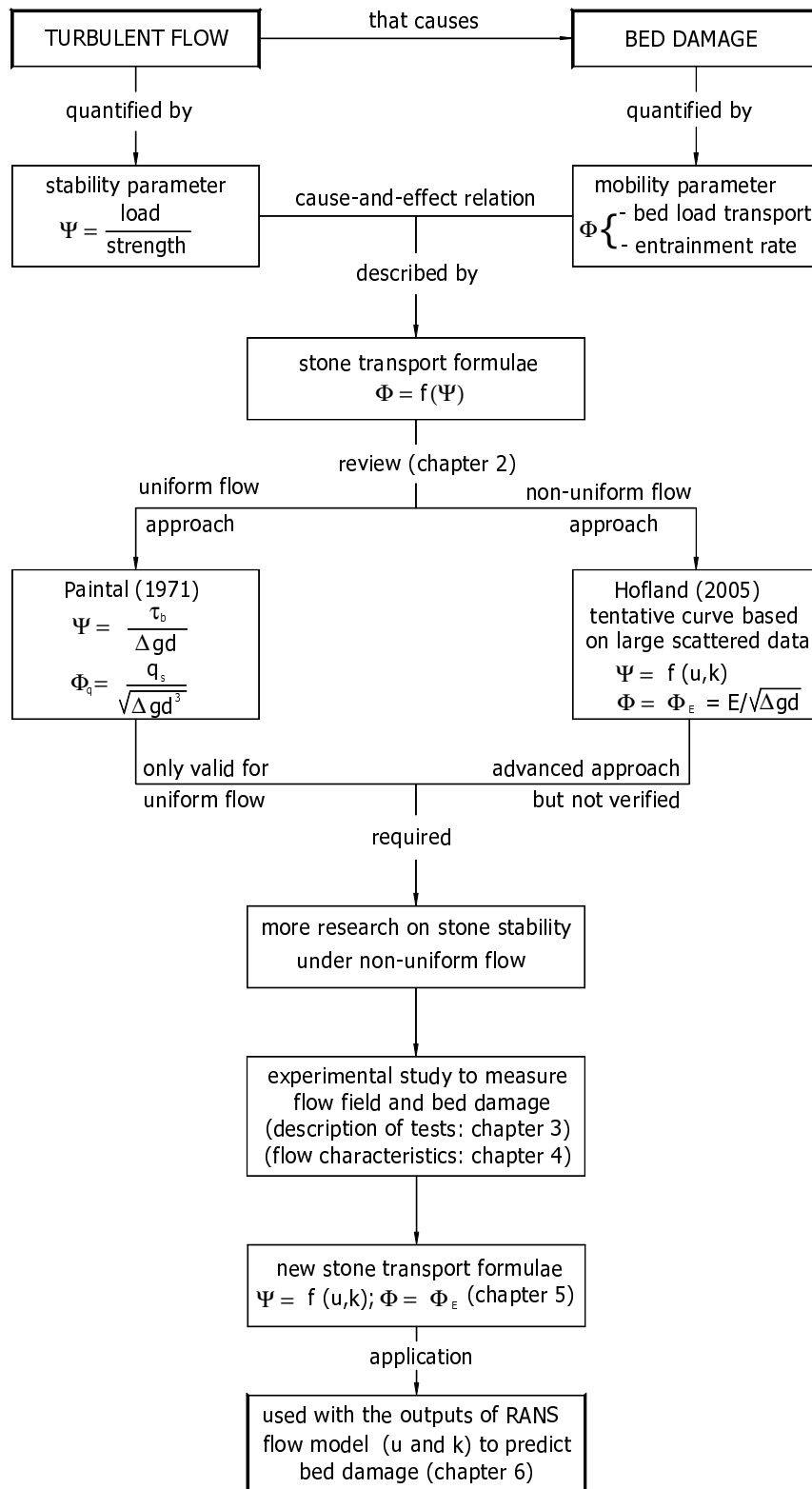


Figure 1.1: Graphical presentation of the research methodology and thesis layout.



# Chapter 2

## Literature review

### 2.1 Introduction

In this chapter, we present some of the background information that is essential for studying the interaction between flow and stone stability. The governing equations of turbulent flow and stone stability are presented. The physical meaning of various terms in the equations is discussed, indicating the importance to measure them. As a result, the requirements for the development of new stone transport formulae for non-uniform flow are derived.

The flow configurations used in the present experiments are the flow in a straight narrow open-channel and the flow along a gradually expanding open-channel. As hardly any research is available about this exact flow configuration, the characteristics of the related turbulent flows are discussed instead (Section 2.2). In Section 2.3 the physical concepts of stability of a single stone are treated, focusing on the hydrodynamic forces on the stones. The parameters used to quantify the flow forces acting on a bed are treated in Section 2.4. Several aspects that play a role in stone stability like turbulence effects and stone characteristics are discussed. It is followed by a discussion on how the bed damage should be quantified (Section 2.5). In Section 2.6 the methods for stone stability assessment are discussed. The chapter ends with concluding remarks in Section 2.7.

### 2.2 Turbulence and flow properties

#### 2.2.1 Uniform open-channel flow over a rough bed

In this section some characteristics of uniform open-channel flow over a rough bed are discussed. This is used to compare with the flow in the present study. In this thesis we define  $x$  to be the streamwise coordinate,  $y$  the transverse coordinate,  $z$  the upward coordinate and  $u$ ,  $v$ ,  $w$  are the velocity components in the respective directions. An over bar is used to represent the stationary mean

part (e.g.  $\bar{u}$ ) and a prime represents the fluctuating part with zero mean (e.g.,  $u' = u - \bar{u}$ ).

## Velocity distribution

Hydraulically rough flow is characterized by a large value of the ratio of the Nikuradse's equivalent particle roughness ( $k_s$ ) and the length scale of the viscous sublayer ( $\nu/u_*$ ), i.e.,  $u_*k_s/\nu$ . Here  $\nu$  is the kinematic viscosity coefficient,  $u_* = \sqrt{\tau_b/\rho}$  the shear velocity,  $\tau_b$  the bed shear stress and  $\rho$  the water density. In general,  $k_s$  is a function of the shape, height, width of the roughness elements, as well as their spatial distribution on the channel surface. [Van Rijn \(1994\)](#) argues that the roughness elements mainly influence the velocity distribution close to the bottom, because the roughness elements generate eddies (with a characteristic size of the order of the roughness elements) which affect the turbulence structure and hence the velocities close to the bottom. Further away, the eddies will rapidly be absorbed in the general existing turbulence pattern.

The vertical distribution of the streamwise velocity in a turbulent open-channel flow is quite complex. In the wall region ( $z/h < 0.2$ ,  $z$  is the distance above the boundary,  $h$  the water depth), the logarithmic law is widely accepted. It reads

$$\frac{\bar{u}}{u_*} = \frac{1}{\kappa} \ln \frac{z}{z_0} \quad (2.1)$$

where  $\kappa$  is the von Karman constant,  $\kappa \approx 0.4$  and  $z_0$  the zero-velocity level. In Eq. (2.1)  $z$  directly depends on where the theoretical wall level be defined, i.e. where  $z = 0$ . No definite standard is available yet, but according to [Nezu and Nakagawa \(1993\)](#) this level can be set at a  $\delta$  position below the top of the roughness elements. The value of  $\delta$  can be determined so that the mean velocity distribution best fits the log law. In physical applications, the value of  $\delta$  should be at some intermediate point in the range  $0 < \delta < k_s$ . From previous research (e.g., [Grass, 1971](#), [Blinco and Partheniades, 1971](#), [Nakagawa et al., 1975](#))  $\delta$  varies from  $0.15k_s$  to  $0.30k_s$ . According to [Van Rijn \(1994\)](#),  $\delta$  is approximately  $0.25k_s$  for sand and gravel particles. In the present study, in order to make the results comparable for different profiles and flow conditions a fixed value of  $\delta$  should be used for all flow conditions. The value of  $\delta = 0.25d_{n50}$  was chosen (with  $d_{n50}$  is the nominal diameter).

[Nezu and Rodi \(1986\)](#) discuss that the logarithmic law is inherently valid only in the wall region and that deviations of the velocity distribution from this law in the outer region should be accounted for by considering a wake function such as that proposed by [Coles \(1956\)](#):

$$\frac{\bar{u}}{u_*} = \frac{1}{\kappa} \ln \frac{z}{z_0} + \frac{2\Pi}{\kappa} \sin^2 \left( \frac{\pi z}{2h} \right) \quad (2.2)$$

where  $h$  is the water depth and  $\Pi$  the Coles wake strength parameter. The Coles parameter describes the deviation from the log law in outer region.

### Turbulence intensity distribution

According to [Nezu and Nakagawa \(1993\)](#) the vertical distributions of turbulence intensities can be described by an exponential law. It reads

$$\frac{\sigma(u_i)}{u_*} = \alpha_i e^{-\beta_i \frac{z}{h}} \quad (2.3)$$

where  $\alpha_i$  and  $\beta_i$  are empirical constants,  $i$  stands for  $u$ ,  $v$  and  $w$ . Based on hot-film data of smooth open-channel flows following values were established for those empirical constants:

$$\beta_u = \beta_v = \beta_w = 1.0, \quad \alpha_u = 2.30, \quad \alpha_v = 1.27, \quad \alpha_w = 1.63 \quad (2.4)$$

### Shear stress distribution

The shear stress in a turbulent flow at height  $z$  can be described as

$$\tau = \rho \nu \frac{d\bar{u}}{dz} - \rho \overline{u'w'} \quad (2.5)$$

As  $-\rho \overline{u'w'}$  component comes from the Reynolds averaging procedure, it is also called Reynolds shear stress. In most cases, the viscous shear stress ( $\rho \nu d\bar{u}/dz$ ) is much smaller than the Reynolds shear stress ( $-\rho \overline{u'w'}$ ) and can be neglected. For uniform flow, the equilibrium of forces in  $x$ -direction yields the following expression for the shear stress at height  $z$ :

$$\tau = -\rho g(h-z)i = \rho \left(1 - \frac{z}{h}\right) u_*^2 \quad (2.6)$$

where  $i$  is the energy slope. This relation shows a linear shear stress distribution over the depth.

### Mixing length and eddy viscosity

In analogy with the kinematic viscosity ( $\nu$ ) in the viscous shear stress  $\tau_v = \rho \nu d\bar{u}/dz$ , Boussinesq introduced the concept of eddy viscosity ( $\nu_t$ ) for the turbulent shear stress. Thus, the Reynolds shear stress can be expressed as:

$$\tau_t = \rho \nu_t \frac{d\bar{u}}{dz} \quad (2.7)$$

Prandtl (1875-1953) expressed the eddy viscosity as the product of a length and a velocity scale. This author introduced a mixing length  $l_m$  as the transverse

distance over which fluid particles travel due to turbulent fluctuations. Thus, the characteristic velocity scale of the fluctuating motion can be expressed as  $l_m d\bar{u}/dz$ . By using  $l_m$  again as the governing length scale, the eddy viscosity can be written as:

$$v_t = l_m^2 \left| \frac{d\bar{u}}{dz} \right| \quad (2.8)$$

Substituting Eq. (2.8) into Eq. (2.7) yields

$$\tau_t = \rho l_m^2 \left| \frac{d\bar{u}}{dz} \right| \frac{d\bar{u}}{dz} \quad (2.9)$$

This is known as Prandtl's *mixing length hypothesis*. The problem of determining the eddy viscosity has now shifted to the determination of the mixing length  $l_m$  (Uijttewaal, 2005). The mixing length is a local parameter, which may vary through the flow field. Close to a wall, Prandtl assumed that the mixing length  $l_m$  is proportional to the distance to the wall. The proportional factor is known as the constant of von Karman  $\kappa$  ( $\kappa \approx 0.4$ ):

$$l_m = \kappa z \quad (2.10)$$

Prandtl's mixing length model has been proven to be useful in describing uniform open channel flows. However, it is not suitable for flows with strong pressure gradients. In such cases more complex models should be used.

To examine the distribution of the eddy viscosity over the entire flow depth, one can use the shear stress distribution expressed in Eq. (2.6). The eddy viscosity distribution can then be determined as:

$$v_t = \frac{(1 - z/h) u_*^2}{d\bar{u}/dz} \quad (2.11)$$

In case the log-wake law is used to describe the velocity distribution, Eq. (2.2) leads to

$$\frac{d\bar{u}}{dz} = \frac{u_*}{\kappa} \left[ \frac{1}{z} + \frac{\Pi\pi}{h} \sin\left(\frac{\pi z}{h}\right) \right] \quad (2.12)$$

Eq. (2.11) and Eq. (2.12) yield the following distribution of  $v_t$ :

$$\frac{v_t}{u_* h} = \frac{\kappa (1 - z/h)}{\frac{h}{z} + \Pi\pi \sin\left(\frac{\pi z}{h}\right)} \quad (2.13)$$

When the logarithmic law is expanded to the outer region, i.e.  $\Pi = 0$ , a parabolic distribution of the eddy viscosity results.

In the same manner, the mixing length  $l_m$  can be obtained as:



$$\frac{l_m}{h} = \frac{\kappa \sqrt{(1 - z/h)}}{\frac{h}{z} + \Pi \pi \sin\left(\frac{\pi z}{h}\right)} \quad (2.14)$$

### 2.2.2 Non-uniform open-channel flow

In this section a brief overview of non-uniform open-channel flow is given, focusing on the characteristics of decelerating flow. This is used to make a qualitative comparison with the gradual-expansion open-channel flow in the present study.

Over the past few decades, several studies have been carried out to investigate the effect of non-uniformity on the velocity distribution and the turbulence characteristics of the flow (e.g. [Balachandar et al., 2002a](#); [Kironoto and Graf, 1995](#); [Nezu et al., 1994](#); [Cardoso, 1990](#); [Tsujimoto et al., 1990](#), among others). In most studies the flow is accelerated or decelerated by using a sloping bed. By changing the bed slope one can produce a spatial variation of the flow depth in the flow direction, forcing the flow to accelerate or decelerate. This configuration reproduces realistic bed forms, such as ripples, dunes, and anti-dunes.

In contrast, non-uniform flow induced by variation of the channel width - which is the case for the flow configuration used in the present experiments - has hardly been examined. The most important contributions related to the flow configuration in the present study were made by [Papanicolaou and Hildale \(2002\)](#), [El-Shewey and Joshi \(1996\)](#) and [Mehta \(1981\)](#). Of those studies only [Papanicolaou and Hildale \(2002\)](#) investigated the flow in a gradual channel transition. However, this concerns a field study and it does not give enough information for a systematic comparison to the present data.

#### Non-uniform flow induced by an inclined bed slope

[Kironoto and Graf \(1990a, 1995\)](#) and [Song and Graf \(1994\)](#) studied steady decelerating flow over a gravel bed. Their works were mostly aimed at the description of the turbulence structure of decelerating flows in laboratory equilibrium boundary-layer conditions in which the main characteristics of turbulence do not change in the flow direction. They found that the velocity and turbulence distributions are self similar over the entire depth. The log-wake law explains the mean velocity data sufficiently well over the entire depth. In a similar study, [Kironoto and Graf \(1990b\)](#) found that the turbulence intensities increase when the flow is decelerated and decrease when the flow is accelerated.

[Afzalimehr and Anctil \(1999\)](#) studied the behavior of the bed shear stress in a decelerating flow over a gravel bed. The study revealed that the velocity distribution can be described by a parabolic law in the outer region and by a logarithmic law in the inner region of the boundary layer.

[Song and Chiew \(2001\)](#) studied both accelerating and decelerating open-channel flows. The velocity was measured by a 3D acoustic Doppler velocimeter. Their

data show that the log law is still valid for both accelerating and decelerating flows in the inner region. The Coles law can be used for the entire region, but the wake-strength parameter  $\Pi$  depends on the pressure-gradient parameter value. The turbulence intensities and the Reynolds shear stress decrease in accelerating flow and increase in decelerating flow, when compared with those in uniform flow. By using the Reynolds equation and the continuity equation of 2D open-channel flow, they developed theoretical expressions for the distribution of vertical velocity and the Reynolds shear stress.

[Balachandar et al. \(2002a,b\)](#) studied the velocity distributions in a decelerating open channel flow over rough and smooth surfaces. Their study showed that the size of the roughness and the nature of the roughness both had an effect on the mean velocity profiles. The wake parameter was influenced by the channel slope. For the boundary layer generated in decelerating open channel flow, the power laws adequately described the mean velocity profile.

## Non-uniform flow induced by contractions and expansions

[Papanicolaou and Hildale \(2002\)](#) carried out a field study to determine the effects of a channel transition on turbulence characteristics. Three velocity components were measured at a cross section that was located downstream of a gradual channel expansion. These measurements were obtained via an Acoustic Doppler Velocimeter. Analysis of the 3D flow data indicates that the turbulent flow on the outer bank of the channel is anisotropic. The turbulence intensities in the vertical and transverse directions on the outer bank section are different in magnitude, creating turbulence anisotropy in the cross-sectional plane and secondary flows. The turbulence intensities increase toward the free surface. Results for the normalized stress components in the streamwise and transverse direction show similar behavior as the turbulence intensities.

[Mehta \(1981\)](#) studied the flow patterns for large, sudden expansions. The experimental studies revealed that flow patterns for large expansions are highly asymmetric and unsteady. Later, [El-Shewey and Joshi \(1996\)](#) studied in detail the effects of a sudden channel expansion on turbulence characteristics over smooth boundaries. They carried out experiments in a rectangular cross-sectional flume over a smooth bed by using Laser Doppler Velocimeter. They found that turbulence intensities downstream of the sudden expansion point increase towards the free surface. [Figure 2.1](#) illustrates the variation of the streamwise and vertical components of turbulence intensities normalized by the mean free stream velocity. The maximum turbulence intensities occur near bed or at free surface. [El-Shewey and Joshi](#) attributed this paradoxical behavior to the strong secondary flows developed at the transition point.

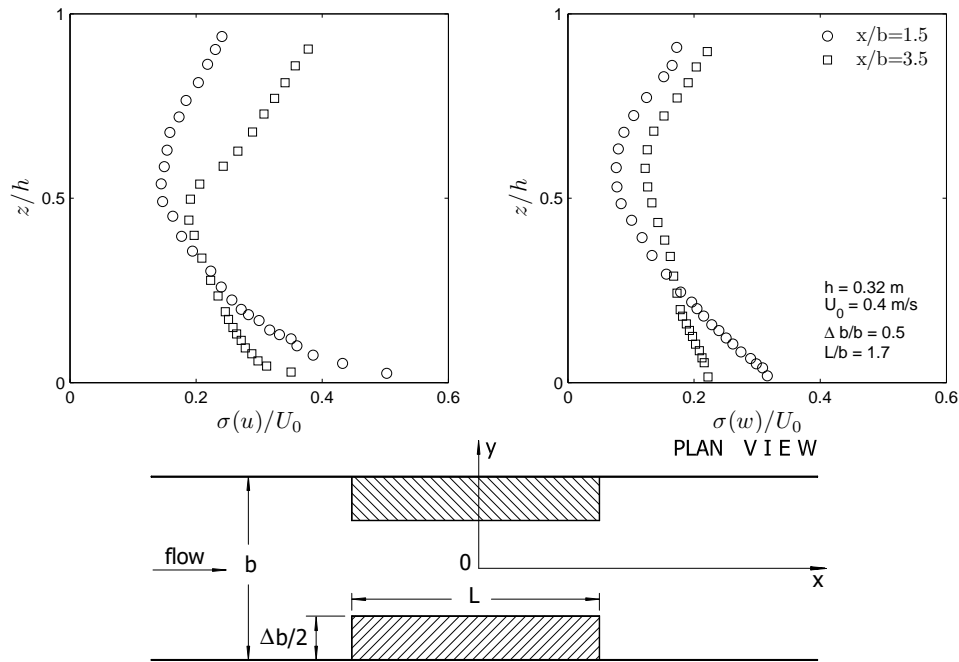


Figure 2.1: Turbulence intensity distributions downstream of a sudden expansion after [El-Shewey and Joshi \(1996\)](#).

## 2.3 Hydrodynamic forces on a single stone

If a stone is exposed to a fluid flow, a frictional force  $F_1$  is presented on the rough surface of the stone (Figure 2.2). This surface friction is the main force acting on the stone if the particle Reynolds number ( $u_*d/\nu$ ) is less than 3.5. If the particle Reynolds number is larger than 3.5, however, separation of streamlines in the form of a small wake occurs behind the top of the particles and vortexes form there. This causes a pressure difference between the front and the back surface of the particle, forming the resistance  $F_2$  ([Chien and Wan, 1999](#)). The resultant of  $F_1$  and  $F_2$  is called drag force ( $F_D$ ). When the particle Reynolds number is high, let's say, larger than 500, the frictional force  $F_1$  can be negligible.

The velocity at the top is higher than the velocity at the bottom of the stone, causing a lift force ( $F_L$ ). This lift force can be considered to act through the center of the stone. Both drag force and lift force are the results of the pressure differences between the front and the back, the top and the bottom of the grain surface, which are the result of the difference of velocities. According to the Bernoulli law, these forces are proportional to the velocities in the vicinity of the stone. The drag force and the lift force can be expressed in general form as follows:

$$F_D = \frac{1}{2}C_D A_D \rho u |u| \quad (2.15)$$

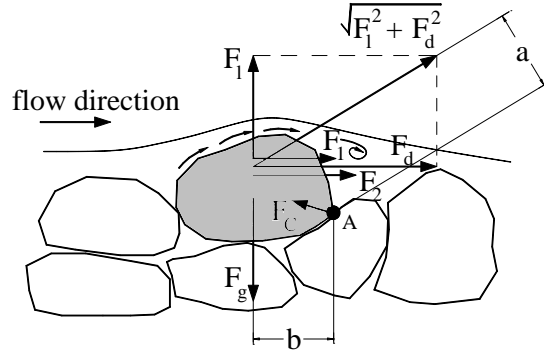


Figure 2.2: Forces acting on particles resting on a bed surface

$$F_L = \frac{1}{2} C_L A_L \rho u |u| \quad (2.16)$$

in which  $C_D$  and  $C_L$  are the drag and lift coefficients, respectively, and  $u$  is the velocity near the grain.  $A_D$  and  $A_L$  are the exposed surface areas. In general,  $A_D$  and  $A_L$  are proportional to the squared value of the nominal diameter  $d_n$ .

Much research has been done on the drag and lift coefficients (see [Hofland, 2005](#), for a review). The drag and lift coefficients depend on the flow pattern around the bed particle and the method of estimating  $u$ . The difference in definition of  $u$  in the vicinity of the stone causes the difference in the coefficient values. The common velocities used to determine drag and lift coefficients are  $\bar{u}$  at  $0.15d$  above the top of the grain (e.g. [Einstein and El-Samni, 1949](#); [Chepil, 1958, 1959](#)),  $\bar{u}$  measured at the height of the center of the grain (e.g. [Coleman, 1967, 1972](#); [Patnaik et al., 1992, 1994](#)), and the shear velocity  $u_*$  (e.g. [Watters and Rao, 1971](#)). The coefficients become fairly constant for high grain Reynolds numbers, but most authors still find a small dependency of  $C_D$  on the grain Reynolds numbers. The drag and lift coefficients are rather constant if  $u_{0.15}$  is used as the reference velocity in Eq. (2.15) and Eq. (2.16).

The averaged velocity near the stone is commonly used to determine the drag and lift forces. However, the velocity is not constant and the fluctuations of the velocities near the stone cause the forces to fluctuate as well. These forces are often referred to as quasi-steady forces (QSF). Generally, the fluctuating parts of the velocity,  $u'$ , is much less than the averaged value so the fluctuating parts of the drag and lift forces can be negligible. However, the velocity used in Eqs. (2.15) and (2.16) is the velocity in the vicinity of the stone and close to the bed the extreme values of  $|u'|$  can be of the same order of magnitude as  $|\bar{u}|$  so the fluctuating parts of drag and lift forces are of importance for the entrainment of stones.

From Eqs. (2.15) and (2.16) it can be inferred that:

$$F_D' \propto 2\bar{u}u' + u'^2 - \overline{u'^2} \quad (2.17)$$

$$F'_L \propto 2\bar{u}u' + u'^2 - \overline{u'^2} \quad (2.18)$$

For the fluctuating part of the lift force another relation was also proposed (Radecke and Schulz-DuBois, 1988):

$$F'_L \propto a\bar{u}u' + b\bar{u}v' \quad (2.19)$$

in which  $a$  and  $b$  are coefficients. The second term in the right hand side accounts for the vertical force component which is caused by the vertical velocity.

In the threshold condition, the fluctuating part of the drag and lift forces are expected to play an important role in dislodging stones on the bed.

Xingkui and Fontijn (1993), in their backward-facing step (BFS) experiments, found an increase of  $C_D$  for growing distances from the step. The drag coefficient in their experiments was determined by using the mean of the measured horizontal velocities. In BFS flow conditions, the fluctuating parts of horizontal velocities are high and can attribute largely to the instantaneous drag force and hence the mean drag force. Therefore, using mean velocities is not a proper choice. Let's find the drag coefficient for the experiment if instantaneous velocities are used:

$$\overline{F_D} = \frac{1}{2}C_D A_D \rho_w \overline{u^2} \quad (2.20)$$

$$\overline{F_D} = \frac{1}{2}C_D A_D \rho_w [\overline{u^2} + \sigma(u)^2] \quad (2.21)$$

The drag coefficient determined by Xingkui and Fontijn ( $C_{dxf}$ ) is expressed as follows:

$$\overline{F_D} = \frac{1}{2}C_{dxf} A_D \rho_w \overline{u^2} \quad (2.22)$$

From Eq. (2.21) and (2.22) we have:

$$C_{dxf} = C_D \left(1 + r_u^2\right) \quad \text{with} \quad r_u = \frac{\sigma(u)}{\bar{u}} \quad (2.23)$$

As mentioned above,  $C_D$  can be considered a constant and does not depend on the flow conditions. Hence, the observed increase of drag coefficient  $C_{dxf}$  with the distance from the step is not in line with the decrease of the relative turbulence intensity  $r_u$  in the streamwise direction downstream of the reattachment point. Perhaps that was caused by the fact that not all horizontal forces that were measured by their dynamometer are covered by Eq. (2.15). Some horizontal forces may have been caused by turbulence wall pressure (TWP) originating from turbulent structures that did not affect the velocities in the vicinity of the dynamometer (Hofland, 2005). Another possible factor is the pressure gradient caused by acceleration or deceleration (see Hoan, 2005, for a discussion).

## 2.4 Stability parameters

### 2.4.1 Governing variables

A stone transport formula should present a method of determining the bed response (i.e., bed damage level) as a function of all the variables involved. The review in the previous sections describes a large number of variables affecting the stone stability. The dominant governing variables are summarized in Table 2.1. In the present study, these variables can be obtained directly or indirectly from the measurements.

Table 2.1: List of dominant governing variables.

Governing variables	Expression	Dimension
The bed shear stress	$\tau = \rho u_*^2$	N/m <sup>2</sup>
The velocity	$u, v, w,$	m/s
The turbulence	$k, \sigma(u), \sigma(v), \sigma(w)$	m <sup>2</sup> /s <sup>2</sup>
The stone size	$d_{n50}$	m
The gradation of the stones	$d_{85}/d_{15}$	-
The shape of the stones	$SF = a/\sqrt{bc}$	-
The specific submerged density of stone	$\Delta = (\rho_s - \rho)/\rho$	-

The bed shear stress has been widely used as the only governing variable representing the flow forces (Shields, 1936). It can be used to define the threshold condition at which the stones start to move. In most transport formulae, the bed load transport is driven by the bed shear stress. In uniform flow the bed shear stress is a function of the depth-averaged velocity, the Chezy coefficient  $C$  and the water depth. Therefore, the depth-averaged velocity is sometimes used in the stone stability equation.

Apart from the bed shear stress, the longitudinal flow velocity is commonly used to quantify the flow forces on a particle (e.g., Isbash, 1932; Nordin, 1964; Hoffmans and Akkerman, 1998; Hoffmans, 2006). The drag force and the lift force are often expressed as a proportion to the square of the velocity near the grain. In stability formulae, the influence of velocity can be described by a mean velocity (Isbash, 1932), the depth-averaged velocity (Nordin, 1964; Hoffmans and Akkerman, 1998; Hoffmans, 2008), or the velocity distribution (Jongeling et al., 2003; Hofland, 2005; Hofland and Booij, 2006). Since near-bed velocities cause the main forces on bed material, the use of velocities and other flow quantities such as turbulence higher up in the water column is unlikely to be correct. However, Hofland (2005) has shown that stones often get moved when an increased  $u$ -velocity fluid package reaches the bed. The chance that a high momentum fluid package reaches the bottom is related to flow parameters such as velocity and

turbulence from higher up in the water column. Therefore, flow parameters at different depths should be used to represent the flow forces exerting on the bed.

For uniform flow, the turbulence effect is sometimes incorporated in some empirical coefficient such as  $\Psi_{s,c}$  in the Shields curve. In non-uniform flow, the influence of turbulence can be given by applying a correction for turbulence effect after the stone diameter in uniform flow has been determined (Pilarczyk, 2001; Schiereck, 2001). The values for the turbulence factor are given for various flow situations. Since the turbulence effect is not physically explained and the uncertainty in the choice of the correction factor is usually high, the expressions can only be used as rules-of-thumb. The turbulence factor sometimes can be determined based on the normalized depth-averaged longitudinal turbulence intensity:  $\langle \sigma(u) \rangle_h / \langle \bar{u} \rangle_h$  (Hoffmans and Akkerman, 1998). In the recent approach developed by Jongeling et al. (2003) and Hofland (2005), the profiles of the mean velocity and turbulent kinetic energy in the water column above the bed are used to formulate local stability parameters. In this approach, the influence of turbulence is incorporated explicitly.

For stability, the size of a stone is one of the most important parameters since it defines both the resisting forces of the stone as well as the dislodging forces of the flow acting on the stone. The stone size is often described by a characteristic diameter, namely (Hofland, 2005):

- nominal diameter,  $d_n$  (size of an equivalent-volume cube),
- sieve diameter,  $d_s$  (diameter of a sphere equal to the length of the side of a square sieve opening through which the stone can pass),
- standard fall diameter (diameter of a sphere that has the same density and has the same standard fall velocity as the stone).

Other factors that may influence the stability are the shape and the gradation of the stones (see Mosselman and Akkerman, 1998, for a review). The shape of a stone can be angular, rounded or flat. The stone shape can be quantified by a shape factor  $SF$  defined in Table 2.1 where  $a$ ,  $b$  and  $c$  are the shortest, intermediate, and longest body axes of the stone, respectively. The grading of the stones is often expressed by  $d_{85}/d_{15}$ , where the subscripts refer to the 85 and 15 percent value of the sieve curve, respectively. The stones used in bed protections are often classified as a narrow grading, defined as  $d_{85}/d_{15} < 1.5$ . The studies of Breusers (1965); Boutovski (1998) (flow), Van der Meer and Pilarczyk (1986); Van der Meer (1988, 1993) (waves) and others have revealed that the grading and the shape of stones practically have no influence on the stone stability when the nominal diameter  $d_{n50}$  is used as the characteristic dimension.

$$d_{n50} = \left( \frac{m_{50}}{\rho_s} \right)^{1/3} \quad (2.24)$$

where  $m_{50}$  is the mass of median size of the stones (exceeded by 50% of stone weight).

The influence of the stone density is given by the specific submerged density of stones  $\Delta = (\rho_s - \rho)/\rho$ , where  $\rho_s$  is the stone density and  $\rho$  is the water density.

The influence of all dominant governing variables can be weighed and expressed in a Shields-like stability parameter which describes the ratio of the flow forces to the resisting forces. The ways in which these variables are grouped to form various stability parameters are described and discussed below.

### 2.4.2 The Shields stability parameter

Shields (1936) assumed that the factors in determining the stability of the particles on a bed are the bed shear stress  $\tau_b$  and the submerged weight of the particles. These two quantities are used to form the dimensionless shear stress known as the Shields stability parameter  $\Psi_s$ . This is roughly the ratio of the load on the particle ( $\propto \tau \times d^2$ ) to the strength of the particle (i.e the gravitational force that resists movement,  $\propto g(\rho_s - \rho)d^3$ ).

$$\Psi_s = \frac{\text{load}}{\text{strength}} = \frac{\tau_b \times d^2}{g(\rho_s - \rho)d^3} = \frac{\tau_b}{\rho\Delta g d} \quad (2.25)$$

in which  $d$  is the stone diameter. In the present analysis the nominal diameter  $d_{n50}$  is used. Since the bed shear stress can be expressed as  $\tau_b = \rho u_*^2$ , Eq. (2.25) becomes:

$$\Psi_s = \frac{u_*^2}{\Delta g d} \quad (2.26)$$

Because the turbulence also plays an important role, it is questionable whether the bed shear stress should be used as the only quantity representing the flow forces. This is discussed in Chapter 5.

### 2.4.3 The Jongeling et al. stability parameter

Jongeling et al. (2003) developed a method that uses the outputs of numerical computations for determining damage of bed protections. A combination of velocity and turbulence distributions over a certain water column above the bed is used to quantify the flow forces. The turbulence is incorporated to account for the peak values of the forces that occur in the flow. A Shields-like stability parameter was proposed and it reads:

$$\Psi_{WL} = \frac{\langle (\bar{u} + \alpha\sqrt{k})^2 \rangle_{hm}}{\Delta g d} \quad (2.27)$$



where  $k$  denotes the turbulent kinetic energy,  $\alpha$  is an empirical turbulence magnification factor,  $\langle \dots \rangle_{hm}$  is a spatial average over a distance of  $hm$  above the bed.

The determination of  $\alpha$  and  $hm$  for the new stability  $\Psi_{WL}$  and its critical value  $\Psi_{WL,c}$  is based on the stability threshold concept. First, experiments were carried out for various flow configurations at incipient conditions. Second, these experiments were simulated by numerical flow models. Finally, the outputs of a numerical flow model were used to compute the new stability parameter with several combinations of  $\alpha$  and  $hm$ . The values of  $\alpha$  and  $hm$  that give more or less equal values of  $\Psi_{WL,c}$  at incipient motion for all considered geometries were chosen to formulate  $\Psi_{WL}$  (Jongeling et al., 2006). After a mutual comparison of the various geometries,  $\alpha = 6$  was chosen since it gives the least variation of  $\Psi_{WL,c}$ . The water column above the bed was chosen as  $hm = 5d + 0.2h$  with  $d$  is the stone diameter and  $h$  is the water depth. The value of  $\Psi_{WL,c}$  ranging from 9 to 14 was calculated based on the output of RNG  $k - \epsilon$  turbulence model.

This approach has the advantage that the turbulence effect is explicitly modeled. However, the method of choosing  $\alpha$  and  $hm$  is questionable because there is no proof that the critical stability parameter  $\Psi_{WL,c}$  has to be a constant value. Also as pointed out by Hofland (2005) and others, using a subjective definition of incipient motion will not yield consistent design criteria. It appears that Jongeling et al. defined the incipient motion by the visual observation method since the flow conditions in their experiments are described as: "In all cases the bed was protected with stones and the flow conditions were such that individual stones were now and then moved by the flow (*incipient motion* condition)" (Jongeling et al., 2006). Therefore, the link between  $\Psi_{WL,c}$  and the stability state of bed material is not clear.

#### 2.4.4 The Hofland stability parameter

Hofland (2005) proposed a method for evaluating the stability of bed protections under non-uniform flow using output of a 3D RANS model. The profiles of the mean velocity and turbulent kinetic energy in the water column above the bed are used to formulate a local stability parameter. The maximum over the depth of the local values of  $(\bar{u} + \alpha\sqrt{k})$  weighted with the relative mixing length  $Lm/z$  is used. The stability parameter,  $\Psi_{Lm}$ , is expressed as

$$\Psi_{Lm} = \frac{\max \left[ \left\langle \bar{u} + \alpha\sqrt{k} \right\rangle_{Lm} \frac{Lm}{z} \right]^2}{\Delta g d} \quad (2.28)$$

where  $Lm$  denotes the Bakhmetev mixing length ( $Lm = \kappa z \sqrt{1 - z/h}$ ),  $\langle \dots \rangle_{Lm}$  is a moving average with varying filter length  $Lm$ , and  $z$  is the distance from the bed. A correlation between the Hofland stability parameter and the bed damage was

analyzed based on the data of [Jongeling et al. \(2003\)](#) and [De Gunst \(1999\)](#). From the analysis  $\alpha = 6$  visually yielded the best collapse of data.

## 2.5 Mobility parameters

A clearly defined and quantified measure of damage is essential for assessing the stability of a granular bed. This quantity is often referred to as mobility parameter (or bed damage indicator, or transport indicator). This parameter should adequately quantify the bed response (also the bed damage level) for a variety of flow conditions - uniform and non-uniform. For non-uniform flow, it is important that the mobility parameter is dependent on the local hydrodynamic conditions ([Hofland, 2005](#)).

[Mosselman and Akkerman \(1998\)](#) distinguish two ways of defining the mobility of particles: i) the number of pick-ups ( $n$ ) per unit time ( $T$ ) and area ( $A$ ) or ii) the number of particles that is transported through a cross-section per unit time. The former if expressed in terms of volume of entrainment is often called (volume) entrainment rate,

$$E = \frac{nd^3}{AT} \quad (2.29)$$

The latter is often called bed load transport,  $q_s$ , expressed as:

$$q_s = \frac{nd^3}{BT} \quad (2.30)$$

where  $B$  is the section width. The entrainment is linked to the bed load transport by:

$$q_s = E \times l \quad (2.31)$$

where  $l$  is the displacement length. In the studies of bed protections, both the bed load transport ( $q_s$ ) and the entrainment rate ( $E$ ) can be used as bed damage indicators and are often expressed in dimensionless form as ([Einstein, 1950](#); [Hofland, 2005](#)):

$$\Phi_q = \frac{q_s}{\sqrt{\Delta g d^3}} \quad (2.32)$$

$$\Phi_E = \frac{E}{\sqrt{\Delta g d}} \quad (2.33)$$

in which  $d$  is the characteristic particle diameter,  $g$  is the gravitational acceleration,  $\Delta$  is the specific submerged density of particles.

The use of (dimensionless) bed load transport as a bed damage indicator is conventional for uniform flow (e.g. [Paintal, 1971](#)). However, bed load transport

is dependent on the upstream hydraulics; all the stones passing a certain cross section (i.e., the transport) have been entrained upstream of this section. Bed load transport is therefore considered as a non-local parameter. Stability parameters are local parameters, making  $\Psi - \Phi$  a relationship of local and non-local parameters. Such a relationship can only be valid for uniform flow where the flow condition is unchanged along the channel.

To adapt to various flow conditions, [Hofland \(2005\)](#) points out that the dimensionless entrainment rate ( $\Phi_E$ ) could be used as a bed damage indicator because it is completely dependent on the local hydrodynamic parameters.

## 2.6 Methods for stone stability assessment

The basic approaches used for stone stability assessment are the deterministic and probabilistic methods (see the review by [Mosselman et al., 2000](#)). Due to the stochastic nature of the flow and the particle resistance properties, the probabilistic approach seems more realistic than the deterministic approach. However, the results based on a probabilistic approach are not more accurate than those based on a deterministic approach because of the statistics involved ([Van Rijn, 1993](#)). Examples of studies using probabilistic approach are [Einstein \(1950\)](#); [Paintal \(1969\)](#); [Grass \(1970\)](#); [De Ruiter \(1982\)](#); [Bridge \(1992\)](#); [Van Rijn \(1993\)](#); [Uittenbogaard et al. \(1998\)](#); [Kleinhans and Van Rijn \(2002\)](#), among others. In spite of the sophisticated theories, the probabilistic approach is not a popular one for engineering applications due to the complex computational procedures required ([Bureau of Reclamation U.S. Department of the Interior, 2006](#)). For the aforementioned reasons, in the present study the deterministic approach is followed.

Apart from these two basic approaches, [Mosselman et al. \(2000\)](#) distinguished two concepts for the assessment of stone stability: i) the stability threshold concept and ii) the stone transport concept. Together they form four mechanical model concepts for stone stability, as shown in [Figure 2.3](#).

Next in this section, the deterministic threshold and transport concepts are described and discussed. The concept that is most appropriate will be used for the present study.

### 2.6.1 The stability threshold concept

In this approach, the stability of bed material is assessed using incipient motion condition at which the bed material starts to move (see [Buffington and Montgomery, 1997](#), for a review). In principle, when the dislodging force on the particle exceeds the resisting (gravitational) force, the particle will start to move ([White, 1940](#); [Wang and Shen, 1985](#); [Wiberg and Smith, 1987](#); [Bridge, 1992](#); [Andrews and Smith, 1992](#); [Ling, 1995](#), for example). In practice, the incipient motion of bed material can be defined by i) a critical stability parameter (or critical shear

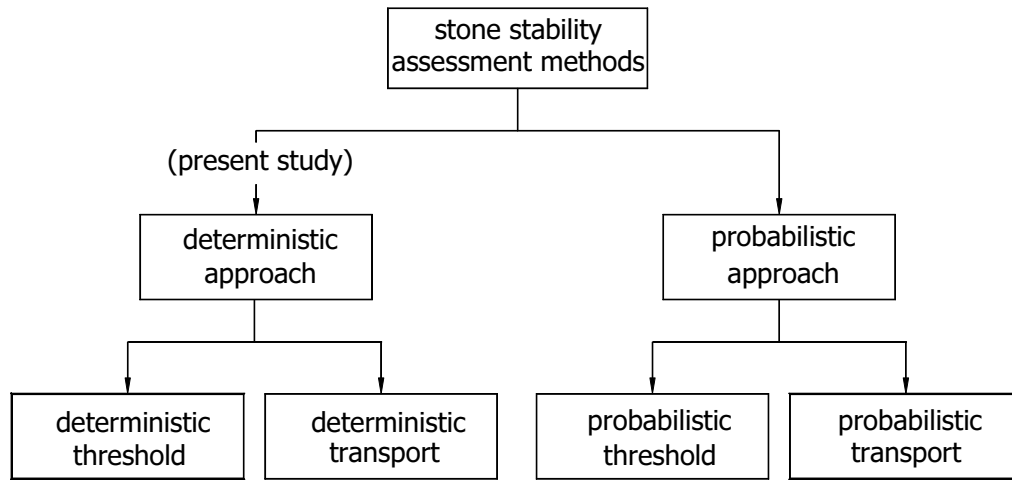


Figure 2.3: Four mechanical model concepts after [Mosselman et al. \(2000\)](#).

stress), ii) the number of particles displaced per unit area and time or iii) visual observation.

### Definition based on critical stability parameters

[Shields \(1936\)](#) pioneered the dimensionless critical shear stress to define incipient motion of a particle size of interest. Since then, the dimensionless critical shear stress (sometimes called the critical Shields stability parameter) or its modifications were used by many researchers to study the threshold conditions in which bed material starts to move. The corresponding bed shear stress is referred to as the critical shear stress,  $\tau_c$ . The Shields curve - often used for the assessment of stone stability - presents the critical dimensionless shear stress parameter  $\Psi_{s,c}$  as a function of the particle Reynolds numbers  $Re_*$  (see Figure 2.4). The stones on a bed are considered stable if the Shields stability parameter  $\Psi_s$  is smaller than the critical Shields stability parameter  $\Psi_{s,c}$ :

$$\Psi_s = \frac{\tau_b}{\rho\Delta gd} = \frac{u_*^2}{\Delta gd} < \Psi_{s,c} = \frac{\tau_c}{\rho\Delta gd} = \frac{u_{*c}^2}{\Delta gd} = f\left(\frac{u_{*c}d}{\nu}\right) = f(Re_*) \quad (2.34)$$

in which  $\tau_b$  is the bed shear stress,  $\tau_c$  is the critical shear stress,  $u_{*c}$  is the critical shear velocity and  $d$  is the characteristic diameter of the stones.

Since the stones used in bed protections are large, the particle Reynolds number is usually high, i.e.  $Re_* > (300 - 500)$ . According to the Shields curve, the value of the critical Shields stability parameter for that high particle Reynolds number is a constant value of about 0.055.

It is noted that the Shields curve is developed for uniform open-channel flow and turbulence is not explicitly accounted for. Its effect is incorporated implicitly through the empirically estimated values of  $\Psi_{s,c}$ . This is a valid approach for uniform flows, for which the ratio of turbulence intensity to  $u_*$  is virtually constant (Hofland, 2005). Therefore, the use of the Shields curve in the design of bed protections - where the flow is usually non-uniform - is not straightforward. In practice, the value of  $\Psi_c = 0.03 - 0.04$  is often used as a safe limit for the design of bed protections.

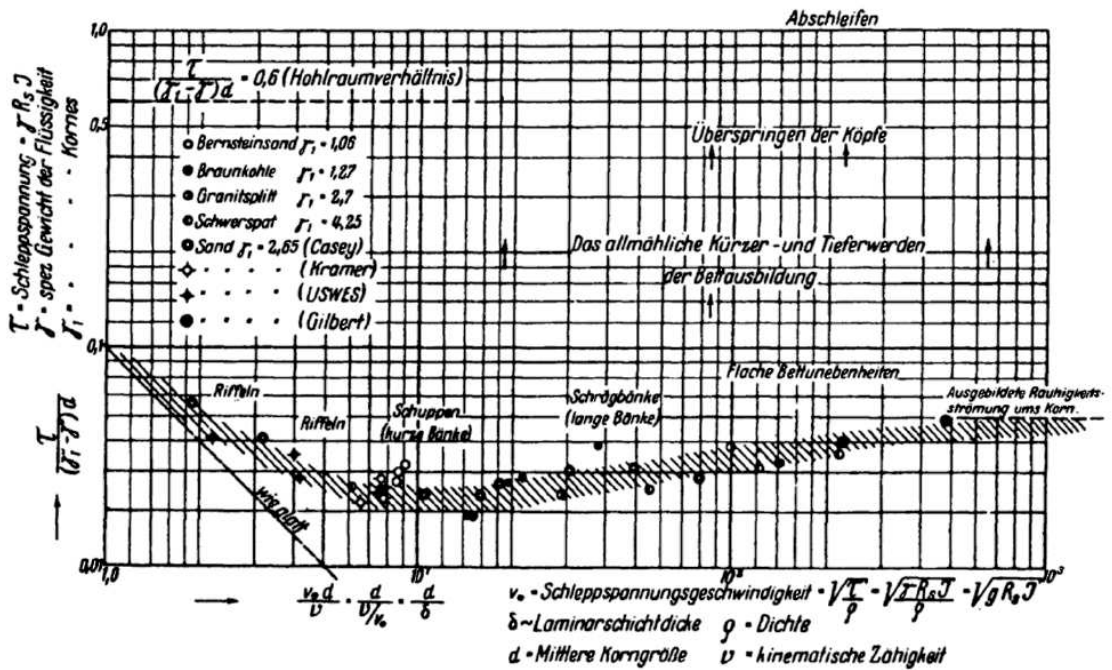


Figure 2.4: Original Shields curve (1936). The hatched area shows the critical shear stress as a function of the particle Reynolds number.

**Uniform flow.** In uniform open-channel flow, the shear velocity can be expressed as (Schiereck, 2001):

$$u_* = \frac{\langle \bar{u} \rangle_h \sqrt{g}}{C} \tag{2.35}$$

where  $\langle \bar{u} \rangle_h$  is the mean velocity averaged over the water depth  $h$  or the cross section and  $C$  is the Chezy coefficient, determined as  $C = 18 \log(12R/k_s)$  with  $R$  is the hydraulic radius,  $k_s$  is the equivalent roughness. Substituting Eq. (2.35) into Eq. (2.34) yields

$$d_{n50} = \frac{\langle \bar{u} \rangle_h^2}{\Psi_{s,c} \Delta C^2} \tag{2.36}$$

This formula is the basis for the design of bed protections in uniform flow conditions. Note that the effect of water depth is implicitly incorporated in Eq. (2.36) via  $C$ .

*Non-uniform flow.* As Eq. (2.36) is only valid for uniform flow condition, several correction factors are often applied to account for non-horizontal bottoms and flow situations that deviate from uniform flow (Schiereck, 2001). The way in which this is done is the main difference between the various design approaches (Hofland, 2005).

Pilarczyk (2001) proposed:

$$d_{n50} = 0.035 \frac{S}{\Delta\Psi_{s,c}} \frac{K_T K_h}{K_s} \frac{\langle \bar{u} \rangle_h^2}{2g} \quad (2.37)$$

where  $S$  is an empirical factor accounting for the way the stones are placed,  $S = 0.5 - 1.0$ .  $K_T$  is a turbulence factor, varying from 1.0 (for uniform flow) to 2.0 (for hydraulic jump) and to 3.0 – 4.0 (for load due to water jet).  $K_h$  is the water depth parameter used to translate the depth-averaged velocity into the velocity just above the bottom.  $K_s$  is the slope parameter accounting for slopes of the bed protection. Eq. (2.37) can only be used as a rule-of-thumb since the various correction coefficients are rather arbitrary.

Another approach is (Franken et al., 1995; Schiereck, 2001):

$$d_{n50} = \frac{(K_v \langle \bar{u} \rangle_h)^2}{K_s \Delta\Psi_{s,c} C^2} \quad (2.38)$$

in which  $K_s$  is the slope correction factor,  $K_v$  is the velocity/turbulence factor used to account for a load deviation from uniform flow.  $K_v$  has been determined from measurements for various types of structures as:

$$K_v = \frac{u_{c,u}}{u_{c,nu}} \quad (2.39)$$

where  $u_{c,u}$  and  $u_{c,nu}$  are the critical flow velocity under uniform and non-uniform flow, respectively.

As an alternative to the critical Shields parameter, the critical Jongeling et al. (2003) stability parameter can be used to determine stone size in bed protections under non-uniform flow. Substituting  $\Psi_{WL,c}$  into Eq. (2.27) yields

$$d_{n50} = \frac{\langle (\bar{u} + \alpha\sqrt{k})^2 \rangle_{hm}}{\Delta g \Psi_{WL,c}} \quad (2.40)$$

An analysis using numerical flow outputs gave a large range of  $\Psi_{WL}$  for all critical flow conditions ( $\Psi_{WL} = 9 - 14$ ), and therefore a conservative value of  $\Psi_{WL,c} = 8$  was chosen. In order to use Eq. (2.40), information on the vertical distributions of velocity  $\bar{u}$  and turbulent kinematic energy  $k$  is needed. A detailed discussion on this approach is presented in Section 2.4.3.

### Other definitions of threshold condition

Apart from the use of the critical stability parameters, there are two other commonly used definitions for incipient motion: i) the number of particles displaced per unit area and time (e.g. [Breusers and Schukking, 1971](#); [Graf and Pазis, 1977](#); [Tromp, 2004](#); [Dessens, 2004](#)) and ii) visual observation. The use of a certain number of displaced stones to define incipient motion is not suggested since it is not possible to compare different investigations using different stone sizes (i.e., inconsistent design criteria). For the visual observation method, the bed movement can be defined as ([Kramer, 1932](#)):

1. None.
2. Weak (“...several of the smallest particles are in motion, in isolated spots, and in countable numbers.”).
3. Medium (“...grains of mean diameter are in motion in numbers too large to be countable ... movement is no longer local in character. It is not strong enough to affect bed configuration and does not result in transportation of an appreciable quantity of material.”).
4. General (“...grains up to and including the largest are in motion .... It is sufficiently vigorous to change the bed configuration .... There is an appreciable quantity of material transported ...”).

Another definition of the bed movement suggested by [WL|Delft Hydraulics \(1972\)](#) can be described as:

1. no movement at all.
2. occasional movement at some locations.
3. frequent movement at some locations.
4. frequent movement at several locations.
5. frequent movement at many locations.
6. frequent movement at all locations.
7. continuous movement at all locations.
8. general transport of the grains.

The above two common definitions clearly show that the visual observation method is rather subjective. However, this method is helpful for the study of mixed sediments ([Shields, 1936](#); [Buffington, 1999](#)). Also visual observation can always be a good supplement for the other methods.

## 2.6.2 The stone transport concept

This approach is widely used in sediment transport studies where the transport formulae can be expressed deterministically in a cause-and-effect relationship between independent and dependent variables. Conventional, dominant independent variables used in sediment transport studies are i) the flow parameters such as flow discharge, velocity, shear stress, turbulence and ii) the particle properties such as the diameter, the gradation and the density of particles. The dependent variables used in sediment transport formulae are the amount of transported particles and their displacement lengths. They are often grouped to form a transport indicator (i.e. mobility parameter). These independent and dependent variables are often grouped into dimensionless quantities and the transport formulae have the following general form:

$$\Phi = f(\Psi) \quad (2.41)$$

where  $\Psi$  is the stability parameter used to quantify the flow forces acting on the bed (see Section 2.4) and  $\Phi$  is the transport indicator used to quantify the bed response (see Section 2.5).

The transport formulae are often expressed by an exponential relation and can be divided into two main groups as defined by the involvement of a critical stability parameter (Mosselman and Akkerman, 1998). The formulae without a critical stability parameter are of the following form (type 1):

$$\Phi = a\Psi^b \quad (2.42)$$

in which  $a$  is a coefficient,  $b$  is an exponent. The transport formulae with a critical stability parameter are of the following form (type 2):

$$\Phi = a(\Psi - \Psi_c)^b \quad (2.43)$$

where  $\Psi_c$  is a critical stability parameter defining the incipient motion state.

**Type 1 formula.** Examples are the well-known stone transport formulae of Paintal (1971) developed for uniform flow conditions. In that study, the Shields stability parameter ( $\Psi_s$ ) and the dimensionless bed load transport ( $\Phi_q$ ) were used to quantify the flow forces on the bed and the bed response, respectively. The stone diameters of 2.5, 7.95 and 22.2 mm (sieve diameter) were used. Paintal (1971) found a strong dependence of  $\Phi_q$  on  $\Psi_s$ :

$$\Phi_q = 6.56 \times 10^{18} \Psi_s^{16} \quad \text{for } 0.015 < \Psi_s < 0.055 \quad (2.44)$$

Since the flow over the smallest stones was not completely hydraulically rough, only the data of the other two stone sizes are relevant for the studies of bed protections. A correlation analysis using the data of the large stones ( $d = 7.95$  and  $22.2$  mm) is shown in Figure 2.5. The corresponding stone transport formula is written as:



$$\Phi_q = 3.4 \times 10^7 \Psi_s^{8.87} \quad \text{for } 0.015 < \Psi_s < 0.055 \quad (R^2 = 0.816) \quad (2.45)$$

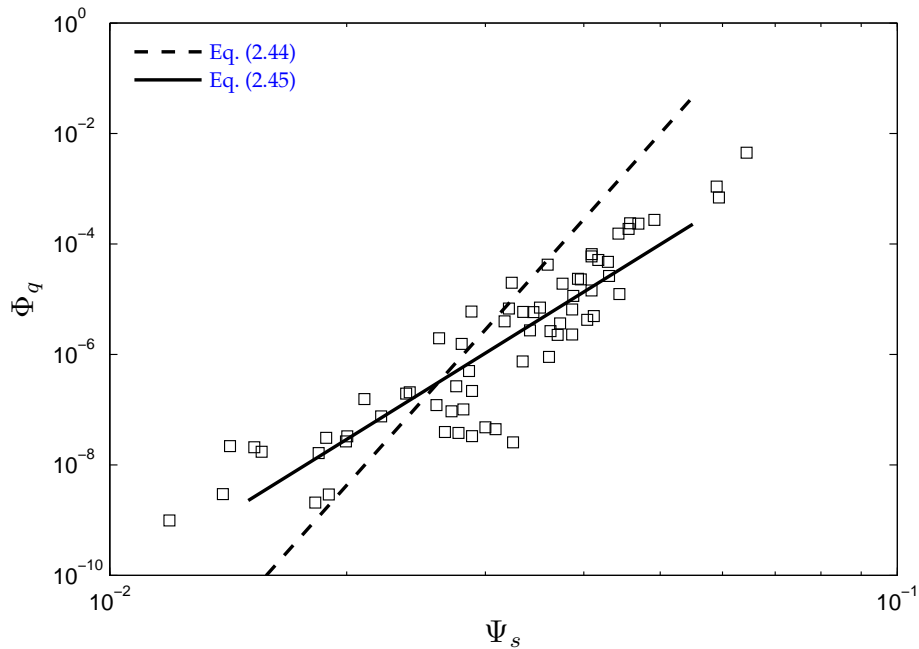


Figure 2.5: Variation of the dimensionless bed load transport with the Shield stability parameter after [Paintal \(1971\)](#) (large particles only).

**Type 2 formula.** Examples of this group are the formulae of [Meyer-Peter and Muller \(1948\)](#) and [Van Rijn \(1984\)](#) for sediment transport. The critical Shields parameter is often used in sediment transport formulae. This type of formulae is suitable for high transport levels where the stability parameter is large. An advantage of this approach is that the transport parameter is not as sensitive to the change of the stability parameter as in type 1 formula. However, for low mobility transport, i.e. the stability parameter is less than or close to the critical stability parameter, this type of formulae is not physically applicable.

Using the data of [Jongeling et al. \(2003\)](#) and [De Gunst \(1999\)](#), [Hofland \(2005\)](#) made the first attempt to develop stone transport formulae for non-uniform flow. He used the dimensionless entrainment rate  $\Phi_E$  as the bed damage indicator and the stability parameters of [Jongeling et al. \(2003,  \$\Psi\_{WL}\$ \)](#) and [Hofland \(2005,  \$\Psi\_{Lm}\$ \)](#) to quantify the flow forces. The correlation between these parameters is given in [Figure 2.6](#).

As the data are highly scattered, a physical relationship between these parameters could not be obtained. Therefore, a tentative curve was drawn more or less as an upper envelope of the data points for the Hofland stability parameter:

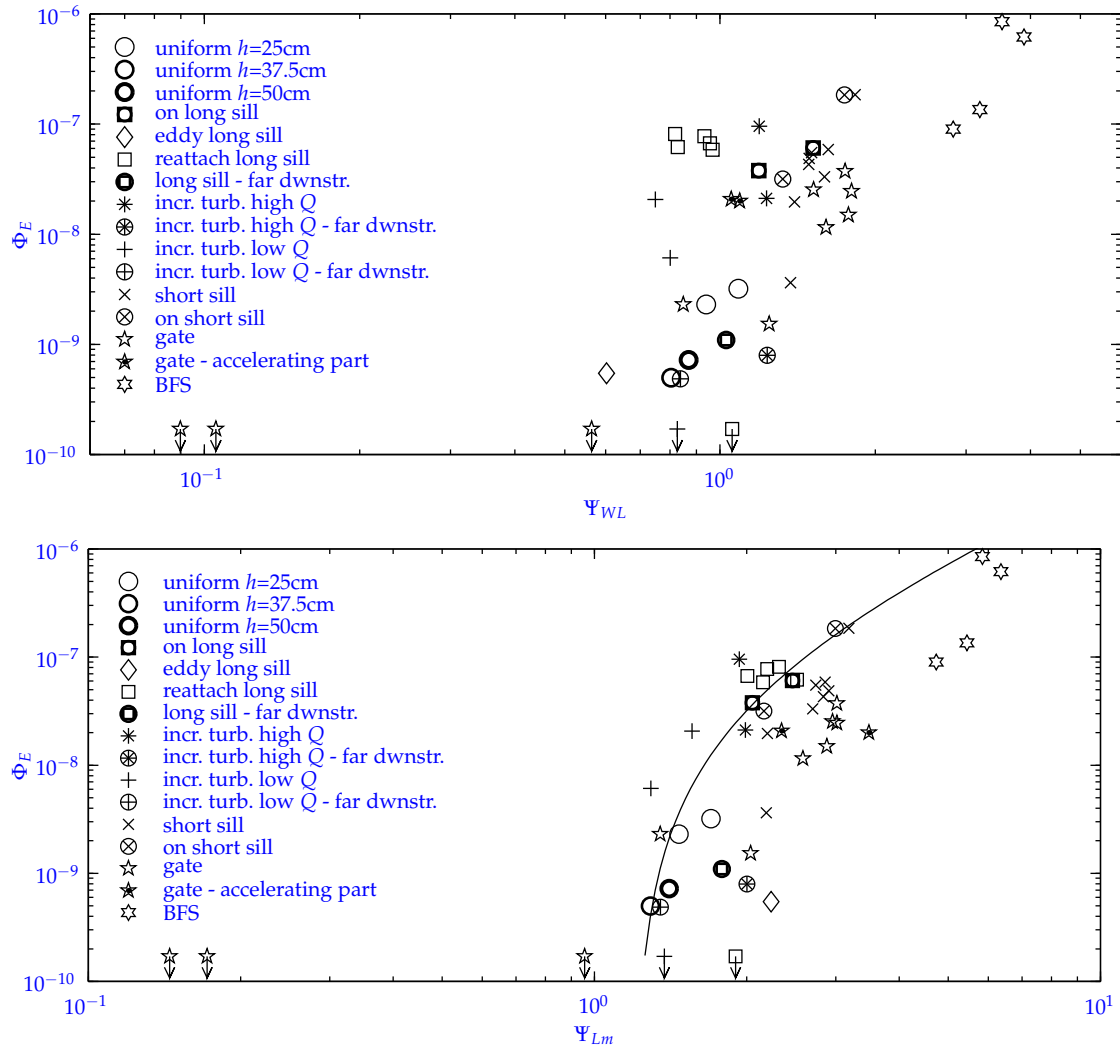


Figure 2.6: Top: measured  $\Phi_E$  versus the measured  $\Psi_{WL}$  for a variety of flow conditions. Bottom: measured  $\Phi_E$  versus the measured  $\Psi_{Lm}$  for the same flow conditions with the tentative curve expressed by Eq. (2.46) (Hofland, 2005).

$$\Phi_E = 5 \times 10^{-8} (\Psi_{Lm} - 1.2)^2 \text{ for } 1.2 < \Psi_{Lm} < 7 \quad (\alpha = 6) \quad (2.46)$$

### 2.6.3 Comparison and selection of methods

A summary of stone stability assessment methods is presented in Figure 2.7. Despite its popular and successful usage in engineering applications, the stability threshold method has several limitations. First, the threshold of movement is a subjective matter and depends on the definition of incipient motion, making it difficult to compare among different investigations. Due to the stochastic nature of bed material movement, it is difficult to define precisely at what flow condition the stones begin to move. The studies of [Paintal \(1971\)](#) and [WL|Delft Hydraulics \(1972\)](#) clearly show that a distinct condition for the beginning of movement does not exist and that significant particle movement occurred below the critical Shields stability parameter. [Paintal \(1971\)](#) concluded that only for practical purposes a limiting bed shear stress can be defined below which the bed load transport is of no practical importance.

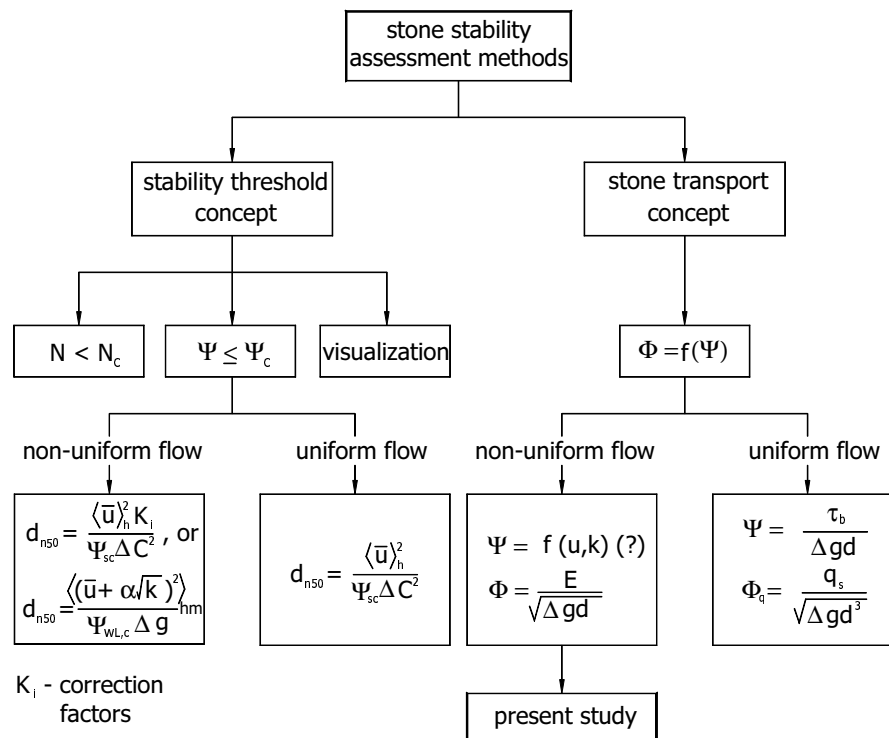


Figure 2.7: A summary of stone stability assessment methods.

Second, the threshold stability method does not give any relation between the flow parameters and the bed damage level. Therefore, it is not possible to

estimate the damage for a given flow condition. The problems that arise from the threshold stability approach are discussed in Section 2.4.3 with the example of Jongeling et al. stability parameter.

Physically, the stone transport approach is more realistic because it expresses a cause-and-effect relationship between the flow parameters and the bed response. Such a relation allows an estimate of the lifetime and a planning of maintenance for a certain stone protection design as well as for an existing stone protection layer (Mosselman et al., 2000). The appropriateness of the approach is confirmed by the success of sediment transport formulae. This approach has also been proven appropriate for lower transport conditions and larger particle sizes such as stones (e.g. Paintal, 1971 and Hofland, 2005). If established, the stone transport formulae can be used to predict the bed damage level for a given flow condition. Therefore, this approach is selected for the present study with special attention being paid to the turbulence effect. Since bed protections mean low-mobility transport, Eq. (2.42) is employed.

## 2.7 Concluding remarks

In the foregoing sections, most important aspects of stone stability under flowing water were presented and discussed. The following concluding remarks are drawn as implications for the development of new stone transport formulae addressed in the next four chapters.

First of all, it is important that the flow forces acting on a bed are adequately quantified. A stability parameter - expressed as a dimensionless relationship between hydraulic load and bed strength - is often used to quantify the influence of these forces on the bed. As the turbulence fluctuations in the flow are of importance for the stability of stones, their effect has to be taken into account, especially for non-uniform flow. Three available stability parameters that can be used are those of Shields (1936) [Eq. (2.26)], Jongeling et al. (2003) [Eq. (2.27)] and Hofland (2005) [Eq. (2.28)].

The Shields stability parameter was developed for uniform flow conditions and utilizes only the bed shear stress to quantify the flow forces. Turbulence fluctuations are not explicitly represented, but their effect is incorporated implicitly through empirical constants such as  $\Psi_{s,c}$ . This is a valid approach for uniform flows, for which the ratio of turbulence intensity to the shear velocity (and hence the bed shear stress) is virtually constant. In non-uniform flow, correction factors are conventionally applied to account for the turbulence fluctuations and the non-horizontal bottoms. This approach, however, does not physically explain the influence of turbulence source in the upper high water column and can only be used as a rule-of-thumb since the various correction factors are given rather arbitrary.

Stones often get moved when an increased  $u$ -velocity fluid package reaches

the bed. The probability that a high momentum fluid package reaches the bottom is related to flow parameters such as velocity and turbulence from higher in the water column. Therefore, flow parameters at different depths should be used to represent the flow forces exerted on the bed. This was done in the stability parameters of [Jongeling et al. \(2003\)](#) and [Hofland \(2005\)](#). These parameters were developed to explicitly account for the effect of turbulence in non-uniform flow. However, the appropriateness of these parameters have not been verified due to the high scatter level of the data that were used.

A clearly defined and quantified measure of damage is essential for assessing the stability of a granular bed. For non-uniform flow, this quantity should be dependent on the local hydrodynamic conditions. Since bed load transport is dependant on the upstream hydraulics, it is only suitable for uniform flow where the flow is unchanged along the channel. For non-uniform flow the dimensionless entrainment rate  $\Phi_E$  should be used.

The assessment of stone stability is based on two concepts: i) the stability threshold concept and ii) the stone transport concept. Since the stability threshold concept utilizes a subjective definition of incipient motion, it often yields inconsistent design criteria. In contrast, the stone transport approach often leads to a result with a cause-and-effect relationship between the flow parameters and the bed response. Such a relationship provides consistent design criteria and allows an estimate of the cumulative damage over time which is important for making decisions regarding maintenance frequency and lifetime analysis of hydraulic structures. Therefore, the stone transport approach is recommended for investigating the stability of stones in bed protections. In the present study, Eq. (2.42) will be used as the basis for the analysis of the experimental data and the evaluation of the various stability parameters.

Although there has been much research on stone stability, the stone transport approach has rarely been applied. Two studies that used this approach are [Paintal \(1971\)](#), for uniform flow) and [Hofland \(2005\)](#), for non-uniform flow). The stone transport formulae developed by Paintal cannot be used for non-uniform flow because the flow forces are quantified by the Shields stability parameter (i.e., no turbulence effect) and the bed damage is quantified by the dimensionless bed load transport (i.e., non-local parameter).

No physical relationship between flow forces and bed damage is available for non-uniform flow. Eq. (2.46) is only a tentative curve describing the upper envelope of the highly scattered data of [Jongeling et al. \(2003\)](#) and [De Gunst \(1999\)](#). From an engineering point of view, Eq. (2.46) can be used for the design of bed protections if verified. However, physically, this equation does not reflect the actual relationship between the flow forces and the bed damage.



# Chapter 3

## Experimental arrangement and data processing methods

### 3.1 Introduction

In Chapter 2 we concluded that turbulence has an important influence on stone stability and that in non-uniform flow it should be modeled explicitly. The dimensionless entrainment rate could be used to describe the bed response because of its complete dependence on local hydrodynamic conditions and independencies on time and bed material. In all studies where entrainment rate data are available, the correlation between the flow forces and the bed response still shows a high scatter level (e.g. Jongeling et al., 2003 and De Gunst, 1999). Therefore, more experiments are needed to increase the understanding of this cause-and-effect relationship and to verify the available stability parameters for non-uniform flow. To this end, experiments were carried out in which both the bed response (quantified by the dimensionless entrainment rate) and the flow field (velocity and turbulence intensity distributions) were measured. The flow in gradually expanding open-channels and its influence on stone stability were focused on because under these conditions the turbulence intensity is high. Three experimental configurations<sup>1</sup> with three different expansion dimensions were used to create different combinations of velocity and turbulence.

In this chapter the experimental arrangement and data processing methods that are employed are described. In Section 3.2 the experimental configurations are described in addition to the instrumentation. Next, in Section 3.3 the choice of stone size and weight that were used is discussed. The test program is given in Section 3.4. It is followed by a discussion on the selected time series (Section 3.5). Finally, in Section 3.6 the data processing methods are briefly presented.

---

<sup>1</sup>Also called *set-up* in all figures in this thesis.

## 3.2 Experimental configuration

### 3.2.1 Geometry

The experiment was undertaken in a laboratory open-channel flume with a length of 14.00 m, a height of 0.7 m and an available width of 0.5 m. The water is pumped through the flume from a central system in the laboratory and the water level is controlled at the downstream side using a manually controlled tailgate. To decelerate the flow, an expansion is made near the end of the flume. To this end, the first part of the flume was narrowed at both sides. Then the extension was made by gradually increasing the width from the first segment to the width of the flume. By changing the expansion length (expansion angle), different combinations of velocity and turbulence can be obtained. Three different configurations with expansion angles  $\alpha$  of 3, 5 and 7 degrees were built. The experimental installation is presented in Figure 3.1.

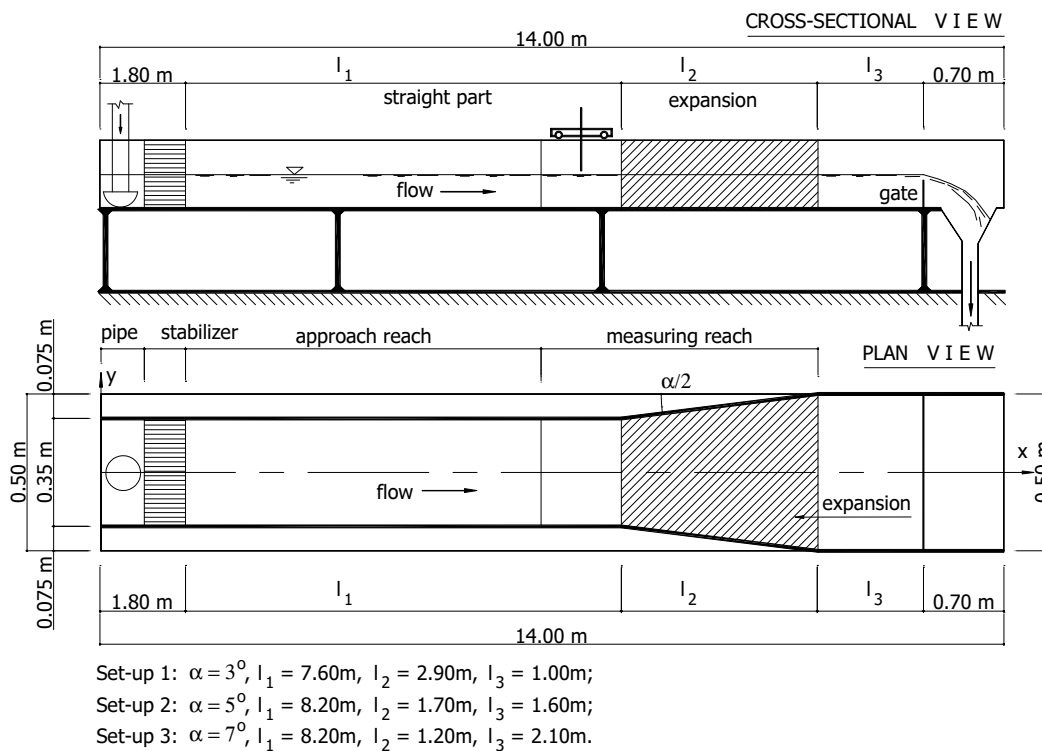


Figure 3.1: Experimental installation (not to scale).

Natural stones having a density of  $2700\text{ kg/m}^3$ , a nominal diameter  $d_{n50}$  of 0.80 cm and  $d_{n85}/d_{n15}$  of 1.27 were used to create a 4-cm-thick rough and permeable bottom. The bottom was flat and the stones were angular, i.e. the edges were sharp, like stone used for bed protections. The flow velocity during the



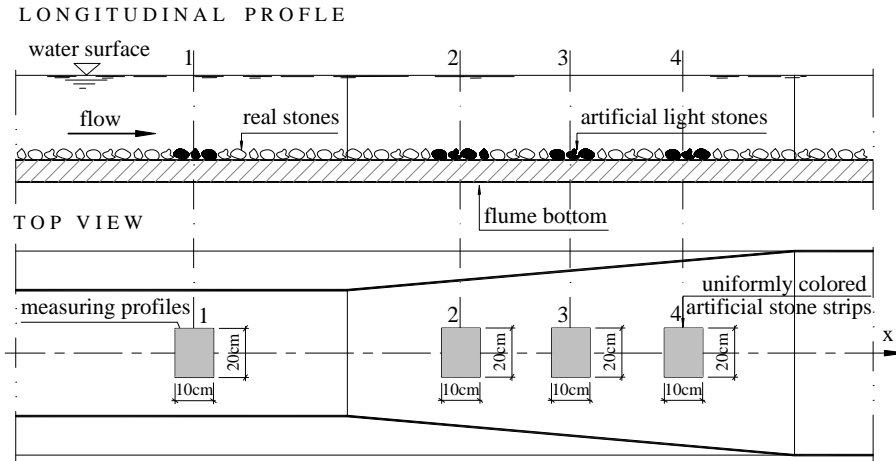


Figure 3.2: The first experimental configuration indicating the placement of uniformly colored artificial stone strips (not to scale).

experiments was too low to displace the natural stones. To examine stone stability, two layers of uniformly colored strips of artificial light stones were placed at designated locations before and along the expansion, see Figures 3.2 and 3.3. Figure 3.2 shows a schematic representation of the first experimental configuration indicating the location of the uniformly colored artificial stone strips. These stones are made of epoxy resin with densities in the range of  $1320$  to  $1971 \text{ kg/m}^3$ , mimicking shapes and sizes of natural stones. The artificial stones have a nominal diameter  $d_{n50}$  of  $0.82 \text{ cm}$  and  $d_{n85}/d_{n15}$  of  $1.11$ . More information on the stones used in the experiments is presented in Section 3.3.

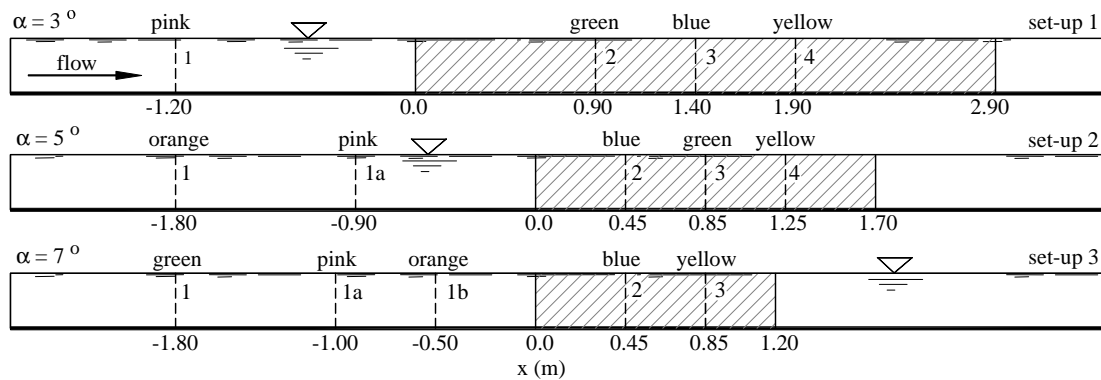


Figure 3.3: Longitudinal sections of the three experimental configurations. Hatched areas depict the expansion regions. Dashed lines are stone entrainment-measurement locations. The stone colors are also indicated.

### 3.2.2 Instrumentation

This section describes the instruments used in the experiment to measure the velocity distribution, the discharge, the water depth and the water level. Special attention is paid to the velocity measurement due to the complexity of the instruments and the importance of this quantity. There are two types of velocity measurement instruments used in the experiment: a Laser Doppler Velocimeter and an Electro Magnetic velocity Sensor. Of the two, the latter was used in some tests to get more information on i) the transverse velocity components ( $v$ ) and ii) the horizontal velocity distribution in the flume.

A two-component, Laser Doppler Velocimetry (LDV) system was used, measuring  $u$  and  $w$  components of the velocity in the streamwise vertical plane. A light source Helium-Neon (HeNe) laser with a power of 15mW was used. The LDV uses the forward-scatter, reference-beam method. In the present study, a 400 mm lens was used, resulting in a measuring volume with dimensions of about 10 mm in spanwise direction and 1 mm in the other directions. Each time series lasted 2 minutes with a sampling frequency of 500 Hz. The rationale for this choice is discussed in Section 3.5.

As the flow structures in the present study are different from standard uniform open-channel flow, it is necessary to check the reliability of the LDV measurements. Therefore, a measurement of a nearly-uniform open-channel flow on a smooth bed was conducted. The flow has a discharge of 12 l/s, a water depth of 5.9 cm and  $B/h = 5.9$ . The results are shown in Figure 3.4, showing that the data agree well with findings of previous studies.

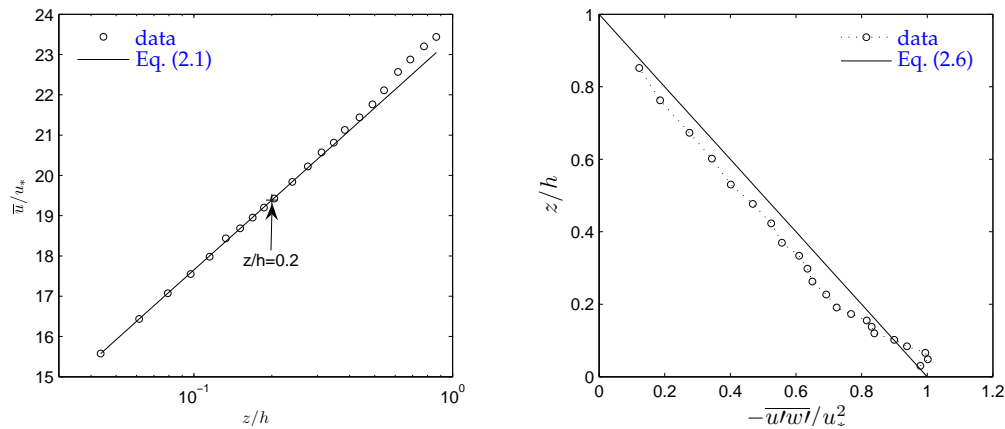


Figure 3.4: Distributions of velocity and Reynolds shear stress.

In addition to the LDV measurement, the Electro Magnetic velocity Sensor (EMS) was used to measure  $u$  and  $v$  components of the velocity. The reasons for the use of EMS are twofold. First, the EMS can measure the horizontal velocity distributions of the  $v$  component in the flume which cannot be done with

the available LDV instrument in the laboratory. This was done to check for the symmetry of the flume set-ups and the flow field. Second, since the LDV only measures  $u$  and  $w$  components of the velocity, information on the  $v$  component can be obtained via the EMS measurement. This information is important for the determination of the turbulent kinetic energy. However, the disadvantage of EMS measurement is that i) it disturbs the flow being measured, ii) the sampling volume is rather large ( $> 3 \text{ cm}^3$ ) iii) it could not measure the velocity near the flume bottom and iv) it is susceptible for electronic noise and zero-offset drift. Therefore, the EMS measurement is only used as a supplement to the LDV measurement in the present study.

In the EMS measurements, each time series lasted 1 minute with a sampling frequency of 200 Hz. Figure 3.5 shows the horizontal velocity distributions at the middle cross section of the expansion measured by the EMS. The velocity was measured at  $z = 0.2h$  and  $z = 0.6h$ . The measurement was undertaken for two flume set-ups (2 & 3) with flow condition B (smallest Reynolds number and water depth) and L (largest Reynolds number and water depth). Information on the flow conditions and the names of the experiments are presented in Section 3.4.

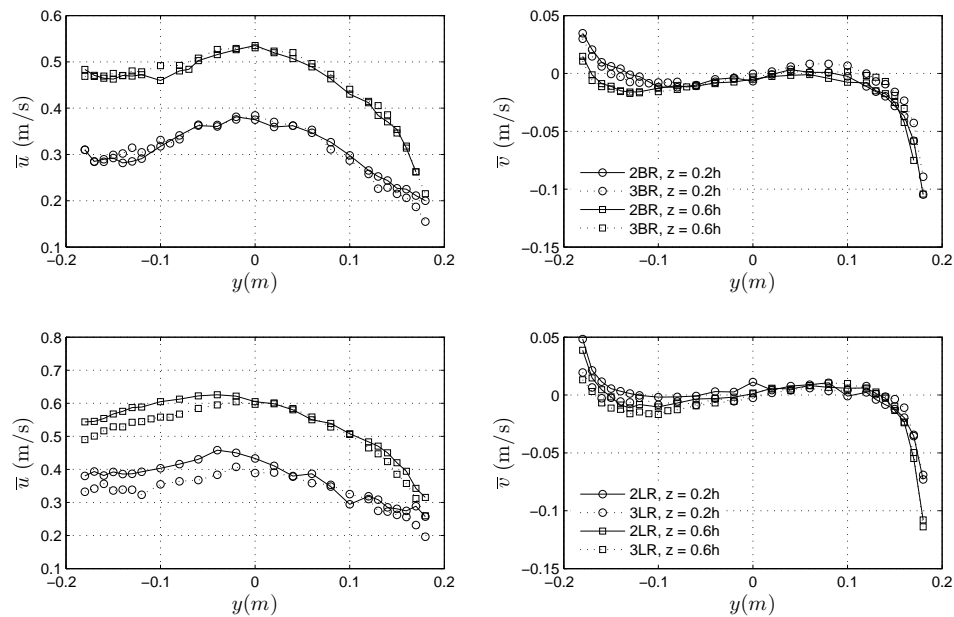


Figure 3.5: Horizontal distributions of mean velocity ( $u$  and  $v$ ) at the middle cross section of the expansion. The measurement was undertaken for flow condition B (top panel) and L (bottom panel).

In the experiment, the discharge could be regulated using an orifice plate in the water supply pipe. By measuring the difference in water pressure before and

after the orifice plate, the discharge was determined. Due to the pressure fluctuations, the water column has an accuracy of about 0.5 cm water column. This means an accuracy of approximately 0.2 l/s. The water levels were measured by a needle. The needle has an accuracy of 0.1 mm. However, due to the presence of small surface waves in the flume the measurement accuracy is about 2 mm.

### 3.3 Stones

The purpose of the experiments was to obtain stone entrainment rate data at the proximity of the incipient motion condition. This is done to investigate the effects of hydraulic parameters such as velocity and turbulence distributions on stone stability in bed protections under flowing water. Therefore, the following characteristics of granular bed protections should be attained in the experiments:

- hydraulically rough flow regime ( $Re_* > 300 - 500$ );
- non-cohesive stones;
- narrow grading of sizes;
- angular stones.

In granular bed protections the use of large stone size results in large particle Reynolds numbers ( $Re_* = u_*d/\nu$  is usually larger than 500). The value of  $Re_* = 300 - 500$  is often referred to because the critical Shields number is constant ( $\Psi_{s,c} \approx 0.05$ )<sup>2</sup> when the particle number  $Re_*$  is larger than (300-500). In the experiments this important characteristic can be accomplished by using large stone size and/or large velocity. However, the larger the stone sizes, the higher the uncertainty of stone entrainment rate data. The use of large stone size also makes the ratio of  $d$  and  $h$  in the experiment differ significantly from the prototype. Therefore, in the experiments the smallest stone size that fulfills the flow regime and  $h/d$  ratio conditions was chosen. A range of 10 to 25 was chosen for  $h/d$  ratio as a guideline. A rough estimation based on the knowledge of uniform open-channel flow and the Shields curve has shown that if natural stones were used, to satisfy the aforementioned conditions the velocity must be large. This results in large Froude numbers in the experiments, leading to undulating water surfaces which alter the turbulence and pressures in a way that is difficult to control. In such conditions not only the turbulence but also other phenomena will influence the stone stability, which is outside the scope of the present study.

Thus, the only solution to overcome the problem is to use lighter stones. The results are still valid for natural stones and any other material as long as the

---

<sup>2</sup>The critical Shields number defines the so called incipient motion condition. When the Shields number  $\Psi_s = u_*^2/\Delta gd$  is larger than the critical Shields number  $\Psi_{s,c}$ , the stones will move.

influence of stone density is well incorporated in the governing variables, i.e., stability parameters and dimensionless entrainment rate. A well-known example for this approach is the work of Shields (1936) where materials with the densities from 1060 to 4250 kg/m<sup>3</sup> were used.

In the present study both natural and artificial stones were used. The natural stones were used to construct a granular bed where the stones are too heavy to be moved under simulated flow conditions. These stones are angular, i.e., the edges are sharp, similar to stones used in bed protections. The artificial lighter stones (i.e.,  $\rho_s = 1032 - 1971$  kg/m<sup>3</sup>) were used to study the stability of stones. The shape and size of the artificial stones are copied from those of approximately 100 samples of the natural stones. This ensures that all the stones placed on the bottom have more or less the same characteristics, except the density. The process of creating the artificial stones is described in Appendix A.

An additional advantage of using artificial stones is the possibility to freely choose the density to be used. Therefore, we have more control on the range of the stability parameters. Because the flow condition varies along the flume and to ensure the stability parameters to be within a certain range, different stone densities were used. These stones and the natural stones are described in Table 3.1. The grading of the stones used in the experiments is classified as narrow which is typical for most bed protections ( $d_{85}/d_{15} < 1.5$ ).

Table 3.1: The main characteristics of stones used in the experiments.

Type	Color	$\rho_s$	$\sigma(\rho_s)$	$d_{n50}$	$d_{n85}/d_{n15}$	Location
[-]	[-]	[ $\frac{\text{kg}}{\text{m}^3}$ ]	[ $\frac{\text{kg}}{\text{m}^3}$ ]	[mm]	[-]	[-]
1	blue, green, yellow	1341	26.0	8.2	1.1	along the expansion
2	pink	1384	10.9	8.2	1.1	in the straight part
3	orange [light]	1320	15.0	8.2	1.1	in the straight part
4	orange [heavy]	1971	11.0	8.2	1.1	all profiles in 3MR
5	grey (natural stones)	2707	59.8	8.0	1.3	whole flume

## 3.4 Test program

### 3.4.1 Hydraulic conditions

The hydraulic condition is the main criterion for the entire experiment and involves the choice of the dimensions of the flume set-ups (i.e., expansion dimensions), the stone size and weight. The hydraulic conditions have been chosen based on the following analysis.

First, several possible flow conditions in the straight part of the flume were considered. For the sake of simplicity, the flow in this part is considered uniform.

Therefore, it can be formulated based on uniform open-channel flow. A possible set of flow conditions is presented in Table 3.2 where the mean bulk velocity upstream of the expansion ( $U$ ) was determined as:

$$U = \frac{Q}{Bh} \quad (3.1)$$

where  $Q$  is the discharge,  $B$  and  $h$  are the flume width and water depth, respectively. The Reynolds number was calculated as

$$Re = \frac{Uh}{\nu} = \frac{Q}{B\nu} \quad (3.2)$$

where  $\nu = 1.01 \times 10^{-6} m^2/s$  is the kinematic viscosity. The Froude number was obtained as:

$$Fr = \frac{U}{\sqrt{gh}} \quad (3.3)$$

Table 3.2: A possible set of hydraulic conditions.

Series	$Q$	$h$	$B$	$U$	$Re$	$Fr$	$d_{n50}$	$\rho_s$	$\rho$	$C$	$u_*$	$Re_*$	$\Psi_s$	$\frac{h}{d_{n50}}$
[-]	$[\frac{l}{s}]$	[m]	[m]	$[\frac{m}{s}]$	$[10^4]$	[-]	[cm]	$[\frac{kg}{m^3}]$	$[\frac{kg}{m^3}]$	$[\frac{m^{0.5}}{s}]$	$[\frac{m}{s}]$	[-]	[-]	[cm]
A	22.0	0.120	0.35	0.52	62235	0.48	0.82	1384	1000	36.32	0.045	367	0.066	14.6
B	20.0	0.120	0.35	0.48	56577	0.44	0.82	1384	1000	36.32	0.041	333	0.055	14.6
C	23.0	0.130	0.35	0.51	65064	0.45	0.82	1384	1000	36.68	0.043	350	0.060	15.9
D	26.5	0.140	0.35	0.54	74965	0.46	0.82	1384	1000	37.01	0.046	372	0.068	17.1
E	24.0	0.140	0.35	0.49	67893	0.42	0.82	1384	1000	37.01	0.041	337	0.056	17.1
F	27.0	0.150	0.35	0.51	76379	0.42	0.82	1384	1000	37.31	0.043	351	0.060	18.3
G	31.0	0.160	0.35	0.55	87694	0.44	0.82	1384	1000	37.57	0.046	375	0.069	19.5
H	28.0	0.160	0.35	0.50	79208	0.40	0.82	1384	1000	37.57	0.042	338	0.056	19.5
I	31.5	0.170	0.35	0.53	89109	0.41	0.82	1384	1000	37.82	0.044	356	0.062	20.7
J	35.5	0.180	0.35	0.56	100424	0.42	0.82	1384	1000	38.04	0.046	377	0.070	22.0
K	32.0	0.180	0.35	0.51	90523	0.38	0.82	1384	1000	38.04	0.042	340	0.057	22.0
L	36.0	0.190	0.35	0.54	101839	0.40	0.82	1384	1000	38.25	0.044	360	0.064	23.2
M	36.0	0.120	0.35	0.86	101839	0.79	0.82	1971	1000	36.32	0.074	600	0.070	14.6

The Chezy coefficient  $C$  was determined as (e.g., Schiereck, 2001):

$$C = 18 \log \frac{12R}{k_s} \quad (3.4)$$

in which  $R$  is the hydraulic radius,  $R = \omega/\chi = Bh/(B + 2h)$ ;  $k_s$  is the equivalent roughness. In uniform open-channel flow the shear velocity,  $u_*$ , can be expressed as follows (Schiereck, 2001):

$$u_* = \frac{U\sqrt{g}}{C} \quad (3.5)$$

The particle Reynolds number,  $Re_*$ :

$$R_{e*} = \frac{u_* d_{n50}}{\nu} \quad (3.6)$$

And the Shields stability parameter,  $\Psi_s$ :

$$\Psi_s = \frac{u_*^2}{\Delta g d_{n50}} \quad (3.7)$$

Under these flow conditions the Shields stability parameter of the natural stones is rather small ( $\Psi_s \approx 0.01$ ), assuring that these stones are not moved during the experiments.

Second, detailed information on the flow along the expansion must be estimated in order to choose the proper expansion dimensions and stone densities. Therefore, the flows formulated in Table 3.2 were examined for several possible configurations with different expansion dimensions by means of numerical simulations. These RANS<sup>3</sup> computations were executed with the flow simulation package PHOENICS of CHAM Ltd. The simulation results led to the choice of the 3 expansion angles and the densities of artificial stones mentioned in the previous sections. The simulations confirmed the suitability of the flow conditions listed in Table 3.2.

The twelve flow conditions listed in Table 3.2 are denoted as A to L (with the water depth varying from 12 cm to 19 cm). This set of flow conditions was applied to all the three experimental configurations, resulting in a total of 36 flow conditions. The names of the experiments have been defined in this research as follows. The names consist of 3 components: i) the set-up number (1 to 3), ii) the name of the basic flow condition (A to L, Table 3.2) and iii) the type of flume bottom. For instance, series 1AR indicates the experiment in set-up 1 with flow condition A ( $Q = 22.0$  l/s,  $h \approx 12$  cm) and a rough flume bottom (R stands for rough, S stands for smooth). Similarly, profile names consist of series name and profile number, i.e., 1AR2 is the name for profile 2 of series '1AR'. The locations of the test sections are depicted in Figure 3.3. The actual flow conditions that are measured in the experiments are summarized in Table 3.3.

In the experiments, the artificial stones having the density from 1320 to 1384 kg/m<sup>3</sup> were used to obtain the stone entrainment rate data. These stones are colored and listed in Table 3.1. The locations of these stones are indicated in Figures 3.2 & 3.3. Strip sizes of 10 cm in streamwise and 20 cm in transverse directions were chosen for all stone strips.

To check whether the effect of the stone density is properly incorporated, an extra experiment was undertaken where heavier artificial stones was used ( $\rho_s = 1971$  kg/m<sup>3</sup>). As a result, a stronger flow condition was required. This flow condition is referred to as 3MR and is presented in Table 3.3.

---

<sup>3</sup>Reynolds-Averaged Navier-Stokes

Table 3.3: Summary of hydraulic conditions measured from the experiments.

No	Series	Q	h	Profile 1		Profile 2			Profile 3			Profile 4		
				Re	Fr	h	Re	Fr	h	Re	Fr	h	Re	Fr
[-]	[-]	[l/s]	[cm]	[10 <sup>4</sup> ]	[-]	[m]	[10 <sup>4</sup> ]	[-]	[m]	[10 <sup>4</sup> ]	[-]	[m]	[10 <sup>4</sup> ]	[-]
1	1AR	22.0	11.7	6.2	0.498	12.1	5.5	0.423	12.1	5.2	0.394	12.3	4.9	0.362
2	1BR	20.0	12.0	5.7	0.439	12.1	5.0	0.385	12.2	4.7	0.357	12.3	4.4	0.331
3	1CR	23.0	13.0	6.5	0.448	13.0	5.7	0.396	13.2	5.4	0.363	13.3	5.1	0.338
4	1DR	26.5	13.9	7.5	0.466	14.3	6.6	0.395	14.5	6.2	0.363	14.5	5.9	0.343
5	1ER	24.0	13.9	6.8	0.422	13.9	6.0	0.371	14.1	5.6	0.344	14.3	5.3	0.316
6	1FR	27.0	15.0	7.6	0.425	14.8	6.7	0.381	15.2	6.3	0.346	15.3	6.0	0.323
7	1GR	31.0	15.7	8.8	0.456	16.1	7.7	0.385	16.2	7.3	0.361	16.2	6.9	0.338
8	1HR	28.0	15.8	7.9	0.407	15.9	7.0	0.355	16.2	6.6	0.324	16.5	6.2	0.299
9	1IR	31.5	17.0	8.9	0.412	17.1	7.9	0.359	17.4	7.4	0.329	17.8	7.0	0.300
10	1JR	35.5	17.9	10.0	0.428	18.1	8.9	0.372	18.3	8.3	0.343	18.5	7.8	0.318
11	1KR	32.0	18.0	9.1	0.383	18.1	8.0	0.333	18.3	7.5	0.308	18.5	7.1	0.287
12	1LR	35.5	19.0	10.0	0.391	19.1	8.9	0.343	19.1	8.3	0.321	19.3	7.8	0.298
13	2AR	22.0	11.6	6.2	0.507	11.6	5.6	0.459	11.6	5.1	0.419	11.8	4.7	0.379
14	2BR	20.0	12.0	5.7	0.442	11.9	5.1	0.401	11.8	4.7	0.373	11.8	4.3	0.341
15	2CR	23.0	12.8	6.5	0.459	12.6	5.8	0.420	12.7	5.4	0.382	12.9	5.0	0.345
16	2DR	26.5	13.8	7.5	0.471	13.8	6.7	0.424	13.7	6.2	0.391	13.9	5.7	0.355
17	2ER	24.0	13.2	6.8	0.458	13.2	6.1	0.409	13.3	5.6	0.373	13.3	5.2	0.343
18	2FR	27.0	14.4	7.6	0.448	14.1	6.9	0.418	14.2	6.3	0.379	14.3	5.8	0.345
19	2GR	31.0	16.0	8.8	0.443	15.9	7.9	0.402	15.9	7.2	0.368	16.1	6.7	0.335
20	2HR	28.0	15.9	7.9	0.404	15.8	7.1	0.367	15.9	6.5	0.332	15.9	6.0	0.308
21	2IR	31.5	16.9	8.9	0.413	16.7	8.0	0.379	16.6	7.3	0.350	16.8	6.8	0.318
22	2JR	35.5	17.5	10.0	0.442	18.0	9.0	0.382	17.9	8.3	0.351	18.1	7.6	0.320
23	2KR	32.0	17.8	9.1	0.390	17.9	8.1	0.347	17.8	7.5	0.320	17.9	6.9	0.293
24	2LR	35.5	18.6	10.0	0.405	18.2	9.0	0.375	18.5	8.3	0.335	18.6	7.6	0.306
25	3AR	22.0	12.1	6.2	0.474	12.6	5.4	0.393	12.8	4.8	0.343	-	-	-
26	3BR	20.0	12.0	5.7	0.438	12.7	5.0	0.351	13.0	4.4	0.303	-	-	-
27	3CR	23.0	12.9	6.5	0.454	13.3	5.7	0.379	13.4	5.1	0.333	-	-	-
28	3DR	26.5	13.8	7.5	0.474	14.4	6.6	0.387	14.7	5.8	0.332	-	-	-
29	3ER	24.0	14.1	6.8	0.411	14.7	5.9	0.340	15.0	5.3	0.292	-	-	-
30	3FR	27.0	14.9	7.6	0.428	15.5	6.7	0.355	15.6	5.9	0.310	-	-	-
31	3GR	31.0	15.7	8.8	0.456	16.4	7.7	0.373	16.8	6.8	0.319	-	-	-
32	3HR	28.0	15.8	7.9	0.406	16.4	6.9	0.336	16.6	6.2	0.294	-	-	-
33	3IR	31.5	16.9	8.9	0.412	17.8	7.8	0.335	17.5	6.9	0.305	-	-	-
34	3JR	35.5	17.5	10.0	0.442	18.0	8.8	0.370	18.5	7.8	0.316	-	-	-
35	3KR	32.0	17.7	9.1	0.391	18.0	7.9	0.335	18.2	7.0	0.292	-	-	-
36	3LR	35.5	18.3	10.0	0.414	19.2	8.8	0.336	19.5	7.8	0.293	-	-	-
37	3MR	36.0	12.4	10.2	0.752	11.8	8.9	0.710	12.7	7.9	0.562	-	-	-

### 3.4.2 Measurements

The data collected in each experiment are the discharge, the water level, the water depth, the velocity distributions and the stone entrainment rate. Table 3.4 provides an overview of the equipment used during the experiments.

Since the measurements of the hydraulic conditions and the stone entrainment require different procedures, they were undertaken separately. Each series consists of five repetitive tests with the same flow conditions. The first test is dedicated to the measurements of the flow conditions while the next four tests are used to measure the stone entrainment data. The experimental procedure of one series was as follows.

In the first test of the series, the whole flume bottom was covered by only the



Table 3.4: Summary of measurements and equipments used in the experiment.

Measurement	Measuring equipment	Number of		
		instruments	locations	times
Water level	Needle	1	3 to 4	variable
Bed level	Needle	1	3 to 4	variable
Velocity	LDV	1	3 to 4	1 @ 6 hours
Stone entrainment	Video, counting	1	4 to 5	4 @ 2.5 hour

natural stones, ensuring that no stones were displaced during the measurements. In this first run, the desired discharge was generated and the desired water depth was obtained by adjusting the weir at the downstream end of the flume. After the flow became stationary, the water level and the velocity could be measured. The LDV could measure the velocity as close as 3 mm from the bottom. The spacing between the measuring points  $\Delta z$  of 1 mm is applied for the first 5 measurements near the bottom and increases to 3 mm in the upper part of the inner region ( $z/h < 0.2$ ). In the outer region, the spacing between the measuring points increases towards the free surface with the maximum value of 15 mm. In total there are about 19 to 25 measuring points for each profile depending on the water depth. The number of measuring points in the inner region ( $z/h < 0.2$ ) varies from 10 to 13.

After the hydraulic conditions were measured, the same flow condition was reproduced to measure the stone entrainment data. Uniformly colored strips of light artificial stones were placed at the designated locations. In order to obtain statistically reliable entrainment rate data, the entrainment test was repeated four times. The following procedure was applied to the entrainment test. A 30-minute initial settling period was applied prior to the actual test to remove loose stones that do not determine the strength of the bed. To start the actual entrainment test the flume was flooded slowly to the designated condition. After two hours, the flow was stopped and the number of displaced stones was registered. The entrainment rates obtained from the four tests are averaged to obtain the entrainment rate for the series. The measured data are summarized in Appendix B.

### 3.5 Selected time series

In this section, the choice of the signal length for one velocity measurement is discussed. The data obtained from the velocity measurement were the mean velocity, the turbulence intensity and the Reynolds shear stress. The evaluation of various possible signal lengths was made for these quantities based on preliminary tests where the velocity was measured for a rather long duration.

The length of a time series must satisfy the following two requirements: i) It

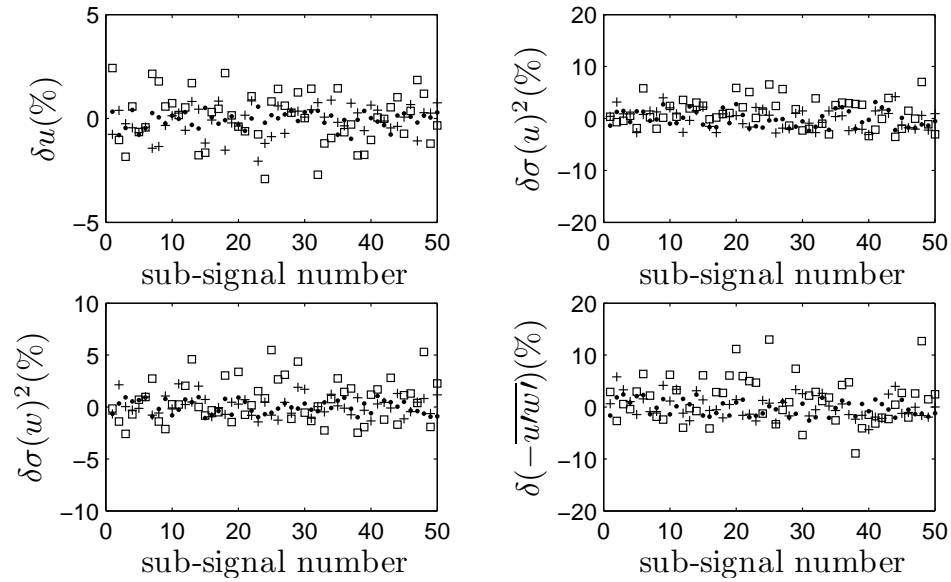
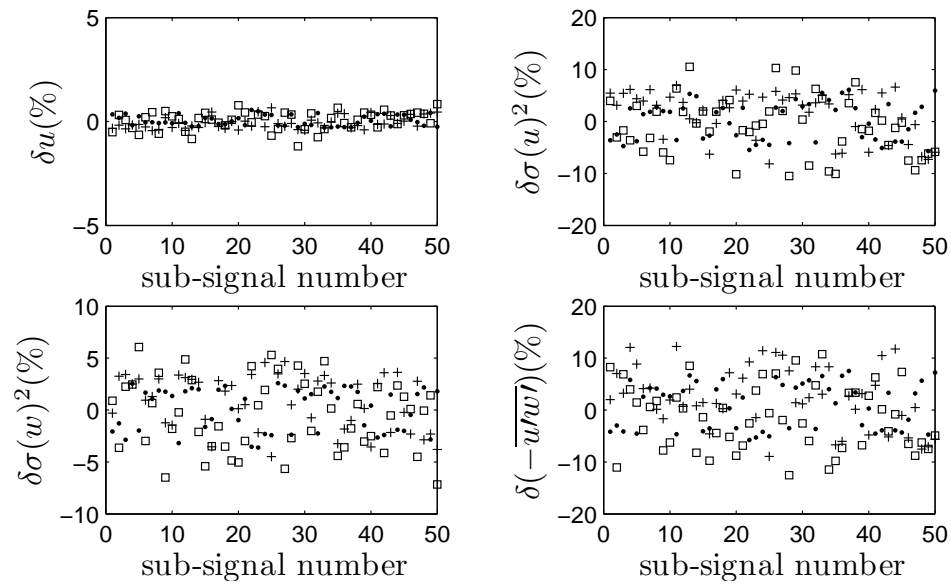
a) The signal was measured at  $z \approx 0.1h$ .b) The signal was measured at  $z \approx 0.5h$ .

Figure 3.6: The relative errors ( $\delta$ ) of 2-minute (square), 5-minute (plus) and 10-minute (dot) sub-signals to the 30-minute signal. The measurements were carried out at profile 1 under flow condition 1FR.

should be sufficiently long so that the sample is representative of the quantities; ii) On the other hand, it should not be too large since the number of measurements is rather large. The following process was used to determine the measuring duration for the LDV measurement.

In order to choose an appropriate length for a time series, the velocity was measured for a 30-minute duration. The measurements were carried out at various positions for several flow conditions. The mean velocity, turbulence intensity and the Reynolds shear stress were then determined for this entire 30-minute long series. These values were used as standards to evaluate the appropriateness of possible shorter measuring lengths. Next, 50 sub-series were randomly selected from the original 30-minute series, where all possible samples are equally likely to be selected. The mean velocity, the turbulence intensity and the Reynolds shear stress were then calculated for the 50 sub-series. These quantities were compared with the standard values using:

$$\delta x = \frac{x_s - x_0}{x_0} \times 100\% \quad (3.8)$$

where  $\delta x$  is the relative error of quantity  $x$  ( $x$  can be  $u$ ,  $\sigma(u)^2$ ,  $\overline{u'w'}$ , etc.),  $x_s$  is the value obtained from the sub-series,  $x_0$  is the true value of quantity  $x$ . In this case, the value obtained from the 30-minute measurement is regarded as  $x_0$ .

Figure 3.6 shows the relative errors of different quantities for two measurements under flow condition 1FR as examples of the analysis. The measurements were carried out at  $z = 0.1h$  (low velocity, high turbulence) and  $z = 0.5h$  (high velocity, low turbulence). The sub-series of 2, 5 and 10 minutes were chosen to analyze. Since the relative errors are small for 2-minute sub-series, the length of 2 minutes was chosen for a time series.

A similar analysis was done for the EMS measurements, leading to the choice of 1 minute as an appropriate duration for its time series.

## 3.6 Data processing methods

### 3.6.1 Velocity and turbulence data

The velocity data collected from the measurements can be used to directly compute the following properties of the turbulent flow: the mean velocity, the turbulence intensity and the turbulent kinetic energy. These are the basic quantities of the flow and could be used for further analysis for various properties such as the shear velocity, the mixing length, the stability parameters, etc. Following are the methods to derive these basic quantities from the measured data.

As previously mentioned, a time series with 60000 samples<sup>4</sup> was obtained for a given point velocity. From this data record of measured velocity samples  $u(i)$ ,

---

<sup>4</sup>2 minute duration with the sampling frequency of 500 Hz

an estimate of the mean velocity  $\bar{u}$  is computed as<sup>5</sup>:

$$\bar{u} = \frac{1}{N} \sum_{i=1}^N u(i) \quad (3.9)$$

where  $N$  is the number of samples ( $N = 60000$ ). As the number of samples is high, the averaged value is expected to converge to the true mean value (with the relative error  $\delta\bar{u} < 3\%$ , see Figure 3.6). The velocity fluctuation  $u'(i)$  is obtained as:

$$u'(i) = u(i) - \bar{u} \quad (3.10)$$

The turbulence intensity of  $u$  is defined as  $\sqrt{\overline{u'^2}}$  and is therefore identical to the standard deviation of  $u$ :

$$\sigma(u) = \sqrt{\frac{1}{N} \sum_{i=1}^N [u(i) - \bar{u}]^2} = \sqrt{\overline{u'^2}} \quad (3.11)$$

The turbulent kinetic energy is defined as

$$k = \frac{1}{2} \left( \overline{u'^2} + \overline{v'^2} + \overline{w'^2} \right) \quad (3.12)$$

Since only two velocity components ( $u$ – streamwise and  $w$ – upward) are available, the turbulent kinetic energy in Eq. (3.12) was approximated by assuming that  $\sigma(v) \approx \sigma(u)/1.9$ . The approximation is based on the EMS measurement of the flow conditions where both  $u$ – and  $v$ – velocity components were measured.

### 3.6.2 Stone entrainment rate data

The data collected from the experiment was the number of stones that was removed from their colored strip during the test. For each flow condition (i.e., each series) the entrainment test was repeated 4 times, resulting in four values of the number of the entrained stones ( $n_1, n_2, n_3$  and  $n_4$ ) for each uniformly colored stone strip. The representative value of the displaced stone number of that strip was determined as

$$n = \frac{n_1 + n_2 + n_3 + n_4}{4} \quad (3.13)$$

The entrainment rate  $E$  - which is the pick-up rate in volume per unit area and time - is determined as

$$E = \frac{V}{AT} = \frac{nd_{n50}^3}{AT} \quad (3.14)$$

---

<sup>5</sup>The overbar is often left out in normal text and figures.

where  $V = nd_{n50}^3$  is the total volume of the displaced stones,  $n$  is the number of displaced stones,  $d_{n50}$  is the nominal diameter of the stones ( $d_{n50} = 8.2$  mm),  $A$  is the strip area (movable surface,  $A = 0.2 \times 0.1$  m<sup>2</sup>),  $T$  is the measuring period ( $T = 2$  hours). In the present study the damage of a bed is quantified by the dimensionless entrainment rate  $\Phi_E$  and is determined as:

$$\Phi_E = \frac{E}{\sqrt{\Delta g d_{n50}}} \quad (3.15)$$

where  $\Delta = (\rho_s - \rho)/\rho$  is the specific submerged density of stone,  $\rho$  is the water density,  $\rho_s$  is the stone density and  $g$  is the gravitational acceleration. The dimensionless entrainment rate data are presented in Appendix B.

### 3.6.3 Correlation analysis

In Chapter 5 new stone transport formulae are developed for various stability parameters based on the present data. The general form of the formulae is expressed as Eq. (2.42). The suitability of a stability parameter is judged based on how well it correlates with the dimensionless entrainment rate. This is measured by the coefficient of determination from the correlation analysis, expressed as:

$$R^2 = 1 - \frac{SSE}{TSS} \quad (3.16)$$

in which  $SSE$  is the error sum of squares and  $TSS$  is the total sum of squares. The error sum of squares is expressed as

$$SSE = \sum_i (y_i - \hat{y}_i)^2 \quad (3.17)$$

in which  $y_i$  and  $\hat{y}_i$  are the measured value and the predicted value from the regression. The total sum of squares is expressed as

$$TSS = \sum_i (y_i - \bar{y})^2 \quad (3.18)$$

where  $\bar{y}$  is the mean value of the data.

The measured stability parameters and the measured dimensionless entrainment rate are presented in Appendix B. The nominal stone diameter  $d_{n50}$  of 0.82 cm was used.



# Chapter 4

## Flow characteristics

### 4.1 Introduction

The characteristics of turbulent boundary layers have been extensively studied in fluid mechanics, especially for uniform open-channel flow. Most conventional turbulence and sediment transport models are developed for uniform flow. However, a vast majority of the flows in natural channels and in engineering applications is non-uniform. Therefore, the use of these models at specific sites may not correctly predict such flows and the associated bed load transport. Understanding the flow structures in non-uniform flow increases the understanding of their influence on sediment transport and on the (in)stability of bottom protections.

As the first step of the investigation on stone stability under non-uniform flow, in this chapter the flow structures measured from the experiments are analyzed and compared to the characteristics of uniform open-channel flow. The analysis focuses on the flow structures at the center of the flume since these flows are the main cause to displace the stones from their uniformly colored strips. The relationship between these flows and their induced-damage to the bottom is examined in the next chapter.

The outline of this chapter is as follows. In Section 4.2 the measured and calculated flow quantities are presented. The methods that are used to determine the shear velocity are described in Section 4.3. Next, in Section 4.4 the mean velocity is analyzed and compared with the law-of-the-wall and the log-wake law. The eddy viscosity and the mixing length are evaluated in Section 4.5. This is followed by the analysis of the turbulence intensity data (Section 4.6) and the Reynolds shear stress data (Section 4.7). Finally, the chapter ends with concluding remarks in Section 4.8. Part of this chapter was published as [Hoan et al. \(2007c\)](#).

## 4.2 Flow quantities

The main flow quantities (measured and calculated) are summarized in Tables 4.1, 4.2 and 4.3. Twelve experiments with different flow conditions were conducted for each flume set-up. The locations of the test sections are depicted in Figures 3.1 and 3.3, namely profile 1 to profile 4. Though profile 1 is located in the straight part of the flume, the flow there is still far from standard uniform open-channel flow as the ratio of channel width and water depth is small, i.e., varying from 1.8 to 2.9. The flow along the expansion is in non-equilibrium as Clauser's parameter ( $\beta$ ) is expected to change along the flow direction (Cardoso, 1990):

$$\beta = \frac{\delta_*}{\rho u_*^2} \frac{dp}{dx} \quad (4.1)$$

where  $\rho$  is the water density,  $dp/dx$  is the pressure gradient and  $\delta_*$  is the displacement thickness given by:

Table 4.1: Summary of measured and calculated flow parameters (set-up 1).

Series	1AR	1BR	1CR	1DR	1ER	1FR	1GR	1HR	1IR	1JR	1KR	1LR
Q [l/s]	22.0	20.0	23.0	26.5	24.0	27.0	31.0	28.0	31.5	35.5	32.0	35.5
Profile 1												
$h$ [m]	0.117	0.120	0.130	0.139	0.139	0.150	0.157	0.158	0.170	0.179	0.180	0.190
$Re$ [ $10^4$ ]	6.223	5.658	6.506	7.496	6.789	7.638	8.769	7.921	8.911	10.042	9.052	10.042
$Fr$ [-]	0.498	0.439	0.448	0.466	0.422	0.425	0.456	0.407	0.412	0.428	0.383	0.391
$\Pi$ [-]	0.425	0.100	0.150	0.325	0.350	0.275	0.550	0.525	0.550	0.550	0.425	0.525
$u_{*1}$ [m/s]	0.056	0.046	0.051	0.053	0.048	0.049	0.053	0.048	0.049	0.054	0.049	0.052
$u_{*2}$ [m/s]	0.046	0.051	0.054	0.050	0.048	0.049	0.047	0.044	0.047	0.051	0.048	0.050
$\delta$ [%]	18.4	-10.9	-4.9	5.2	0.2	0.6	11.0	8.9	2.9	4.5	0.9	4.4
Profile 2												
$h$ [m]	0.121	0.121	0.130	0.143	0.139	0.148	0.161	0.159	0.171	0.181	0.181	0.191
$Re$ [ $10^4$ ]	5.487	4.988	5.736	6.609	5.985	6.734	7.731	6.983	7.856	8.854	7.981	8.854
$Fr$ [-]	0.423	0.385	0.396	0.395	0.371	0.381	0.385	0.355	0.359	0.372	0.333	0.343
$\Pi$ [-]	0.075	0.250	0.100	0.200	0.275	0.300	0.300	0.400	0.450	0.450	0.600	0.375
$u_{*1}$ [m/s]	0.052	0.043	0.051	0.052	0.047	0.047	0.056	0.048	0.051	0.055	0.050	0.051
$u_{*2}$ [m/s]	0.061	0.043	0.050	0.051	0.047	0.045	0.053	0.039	0.045	0.049	0.042	0.048
$\delta$ [%]	-16.5	-0.2	1.8	1.9	-0.1	5.8	4.8	17.4	11.7	9.9	16.9	6.5
Profile 3												
$h$ [m]	0.121	0.122	0.132	0.145	0.141	0.152	0.162	0.162	0.174	0.183	0.183	0.191
$Re$ [ $10^4$ ]	5.162	4.692	5.396	6.217	5.631	6.335	7.273	6.569	7.391	8.329	7.508	8.329
$Fr$ [-]	0.394	0.357	0.363	0.363	0.344	0.346	0.361	0.324	0.329	0.343	0.308	0.321
$\Pi$ [-]	0.250	0.350	0.325	0.175	0.300	0.250	0.550	0.275	0.425	0.225	0.325	0.350
$u_{*1}$ [m/s]	0.050	0.041	0.046	0.050	0.046	0.049	0.053	0.047	0.051	0.055	0.052	0.051
$u_{*2}$ [m/s]	0.044	0.039	0.044	0.045	0.044	0.043	0.038	0.040	0.043	0.051	0.045	0.046
$\delta$ [%]	10.8	4.9	5.5	9.6	4.8	13.5	29.2	15.1	15.1	7.7	13.7	10.2
Profile 4												
$h$ [m]	0.123	0.123	0.133	0.145	0.143	0.153	0.162	0.165	0.178	0.185	0.185	0.193
$Re$ [ $10^4$ ]	4.862	4.420	5.083	5.857	5.304	5.967	6.851	6.188	6.962	7.846	7.072	7.846
$Fr$ [-]	0.362	0.331	0.338	0.343	0.316	0.323	0.338	0.299	0.300	0.318	0.287	0.298
$\Pi$ [-]	0.300	0.300	0.250	0.225	0.200	0.100	0.175	0.200	0.325	0.275	0.575	0.575
$u_{*1}$ [m/s]	0.050	0.039	0.046	0.050	0.044	0.045	0.050	0.045	0.045	0.049	0.048	0.047
$u_{*2}$ [m/s]	0.045	0.040	0.044	0.047	0.044	0.048	0.046	0.043	0.042	0.045	0.035	0.038
$\delta$ [%]	9.2	-2.9	4.2	5.6	-2.1	-4.7	7.0	3.1	5.2	8.8	27.7	19.0



$$\delta_* = \int_0^h \left(1 - \frac{u}{u_{\max}}\right) dz \quad (4.2)$$

where  $u_{\max}$  is the maximum velocity and  $h$  the water depth. Due to the accuracy of water level measurement, the available data are not sufficient to verify the equilibrium conditions.

Table 4.2: Summary of measured and calculated flow parameters (set-up 2).

Series	1AR	1BR	1CR	1DR	1ER	1FR	1GR	1HR	1IR	1JR	1KR	1LR
Q [l/s]	22.0	20.0	23.0	26.5	24.0	27.0	31.0	28.0	31.5	35.5	32.0	35.5
Profile 1												
$h$ [m]	0.116	0.120	0.128	0.138	0.132	0.144	0.160	0.159	0.169	0.175	0.178	0.186
$Re$ [ $10^4$ ]	6.223	5.658	6.506	7.496	6.789	7.638	8.769	7.921	8.911	10.042	9.052	10.042
$Fr$ [-]	0.507	0.442	0.459	0.471	0.458	0.448	0.443	0.404	0.413	0.442	0.390	0.405
$\Pi$ [-]	0.150	0.150	0.200	0.450	0.175	0.300	0.400	0.375	0.400	0.425	0.500	0.400
$u_{*1}$ [m/s]	0.046	0.043	0.048	0.051	0.046	0.048	0.051	0.049	0.050	0.051	0.047	0.051
$u_{*2}$ [m/s]	0.049	0.047	0.048	0.042	0.050	0.051	0.049	0.046	0.046	0.051	0.046	0.050
$\delta$ [%]	-6.5	-9.0	-1.8	18.2	-8.3	-5.3	3.9	6.3	7.3	-1.2	2.0	1.7
Profile 2												
$h$ [m]	0.116	0.119	0.126	0.138	0.132	0.141	0.159	0.158	0.167	0.180	0.179	0.182
$Re$ [ $10^4$ ]	5.585	5.077	5.839	6.728	6.093	6.855	7.870	7.108	7.997	9.012	8.124	9.012
$Fr$ [-]	0.459	0.401	0.420	0.424	0.409	0.418	0.402	0.367	0.379	0.382	0.347	0.375
$\Pi$ [-]	0.450	0.275	0.250	0.300	0.250	0.425	0.325	0.300	0.300	0.375	0.375	0.400
$u_{*1}$ [m/s]	0.049	0.046	0.050	0.057	0.050	0.051	0.056	0.051	0.053	0.055	0.049	0.053
$u_{*2}$ [m/s]	0.048	0.045	0.050	0.053	0.050	0.048	0.053	0.052	0.053	0.055	0.049	0.052
$\delta$ [%]	3.1	1.6	-0.7	7.0	0.1	5.6	4.2	-1.8	0.1	0.0	0.1	1.0
Profile 3												
$h$ [m]	0.116	0.118	0.127	0.137	0.133	0.142	0.159	0.159	0.166	0.179	0.178	0.185
$Re$ [ $10^4$ ]	5.125	4.659	5.358	6.174	5.591	6.290	7.222	6.523	7.338	8.270	7.455	8.270
$Fr$ [-]	0.419	0.373	0.382	0.391	0.373	0.379	0.368	0.332	0.350	0.351	0.320	0.335
$\Pi$ [-]	0.450	0.575	0.550	0.600	0.575	0.475	0.875	0.900	0.725	1.000	0.825	0.825
$u_{*1}$ [m/s]	0.048	0.039	0.049	0.053	0.049	0.052	0.054	0.049	0.052	0.056	0.050	0.054
$u_{*2}$ [m/s]	0.042	0.035	0.039	0.042	0.039	0.043	0.037	0.035	0.039	0.038	0.036	0.039
$\delta$ [%]	12.8	10.4	19.5	20.4	20.0	17.6	31.4	29.4	24.8	31.6	27.9	28.5
Profile 4												
$h$ [m]	0.118	0.118	0.129	0.139	0.133	0.143	0.161	0.159	0.168	0.181	0.179	0.186
$Re$ [ $10^4$ ]	4.735	4.305	4.950	5.704	5.166	5.811	6.672	6.027	6.780	7.641	6.888	7.641
$Fr$ [-]	0.379	0.341	0.345	0.355	0.343	0.345	0.335	0.308	0.318	0.320	0.293	0.306
$\Pi$ [-]	0.375	0.275	0.350	0.325	0.250	0.400	0.550	0.450	0.550	0.700	0.600	0.625
$u_{*1}$ [m/s]	0.046	0.041	0.047	0.051	0.047	0.049	0.051	0.048	0.049	0.053	0.046	0.051
$u_{*2}$ [m/s]	0.044	0.041	0.046	0.048	0.046	0.044	0.042	0.040	0.041	0.042	0.039	0.042
$\delta$ [%]	4.5	-2.1	2.7	5.4	3.1	9.8	18.3	16.5	15.8	20.7	16.0	18.1

In Tables 4.1, 4.2 and 4.3, the Reynolds number and the Froude number at a specific section are determined as indicated in Section 3.4 with the flow discharge ( $Q$ ) and the water depth ( $h$ ) measured from the experiments:

$$Re = \frac{Uh}{\nu} = \frac{Q}{B\nu} \quad (4.3)$$

$$Fr = \frac{U}{\sqrt{gh}} = \frac{Q}{Bh\sqrt{gh}} \quad (4.4)$$

where  $B$  is the section width,  $g$  is the gravitational acceleration and  $U$  is the mean bulk velocity of the section,  $U = Q/Bh$ .

The shear velocity was determined from the Reynolds shear stress distribution (for  $u_{*1}$ ) and from the log law applied to the flow near the bottom (for  $u_{*2}$ ). This is described in the next section. The Coles wake parameter ( $\Pi$ ) was determined by fitting the velocity data in the outer region to the log-wake law, i.e., Eq. (2.2). Due to the influence of small surface waves, only the velocity data in the core of the outer region ( $0.2 < z/h < 0.7$ ) were used for the fit. The difference between  $u_{*1}$  and  $u_{*2}$  is expressed as

$$\delta = \frac{u_{*1} - u_{*2}}{u_{*1}} \times 100\% \quad (4.5)$$

Table 4.3: Summary of measured and calculated flow parameters (set-up 3).

Series	3AR	3BR	3CR	3DR	3ER	3FR	3GR	3HR	3IR	3JR	3KR	3LR
Q [l/s]	22.0	20.0	23.0	26.5	24.0	27.0	31.0	28.0	31.5	35.5	32.0	35.5
Profile 1												
$h$ [m]	0.121	0.120	0.129	0.138	0.141	0.149	0.157	0.158	0.169	0.175	0.177	0.183
$Re$ [ $10^4$ ]	6.223	5.658	6.506	7.496	6.789	7.638	8.769	7.921	8.911	10.042	9.052	10.042
$Fr$ [-]	0.474	0.438	0.454	0.474	0.411	0.428	0.456	0.406	0.412	0.442	0.391	0.414
$\Pi$ [-]	0.025	0.075	0.100	0.225	0.125	0.200	0.350	0.350	0.300	0.250	0.400	0.350
$u_{*1}$ [m/s]	0.048	0.042	0.049	0.050	0.044	0.048	0.049	0.046	0.049	0.050	0.047	0.051
$u_{*2}$ [m/s]	0.058	0.052	0.058	0.056	0.052	0.053	0.053	0.050	0.053	0.057	0.051	0.052
$\delta$ [%]	-20.6	-22.6	-17.8	-11.5	-17.6	-10.6	-7.9	-8.3	-8.2	-13.1	-8.4	-2.8
Profile 2												
$h$ [m]	0.126	0.127	0.133	0.144	0.147	0.155	0.164	0.164	0.178	0.180	0.180	0.192
$Re$ [ $10^4$ ]	5.446	4.950	5.693	6.559	5.941	6.683	7.673	6.931	7.797	8.787	7.921	8.787
$Fr$ [-]	0.393	0.351	0.379	0.387	0.340	0.355	0.373	0.336	0.335	0.370	0.335	0.336
$\Pi$ [-]	0.200	0.100	0.525	0.025	0.225	0.225	0.325	0.450	0.425	0.300	0.425	0.475
$u_{*1}$ [m/s]	0.050	0.045	0.049	0.053	0.046	0.051	0.054	0.052	0.055	0.056	0.052	0.053
$u_{*2}$ [m/s]	0.057	0.055	0.052	0.069	0.052	0.056	0.056	0.050	0.053	0.062	0.050	0.053
$\delta$ [%]	-13.9	-21.1	-5.9	-30.7	-13.8	-10.2	-4.4	4.0	3.3	-9.2	3.2	-0.7
Profile 3												
$h$ [m]	0.128	0.130	0.134	0.147	0.150	0.156	0.168	0.166	0.175	0.185	0.182	0.195
$Re$ [ $10^4$ ]	4.840	4.400	5.061	5.831	5.281	5.941	6.821	6.161	6.931	7.811	7.041	7.811
$Fr$ [-]	0.343	0.303	0.333	0.332	0.292	0.310	0.319	0.294	0.305	0.316	0.292	0.293
$\Pi$ [-]	0.350	0.650	0.525	0.550	0.500	0.600	0.725	0.875	0.775	0.750	0.825	1.000
$u_{*1}$ [m/s]	0.049	0.042	0.050	0.053	0.045	0.051	0.056	0.052	0.054	0.056	0.054	0.056
$u_{*2}$ [m/s]	0.047	0.037	0.042	0.044	0.040	0.042	0.042	0.037	0.041	0.046	0.039	0.040
$\delta$ [%]	2.3	11.9	16.7	17.7	9.7	17.8	23.9	28.9	25.4	18.5	28.6	29.7

### 4.3 Shear velocity

The shear velocity  $u_*$  is a fundamental velocity scale, widely used for scaling various flow quantities such as mean velocity and turbulence intensities. The shear velocity is also a key parameter representing the flow forces on a bed (i.e., in stone entrainment and sediment transport studies). In uniform open-channel flow the shear velocity can be determined from various methods, some of which are listed below (Nezu and Nakagawa, 1993):

1.  $u_{*1}$  from the Reynolds shear stress distribution, i.e., Eq. (2.6);
2.  $u_{*2}$  from the log law applied to the flow near the bottom, i.e., Eq. (2.1);
3.  $u_{*3}$  from the water level slope, i.e.,  $u_{*3} = \sqrt{ghi}$  (with  $i$  is the water slope).

Of the three methods the last one is considered less reliable for the present data because of the non-uniformity of the flow and the uncertainty in the accuracy of the water level measurement. Due to the existence of small surface waves in the flume, this third method will not be used. Regarding non-uniform flow situation the other methods can still be used if the Reynolds shear stress distribution is linear (for the first method) and the flow in the inner region follows the log law (for the second method). This is checked by comparing the shear velocity calculated from the two methods.

The velocity gradient  $du/dz$  is needed to calculate the eddy viscosity, the mixing length and the shear velocity from Eq. (2.6). It can be obtained from the measured mean velocity distribution using following technique employed by Nezu and Rodi (1986). A cubic spline data interpolation technique was applied to the measured velocity against  $\ln z$ . After differentiating  $u$  to  $z$ ,  $u_{*1}$  was determined with the least-square method so that the data  $-\overline{u'w'}$  gave the best fit to Eq. (2.6). In the same manner,  $u_{*2}$  was determined so that the mean velocity data gave the best fit to Eq. (2.1). It is noted that in the inner region ( $z \leq 0.2h$ ) there always exist 10 to 13 measuring points available, giving enough velocity data to evaluate the shear velocity.

The values of  $u_{*1}$  and  $u_{*2}$  for all flow conditions are presented in Tables 4.1, 4.2 and 4.3, showing that  $u_{*1}$  and  $u_{*2}$  are in fairly good agreement. The difference is larger for the flows at profile 3 and 4 of set-up 2 and profile 2 and 3 of set-up 3. This agrees with the high non-uniformity of the flow at these profiles. In general, the shear velocity decreases along the expansion for set-up 1, 2 and somewhat set-up 3. In the first set-up the shear velocity at profile 2 is smaller than that at profile 1 when the water depth is small (i.e., from series 1AR to 1FR). When the water depth is higher or for all cases of the second and third set-ups, the shear velocity at profile 2 is usually larger than that of profile 1. This can be attributed to the increase of turbulence and hence to the increase of the Reynolds shear stress  $-\overline{u'w'}$ .

## 4.4 Mean flow velocity

Figure 4.1 shows the mean streamwise velocity profiles for the three set-ups with flow condition B (smallest Reynolds number and water depth) and L (largest Reynolds number and water depth) as examples of the measured flow results. The results are normalized using the shear velocity determined from the fit of

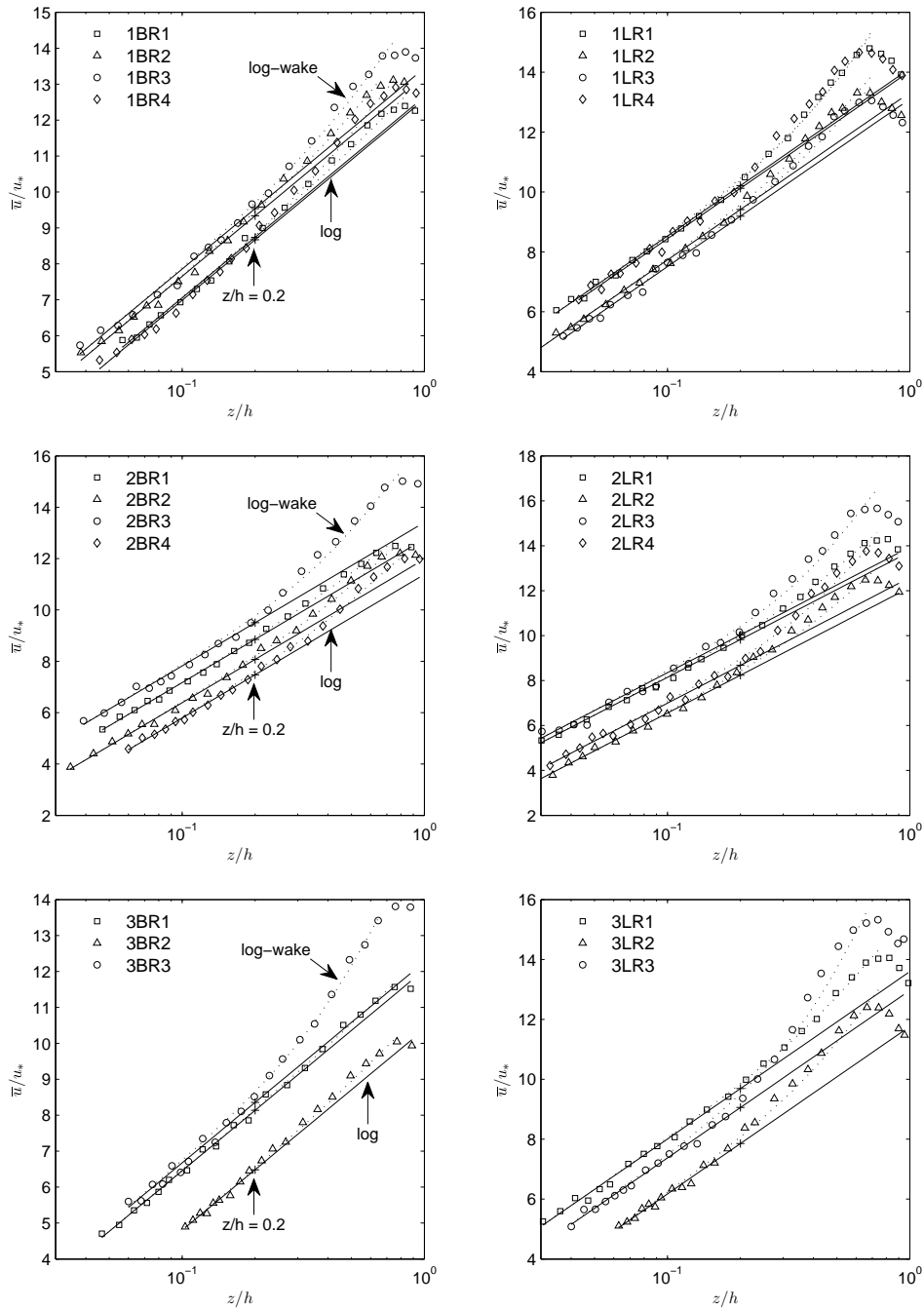


Figure 4.1: Typical velocity profiles.

the Reynolds shear stress distribution ( $u_{*1}$ ). The measured velocity is compared to the log law, i.e., Eq. (2.1) and the log-wake law, i.e., Eq. (2.2).

As can be seen in Figure 4.1, the logarithmic law can still describe the mean velocity in the bottom region (i.e.,  $z/h < 0.2$ ) well for our data. The velocity at profile 1 (i.e., in the straight part of the flume) indeed follows the logarithmic law slightly better compared to the velocity at profiles 2, 3 and 4. However, for all cases the log law fails to describe the data in the outer region. The log wake law can be applied to the outer region as long as a proper Coles wake parameter,  $\Pi$ , is used. This agrees with the results from the previous research on non-uniform flow induced by an inclined bed (e.g. Kironoto and Graf, 1995).

From the measured mean velocity distributions, the Coles wake parameter  $\Pi$  was calculated for all profiles and flow conditions. Due to the influence of small surface waves, only the velocity data in the range of  $0.2 < z/h < 0.7$  were used for the analysis. The  $\Pi$ -values are given in Tables 4.1, 4.2 and 4.3. The results show a dependence of  $\Pi$  on the Reynolds number, i.e., the higher the Reynolds number the larger the  $\Pi$ -value. The variation of flow parameters such as the shear velocity and the Coles wake parameter for different profiles and flow conditions indicates that the flow is in non-equilibrium (Clauser's parameter  $\beta$  in Eq. (4.1) varies along the flow direction), making it impossible to generalize the results.

## 4.5 The eddy viscosity and mixing length

To assess the suitability of the Prandtl mixing length model to the present flow conditions, the eddy viscosity  $\nu_t$  and mixing length  $l_m$  were determined from the measured shear stress data and the mean velocity profile. The velocity gradient  $du/dz$  used in the calculation can be obtained by applying a cubic spline data interpolation technique to the measured velocity against  $\ln z$  as described in Section 4.3. Once the velocity gradient  $du/dz$  is available, the eddy viscosity  $\nu_t$  and the mixing length  $l_m$  can be determined as follows. From Eqs. (2.6) and (2.7) one has:

$$\nu_t = \frac{\nu \frac{du}{dz} - \overline{u'w'}}{\frac{du}{dz}} \quad (4.6)$$

From Eqs. (2.6) and (2.9) one has:

$$l_m = \sqrt{\frac{\nu \frac{du}{dz} - \overline{u'w'}}{\left| \frac{du}{dz} \right| \frac{du}{dz}}} \quad (4.7)$$

where  $\nu$  is the kinematic viscosity.

Figure 4.2 to 4.4 show the distributions of the eddy viscosity and the mixing length at all measuring profiles together with theoretical curves according to

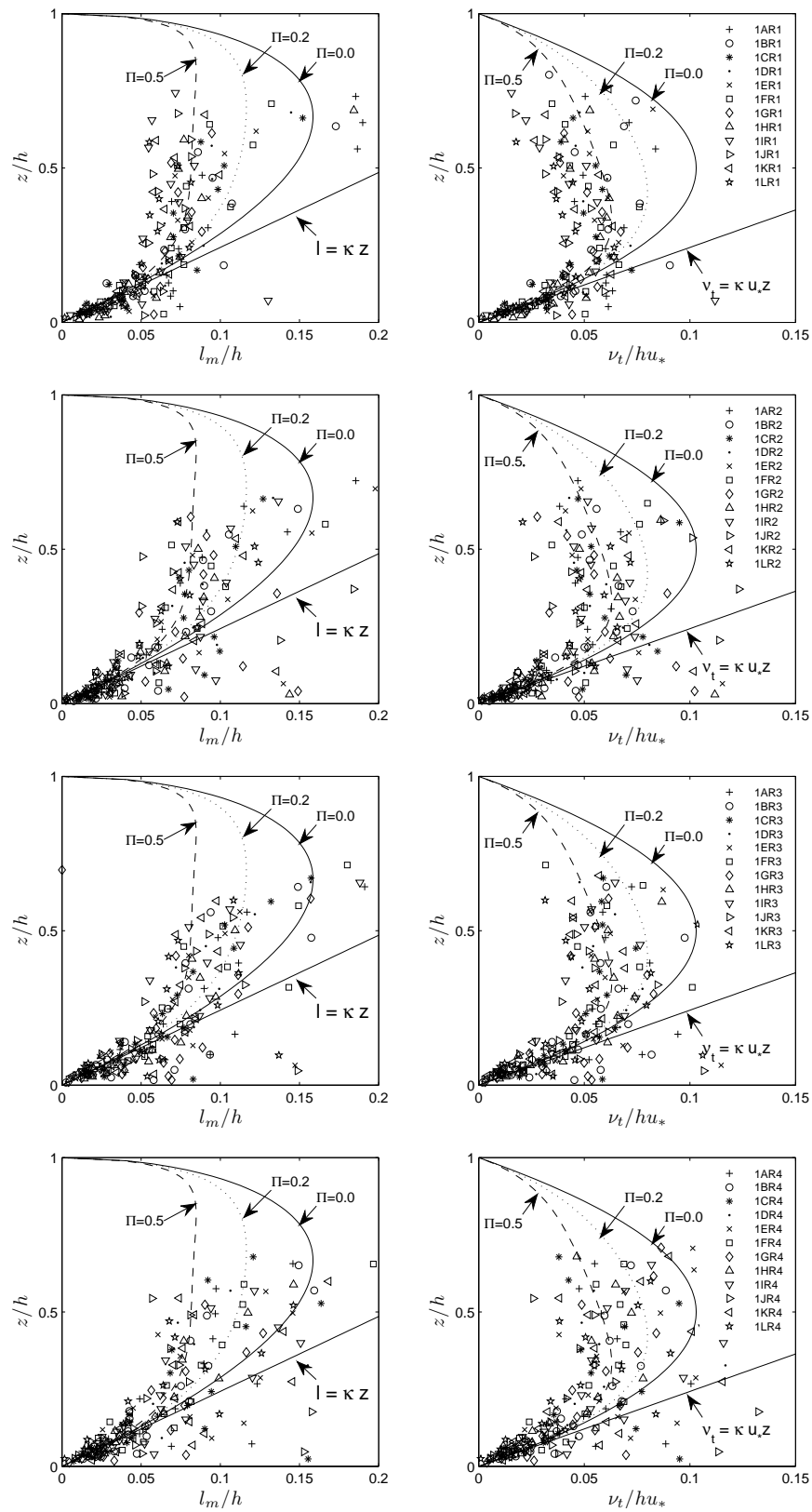


Figure 4.2: Distributions of eddy viscosity and mixing length (set-up 1).

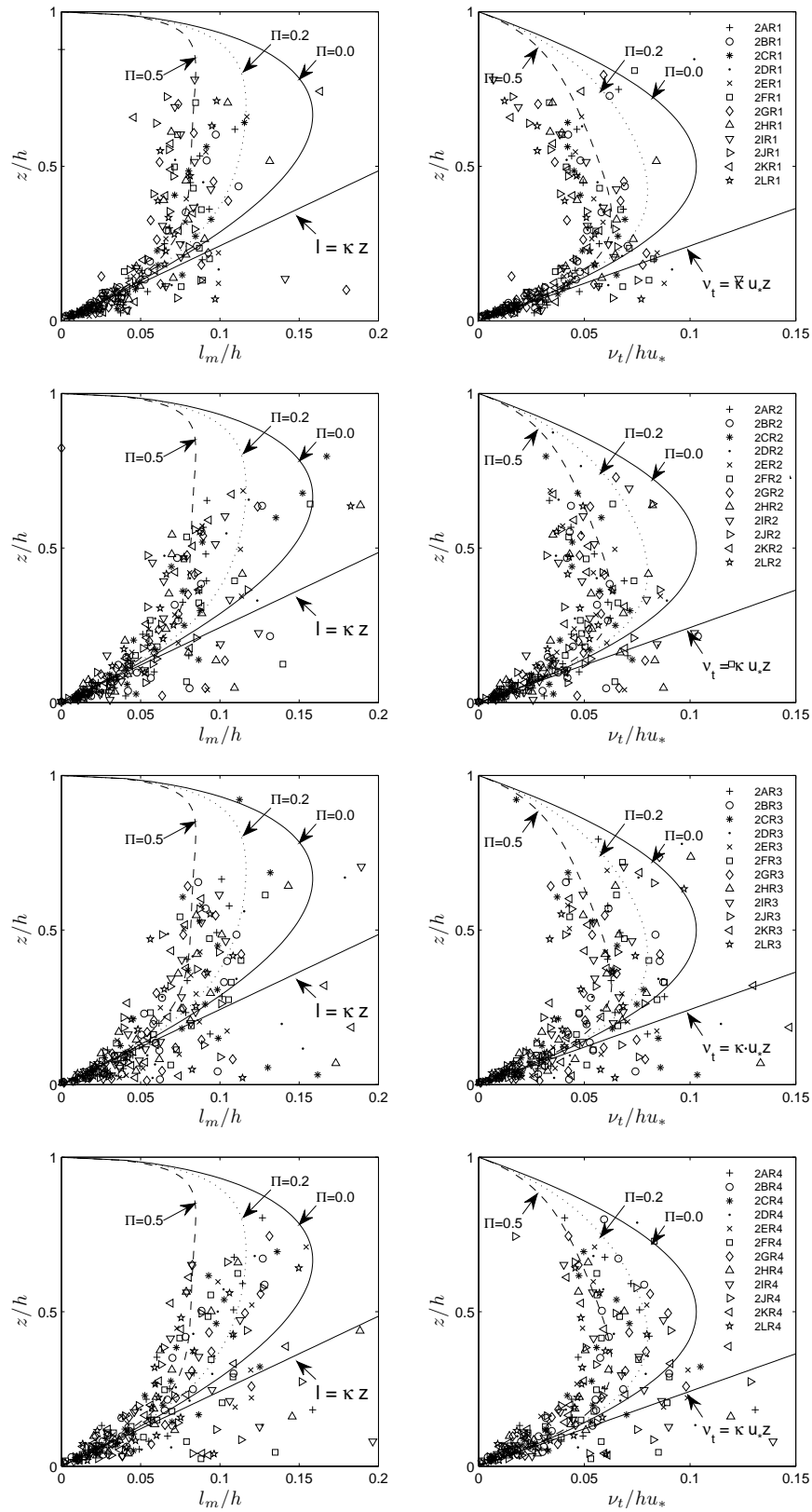


Figure 4.3: Distributions of eddy viscosity and mixing length (set-up 2).

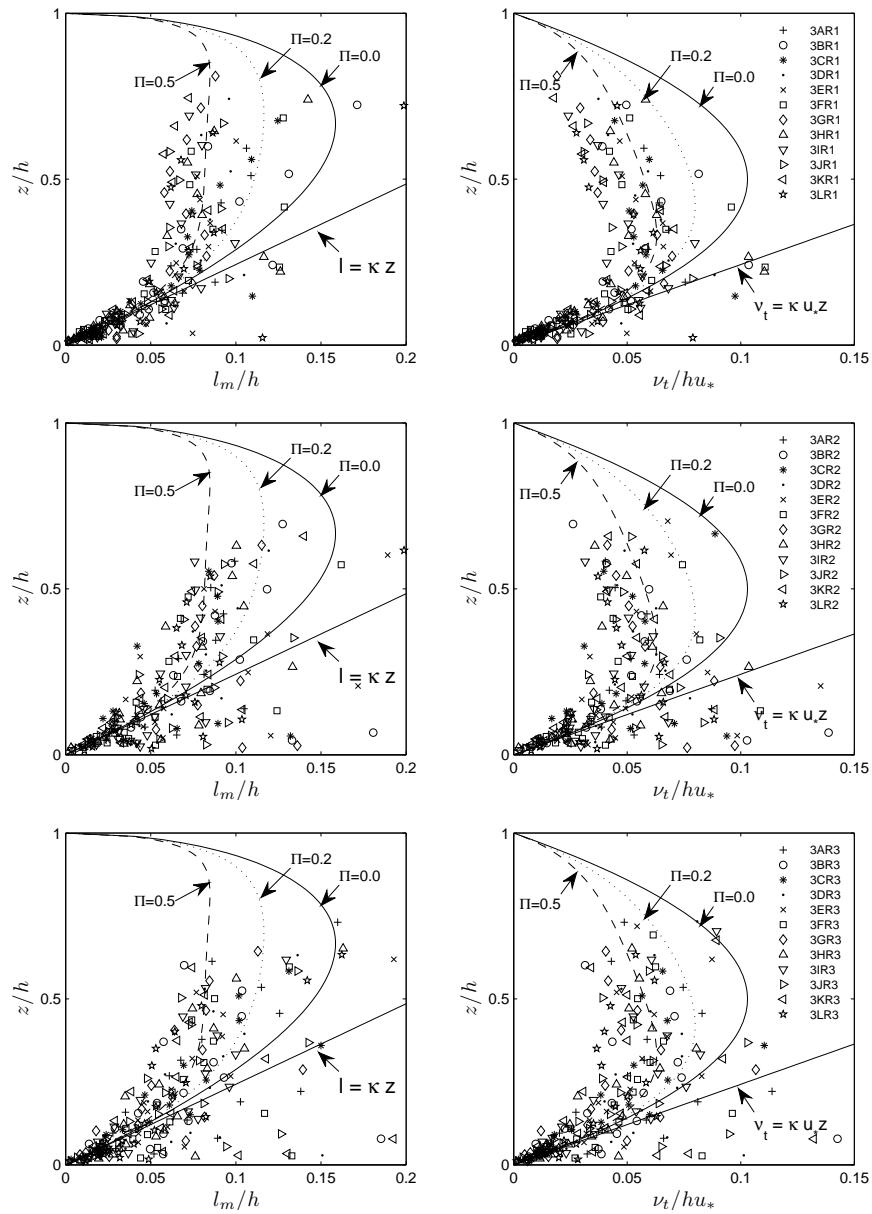


Figure 4.4: Distributions of eddy viscosity and mixing length (set-up 3).



Eqs. (2.13) and (2.14). These profiles show a high scatter level. This can be explained by the fact that small measurement errors occurring in velocity profiles are enhanced in the calculation of  $du/dz$ . The scatter level is higher for the data at profile 2 to 4 in set-up 2 and 3 compared to that of set-up 1. This agrees with the higher non-uniformity of the flow in these two set-ups. However, a good agreement between our data and literature can be seen for profile 1 at  $z/h < 0.2$ . This explains the validity of the log law for our data in the inner region. The deviations from the theoretical curves of the eddy viscosity and the mixing length in the outer region show that the extension of the log law to the whole water depth cannot be applied to the present flow conditions. The scatter in the outer region reflects the fact that the Coles wake parameter  $\Pi$  varies considerably for all flow conditions.

## 4.6 Turbulence intensity data

Figures 4.5, 4.6 and 4.7 show the turbulence intensities normalized by the shear velocity ( $u_{*1}$ ) for all flow conditions. From the measured turbulence intensity distributions, the empirical constants  $\alpha$  and  $\beta$  in Eq. (2.3) can be evaluated. This equation is rewritten as

$$\frac{\sigma(u_i)}{u_*} = \alpha_i e^{-\beta_i \frac{z}{h}} \quad (4.8)$$

The empirical constants  $\alpha_i$  and  $\beta_i$  were determined by least-square fitting to the turbulence data in the range of  $0.15 < z/h < 0.70$ . The fit analysis was made as follows. By taking the logarithm of both sides of Eq. (4.8) and taking  $Y = \ln[\sigma(u_i)/u_*]$ ,  $X = z/h$ ,  $A = -\beta_i$ , and  $B = \ln(\alpha_i)$ , we have

$$\ln \left[ \frac{\sigma(u_i)}{u_*} \right] = \ln(\alpha_i) - \beta_i \frac{z}{h} \rightarrow Y = AX + B \quad (4.9)$$

Table 4.4: The empirical constants  $\alpha$  and  $\beta$  determined from the present data.

profile	set-up 1				set-up 2				set-up 3			Nezu (1977)
	1	2	3	4	1	2	3	4	1	2	3	for uniform flow
$\alpha_u$	2.33	2.31	2.20	2.21	2.27	2.38	2.35	2.21	2.29	2.41	2.32	2.30
$\beta_u$	1.61	1.48	1.35	1.23	1.50	1.49	1.32	1.05	1.41	1.45	1.30	1.00
$R_u^2$	0.92	0.95	0.93	0.92	0.90	0.95	0.88	0.85	0.89	0.96	0.89	-
$\alpha_w$	1.15	1.10	1.09	1.09	1.17	1.12	1.15	1.12	1.17	1.09	1.12	1.63
$\beta_w$	1.06	0.83	0.77	0.65	1.03	0.90	0.83	0.61	0.95	0.80	0.78	1.00
$R_w^2$	0.92	0.91	0.93	0.84	0.91	0.94	0.88	0.81	0.89	0.94	0.90	-

From Eq. (4.9) a linear regression analysis was made for the present data. The results are given in Table 4.4 and shown in Figure 4.5 to 4.7. For all profiles

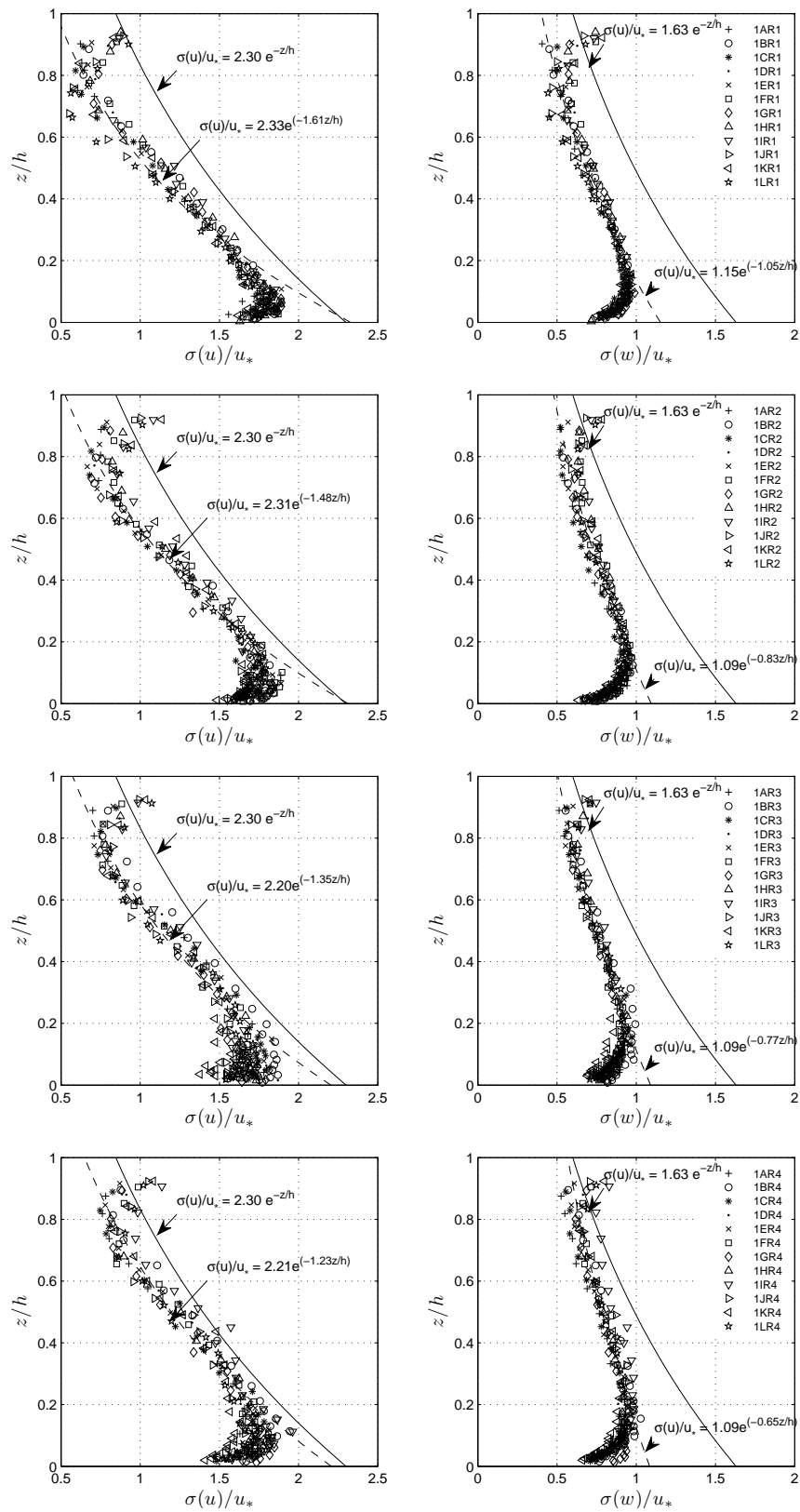


Figure 4.5: Turbulence intensity distributions (set-up 1).

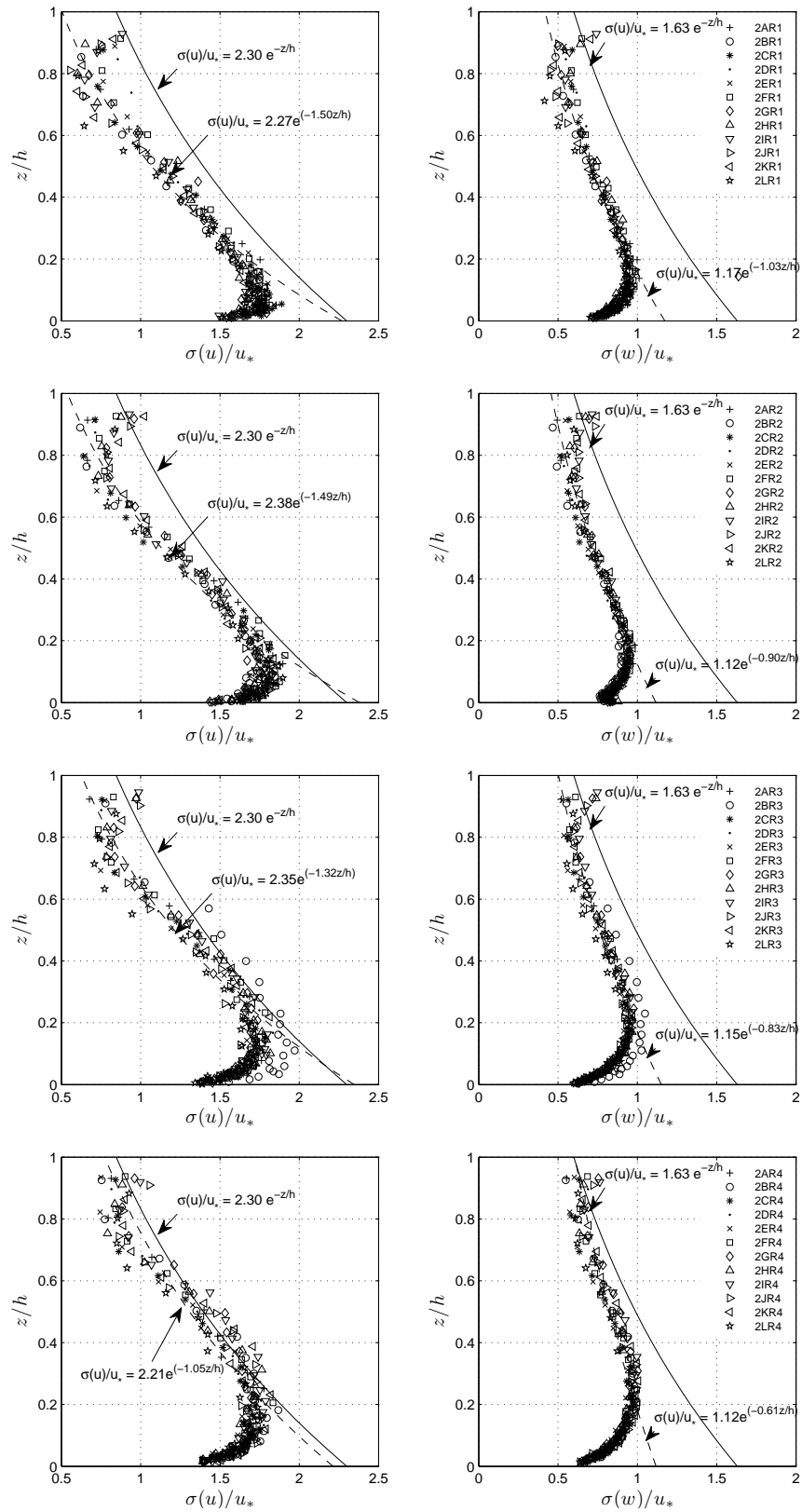


Figure 4.6: Turbulence intensity distributions (set-up 2).

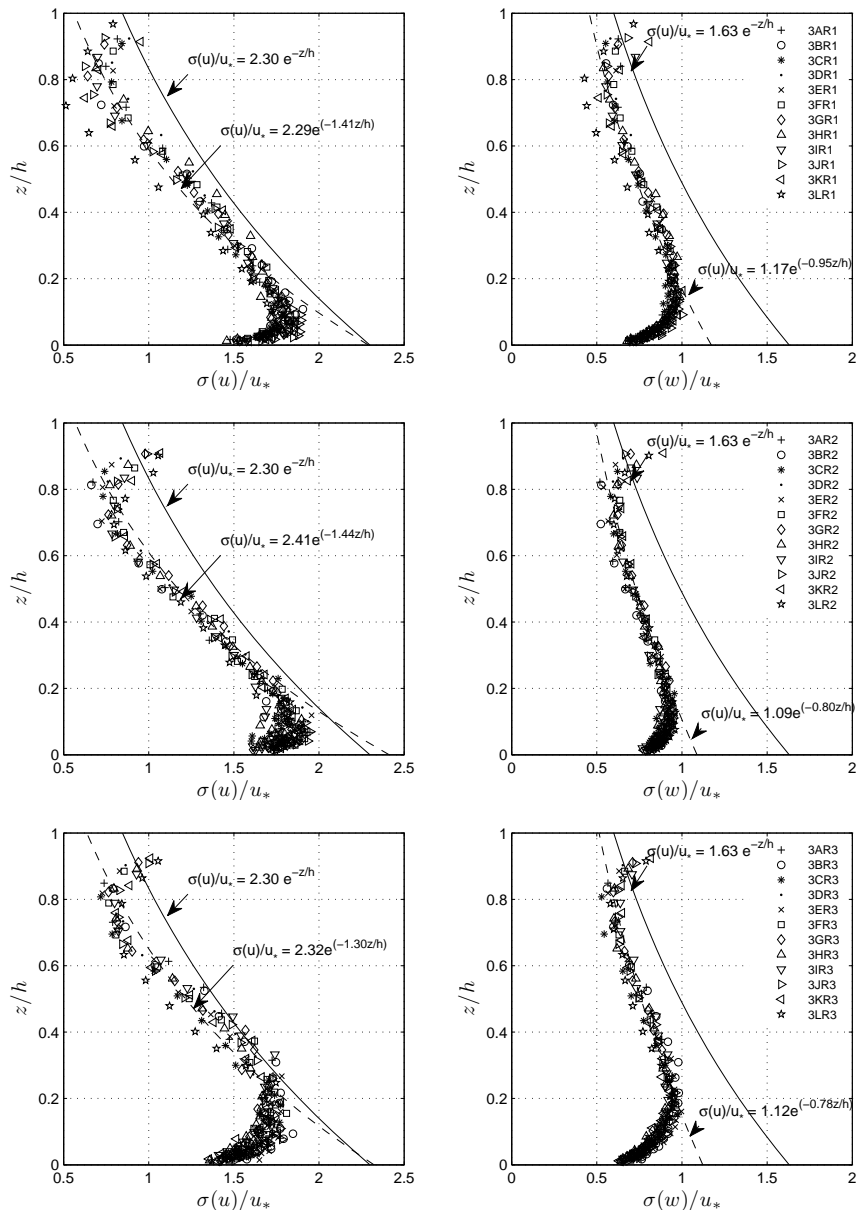


Figure 4.7: Turbulence intensity distributions (set-up 3).

the constants  $\alpha_u$  in Eq. (4.8) are close to the value reported by Nezu and Rodi (1986), i.e.,  $\alpha_u \approx 2.30$ . However,  $\beta_u$  varies considerably from profile 1 ( $\beta_u = 1.50$ ) to profile 4 ( $\beta_u = 1.05$ ). The deviation of  $\sigma(u)/u_*$  from the empirical curve in profile 1 can be attributed to the influence of secondary flow in a relatively narrow channel. The deviation becomes less for profile 2 to 4 due to the widening of the channel and hence increasing the turbulence in the outer region.

The distribution of  $\sigma(w)/u_*$  shows less scatter but still deviates from the empirical curve. The value of  $\alpha_w$  is approximately constant at 1.15 for all profiles while  $\beta_w$  varies from 1.06 (profile 1) to 0.61 (profile 4). For all flow conditions the turbulence intensities reach their maximum at about  $z/h = 0.1$  (for  $\sigma(u)/u_*$ ) and  $z/h = 0.15$  (for  $\sigma(w)/u_*$ ) and then decrease gradually towards the surface. At a height of about  $z/h = 0.8$  the turbulence intensities increase due to the presence of the surface waves.

## 4.7 Reynolds shear stress data

Figure 4.8 shows the distributions of the Reynolds shear stress  $-\overline{u'w'}$  normalized by the shear velocity squared ( $u_{*1}^2$ ), together with the theoretical curves according to Eq. (2.6). The velocity fluctuation  $u'$  and  $w'$  were obtained directly from the instantaneous velocity data as described in Section 3.6.

In Figure 4.8 the high scatter level as well as the deviation of the Reynolds shear stress data from the theoretical curves can be observed. This could be attributed mostly to the secondary currents in the relatively narrow channel as explained by Nezu and Nakagawa (1993, page. 107). The deviation is more pronounced for higher water depths. In most cases the Reynolds shear stress reaches its maximum at  $z/h \approx 0.15$ . It is unclear what causes the decay of Reynolds shear stress near the bottom but it could be attributed to the presence of secondary flow in the relatively narrow channel and/or the effect of measuring volume of the LDV.

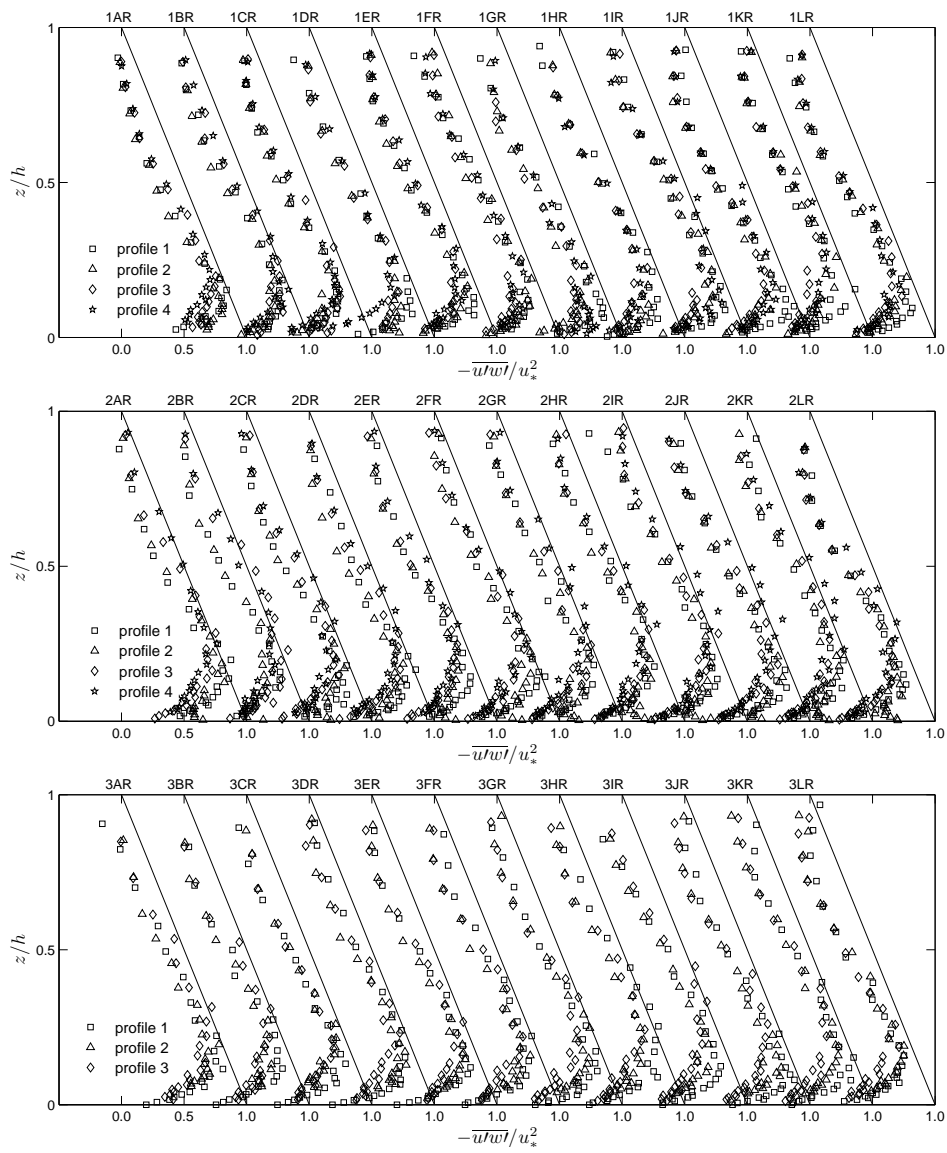


Figure 4.8: Reynolds shear stress distributions.

## 4.8 Concluding remarks

In this chapter the flow structures measured in the experiments are analyzed and compared to those reported for uniform open-channel flow. The analysis was made for the flow measured at the center of the flume since this flow is the main cause to the entrainment of the stones on the bottom. The two-component ( $u$ - and  $w$ -) velocity measurements were used to verify the validity of the log law and the log-wake law for the present flow. From the measured velocity and Reynolds shear stress profiles, the eddy viscosity and the mixing length were evaluated. The measured turbulence intensities were compared with the empirical curves reported in the literature (i.e., in [Nezu and Rodi, 1986](#)). The analysis presented in this chapter leads to the following conclusions.

The logarithmic law, which is shown to be valid in the inner region of uniform open-channel flow, can also describe the mean velocity in the inner region of the present flow, i.e., a decelerating open-channel flow in a gradual expansion. The log law, however, fails to describe mean velocity in the outer region. In this outer region Coles' law can be applied. Due to the non-equilibrium state of the flow, there is no single value of  $\Pi$  that is applicable to all cases.  $\Pi$ -values increase when the Reynolds number increases.

The shear velocity can be determined both by the logarithmic fit of the mean velocity and by the fit of the Reynolds shear stress distributions. The values of the shear velocity determined from these two methods coincide mostly within  $\pm 30\%$ .

The turbulence intensity distributions deviate from the empirical curves reported for uniform open-channel flow. They reach their maximum values at  $z/h = 0.1$  (for  $\sigma(u)/u_*$ ) and  $z/h = 0.15$  (for  $\sigma(w)/u_*$ ). The turbulence intensities do increase along the expansion, especially in the outer region. This is more pronounced for larger Reynolds numbers. The increase of turbulence intensity probably results in a slight increase of the shear velocity at the beginning part of the expansion.

The eddy viscosity and mixing length distributions are self-similar up to  $z/h \approx 0.2$  for the flow in the straight part of the flume (i.e., measured at profile 1). For all cases a high scatter level is observed in the outer region. The scatter of the eddy viscosity and the mixing length can be attributed to the sensitivity of  $du/dz$  on velocity measurement errors. However, when averaged, the results confirm the dependence of the mixing length on the Coles wake parameter, namely the larger the Coles wake parameter, the smaller the mixing length.

In spite of the validity of the log law in the inner region for the studied flow, it is considered non-uniform due to the deviation (and the high scatter level) of the turbulence intensity, the eddy viscosity and the mixing length to the theoretical and empirical curves reported for uniform flow. The non-uniformity of the present flow requires a different approach in investigating the relationship between the flow and its induced damage to the bottom. This matter is treated

in the next chapter.



# Chapter 5

## Stone transport formulae

### 5.1 Introduction

In the design of bed protections the choice of stone sizes and weights to be used is essential. This is, however, complicated by the fact that the actual interaction between flow and stones on a bed is rather complex and that there is only limited knowledge of the mechanism of entrainment of bed material. The review in Chapter 2 has shown that the stone stability assessment method based on the concept of incipient motion of bed material often yields inconsistent and unreliable design criteria and that the stone stability assessment method based on the stone transport concept should be used. The effect of turbulence fluctuations has to be taken into account, especially for non-uniform flow. In this chapter we try to make the link between governing flow parameters and the stability of bed protections in which the effect of turbulence is incorporated. The various ways of quantifying the hydraulic loads exerted on the stones on a bed are verified and extended. The measured flow quantities and the stone entrainment data obtained from the experiment are used for the analysis.

The chapter is structured as follows. In Section 5.2 a new stability parameter based on the approaches of Shields (1936), Jongeling et al. (2003, 2006) and Hofland (2005) is proposed. Next, in Section 5.3 the new stability parameter is evaluated and the formulation of a new stone transport formula is determined based on the correlation analysis of the present data. In Section 5.4 a similar analysis is carried out for the stability parameters of Shields (1936), Jongeling et al. (2003) and Hofland (2005). The performance and the sensitivities of the new stone transport formulae to the dominant variables are discussed in Section 5.5. It is followed by the comparison between the present data and those of Jongeling et al. (2003) and De Gunst (1999). The chapter ends with conclusions in Section 5.6. Parts of this chapter were published as Hoan et al. (2007a,b).

## 5.2 The proposed stability parameter

In attempts to describe flow impact on bed materials, several stability parameters - expressed as the ratio of the load of the flow to the strength of the bed particles (e.g., stones) - have been proposed. Because the actual interaction between the flow and the stones on a bed are rather complicated, assumptions are often needed to describe flow forces. The use of the bed shear stress to quantify the flow forces has been proven insufficient for non-uniform flow due to the lack of turbulence effect. [Jongeling et al. \(2003\)](#) proposed an approach in which a combination of velocity and turbulence distributions (i.e.,  $\bar{u} + \alpha\sqrt{k}$ ) is used to describe the peak values of the forces that occur in the flow. These forces are averaged over a certain water column to quantify the flow forces acting on the bed. The [Jongeling et al.](#) stability parameter, however, was formulated rather arbitrary (see Section 2.4). [Hofland \(2005\)](#) argued that the maximum over the depth of the local values of  $(\bar{u} + \alpha\sqrt{k})$  weighted with the relative mixing length  $Lm/z$  is responsible for dislodging the stones on a bed and gave a well-physical explanation for his approach. However, both the [Jongeling et al.](#) and [Hofland](#) stability parameters have not been validated by reliable data. In other words: the data used to develop and to validate these parameters are highly scattered (see Figure 2.6). These stability parameters will be verified later in this chapter using the present data.

In this section a new stability parameter which incorporates the influence of turbulence sources above the bed is proposed. A qualitative function is introduced to quantify the role of a turbulence source away from the bed. The formulation of the new stability parameter will be based on the correlation analysis of the present data. The physical interpretation for this approach can be discerned from Figure 5.1 and is given below.

Let us assume that the flow force ( $F$ ) exerted on the stone on a bed is proportional to the square of the near bed velocity ( $u$ ) and the exposed surface area of the stone ( $\propto d^2$ ):

$$F \propto \rho u^2 d^2 \quad (5.1)$$

Since the instantaneous flow velocity  $u$  can be expressed as  $u = \bar{u} + u'$  (in which  $\bar{u}$  is the local, time-averaged component and  $u'$  is the fluctuating velocity component), the force can be expressed as

$$F \propto \rho (\bar{u} + u')^2 d^2 \quad (5.2)$$

From this we can estimate a *maximum* (extreme) force as

$$F_{max} \propto \rho [\bar{u} + \alpha\sigma(u)]^2 d^2 \quad (5.3)$$

where  $\sigma(u) = \sqrt{\overline{u'^2}}$  and  $\alpha$  is a turbulence magnification factor which accounts for the velocity fluctuations.

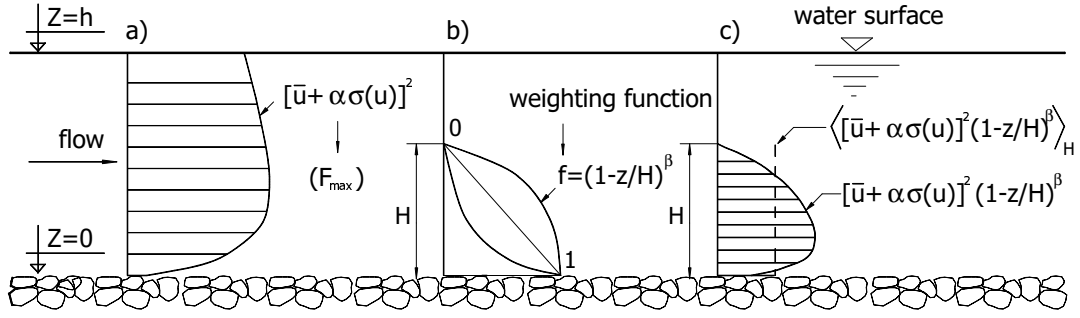


Figure 5.1: The distributions of key parameters used to formulate the new stability parameter. From left to right: extreme force distribution (a), weighting function (b) and weighting average of the extreme forces (c).

If we assume that the turbulence source near the bed has the largest influence on stone stability on the bed and its influence gradually decreases to a negligible amount at a certain distance  $H$  from the bed ( $H \leq h$ ), a weighting function  $f$  can be used to account for the influence of the turbulence source at a distance  $z$  (Figure 5.1):

$$f(z) = \left(1 - \frac{z}{H}\right)^\beta \quad (5.4)$$

where  $\beta$  is an empirical constant. The force from the water column  $H$  acting to move the stone can be averaged as follows:

$$\bar{F} \propto \frac{1}{H} \int_0^H \rho [u + \alpha\sigma(u)]^2 dz \times \left(1 - \frac{z}{H}\right)^\beta \quad (5.5)$$

By dividing the moving force by the resisting force, i.e. the submerged weight of the stone  $\equiv (\rho_s - \rho)gd^3$ , the general form of a new Shields-like stability parameter can be obtained:

$$\Psi_{u-\sigma[u]} = \frac{\langle [u + \alpha\sigma(u)]^2 \times \left(1 - \frac{z}{H}\right)^\beta \rangle_H}{\Delta gd} \quad (5.6)$$

in which  $\langle \dots \rangle_H$  denotes an average over the height  $H$  above the bed ( $H < h$ ).

The suitability of a stability parameter for representing the flow forces on a bed is evaluated by considering the correlation between the stability parameter and the bed response. Therefore, the values of  $\alpha$ ,  $\beta$ , and  $H$  that give the best correlation between the new stability parameter and the dimensionless entrainment rate will be chosen to formulate the final expression of the new stability parameter. This is discussed in the next section.

### 5.3 Final formulation of the proposed stability parameter

The turbulence quantity used in the newly-proposed stability parameter is  $\sigma(u)$ . This turbulence component can be calculated directly from the instantaneous velocity data. To evaluate the new stability parameter, a correlation analysis was made for various possible values of  $\alpha$ ,  $\beta$  and  $H$ . The results are shown in Figure 5.2. The best correlation ( $R^2 = 0.81$ ) can be obtained when  $\alpha = 3.0$ ,  $\beta = 0.7$  and  $H = 0.7h$  are used. With  $H > 0.7h$  the correlation is high, showing that large-scale structures are connected to the entrainment of bed material, which is consistent with the finding by Hofland (2005). The insensitivity to  $H/h$  (above 0.7) and  $\beta$  leads to a choice of the final form of the new stability parameter as follows ( $\alpha = 3$ ):

$$\Psi_{u-\sigma[u]} = \frac{\langle [u + \alpha\sigma(u)]^2 \times \sqrt{1 - z/h} \rangle_h}{\Delta g d} \quad (5.7)$$

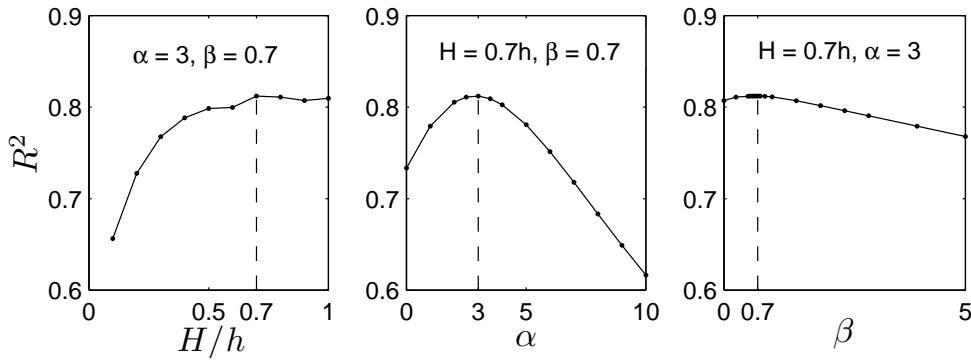


Figure 5.2: Sensitivity analysis of  $\alpha$ ,  $\beta$  and  $H$ .

Figure 5.3 illustrates the role of each parameter in the new stability parameter. In this figure, the distributions of the key parameters in the new stability parameter are calculated using the measured flow quantities at profile 2 in series 2BR. It clearly shows the large influence of the turbulence in the new stability parameter.

The correlation between the new stability parameter and the measured entrainment rate is shown in Figure 5.4. The entrainment curve found by regression analysis is given as

$$\Phi_E = 9.6 \times 10^{-12} \Psi_{u-\sigma[u]}^{4.35} \quad \text{for } 7.5 < \Psi_{u-\sigma[u]} < 18 \quad (R^2 = 0.81, \alpha = 3) \quad (5.8)$$

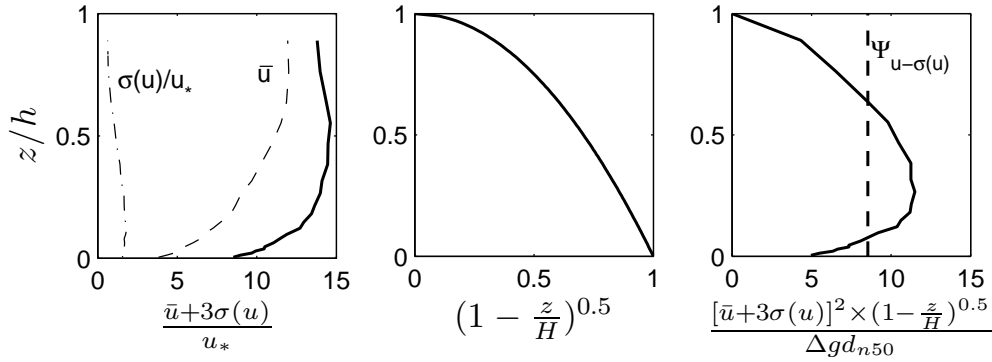


Figure 5.3: Vertical distributions of key parameters in Eq. (5.7).

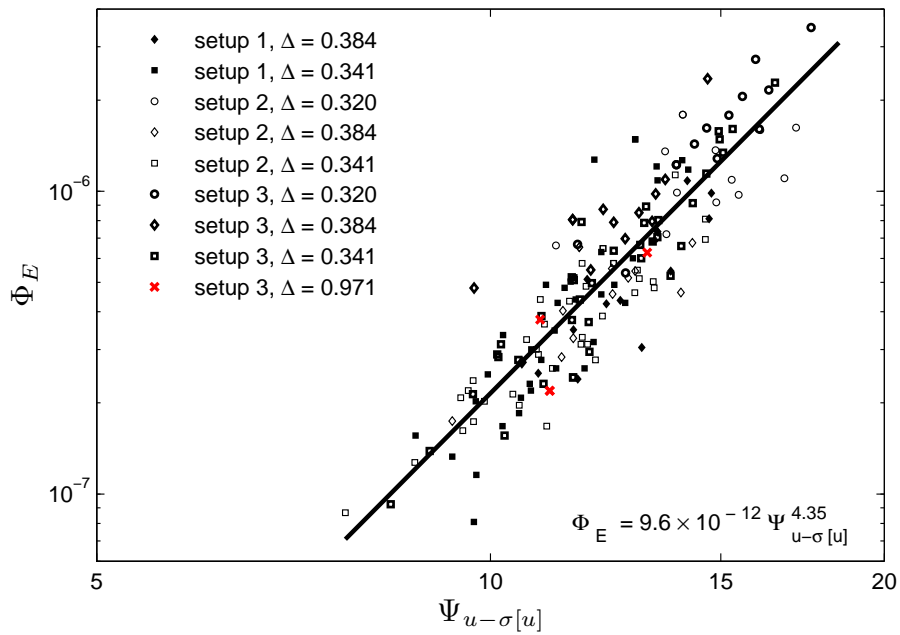


Figure 5.4: Measured  $\Psi_{u-\sigma[u]}$  versus measured  $\Phi_E$ .

## 5.4 Evaluation of the available stability parameters

In this section the stability parameters of [Shields \(1936\)](#), [Jongeling et al. \(2003\)](#) and [Hofland \(2005\)](#) are evaluated using the present data. Correlation analysis is made and the coefficient of determination gives the quantitative confirmation of the validity of these parameters. The analysis results in new stone transport formulae for these stability parameters.

### 5.4.1 The Shields stability parameter

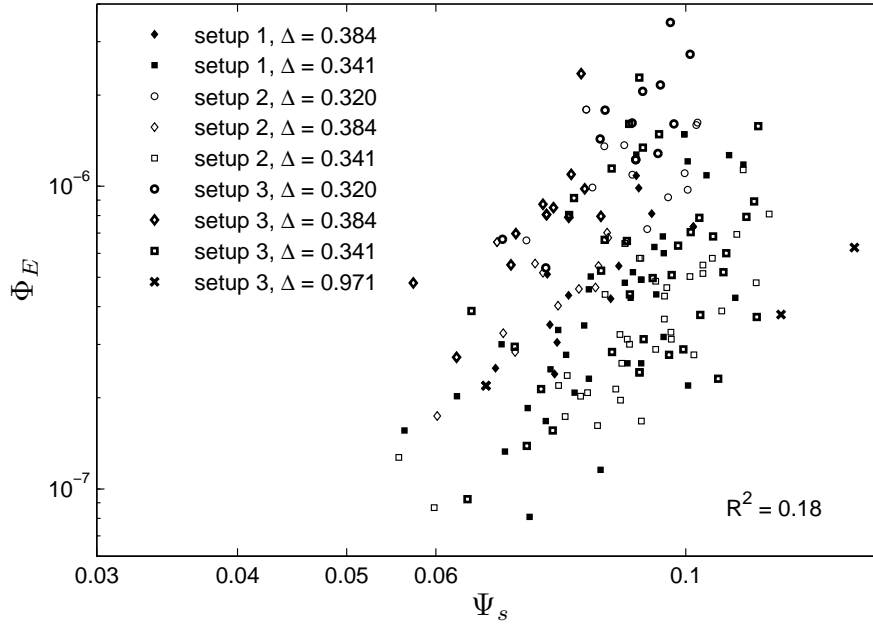
The shear velocity is needed to calculate the measured Shields stability parameter, expressed in Eq. (2.26). In the present analysis the shear velocity was determined in the two following ways: i)  $u_{*1}$  from the Reynolds shear stress distribution and ii)  $u_{*2}$  from the log law applied to the flow near the bottom. The values of  $u_{*1}$  and  $u_{*2}$  for all flow conditions are presented in Table 4.1 to 4.3, showing that  $u_{*1}$  and  $u_{*2}$  are in fairly good agreement. However, correlation analysis between the measured  $\Psi_s$  and the measured  $\Phi_E$  shows less scatter when  $u_{*1}$  is used. In this section, the analysis using  $u_{*1}$  is presented.

Table 5.1 summarizes the correlation analysis between the measured Shields stability parameter and the measured dimensionless entrainment rate for configuration 1, 2, 3 and all configurations. The results show that the correlation deteriorates when the expansion angle is larger, i.e., when the flow is more non-uniform.

Table 5.1: Coefficient of determination for different data sets.

	set-up 1	set-up 2	set-up 3	all set-ups
Expansion angle, $\alpha$ [degree]	3	5	7	3, 5, 7
Number of data [-]	48	60	60	168
$R^2$ [-]	0.48	0.21	0.08	0.18

Figure 5.5 shows the correlation between the Shields stability parameter and the dimensionless entrainment rate for all data. The coefficient of determination  $R^2$  is of 0.18, showing that virtually there is no correlation between  $\Psi_s$  and  $\Phi_E$  for non-uniform flow. It is noted that the flow condition in the straight part of the flume is still far from uniform since the channel is rather narrow. The analysis clearly shows that the bed shear stress alone is not sufficient to quantify the flow forces acting on the bed.

Figure 5.5: Measured  $\Psi_s$  versus measured  $\Phi_E$ .

### 5.4.2 The Jongeling et al. stability parameter

As only two velocity components ( $u$ - streamwise and  $w$ - upward) are available, the turbulent kinetic energy in Eqs (2.27) and (2.28) was approximated by assuming that  $\sigma(v) = \sigma(u)/1.9$  as discussed in Section 3.6. First, the original Jongeling et al. (2003) stability parameter with  $\alpha = 6$  is used.

The correlation between this stability parameter and the dimensionless entrainment rate is shown in Figure 5.6. The results show that, in contrast to the Shields stability parameter, the measured Jongeling et al. stability parameter is strongly correlated to the measured dimensionless entrainment parameter. The correlation analysis leads to the following stone transport formula:

$$\Phi_E = 5.4 \times 10^{-14} \Psi_{WL}^{4.89} \text{ for } 18 < \Psi_{WL} < 39 \quad (R^2 = 0.78, \alpha = 6) \quad (5.9)$$

In Eq. (5.9) a turbulence magnification factor  $\alpha$  of 6 was used as suggested by Jongeling et al. (2003). This was chosen based on the assumption that at the incipient motion, the critical Jongeling et al. stability parameter is a constant. This assumption, however, is questionable as discussed in Section 2.4.3. In the present analysis the value of  $\alpha$  that gives the best correlation between the stability parameter and the dimensionless entrainment rate was used. The recognized analysis of  $\alpha$  in  $\Psi_{WL}$  was based on all data sets (i.e., configuration 1, 2 & 3), showing that  $\alpha = 3.5$  gives the best correlation ( $R^2 = 0.82$ , Figure 5.7).

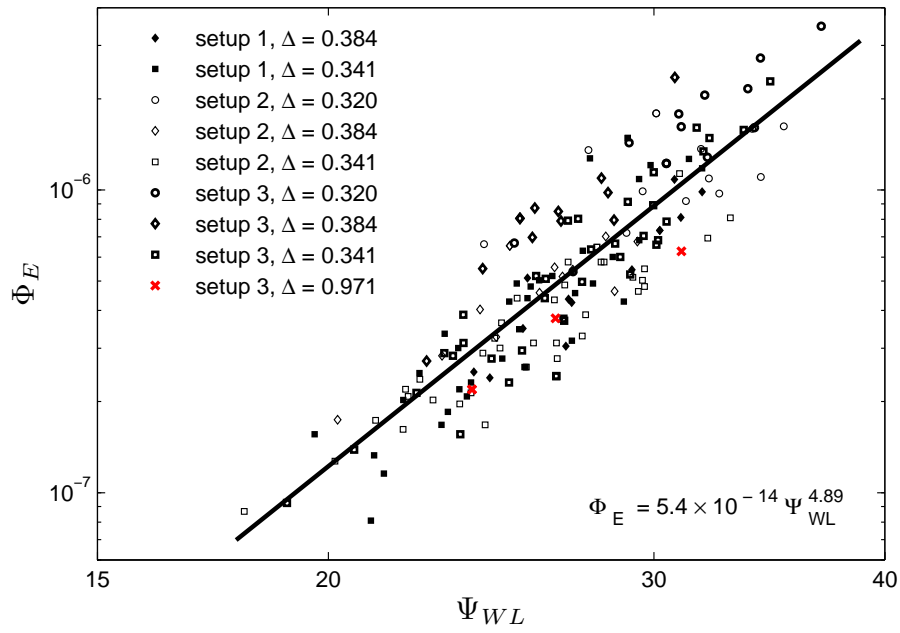


Figure 5.6: Measured  $\Psi_{WL}$  (with  $\alpha = 6$ ) versus measured  $\Phi_E$ .

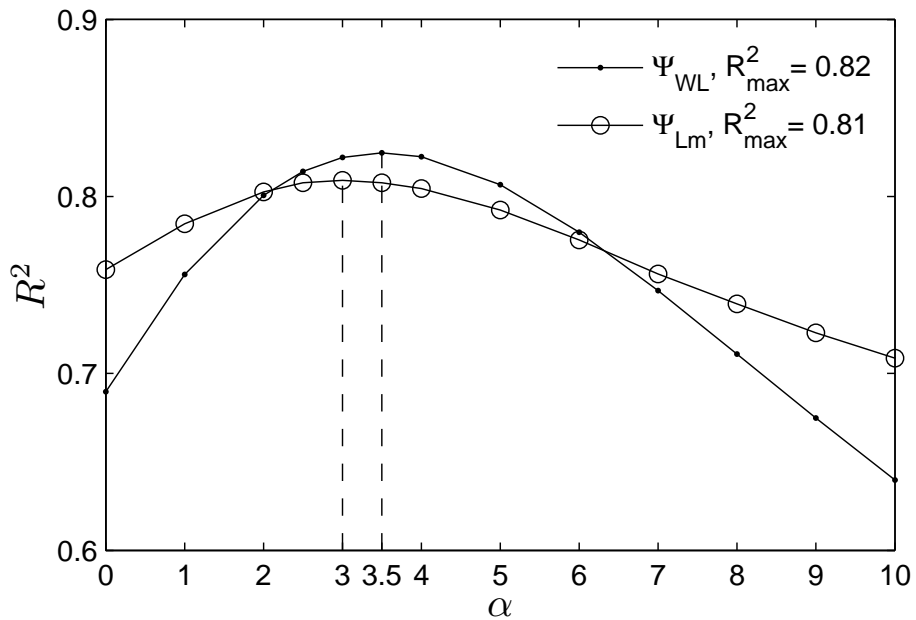


Figure 5.7: Sensitivity analysis of  $\alpha$  in Eqs. (2.27) and (2.28).



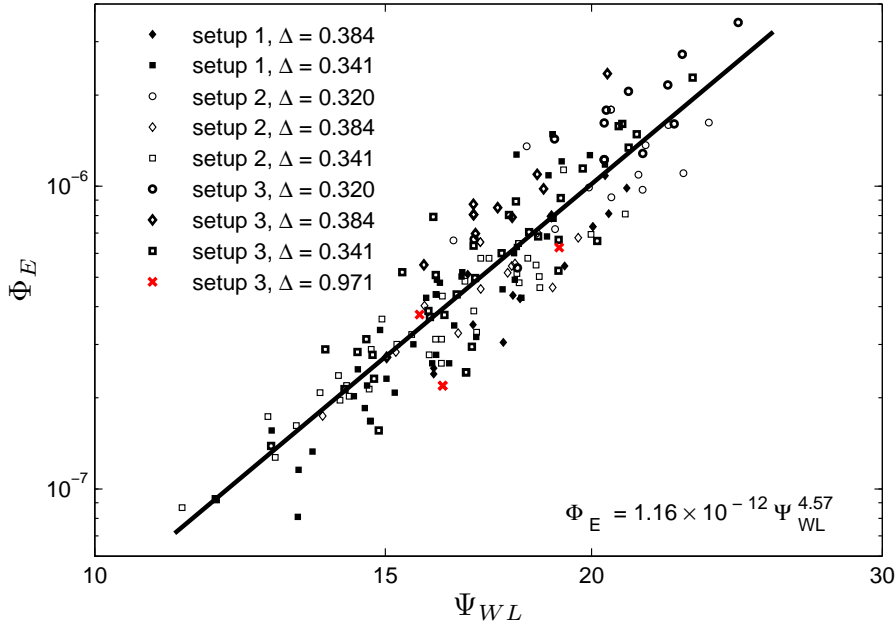


Figure 5.8: Measured  $\Psi_{WL}$  (with  $\alpha = 3.5$ ) versus measured  $\Phi_E$ .

Figure 5.8 shows the correlation between the modified [Jongeling et al.](#) stability parameter (with  $\alpha = 3.5$ ) and the dimensionless entrainment rate. The relationship between the modified stability parameter and the entrainment rate is expressed as follow:

$$\Phi_E = 1.16 \times 10^{-12} \Psi_{WL}^{4.57} \text{ for } 11 < \Psi_{WL} < 25 \quad (R^2 = 0.82, \alpha = 3.5) \quad (5.10)$$

From the analysis, it appears that the [Jongeling et al. \(2003\)](#) stability parameter is sufficient to quantify the flow forces on a bed. The results also confirm that the influence of stone density is well incorporated in the formula.

### 5.4.3 The Hofland stability parameter

Here, the original [Hofland](#) stability parameter was calculated using  $\alpha = 6$ . The analysis was based on all data sets (i.e., configuration 1, 2 & 3). The correlation between this stability parameter and the dimensionless entrainment rate is shown in Figure 5.9, showing a strong correlation between the two parameters. The stone transport formula based on the correlation analysis of the present data for  $\Psi_{Lm}$  is derived as:

$$\Phi_E = 1.15 \times 10^{-9} \Psi_{Lm}^{4.53} \text{ for } 2.5 < \Psi_{Lm} < 5.5 \quad (R^2 = 0.77, \alpha = 6) \quad (5.11)$$

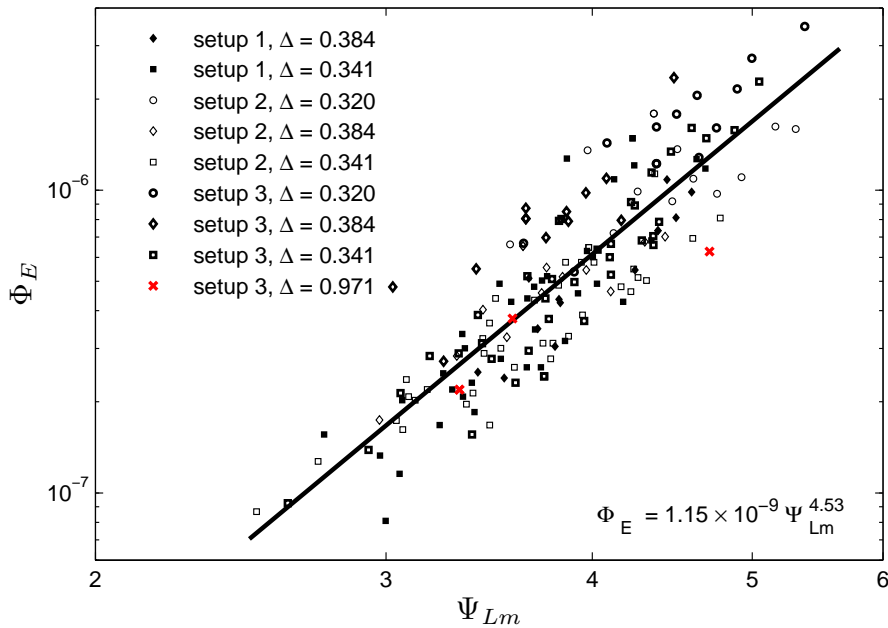


Figure 5.9: Measured  $\Psi_{Lm}$  (with  $\alpha = 6$ ) versus measured  $\Phi_E$ .

Next we examine the turbulence effect in the Hofland stability parameter. Several values of  $\alpha$  were tested. The analysis shows that the best correlation can be obtained when  $\alpha = 3$  is used (see Figure 5.7). The correlation between the modified Hofland stability (with  $\alpha = 3$ ) and the dimensionless entrainment rate is plotted in Figure 5.10. The transport formula for this stability parameter is written as:

$$\Phi_E = 1.90 \times 10^{-8} \Psi_{Lm}^{4.32} \text{ for } 1.3 < \Psi_{Lm} < 3.2 \quad (R^2 = 0.81, \alpha = 3) \quad (5.12)$$

## 5.5 Discussion

In the foregoing sections, the velocity and entrainment data obtained from the present experiment were analyzed. Our aims are to (i) evaluate the performance of the Shields (1936), the Jongeling et al. (2003), the Hofland (2005) and the newly proposed stability parameters, and (ii) establish robust stone transport formulae which can be used to predict bed damage. The present approach can be extended to the study of sediment transport provided that the movement of the sediment on the bed is accurately quantified for non-uniform flow conditions.

It is noted that the present data have certain advantages over the existing data. To the author's knowledge, of the few studies on stone transport, this study

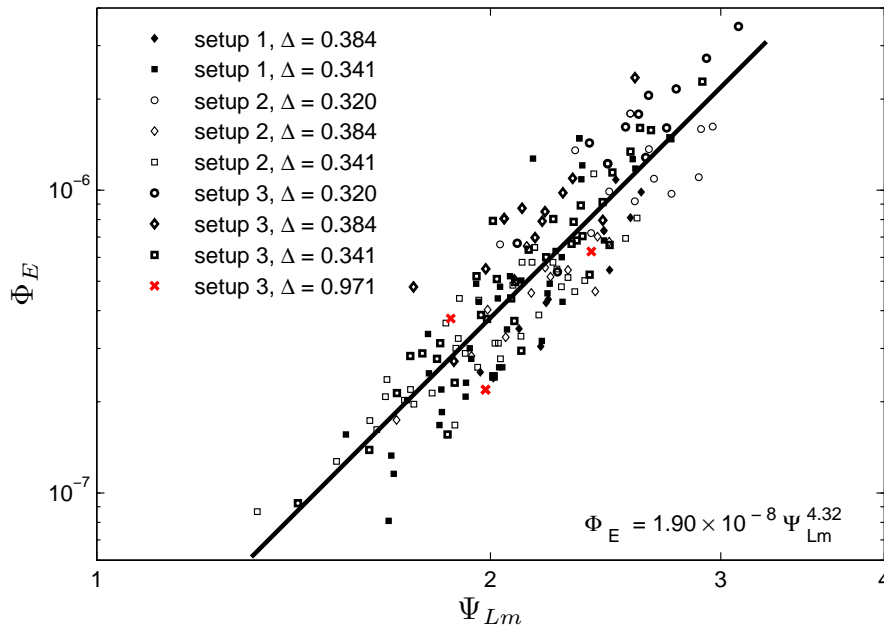


Figure 5.10: Measured  $\Psi_{Lm}$  (with  $\alpha = 3$ ) versus measured  $\Phi_E$ .

probably carried out the most detailed and accurate velocity measurements, especially in the inner region ( $z/h < 0.2$ ). With the LDV instrument, the velocity was measured very close to the bottom (3mm) with a small measuring volume, a high sampling frequency ( $f = 500\text{Hz}$ ) and no flow disturbance. In [Jongeling et al. \(2003\)](#) and [De Gunst \(1999\)](#), with the water depth varying from 25 to 50 cm, only (10 - 12) measuring points were used to measure velocity profiles (compared to (12 - 19) cm water depth and (19 - 25) measuring points in the present study). Velocity measurements were not even needed to formulate the stone transport formulae in the investigation of [Paintal \(1969, 1971\)](#) since the bed shear stress was calculated using the energy slope. In the present study, the entrainment tests were repeated four times. The entrainment rates obtained from the four runs were averaged to get a statistically reliable entrainment rate for the series.

### 5.5.1 Comparison of the stability parameters

The analysis presented in this chapter has quantitatively confirmed that the use of the bed shear stress as the only quantity representing the flow forces is not sufficient for non-uniform flow conditions. This explains the low correlation between the Shields stability parameter ( $\Psi_s$ ) and the dimensionless entrainment rate ( $\Phi_E$ ).

Conversely, the approaches that use the combination of velocity and turbu-

lence distributions over a certain water column above the bed perform well. Three stability parameters that use these approaches are the [Jongeling et al.](#) ( $\Psi_{WL}$ , average of the extreme forces), the [Hofland](#) ( $\Psi_{Lm}$ , maximum of the extreme forces) and the newly-developed ( $\Psi_{u-\sigma[u]}$ , weighting average of the extreme forces) parameters. A graphical comparison of the four stability parameters is given in Figure 5.11. In this figure,  $\langle x \rangle_H$  denotes a spatial average of  $x$  over a distance  $H$ .

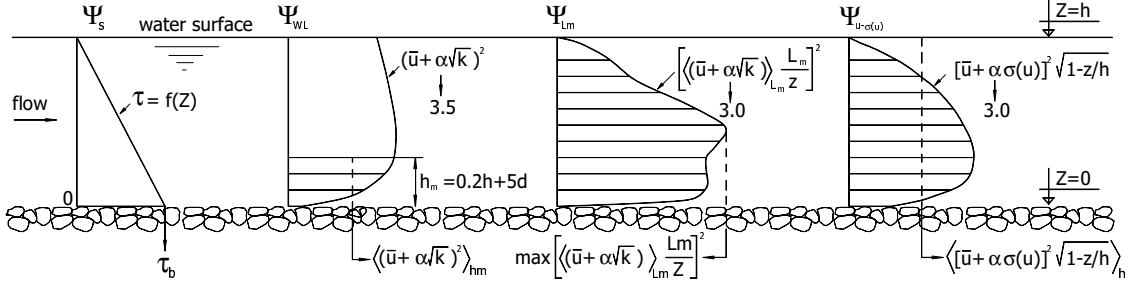


Figure 5.11: Typical distributions of the key parameters according to Eqs. (2.26), (2.27), (2.28) and (5.7).

The correlation analysis shows that the proposed stability parameter performs better than the stability parameters of [Jongeling et al. \(2003\)](#) and [Hofland \(2005\)](#) (i.e.,  $R^2 = 0.81$  vs.  $R^2 = 0.77$ ). The analysis later reveals that the difference in performance of the three stability parameters is not only due to the difference in quantifying the flow forces, but mainly because of the differences in quantifying turbulence (i.e.,  $\alpha$ ). Once appropriate values of the turbulence magnification  $\alpha$  are used, the three stability parameters perform similarly.

Surprisingly, the three approaches using the maximum ( $\Psi_{Lm}$ ), average ( $\Psi_{WL}$ ) and weighting average ( $\Psi_{u-\sigma[u]}$ ) of the extreme forces over a water column above the bed appear to give similar results. This can be explained by i) the insensitivity (of the correlation coefficient) to  $H/h$  (above 0.5) and  $\beta$  (Figure 5.2) and ii) the correlation between the maximum and the (weighting) average of the extreme forces.

It is noted that in the present analysis only the newly-proposed stability parameter can be directly calculated from the measured data. The stability parameters of [Jongeling et al. \(2003\)](#) and [Hofland \(2005\)](#) were calculated using the approximated turbulent kinematic energy discussed in Section 3.6.

### 5.5.2 Sensitivity analysis of key parameters

To evaluate the roles of velocity and turbulence, a sensitivity analysis of these quantities will be made for  $\Psi_{WL}$ ,  $\Psi_{Lm}$  and  $\Psi_{u-\sigma[u]}$  in Eqs. (5.10), (5.12) and (5.8), respectively. By alternatively changing the values of the measured velocity ( $u$ )

and the measured turbulence ( $k$  or  $\sigma[u]$ ) by a certain percentage, the corresponding values of  $\Psi_{WL}$ ,  $\Psi_{Lm}$  and  $\Psi_{u-\sigma[u]}$  can be calculated from Eqs. (2.27), (2.28) and (5.7), respectively. The calculated  $\Psi_{WL}$ ,  $\Psi_{Lm}$  and  $\Psi_{u-\sigma[u]}$  are then used to compute the corresponding entrainment rate using Eqs. (5.10), (5.12) and (5.8). These calculated quantities ( $x_o$ ) are then compared to the corresponding quantities ( $x$ ) computed from the originally (unchanged) measured velocity and turbulence. The analysis is presented in Figure 5.12 in which the relative error ( $\delta$ ) of quantity  $x$  is determined as

$$\delta x = \frac{\Delta x}{x} = \frac{x_o - x}{x} \times 100\% \quad (5.13)$$

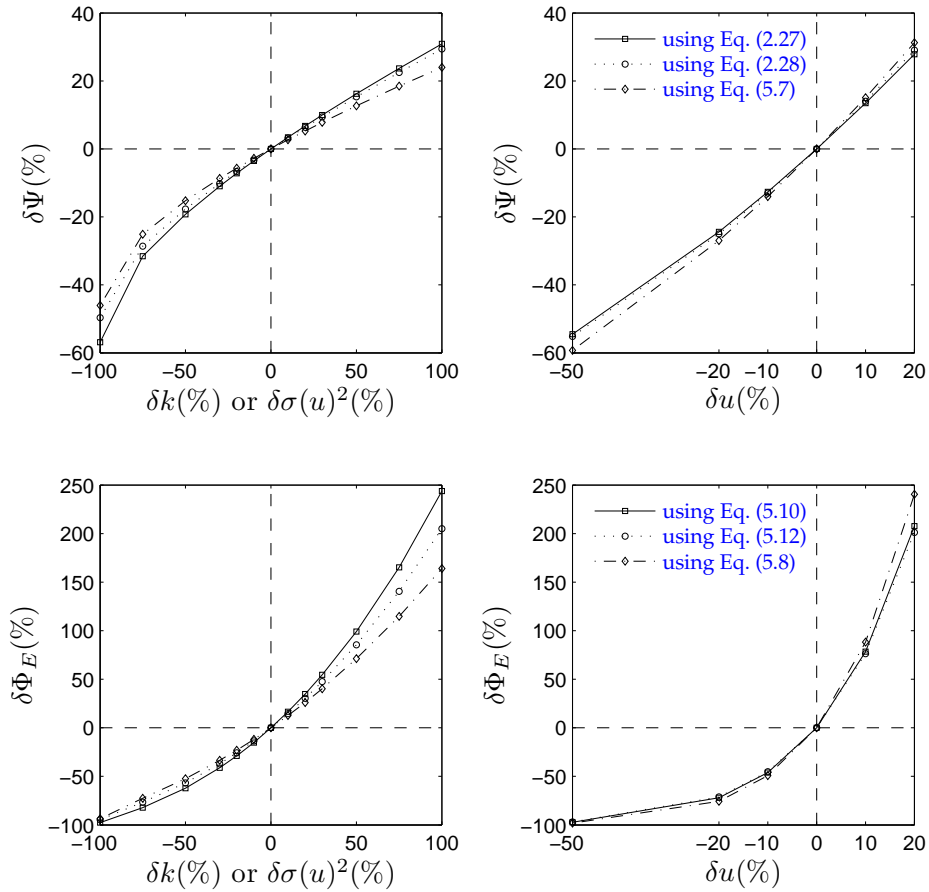


Figure 5.12: Sensitivity analysis of the velocity and turbulence to the bed damage. The  $\alpha$  values of 3.5, 3 and 3 are used in Eqs. (2.27), (2.28) and (5.7), respectively.

### 5.5.3 Entrainment correction

So far the measured stone entrainment rate obtained from the measurements has been used for the analysis. Hofland (2005), however, argues that the entrainment rate directly calculated from the numbers of stones that are removed from their colored strips will be underestimated because some entrained stones will deposit in their strip of origin. This underestimation should be corrected for in order to end up with quality that can be compared between different investigations. He proposed a method for the correction in which the strip width, the stone diameter and the probability distribution of the displacement lengths of the stones are used as the input. He assumes that the probability of a certain displacement length has exponential distribution (based on the finding of Nakagawa and Tsujimoto, 1980) and that the averaged displacement length is proportional to the stone diameter. For more detail on the method the reader is referred to Hofland (2005, Appendix D).

Next in this section an attempt will be made to apply Hofland's correction method to the present data. The relation between the measured ( $E_m$ ) and the corrected entrainment rate ( $E_c$ ) is expressed as (Hofland, 2005):

$$E_c = \frac{\tilde{L}}{1 - e^{-\tilde{L}}} E_m \quad (5.14)$$

in which  $\tilde{L}$  is the dimensionless strip width, expressed as the ratio of the strip width ( $L$ ) to the mean displacement length of the stones ( $\bar{l}$ ):

$$\tilde{L} = \frac{L}{\bar{l}} \quad (5.15)$$

Since the displacement lengths of the stones were not measured in our experiments, we will use the results from measurements by De Gunst (1999, next: DG) and the assumption that  $\bar{l} \propto d$  to determine  $\tilde{L}$  for the present data. The results will be checked using the visual observation from the experiments. From the fit analysis of the DG data on the displacement lengths, Hofland (2005) found that  $\tilde{L}$  is 1.51, leading to an estimate of  $E_c = 1.93E_m$  for the DG data. If we assume that  $\bar{l}/d$  is constant, we have

$$\frac{\bar{l}_H}{d_H} = \frac{\bar{l}_{DG}}{d_{DG}} \quad (5.16)$$

in which subscript  $H$  and  $DG$  denote the present data and the DG data,  $d$  is the stone diameter,  $d = d_{n50}$ . From Eqs. (5.15) and (5.16) we have

$$\frac{L_H}{d_H \tilde{L}_H} = \frac{L_{DG}}{d_{DG} \tilde{L}_{DG}} \quad (5.17)$$

With the strip widths  $L_H = L_{DG} = 10$  cm, the stone diameter  $d_{DG} = d_{n50} = 1.08$  cm,  $d_H = d_{n50} = 0.82$  cm and  $\tilde{L}_{DG} = 1.51$ , we have  $\tilde{L}_H = 1.99$ . Using Eq. (5.14) a corrected entrainment of  $E_c = 2.31E_m$  is found for the present data.

Though the corrected entrainment  $E_c$  is more physics based, especially when used to compare results from different investigations where various stone strips and diameters are used, it must be applied cautiously because of the assumptions involved. Measurements of the displacement lengths of the stones should be available in order to get a reliable correction for the entrainment. For instance, using  $\bar{l}/d = L/\tilde{L}d = 6.1$  from the DG measurements, the corrected entrainment is overestimated for the present data. In our experiments we observed that the stones were usually moved much farther: from few tens centimeters to few meters from their strip of origin. At the end of each test, more often than not, many stones were moved to the end of the flume which is 4 to 5 meters away from the first strip and 1 to 2 meters away from the last strip depending on the set-ups. Therefore, if we roughly estimate the mean displacement lengths of 50 cm, a corrected entrainment of  $E_c = 1.10E_m$  is found for the present data.

#### 5.5.4 Data comparison

In this section, the present data and those of [Jongeling et al. \(2003, next: WL\)](#) and [De Gunst \(1999\)](#) are compared. The WL and DG data were obtained directly from Figure 2.6 with the following quantities:  $\Psi_{WL}$  (with  $\alpha = 6$ ),  $\Psi_{Lm}$  (with  $\alpha = 6$ ) and  $\Phi_{Ec}$ . This information is not enough for comparison using the newly-developed stability parameter or the corrected stability parameters of [Jongeling et al. \(2003\)](#) and [Hofland \(2005\)](#). The comparison will be made for both the measured entrainment rate ( $\Phi_{Em}$ ) and the corrected entrainment rate ( $\Phi_{Ec}$ ). These values are determined as follows:

For the corrected entrainment rate of

- WL:  $\Phi_{EcWL}$ , obtained directly from Figure 2.6.
- DG:  $\Phi_{EcDG}$ , obtained directly from Figure 2.6.
- The present data:  $\Phi_{EcH} = 1.10\Phi_{EmH}$ .

For the measured entrainment rate of

- WL:  $\Phi_{EmWL} = \Phi_{EcWL}/2.83$  ([Hofland, 2005](#), page 149).
- DG:  $\Phi_{EmDG} = \Phi_{EcDG}/1.93$  ([Hofland, 2005](#), page 149).
- The present data:  $\Phi_{EmH}$ , obtained directly from the measurements.

The comparison is plotted in Figure 5.13 (for  $\Phi_{Em}$ ) and 5.14 (for  $\Phi_{Ec}$ ), showing a much larger scatter level in the WL and DG data. It appears that the present data had higher values of the stability parameters compared to those in the WL

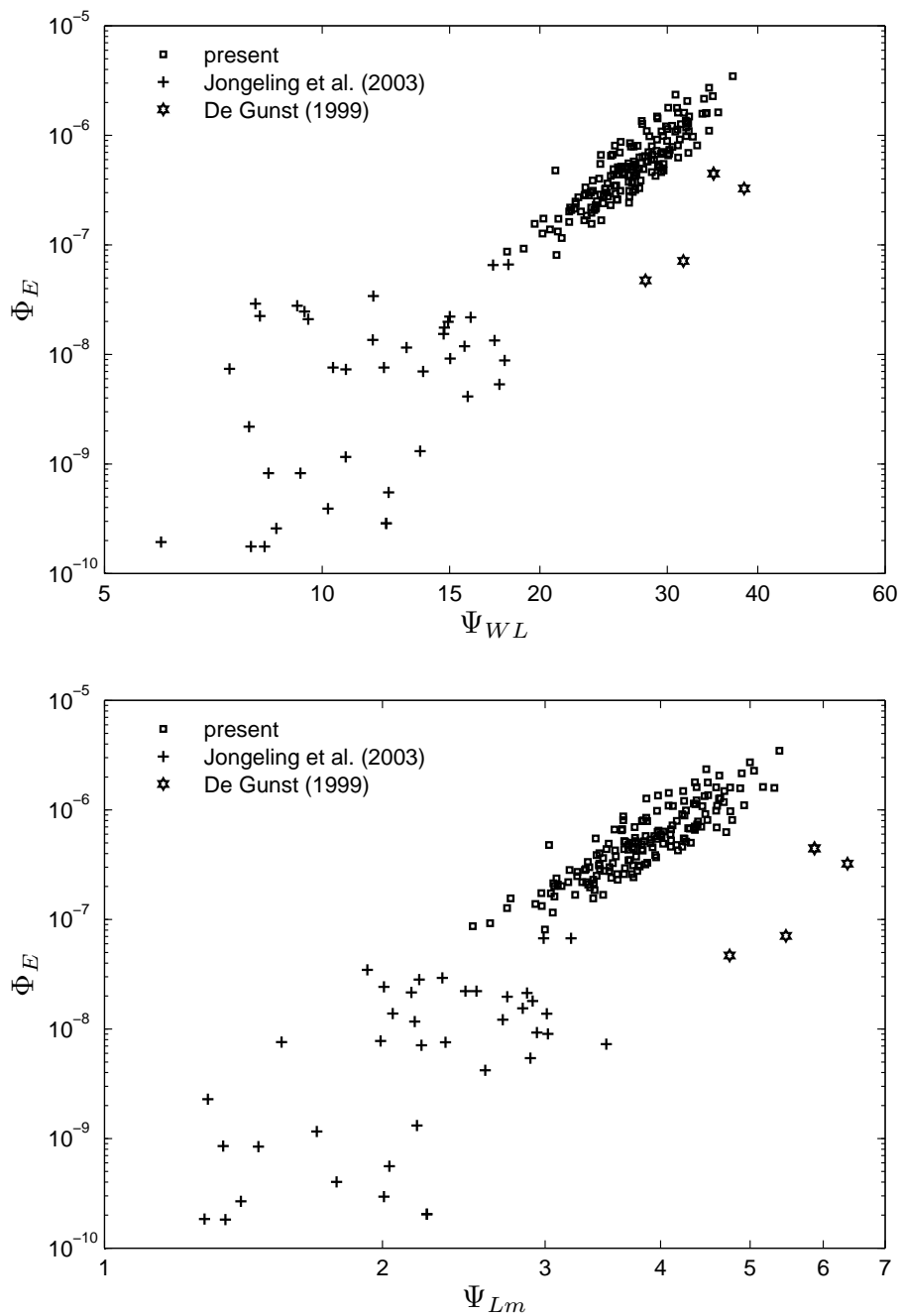


Figure 5.13: Data comparison. The  $\alpha$  value of 6 was used for both  $\Psi_{WL}$  (top) and  $\Psi_{Lm}$  (bottom). The comparison was made for the measured entrainment data, i.e.  $\Phi_E \equiv \Phi_{Em}$ .



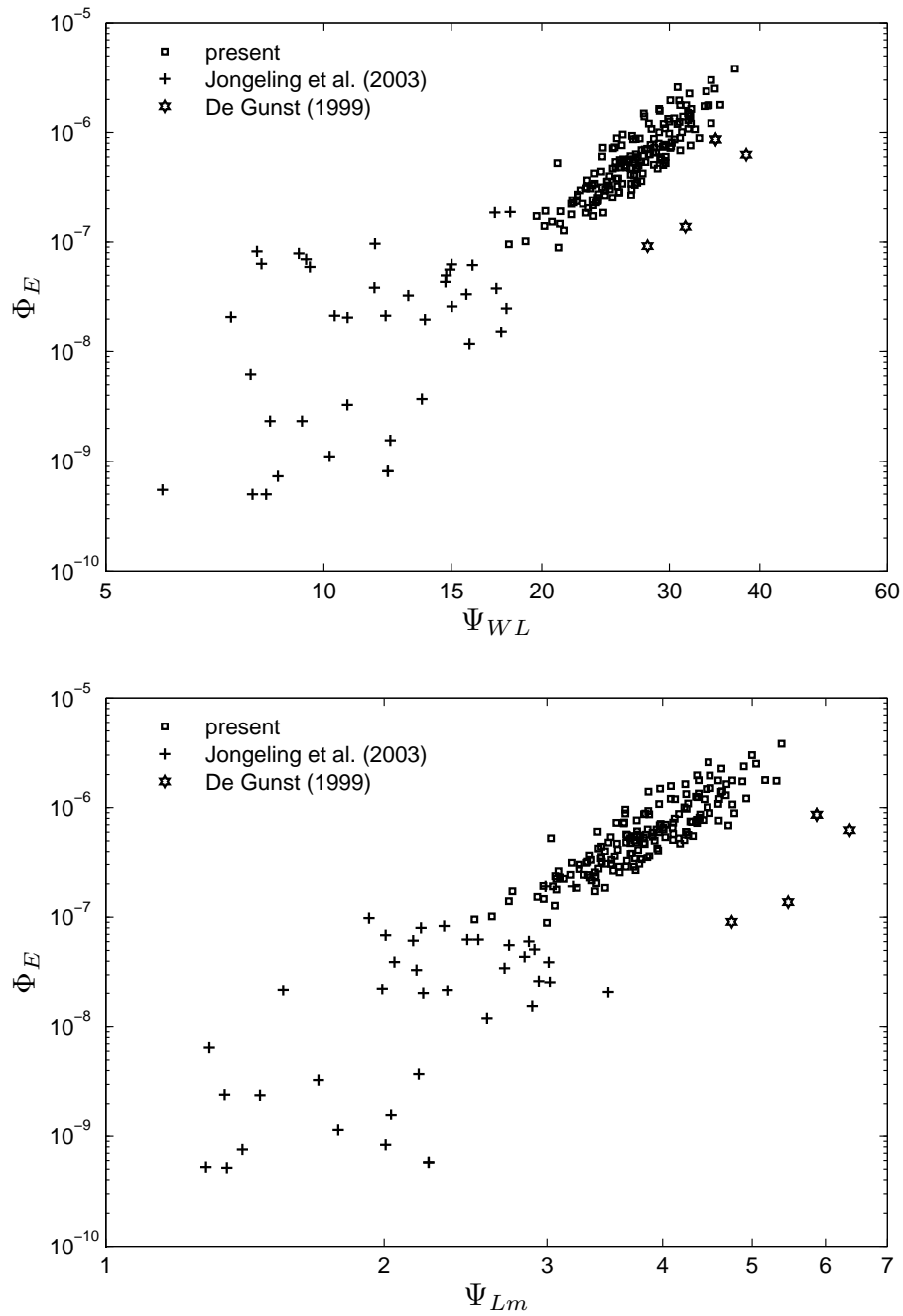


Figure 5.14: Data comparison. The  $\alpha$  value of 6 was used for both  $\Psi_{WL}$  (top) and  $\Psi_{Lm}$  (bottom). The comparison was made for the corrected entrainment data, i.e.  $\Phi_E \equiv \Phi_{Ec}$ .

data, resulting in the larger entrainment rate. For both comparisons the present data are in good agreement with the WL and DG data. The comparison for the corrected entrainment rate shows less scatter for the entire data set. From Figures 5.13 and 5.14 we can conclude that Eqs. (5.8), (5.10) and (5.12) can also be used to predict entrainment rate outside the range of the present experiment, i.e. at a much lower entrainment rate ( $\Phi_E$  of  $10^{-9}$ ).

## 5.6 Conclusions

From the analysis presented in this chapter, the following conclusions can be drawn. Because (i) a variety of flow conditions is used in the present experiments and (ii) the present data are in good agreement with those of Jongeling et al. (2003) and De Gunst (1999), which used different flow configurations, stone sizes and densities, we believe that the present results are representative for general bed protections.

The analysis reported herein indicates that the Shields stability parameter is not sufficient for presenting the flow forces acting on the bed in non-uniform flow. The correlation of the Shields stability parameter to the entrainment deteriorates when the flow is more non-uniform. Conventional turbulence correction for non-uniform flow should not be used as it does not physically explain the influence of turbulence source from the water column above the bed. In non-uniform flow, a different approach should be used to quantify the flow forces acting on the bed.

The formulation of the newly-proposed stability parameter has physically explained and quantitatively described the impact of flow (velocity and turbulence) on stone stability. This provides valuable insight into the understanding of the influence of the different flow quantities on stone stability. The high correlation of the proposed stability parameter [Eq. (5.6)] to the entrainment rate for high water column indicates the role of large-scale flow structures. This confirms the finding by Hofland (2005) about the responsibility of large flow structures to stone stability. Based on the physical analysis and practical considerations, the final expression for the new stability parameter was formulated, expressed as Eq. (5.7). This stability parameter properly quantifies the flow forces acting on the bed.

For the first time since it was proposed by Jongeling et al. (2003), the approach that use a combination of velocity and turbulence distributions to quantify the flow forces is verified by reliable data. The analysis indicates that different turbulence factors should be used for Jongeling et al. ( $\alpha = 3.5$ ) and Hofland ( $\alpha = 3.0$ ) stability parameters instead of  $\alpha = 6$ . The proposed stability parameter and the modified stability parameters of Jongeling et al. (2003) and Hofland (2005) perform similarly for the present data. This is explained by the insensitivity (of the correlation coefficient) to  $H/h$  (above 0.5) and  $\beta$  (Figure 5.2) and probably the correlation between the maximum and the (weighting) average of the extreme

forces.

For the first time, the actual relationship between the flow and the stone stability has been established for non-uniform flow. This relationship is described by stone transport formulae developed using the newly-proposed stability parameter and the modified stability parameters of [Jongeling et al. \(2003\)](#) and [Hofland \(2005\)](#), namely Eqs. (5.8), (5.10) and (5.12), respectively. These formulae can be used to predict the damage of bed protections. Although similar correlation is found for the three stone transport formulae, Eq. (5.8) was developed using purely measured data while Eqs. (5.10) and (5.12) were based on the approximated turbulent kinematic energy data. Therefore, Eq. (5.8) is recommended with the alternatives being Eqs. (5.10) and (5.12) when only velocity  $u$  and turbulent kinematic energy  $k$  are available.

Since a good collapse of the data is obtained for a variety of stone densities (varying from 1320 to 1970 kg/m<sup>3</sup>), the influence of stone density is well incorporated into the formulae. Therefore, the newly-developed stone transport formulae are likely to be valid for other bed materials with different densities, including natural stones.



# Chapter 6

## Estimation of stone entrainment using numerical flow modeling

### 6.1 Introduction

Previous chapters have shown that the flow forces acting on a bed and the bed response (damage) have a strong correlation. These relations have been established in the form of Eqs. (5.8), (5.10) and (5.12). Those relations can be used to predict bed damage provided the velocity and turbulence distributions of the flow are available. Since the capabilities of numerical flow models have been improved significantly, the use of such models to predict bed damage becomes interesting. This would make the use of expensive physical models obsolete.

In this chapter, the use of the outputs of a numerical flow modeling is evaluated. First, the governing equations of an incompressible, viscous Newtonian fluid are presented and the numerical method that is to be used to model the flow is assessed (Appendix C). As a Large Eddy Simulation (LES) approach is expensive in terms of computation effort and we are interested in a time-averaged representation of the flow, the use of a Reynolds-Averaged Navier-Stokes (RANS) model is preferred. The  $k - \varepsilon$  model is used as a closure to determine the turbulence viscosity.

Second, a Navier-Stokes solver with  $k - \varepsilon$  model was utilized to simulate the flow in our experiments. A numerical model has been set-up using the Deft incompressible flow solver. The numerical flow outputs were used to determine the stability parameters and the bed damage. The available experimental data were then used as the basis for the evaluation. The aim of this chapter is to judge the applicability of numerical computation to predict bed damage.

This chapter is structured as follows. The flow conditions that were modeled are presented in Section 6.2. This is followed by the description of the numerical flow model (Section 6.3) and the computation results (Section 6.4) where the calculated flow quantities (velocity and turbulence distributions) are compared to the measurements. Then, in Section 6.5 the use of numerical outputs to calculate

the bed damage is discussed. The chapter ends with conclusions and recommendations in Section 6.6. Part of this chapter was published as [Hoan et al. \(2008\)](#).

## 6.2 Flow conditions

In order to check the applicability of numerical computation for predicting bed damage, the measured data of velocity and stone entrainment in our experiments were used. These data are systematically analyzed in Chapters 4 and 5. In this chapter, the flow conditions used in those experiments will be simulated using numerical flow modeling. It consists of 37 flow conditions which are summarized in Table 6.1. These are the flows measured at profile 1 (straight part of the flume) in the experiments and are referred to as *the studied flows* from now on. The flow configurations are described in Figures 3.1 and 3.2.

Table 6.1: The flow conditions that are to be modeled.

	Set-up 1 ( $\alpha = 3^0$ )					Set-up 2 ( $\alpha = 5^0$ )					Set-up 3 ( $\alpha = 7^0$ )			
	Q [l/s]	h [cm]	Re [ $10^4$ ]	Fr [-]		Q [l/s]	h [cm]	Re [ $10^4$ ]	Fr [-]		Q [l/s]	h [cm]	Re [ $10^4$ ]	Fr [-]
1AR	22.0	11.7	6.2	0.50	2AR	22.0	11.6	6.2	0.51	3AR	22.0	12.1	6.2	0.47
1BR	20.0	12.0	5.7	0.44	2BR	20.0	12.0	5.7	0.44	3BR	20.0	12.0	5.7	0.44
1CR	23.0	13.0	6.5	0.45	2CR	23.0	12.8	6.5	0.46	3CR	23.0	12.9	6.5	0.45
1DR	26.5	13.9	7.5	0.47	2DR	26.5	13.8	7.5	0.47	3DR	26.5	13.8	7.5	0.47
1ER	24.0	13.9	6.8	0.42	2ER	24.0	13.2	6.8	0.46	3ER	24.0	14.1	6.8	0.41
1FR	27.0	15.0	7.6	0.43	2FR	27.0	14.4	7.6	0.45	3FR	27.0	14.9	7.6	0.43
1GR	31.0	15.7	8.8	0.46	2GR	31.0	16.0	8.8	0.44	3GR	31.0	15.7	8.8	0.46
1HR	28.0	15.8	7.9	0.41	2HR	28.0	15.9	7.9	0.40	3HR	28.0	15.8	7.9	0.41
1IR	31.5	17.0	8.9	0.41	2IR	31.5	16.9	8.9	0.41	3IR	31.5	16.9	8.9	0.41
1JR	35.5	17.9	10.0	0.43	2JR	35.5	17.5	10.0	0.44	3JR	35.5	17.5	10.0	0.44
1KR	32.0	18.0	9.1	0.38	2KR	32.0	17.8	9.1	0.40	3KR	32.0	17.7	9.1	0.39
1LR	35.5	19.0	10.0	0.39	2LR	35.5	18.6	10.0	0.41	3LR	35.5	18.3	10.0	0.41
										3MR	36.0	12.4	10.2	0.75

The velocity and stone entrainment data are available at several measuring profiles for each series. The computational outputs at the corresponding profiles will be analyzed and compared to the measurements. The location of those measuring profiles is depicted in Figures 3.2 and 3.3. For the information on the hydraulic conditions at all the measuring profiles, the reader is referred to Table 3.3.

## 6.3 Numerical model set-up

The turbulent flows through the flume have been simulated using the Deft incompressible flow solver, formerly known as ISNaS - Information System for Navier-Stokes equations. The ISNaS-project was initiated by the National Aerospace Laboratory NLR - the Netherlands, Delft University of Technology, Delft

Hydraulics and University of Twente. With the Deft code it is possible to compute complex turbulent flows in two or three dimensions.

The Deft code has implemented different turbulence models, among others the standard  $k - \varepsilon$  model and RNG  $k - \varepsilon$  model. Both turbulence models were employed in the early stage of modeling process. The turbulence model that gives better results was then used for all simulations. For the relevant information on the Deft package, the reader is referred to [Mynett et al. \(1991\)](#), [Segal et al. \(1998\)](#), [Segal et al. \(2000\)](#) and [Segal \(2000\)](#). A complete description of typical Deft input files used in our simulations is presented in Appendix C.

The applicability of the model for predicting bed damage was investigated by running the model with input that was based on the experiments. Since we are mainly interested in the output which is then used as input to predict bed damage, we focus on the velocity and turbulence profiles. In order to assess the model results properly, we will compare the computation results (i.e., velocity and turbulence distributions) with the measurements. The deviation of the simulated flow field from the measurements resulted in the differences between the calculated and measured bed damage. This is discussed in the next sections.

### 6.3.1 Grid

Due to the symmetry, only one half of the flume is considered. The model grid measures an area of 11.5 m long ( $x$ ), 0.25 m wide ( $y$ ) and 0.12 to 0.19 m high ( $z$ ) depending on flow conditions. The geometry of the flume set-up leads to the choice of multi block approach. In Deft, it is the task of the multi-block method to couple the solutions of the different subdomains in such a way that the correct solution on the whole domain is obtained ([Segal et al., 2000](#)). Three blocks are used to describe the flume geometry as depicted in Figure 6.1.

Table 6.2: Grid refinement test for set-up 2.

	$nx_1$	$\Delta x_1$	$nx_2$	$\Delta x_2$	$nx_3$	$\Delta x_3$	$ny$	$\Delta y$	$nz$	$\Delta z$
	[-]	[cm]	[-]	[cm]	[-]	[cm]	[-]	[cm]	[-]	[cm]
Grid A	87	4.35-17.39	40	4.25	27	5.93	5	5.00	7	1.18-2.36
Grid B	130	2.91-11.65	60	2.83	40	4.00	8	3.10	10	0.83-1.66
Grid C	160	2.37-9.46	75	2.27	50	3.20	10	2.50	13	0.64-1.28

The flow simulated by numerical model depends, amongst others, on the grid size. The computational time increases with decreasing grid cell size for two reasons: the computational time increases linearly with the amount of grid cells, and the computational time step  $\Delta t$  decreases with decreasing grid cell size. The optimal grid design is therefore a compromise in which all relevant processes are

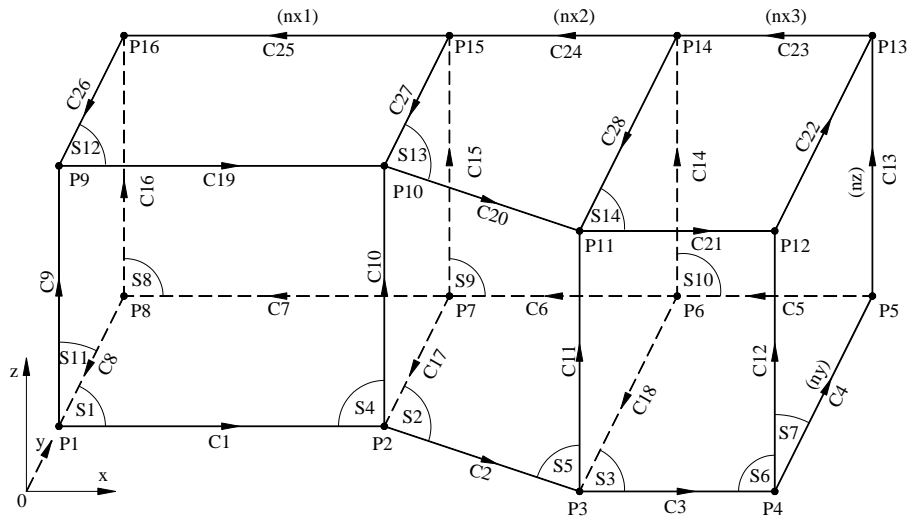


Figure 6.1: Definition region of the model set-up.

accurately numerically simulated while the computational time remains acceptable (Van Maren, 2004). Therefore, computations were performed to examine the grid dependence of the solutions. The standard  $k - \varepsilon$  model was employed. Flow condition 2AR was chosen for the test. Three grids of  $154 \times 5 \times 7$  (A),  $230 \times 8 \times 10$  (B) and  $285 \times 10 \times 13$  (C) cells were used (see Table 6.2). In Table 6.2,  $nx_i$  and  $\Delta x_i$  are the number of cells and the grid size of block  $i$  ( $i = 1$  to 3) in  $x$ -direction, respectively. The same holds for  $ny$ ,  $\Delta y$ ,  $nz$  and  $\Delta z$ . The mesh of the numerical model was made using a structured grid with refinement in regions where steep velocity gradients occur.

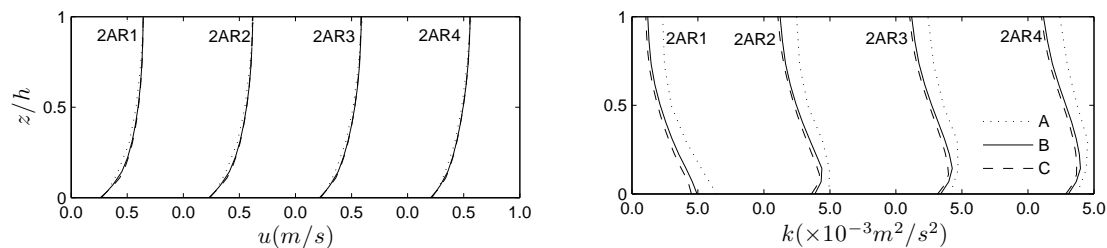


Figure 6.2: Grid refinement test (velocity and turbulence).

The test results are depicted in Figure 6.2 for the streamwise velocity ( $u$ ) and the turbulence intensity ( $k$ ) at profile 1 to 4 (see Figure 3.3 for profile location). The test clearly shows that unlike the turbulence intensity the velocity is already grid independent on grid A ( $154 \times 5 \times 7$ ). Further grid refinement was not pursued,



because it is believed that it gives smaller differences than those simulated by the  $k - \varepsilon$  model. Hence, grid B (230x8x10) is considered optimal.

Table 6.3: Grid refinement for the three flume set-ups. The grid size  $\Delta z$  may vary due to water depth change.

	$nx_1$	$\Delta x_1$	$nx_2$	$\Delta x_2$	$nx_3$	$\Delta x_3$	$ny$	$\Delta y$	$nz$	$\Delta z$
	[-]	[cm]	[-]	[cm]	[-]	[cm]	[-]	[cm]	[-]	[cm]
set-up 1	130	2.70-10.79	100	2.90	35	2.86	8	3.10	10	0.83-1.66
set-up 2	130	2.91-11.65	60	2.83	40	4.00	8	3.10	10	0.83-1.66
set-up 3	130	2.91-11.65	45	2.67	50	4.20	8	3.10	10	0.83-1.66

For flume set-up 2, grid B (230x8x10) was employed for all simulations (2AR to 2LR). For the other flume set-ups (i.e., set-up 1 & 3), different cells were chosen so that the grid sizes are more or less the same as those of grid B. That means the grid size in flow direction ( $\Delta x$ ) gradually decreases from approx. 12 cm to 3 cm in the first straight part of the flume<sup>1</sup> (block 1). The grid size  $\Delta x$  of approx. (2.7 - 2.9) cm is unchanged along the expansion (block 2). An equal grid size  $\Delta x$  of (2.9 - 4.2) cm are implemented in the last part of the flume (block 3). The number of cells in vertical direction ( $z$ ) is 10 for all set-ups and flow conditions. The grid size  $\Delta z$  gradually increases from the bottom to the surface in a way that the last cell is 2 times the first cell. The number of cells in transverse direction ( $y$ ) is 8, resulting in a grid size  $\Delta y$  of approx. 3.1 cm. The actual grids used for each set-up are presented in Table 6.3. A detailed description of the grid is presented in Appendix C.

### 6.3.2 Boundary condition

Figure 6.1 shows the sketch of the domain configuration. Boundary S1, S2, S3 represent the flume bottom. Surface S4, S5, S6 represent the flume side wall. Surface S8, S9, S10 represent the vertical symmetric plan of the flume. Surface S12, S13, S14 model the free surface with free-slip condition. The flume inlet and outlet are represented by surface S11 and S7, respectively.

The inlet profiles for the velocity and turbulence quantities can be regarded as uniform distributions. This close-to-the-experimental-condition assumption was employed in the validation simulation. Because the velocity distribution approaches to logarithmic (or parabolic) form along the flume, to speed up the computation a parabolic velocity distribution was assumed at the inlet in the calibration and actual simulations. In this case, the velocity distribution has the following form:

<sup>1</sup>The length of this part is 7.6m (set-up 1) and 8.2m (set-up 2 and 3).

$$u(z) = az^2 \quad (6.1)$$

where  $a$  is a constant. The discharge ( $Q$ ) at the flume entrance can then be determined as

$$Q = \int_0^h Bu(z)dz = B \int_0^h az^2 dz = B \frac{ah^3}{3} \quad (6.2)$$

where  $B$  is the flume width at the inlet and  $h$  is the water depth. From Eq. (6.2) one has

$$a = \frac{3Q}{Bh^3} \quad (6.3)$$

Thus, velocity distribution at the inlet can be expressed as:

$$u(z) = \frac{3Qz^2}{Bh^3} \quad (6.4)$$

This inlet condition is prescribed in routine *usfunb.f* (see Appendix C). The flow at the end of the flume is described as *outflow* in Deft which prescribes the least restrictive outflow boundary condition, viz. stress equals zero at the boundary. In this case the boundary condition can be interpreted as pressure zero and no restriction to the tangential velocity component (Segal et al., 2000). The flume bottom is described as a rough surface. As the roughness influences both the velocity and turbulence distributions, special attention was paid to choose a correct modeling of the bottom roughness in the calibration simulations. The free water surface was modeled as a rigid lid with free-slip conditions. The flume side wall was modeled as smooth wall in the validation simulation. In the calibration step different roughness values were applied to the side walls to gain better velocity distributions. In the numerical model, the middle of the flume becomes a symmetric boundary condition where normal component of the velocity is zero and the shear stress is zero.

### 6.3.3 Model validation

In the validation stage the computation was made without any tuning of model coefficients. This is done to check whether the model is able to give a good prediction of the the studied flow configuration (Stelling and Booij, 1999). Validation was performed based on the measured data of flow condition 1AR. The numerical outputs were then compared with the measurements.

In the validation simulation, the bottom roughness was described as it is, i.e.,  $k_{sb} = 0.008$  m (stone diameter). The velocity and turbulence are uniformly distributed at the inlet. The side wall was described as *smooth*. The free surface was

modeled as a rigid lid with free-slip condition. The flow at the end of the flume was modeled as *outflow*. The flume middle was modeled as symmetric boundary condition. Both standard  $k - \varepsilon$  and RNG  $k - \varepsilon$  turbulence models were employed. Different time-step  $\Delta t$  and end time  $t_{end}$  were tried. The time-step must satisfy the Courant condition (Wilcox, 1994):

$$\frac{\Delta t}{\Delta l} u < 1 \quad (6.5)$$

with  $\Delta l$  as grid size in flow direction. After several trials, a time-step  $\Delta t$  of 0.008 s was chosen. In all cases the computation converged at an end time less than 20 s. In the computation, an end time  $t_{end}$  of 30 s was chosen, ensuring that the computation was ended by convergence criterion. Figure 6.3 shows the computational results with the standard  $k - \varepsilon$  model.

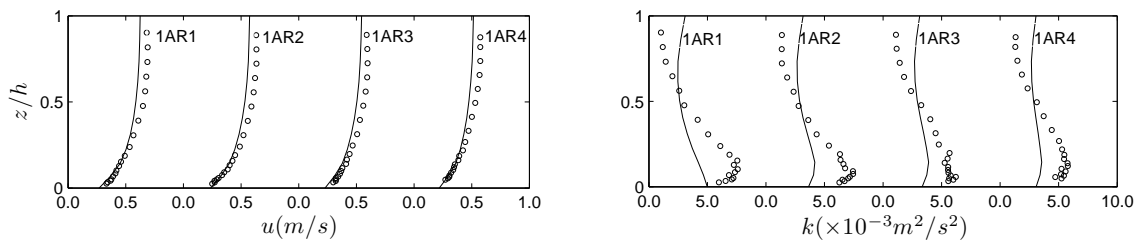


Figure 6.3: Profiles of calculated (lines) and measured (circles) flow parameters over the flume with flow condition 1AR.

The results have shown that the standard  $k - \varepsilon$  and RNG  $k - \varepsilon$  turbulence models give similar results. The velocity distributions were predicted reasonably compared to the measured data though in the upper region ( $z/h > 0.5$ ) the velocity is still underestimated. This could be attributed to the prescription of the boundary conditions of the surface and the side walls. In reality the side walls are not completely smooth. As a result, the flow is blocked near the side walls and hence concentrates more to the middle region. This makes the velocity near the flume center become larger. By adding roughness to the side wall, better velocity distributions are expected. The turbulence intensity in the upper region ( $z/h > 0.5$ ) is rather high mainly because of the prescription of the free-slip condition at the surface. Turbulence is underestimated in the lower region ( $z/h < 0.4$ ) but the distribution shows a similar shape as the measurements. A tuning of the bottom roughness may result in a better prediction of the turbulence near the bottom.

In short, the validation simulations have showed that by employing the  $k - \varepsilon$  turbulence model, the Deft package should be able to model the studied flows. The bottom and side wall roughnesses are the main coefficients to be tuned in the calibration stage. The prescription of the boundary condition at the free surface

needs to be modified to get better velocity and turbulence distributions in the upper region.

### 6.3.4 Model calibration and verification

In order to accurately reproduce physical phenomena, the model needs to be calibrated. Calibration is the process of tuning the model parameter settings in order to get the outputs as closely as possible to the measured data; for hydrodynamic modeling this amounts to the variation of model parameters until the modeled values of e.g. flow velocity, turbulence intensity compare satisfactory with the measured values. Calibration was performed based on the measured data of flow condition 1AR, 2AR, 3AR, 1FR, 2FR and 3FR (which involve all flume set-ups and different water depths). After the calibration, verification is needed to ensure that the model indeed accurately describes these physical phenomena using an additional data set. In the present study, verification process is automatically done when comparing the numerical outputs with the measurements (Section 6.4).

The calibration process primarily included the adjustment of bottom and side-wall roughnesses until good agreement was obtained between the simulated and measured velocity and turbulence intensity distributions. The velocity at the inlet was assumed to have a parabolic distribution as described in Eq. (6.4). The roughness values of the bottom and side wall were tested systematically. Because the measurements have shown that turbulent kinetic energy near free surface in most cases is approximately  $0.9 \times 10^{-3} \text{ m}^2/\text{s}^2$ , this value was used to prescribe turbulence at the free surface in the model. Because the standard  $k - \varepsilon$  and RNG  $k - \varepsilon$  turbulence models perform similarly for the studied flow configuration, the former was mainly used in the calibration process. Once the model had been calibrated (based on the standard  $k - \varepsilon$ ), the RNG  $k - \varepsilon$  model was employed for comparison.

Best results in terms of velocity and turbulence distributions can be obtained when the following parameter settings are used. Bottom roughness  $k_{sb} = 0.02 \text{ m}$  (i.e.,  $k_{sb} \approx 2d$  with  $d$  is stone diameter), side wall roughness  $k_{sw} = 0.005 \text{ m}$ , the velocity condition at the free surface is prescribed as free-slip while turbulent kinetic energy  $k = 0.9 \times 10^{-3} \text{ m}^2/\text{s}^2$ . After the calibration, the standard  $k - \varepsilon$  and RNG  $k - \varepsilon$  turbulence models also give similar results (see Figure 6.4). The standard  $k - \varepsilon$  model, however, gives little better turbulence results near the bottom ( $z/h < 0.4$ ) in addition to less computation time. The standard  $k - \varepsilon$  model, therefore, was used in all simulations.

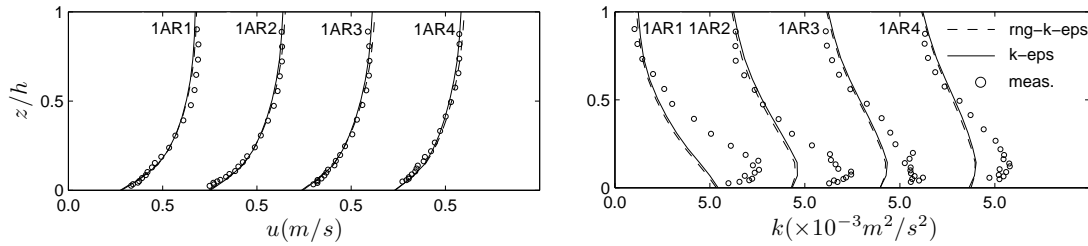


Figure 6.4: Comparison between the standard  $k - \epsilon$  and RNG  $k - \epsilon$  model.

## 6.4 Computation results

In this section, the outputs (velocity and turbulence intensity) of the numerical modeling using the Deft package are presented and discussed. The tuned coefficients and parameter settings of the model obtained from the calibration process were consistently used for all simulations. Since the number of flow conditions is larger, only typical results will be presented as examples of the outputs of the standard  $k - \epsilon$  model. For the comparison between calculations and measurements of all flow conditions, the reader is referred to Appendix B.

The overall results have shown that the model performance is dependant on the Reynolds number, i.e., the lower the Reynolds number, the better the computation results (especially with the turbulence intensity). Better computation outputs are also found for the flume set-up with smaller expansion angle ( $\alpha$ ). The influence of the Froude number is not clearly seen in the computation due to the small variation of the Froude numbers in the flow conditions ( $0.38 \leq Fr \leq 0.51$ ). For one special flow condition (3MR) where the Reynolds and Froude numbers are rather high ( $Re = 10.2 \times 10^4, Fr = 0.75$ ), the model performance is poor, especially at the expansion region (see Figure B.7).

Figure 6.5 shows the calculated and measured profiles of  $u$  and  $k$  for the three set-ups with flow condition B and L (i.e., 1BR, 2BR, 3BR, 1LR, 2LR and 3LR) as examples of the computation results. These two sets of flow conditions represent the smallest (B with  $Re = 5.7 \times 10^4, h = 12$  cm) and largest (L with  $Re = 10.0 \times 10^4, h = 19$  cm) Reynolds numbers and water depths. The mean flow is calculated rather well while the turbulence intensity is reproduced reasonably. Turbulence intensity is underestimated in the bottom region ( $z/h < 0.4$ ). These hold for both the flow in the straight part (profile 1) and the flow along the expansion (profile 2 to 4). Similar results are also found for the other flow conditions. In general, the Deft code models the flow very well (both at before and along the expansion). A good flow field calculation is expected to give a good stability parameter calculation. However, a small variation in the values of the stability parameter is enhanced in the resulting damage. This is examined in the next section.

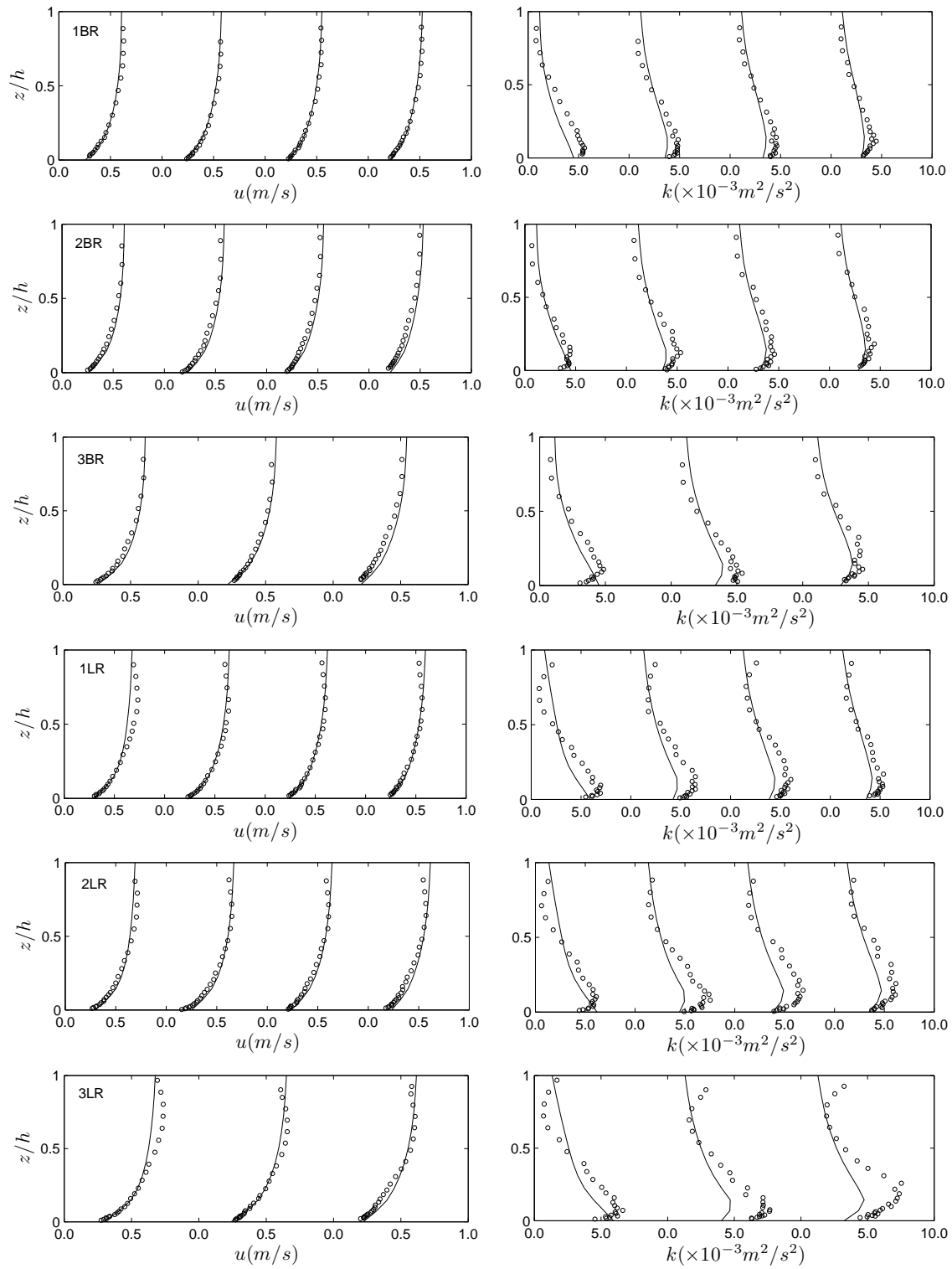


Figure 6.5: Comparison of calculations (lines) and measurements (circles). From top to bottom: flow condition 1BR, 2BR, 3BR, 1LR, 2LR and 3LR. The results at profile 1 to 4 are plotted from left to right.

## 6.5 Estimation of bed damage

Because the  $k - \varepsilon$  model only gives values for  $u$ ,  $k$ ,  $\varepsilon$  and  $p$ , the ratios  $\sigma(u)^2 : \sigma(v)^2 : \sigma(w)^2$  are unknown. Eq. (5.8) requires the values of  $u$  and  $\sigma(u)$  and is therefore not applicable for calculating the bed damage using  $k - \varepsilon$  model outputs. Eqs. (5.10) and (5.12), which require the values of  $u$  and  $k$ , were used for the bed damage estimation and are rewritten as below.

$$\Phi_E = 1.16 \times 10^{-12} \Psi_{WL}^{4.57} \text{ for } 11 < \Psi_{WL} < 25 \quad (R^2 = 0.82, \alpha = 3.5) \quad (6.6)$$

$$\Phi_E = 1.90 \times 10^{-8} \Psi_{Lm}^{4.32} \text{ for } 1.3 < \Psi_{Lm} < 3.2 \quad (R^2 = 0.81, \alpha = 3) \quad (6.7)$$

Before Eqs. (6.6) and (6.7) can be used, the stability parameters ( $\Psi_{WL}$  and  $\Psi_{Lm}$ ) need to be calculated using the velocity ( $u$ ) and the turbulent kinetic energy ( $k$ ) from the numerical simulations. To this end, Eqs. (2.27) and (2.28) were used. Note that the new turbulence magnification factor  $\alpha = 3.5$  and  $\alpha = 3.0$  are used for  $\Psi_{WL}$  and  $\Psi_{Lm}$ , respectively. The *measured* dimensionless stone entrainment rate ( $\Phi_E$ ) and the stability parameters ( $\Psi_{WL}$  and  $\Psi_{Lm}$ ) calculated from the *measured* flow properties are used for comparison. These measured quantities are presented in Appendix B (Tables B.1, B.2 and B.3).

Figure 6.6 compares the calculations and measurements of the key parameters presented in the two stability parameters. Flow condition 2BR and 2IR are chosen as typical examples. 2BR is one of the best computations while 2IR is one of the least accurate simulations. In both cases the velocity is modeled well. Turbulence is modeled well for 2BR condition. In contrast, turbulence is underestimated up to 35% for flow condition 2IR. However, in both cases the calculated  $(\bar{u} + \alpha\sqrt{k})^2$  is in good agreement with the measurements.

Comparison between the calculations and measurements of the stability parameters are depicted in Figure 6.7. Good agreement is found for both  $\Psi_{WL}$  and  $\Psi_{Lm}$ . The Hofland stability parameter ( $\Psi_{Lm}$ ) is better calculated while the Jon-geling et al. stability parameter ( $\Psi_{WL}$ ) is more underestimated. However, the difference is small and the errors for both parameters are within  $\pm 10\%$ .

Though good agreement is found for the calculated and measured stability parameters, the calculated  $\Phi_E$  (bed damage) is expected to have larger errors according to Eqs. (6.6) and (6.7) (i.e., a small error in  $\Psi_{WL}$  or  $\Psi_{Lm}$  can lead to much larger error in  $\Phi_E$ ). Figure 6.8 shows the comparison between the measured and calculated  $\Phi_E$ . It shows that the errors are within  $\pm 50\%$  which is reasonably good for bed damage prediction. Even for sediment transport, Van Rijn (1993) found that with different investigations the deviations of the transport rates vary up to a factor of 2 for similar flow conditions.

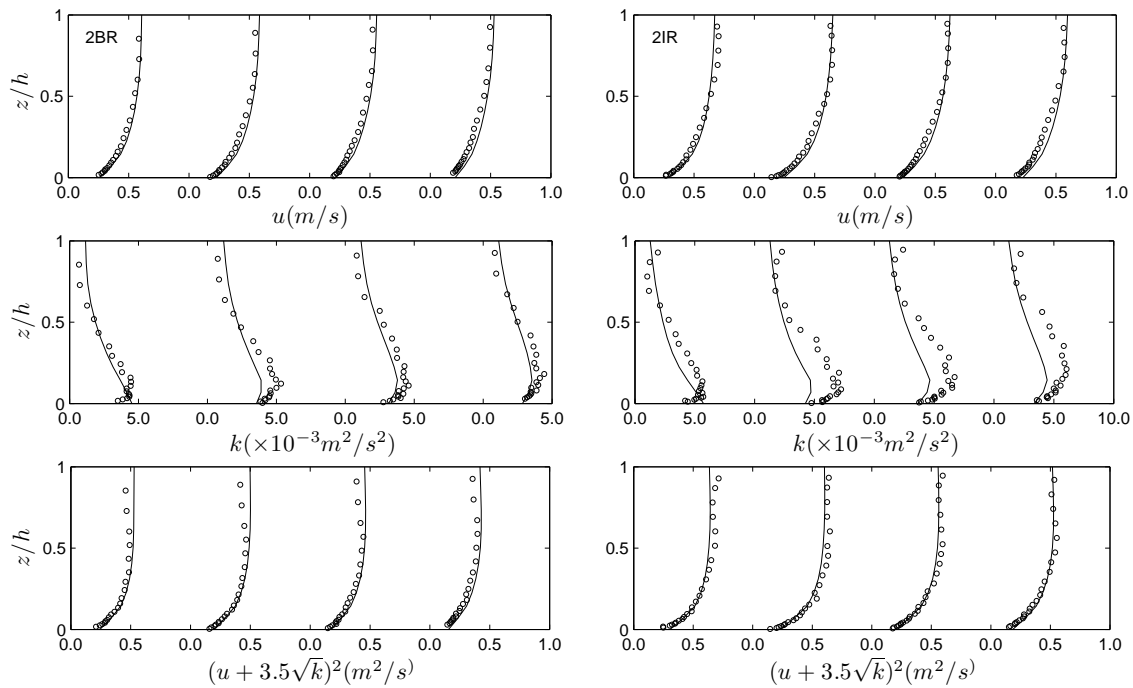


Figure 6.6: Vertical distributions of key parameters in Eqs. (2.27) and (2.28). The turbulence magnification factor  $\alpha = 3.5$  was used. Left: flow condition 2BR. Right: flow condition 2IR.

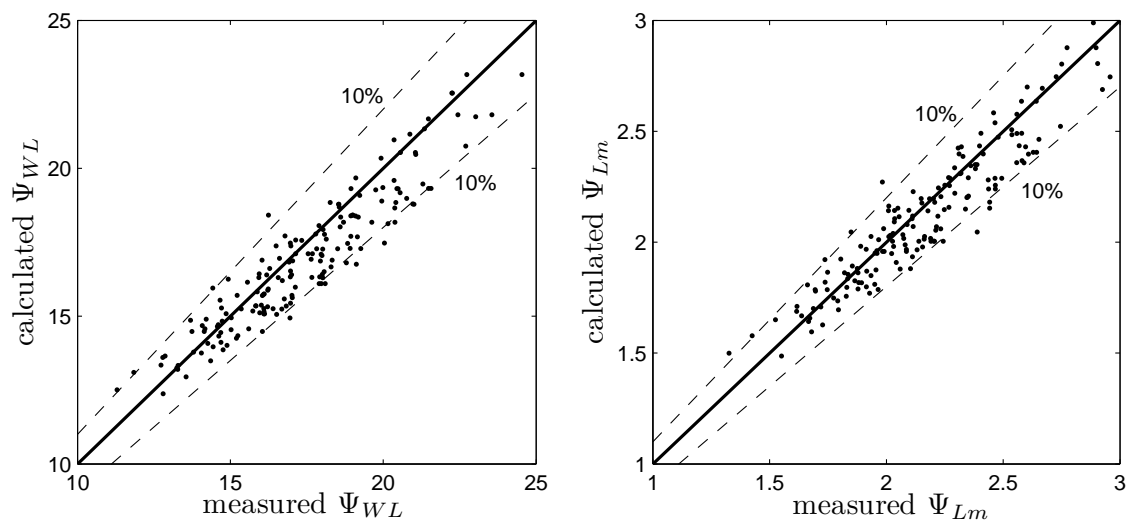


Figure 6.7: Comparison of measured and calculated stability parameters.



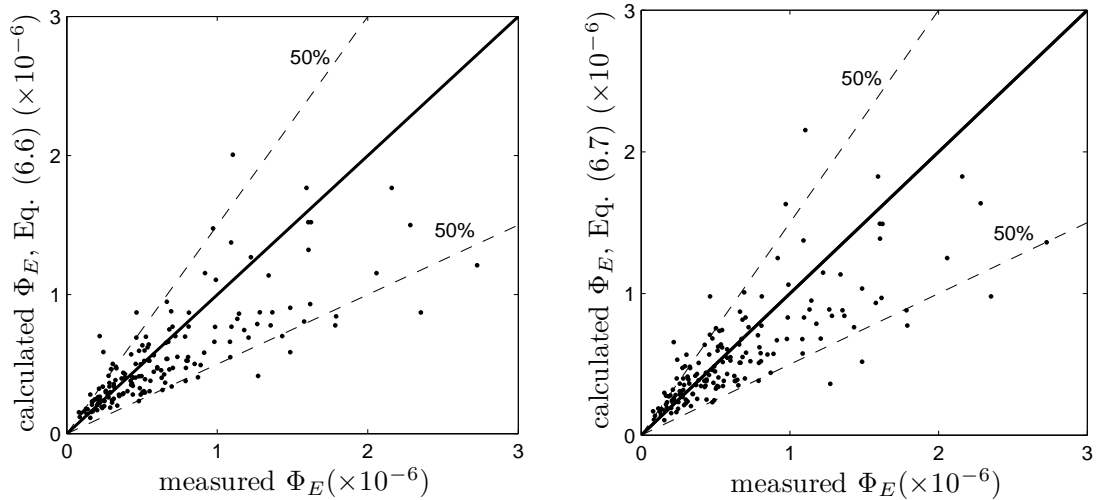


Figure 6.8: Comparison of measured and calculated bed damage ( $\Phi_E$ ). The calculated bed damage was determined using Eq. (6.6) [left] and Eq. (6.7) [right].

## 6.6 Conclusions and recommendations

In this chapter, the applicability of a numerical flow model to predict bed damage has been evaluated. RANS (i.e.,  $k - \varepsilon$  model) computations were used to simulate the flows. The computations were executed with the flow simulation package Deft incompressible flow solver developed at Delft University of Technology. The computed flow properties were then used to calculate the bed damage. The evaluation is made based on the experimental data. The following conclusions could be drawn from the results of the analysis given in this chapter.

It is possible to reproduce the flow in an open-channel with gradual expansion using a  $k - \varepsilon$  turbulence model. However, numerical models should be used with care, especially with the implementation of aspects like the grid and boundary condition. A grid refinement test is often needed to ensure a grid-independent solution. A systematic comparison to the measurements has shown that although the velocity distribution is reproduced very well, the model still underestimates the turbulence intensity in the bottom region. In general, however, the flow field obtained from the Deft package compares well to that measured in the laboratory experiments.

For the estimation of bed damage from the calculated flow properties, relations (5.10) and (5.12) were used. The stability parameters based on the calculated velocity ( $u$ ) and turbulence intensity ( $k$ ) compare well to those obtained from the measurements (errors within  $\pm 10\%$ ). The calculated bed damage ( $\Phi_E$ ) has larger errors (within  $\pm 50\%$ ) due to its high sensitivity to the value of the stability parameters. However, this is reasonably good compared to the typical errors in the

study of sediment transport.

With the availability of the newly-developed stone transport formulae such as (5.8), (5.10), (5.12) and more reliable turbulence models, the bed damage level can be more accurately computed for arbitrary flow conditions.

# Chapter 7

## Conclusions and recommendations

### 7.1 General

The stability of granular bed protections under flowing water was investigated in the present study. These bed protections are defined as hydraulically rough granular beds under non-uniform flow. In this flow regime the turbulence is an important factor that influences the stability of bed materials (i.e., stones). The conventional methods for stone stability assessment are mainly developed for uniform flow and are only partially valid if applied to non-uniform flow. The available methods developed for non-uniform flow, however, can only be used as rules-of-thumb due to the high uncertainty in the choice of the correction factors and/or to the high scatter level of the data. Therefore, more research is needed to increase the understanding of the relationship between turbulent flow and its induced damage to the bottom.

The main objectives of this study are to increase insight into the effect of hydraulic parameters on the stability of stones in bed protections and to develop robust stone transport formulae for non-uniform flow in which the turbulence effect is taken into account explicitly. To this end, a detailed set of measurements was carried out in a laboratory flume. The program comprised the measurement of the flow in gradually expanding open-channels and of the induced damage to the bottom. This flow configuration was chosen because in such a flow the turbulence intensity is high. Three experimental configurations with different expansion dimensions were used to create different combinations of velocity and turbulence. The bed response (quantified by a dimensionless entrainment rate) and the flow field (velocity and turbulence intensity distributions) were measured. The subsequent analysis was directed towards the understanding of the effect of hydraulic parameters to stone stability and the cause-and-effect relationship between the flow and its induced damage to the bottom.

New stone transport formulae have been successfully developed that are capable of predicting the bed damage for non-uniform flow (Chapter 5). More insights into the physics of the interaction between turbulent flow and its induced

damage have been gained. With the newly-developed stone transport formulae, the outputs of a Reynolds-averaged flow model can be used to determine bed damage for a given flow (discussed in Chapter 6). This would make the use of expensive physical models obsolete. In the following the main conclusions and recommendations of this research are given. Since a variety of flow conditions were used in the present experiments, we believe that the results are representative for general bed protections.

## 7.2 Conclusions

The literature review has shown that despite its popular and successful usage in engineering applications, the stability threshold concept often yields inconsistent and unreliable design criteria since it utilizes a subjective definition of incipient motion of bed material. In contrast, the transport concept results in a cause-and-effect relationship between the flow parameters and the bed response. Such a relationship provides consistent and more reliable design criteria and allows an estimate of the cumulative damage over time which is important for making decisions regarding maintenance frequency and lifetime analysis of hydraulic structures. The stone transport concept was, therefore, selected for the present study.

From literature it follows that a clearly defined and quantified measure of damage is essential for assessing the stability of a granular bed. For non-uniform flow, this quantity should be dependent on the local hydrodynamic conditions. As bed load transport is dependant on the upstream hydraulics, it is only suitable for uniform flow where the flow is unchanged along the channel. For non-uniform flow, the dimensionless entrainment rate should be used.

From the literature review it can be concluded that the most challenging issue in studying stone stability under flowing water is how to quantify the hydraulic loads exerted on the stones in bed protections. A stability parameter - expressed as a dimensionless relationship between hydraulic loads and bed strength - is often used to quantify these hydraulic loads. For the first time, the various ways of quantifying these hydraulic loads have been extensively reviewed, verified and extended using reliable data. The physical reasoning behind this is that if a stability parameter properly describes the hydraulic loads exerted on a bed, it should correlate well with the bed response (i.e., the dimensionless entrainment rate) because of the law of cause and effect. This approach requires large amounts of data with detailed information on the hydraulic parameters and the corresponding bed damage in order to give reliable conclusions. Of the many studies on stone stability, such data are only available in the present study.

The correlation analysis between the Shields stability parameter and the entrainment rate data has yielded quantitative confirmation (see Table 5.1) of earlier findings on the inappropriateness of using the bed shear stress alone to represent

the hydraulic loads exerted on a bed in non-uniform flow. The correlation deteriorates when the flow is more non-uniform. The conventional approach that uses correction factors for non-uniform flow should not be used as it does not physically explain the influence of turbulence source from the water column above the bed and often gives uncertain results.

A new stability parameter has been proposed to better quantify the hydraulic loads exerted on the stones. The formulation of the newly-proposed stability parameter has physically explained and quantitatively described the hydraulic loads exerted on the stones in bed protections. This provides valuable insight into the understanding of the influence of the different flow quantities such as velocity and turbulence distributions on stone stability. The high correlation of the proposed stability parameter [Eq. (5.6)] with the entrainment rate for a high water column indicates the role of large-scale flow structures. This confirms the finding by Hofland (2005) about the relevance of large flow structures to stone stability. Based on the physical analysis and practical considerations, the final expression for the new stability parameter was formulated, expressed as Eq. (5.7). This stability parameter properly quantifies the hydraulic loads exerted on the bed.

The approach that uses a combination of velocity and turbulence distributions to quantify the flow forces has been verified for the first time since it was proposed by Jongeling et al. (2003). The analysis indicates that different turbulence factors should be used for the Jongeling et al. ( $\alpha = 3.5$ ) and Hofland ( $\alpha = 3.0$ ) stability parameters instead of  $\alpha = 6$ . The proposed stability parameter and the modified stability parameters of Jongeling et al. (2003) and Hofland (2005) perform similarly for the present data. This is explained by the insensitivity (of the correlation coefficient) to  $H/h$  (above 0.5) and  $\beta$  (Figure 5.2) and probably the correlation between the maximum and the (weighting) average of the extreme forces.

For the first time, the physical relationship between flow parameters and the stone stability has been established for non-uniform flow. This relationship is described by stone transport formulae developed using the newly-proposed stability parameter and the modified stability parameters of Jongeling et al. (2003) and Hofland (2005), namely Eqs. (5.8), (5.10) and (5.12), respectively. These formulae can be used to predict the damage of bed protections. Although similar correlation is found for the three stone transport formulae (i.e.,  $R^2 \approx 0.81$ ), Eq. (5.8) was developed using purely measured data while Eqs. (5.10) and (5.12) were based on the approximated turbulent kinematic energy data. Therefore, Eq. (5.8) is recommended with the alternatives being Eqs. (5.10) and (5.12) when only velocity  $u$  and turbulent kinematic energy  $k$  are available.

Since a good collapse of the data is obtained for a variety of stone densities (varying from 1320 to 1970 kg/m<sup>3</sup>), the influence of stone density is well incorporated into the formulae. Therefore, the newly-developed stone transport formulae are likely to be valid for other bed materials with different densities, including

natural stones.

The applicability of a numerical flow model to predict bed damage has been evaluated. RANS (i.e.,  $k - \varepsilon$  model) computations were used to reproduce the flows in the experiments. The computed flow properties were then used to calculate the bed damage according to stone transport formulae (5.10) and (5.12). The evaluation was made by comparing the calculated bed damage to the measurements. The analysis has shown that the calculated and measured entrainment rate (i.e., damage) are in good agreement (errors within  $\pm 50\%$ ). This is reasonably good compared to the typical errors in the study of sediment transport. With the availability of the newly-developed stone transport formulae such as (5.8), (5.10), (5.12) and the high capability of new numerical models, the bed damage level can be more accurately computed for arbitrary flow conditions.

### 7.3 Recommendations

In this research, the flow before and along gradual expansion open-channels and its induced damage were used to develop new stone transport formulae for non-uniform flow. Though a reasonably wide variety of flow conditions was used in the present experiments, it is recommended that the newly-developed stone transport formulae, i.e., Eqs. (5.8), (5.10) and (5.12) should be verified using different flow conditions, stone sizes, strip widths at both flume and prototype scales (though the main characteristics of a granular bed protection are attained in the present experiments, see Section 3.3).

An initial settling period should be applied prior to an actual entrainment test to remove loose stones that do not determine the *strength* of the bed. As the strength of a bed is a subjective matter, it often confuses. It can be defined as an 'absolute' strength or as a 'relative' strength to the flow condition. A bed is "water-worked" when i) flow has been applied for a certain *time*, i.e., results in the relative strength of the bed or ii) when a certain *number* of stones (per unit of bed area) have moved, i.e., results in the absolute strength of the bed. As stability of bed protections is often examined in relation to a certain flow condition, the relative strength concept is recommended.

Since the movement of stones at low transport rates is highly irregular, entrainment tests should be repeated in order to obtain statistically reliable entrainment rate data.

Measurements of the displacement lengths of the stones should be available in order to get a reliable correction for the entrainment rate using Hofland's correction method. The use of assumption to obtain information on the displacement lengths is not recommended as it may result in an unreliable correction (see Section 5.5).

Critical values of  $\Psi_{u-\sigma[u]}$ ,  $\Psi_{WL}$  and  $\Psi_{Lm}$  - translated from a subjectively chosen low value of  $\Phi_E$  using (5.8), (5.10) and (5.12), respectively - should be used as

consistent design criteria to determine stone size in designing a bed protection. For instance, if  $\Phi_E = 10^{-9}$  is chosen as a critical entrainment rate, the corresponding critical values of these stability parameters are  $\Psi_{u-\sigma[u],c} = 2.9$ ,  $\Psi_{WL,c} = 4.4$  and  $\Psi_{Lm,c} = 0.5$ . The required stone diameter can be determined as

$$d_{n50} = \frac{\langle [u + \alpha\sigma(u)]^2 \times \sqrt{1 - z/h} \rangle_h}{\Delta g \Psi_{u-\sigma[u],c}} \quad \text{with } \alpha = 3.0 \quad (7.1)$$

$$d_{n50} = \frac{\langle (\bar{u} + \alpha\sqrt{k})^2 \rangle_{hm}}{\Delta g \Psi_{WL,c}} \quad \text{with } \alpha = 3.5 \quad (7.2)$$

$$d_{n50} = \frac{\max \left[ \langle \bar{u} + \alpha\sqrt{k} \rangle_{Lm} \frac{Lm}{z} \right]^2}{\Delta g \Psi_{Lm,c}} \quad \text{with } \alpha = 3.0 \quad (7.3)$$

The pressure gradients associated with a strong stationary acceleration of the flow or the effects of the fluctuating accelerations (TWP) mentioned by [Hofland \(2005\)](#) are also considered as sources contributing to the hydraulic loads exerted on the bed. It is recommended that more research should be done to investigate the influence of these factors on the stability of stones.

The newly-developed stone transport formulae are meant for bed protections that are attacked by flow. It is recommended to use the present approach to study sediment transport for non-uniform flow. In this case,  $\Psi_{WL}$ ,  $\Psi_{Lm}$  and  $\Psi_{u-\sigma[u]}$  could be used to quantify the hydraulic loads exerted on the bed. The entrainment rate is not applicable since it is not measurable for sediment. A non-local parameter such as bed load transport should not be used to describe the mobility of sediment. A new mobility parameter for sediment transport should be dependent on local hydrodynamic parameters and measurable for sediment particles.





# References

- Afzalimehr, H. and Anctil, F. O. (1999). Velocity distribution and shear velocity behaviour of decelerating flows over a gravel bed. *Canadian Journal of Civil Engineering*, 26(4):468–476.
- Andrews, E. and Smith, J. (1992). A theoretical model for calculating marginal bedload transport rates of gravel. In: (Billi *et al.*, 1992).
- Balachandar, R., Blakely, D., and Bugg, J. (2002a). Friction velocity and power law velocity profile in smooth and rough shallow open channel flows. *Canadian Journal of Civil Engineering*, 29(2):256–267.
- Balachandar, R., Hagel, K., and Blakely, D. (2002b). Velocity distribution in decelerating flow over rough surfaces. *Canadian Journal of Civil Engineering*, 29(2):211–222.
- Billi, P., Hey, C., Thorne, C., and Tacconi, P. (1992). *Dynamics of gravel-bed rivers*. John Wiley and Sons.
- Blinco, P. and Partheniades, E. (1971). Turbulence characteristics in free surface flows over smooth and rough boundaries. *Journal of Hydraulic Research, IAHR*, 9:43–69.
- Boutovski, A. (1998). *Stabiliteit van gestortte steen*. M.Sc. thesis, Delft University of Technology. In Dutch.
- Breusers, H. and Schukking, W. (1971). Beginning of movement of bed material. Technical Report S159-1, WL|Delft Hydraulics. In Dutch.
- Breusers, H. N. C. (1965). Gradual closure VI, influence of shape and grading on the stability of riprap. Technical Report M731, WL|Delft Hydraulics. In Dutch.
- Bridge, J. S., B. S. J. (1992). A model for the entrainment and transport of sediment grains of mixed sizes, shapes, and densities. *Water Resources Research*, 28(2):337–363.
- Buffington, J. M. (1999). The Legend of A. F. Shields. *Journal of Hydraulic Engineering*, 125(4):376–387.

- Buffington, J. M. and Montgomery, D. R. (1997). A systematic analysis of eight decades of incipient motion studies, with special reference to gravel-bedded rivers. *Water Resources Research*, 33(8):1993–2029.
- Bureau of Reclamation U.S. Department of the Interior (2006). *Erosion and Sedimentation Manual*. U.S. Dept. of the Interior, Bureau of Reclamation, Technical Service Center, Sedimentation and River Hydraulics Group.
- Cardoso, A. H. (1990). *Spatially accelerating flow in a smooth open channel*. Ph.D. thesis, Laboratorio Nacional de Engenharia Civil.
- Chepil, W. (1958). The use of evenly spaced hemispheres to evaluate aerodynamic forces on a soil surface. *Transactions, American Geophysical Union*, 39(3):397–404.
- Chepil, W. (1959). Equilibrium of soil grains at the threshold of movement by wind. *Soil Science Society of America*, 23:422–428.
- Chien, N. and Wan, Z. (1999). *Mechanics of sediment transport*. ASCE Press.
- Coleman, N. (1967). A theoretical and experimental study of drag and lift forces acting on a sphere resting on a hypothetical streambed. In *Proc. 12th IAHR Congress.*, pages 185–192, USA.
- Coleman, N. (1972). The drag coefficient of a stationary sphere on a boundary of similar spheres. *La Houille Blanche*, pages 17–21.
- Coles, D. E. (1956). The law of the wake in the turbulent boundary layer. *Journal of Fluid Mechanics*, 1:191–226.
- De Gunst, M. (1999). *Stone stability in a turbulent flow behind a step*. M.Sc. thesis, Delft University of Technology. (in Dutch).
- De Ruiter, J. (1982). The mechanism of sediment transport on bedforms. pages 137–142. of: Sumer, B. and Muller, A. (eds), *Euromech 156: Mechanics of sediment transport*. Istanbul: A.A. Balkeman, Rotterdam.
- Dessens, M. (2004). *The influence of flow acceleration on stone stability*. M.Sc. thesis, Delft University of Technology.
- Einstein, H. (1950). Bed load function for sediment transportation in open channel flows. Technical Report 1026, U.S. Dept. of Agriculture, Soil Conservation Service, Washington D.C.
- Einstein, H. and El-Samni, E. (1949). Hydrodynamic forces on a rough wall. *Reviews of Modern Physics*, 21(3):520–524.

- El-Shewey, M. I. A. and Joshi, S. G. (1996). A study of turbulence characteristics in open channel transitions as a function of Froude and Reynolds numbers using laser technique. *Adv. Fluid Mech*, 9:363–372.
- Franken, A., Ariëns, E., and Klatter, H. (1995). Manual for the design of bed protections behind two-dimensional outflow constructions. Technical Report BOD-R-95002, Bouwdienst Rijkswaterstaat. In Dutch.
- Graf, W. and Pазis, G. (1977). Les phenomenes de deposition et d'erosion dans un canal alluvionnaire. *Journal of Hydraulic Research*, 15(2). In: (Van Rijn, 1993).
- Grass, A. (1970). Initial instability of fine bed sands. *Journal of the Hydraulics Division, Proceedings of ASCE*, 96(HY3):619–632.
- Grass, A. (1971). Structural features of turbulent flow over smooth and rough boundaries. *Journal Fluid Mechanics*, 50(2):233–255.
- Hinze, J. O. (1975). *Turbulence*. New York : McGraw-Hill, 2nd edition.
- Hoan, N. T. (2005). Report on measurements of velocity and stone movement in accelerating flow. Technical Report 03-05, Delft University of Technology.
- Hoan, N. T. (2007). Experimental data. Technical Report 01-07, Delft University of Technology.
- Hoan, N. T., Booij, R., Hofland, B., Stive, M.J.F., and Verhagen, H. J. (2007a). Stone stability under decelerating open-channel flow. In *The Fifth International Conference on Coastal Structures*, Venice, Italy.
- Hoan, N. T., Booij, R., Hofland, B., Stive, M.J.F., and Verhagen, H. J. (2007b). Stone stability under non-uniform flow. In *The Fifth International Symposium on Environmental Hydraulics*, Tempe, Arizona, USA.
- Hoan, N. T., Booij, R., Hofland, B., Stive, M.J.F., and Verhagen, H. J. (2008). Estimation of bed protection damage using numerical flow modelling. In *The Seventh International Conference on Coastal and Port Engineering in Developing Countries*, Dubai, UAE.
- Hoan, N. T., Booij, R., Stive, M. J., and Verhagen, H. J. (2007c). Decelerating open-channel flow in a gradual expansion. In *The Fourth International Conference on Asian and Pacific Coasts*, Nanjing, China.
- Hoffmans, G. J. (2006). Stability of stones under non-uniform flow. Technical Report DWW-2006-085, Rijkswaterstaat Dienst Weg- and Waterbouwkunde (The Road and Hydraulic Engineering Institute).
- Hoffmans, G. J. (2008). Stability of stones under uniform flow. *Journal of Hydraulic Engineering*. Submitted.

- Hoffmans, G. J. C. M. and Akkerman, G. (1998). Influence of turbulence on stone stability. In *The Seventh International Conference on River Sedimentation*, Hong Kong.
- Hofland, B. (2005). *Rock & roll: turbulence-induced damage to granular bed protections*. Ph.D. thesis, Delft University of Technology.
- Hofland, B. and Booij, R. (2006). Numerical modeling of damage to scour protections. In *Third International Conference on Scour and Erosion*, Amsterdam, The Netherlands.
- Isbash, S. (1932). Construction of dams by dumping stones into flowing water. Technical Report Leningrad, Translated by A. Dovjikov for the War Department of the US Engineer office, Engineering division, Eastport Maine.
- Jongeling, T., Blom, A., Jagers, H., Stolker, C., and Verheij, H. (2003). Design method granular protections. Technical Report Q2933 / Q3018, WL| Delft Hydraulics. In Dutch.
- Jongeling, T. H. G., Jagers, H. R. A., and Stolker, C. (2006). Design of granular bed protections using a RANS 3D-flow model. In *Third International Conference on Scour and Erosion*, Amsterdam, The Netherlands.
- Kironoto, B. A. and Graf, W. H. (1990a). Decelerating flow in a gravel bed flume. Technical Report SEE N91-20432 12-34, Ecole Polytechnique Federale de Lausanne (Switzerland). Abstract.
- Kironoto, B. A. and Graf, W. H. (1990b). Non-uniform turbulent flow in rough beds flume. Technical Report SEE N92-22116 13-34, Ecole Polytechnique Federale de Lausanne (Switzerland). Abstract.
- Kironoto, B. A. and Graf, W. H. (1995). Turbulence characteristics in rough non-uniform open-channel flow. *Proc. Inst. Civ. Eng., Waters. Maritime Energ.*, 112(4):336–348. Abstract.
- Kleinhans, M. G. and Van Rijn, L. C. (2002). Stochastic prediction of sediment transport in sand-gravel bed rivers. *Journal of Hydraulic Engineering*, 128(4):412–425.
- Kramer, H. (1932). Modellgeschiebe und Schleppkraft. *Mitt. der Preusz. Versuchsanstalt fur Wasserbau und Schiffbau*. In: (Buffington, 1999).
- Ling, C. H. (1995). Criteria for incipient motion of spherical sediment particles. *Journal of Hydraulic Engineering*, 121(6):472–478.
- Mehta, P. R. (1981). Separated flow through large sudden expansions. *Journal of the Hydraulics Division*, 107(4):451460. Abstract.

- Meyer-Peter, E. and Muller, R. (1948). Formulas for bed-load transport. In *Proceedings of the 2nd Meeting of the International Association for Hydraulic Structures Research*, pages 39–64, Delft, Netherlands. Int. Assoc. Hydraul. Res.
- Mosselman, E. and Akkerman, G. J. (1998). Low-mobility transport of coarse-grained material. Technical Report Q2395.40, WL|Delft Hydraulics.
- Mosselman, E., Akkerman, G. J., Verheij, H., Hoffmans, G., Jongeling, T., and Petit, H. (2000). Stone stability, progress report. Technical Report Q2539, WL|Delft Hydraulics.
- Mynett, A., Wesseling, P., Segal, A., and Kassels, C. (1991). The ISNaS Incompressible Navier-Stokes Solver - Invariant Discretization. *Applied Scientific Research*, 48(2):175–191.
- Nakagawa, H., Nezu, I., and Ueda, H. (1975). Turbulence of open channel flow over smooth and rough beds. In *Proc. Of Japan Soc. Civil Engrs.*, volume 241, pages 155–168.
- Nakagawa, H. and Tsujimoto, T. (1980). A stochastic model for bed load transport and its applications to alluvial phenomena. In: Shen, H.W., & Kikkawa, H. (eds), *Application of stochastic processes in sediment transport*. Littleton, Colorado: Water resources publications. Chapter 11.
- Nezu, I. (1977). *Turbulent structure in open-channel flows*. Ph.D. thesis, Kyoto University.
- Nezu, I., Kadota, A., and Nakagawa, H. (1994). Turbulence structure in accelerating and decelerating open-channel flows with laser doppler anemometers. In *Proc., 9th Congr. ADP-IAHR*, pages 413–420, Singapore.
- Nezu, I. and Nakagawa, H. (1993). *Turbulence in Open-Channel Flows*. Balkema, Rotterdam.
- Nezu, I. and Rodi, W. (1986). Open-channel flow measurements with a laser doppler anemometer. *Journal of Hydraulic Engineering-Asce*, 112(5):335–355.
- Nordin, C. F. (1964). Aspects of flow resistance and sediment transport Rio Grande near Bernalillo, New Mexico. Technical Report Geological Survey Water-Supply Paper 1498-H, 41 p. Washington, USA.
- Paintal, A. S. (1969). *The probabilistic characteristics of bed load transport in alluvial channels*. Ph.D. thesis, University of Minnisota.
- Paintal, A. S. (1971). Concept of critical shear stress in loose boundary open channels. *Journal of Hydraulic Research*, 9(3):91–113.

- Papanicolaou, A. N. and Hildale, R. (2002). Turbulence characteristics in gradual channel transition. *Journal of Engineering Mechanics*, pages 949–960.
- Patnaik, P., Vittal, N., and Pande, P. (1992). Drag coefficient of a stationary sphere in gradient flow. *Journal of Hydraulic Research*, 30(3):389–402.
- Patnaik, P., Vittal, N., and Pande, P. (1994). Lift coefficient of a stationary sphere in gradient flow. *Journal of Hydraulic Research*, 32(3):471–480.
- Pilarczyk, K. (2001). Unification of stability formulae for revetments. In *Prog. XXIX IAHR congress*, Beijing.
- Radecke, H. v. and Schulz-DuBois, E. O. (1988). Linear response of fluctuating forces to turbulent velocity components. In *Applications of Laser Anemometry to Fluid Mechanics*.
- Rodi, W. (1993). *Turbulence models and their applications in hydraulics; a state-of-the-art-review*. IAHR Monograph series. Balkema, Rotterdam, 3rd edition.
- Schiereck, G. J. (2001). *Introduction to bed, bank and shore protection*. Delft University Press, Delft, 1st edition.
- Segal, A. (2000). *Programmers guide of the ISNaS incompressible flow solver*. Delft University of Technology.
- Segal, A., Bijl, H., Vuik, K., Kuppen, W., Zijlema, M., and Moulinec, C. (1998). *ISNaS-incompressible flow solver: Mathematical manual*. Delft University of Technology. Version 2.1.
- Segal, A., Zijlema, M., Van Nooyen, R., and Moulinec, C. (2000). *User Manual of the Delft incompressible flow solver*. Delft University of Technology.
- Shields, A. (1936). *Anwendung der Aehnlichkeitsmechanik und der Turbulenzforschung auf die Geschiebebewegung*. Mitteilungen der Preussischen Versuchsanstalt fur Wasserbau und Schiffbau, Heft 26, Berlin. in German.
- Song, T. and Chiew, Y. M. (2001). Turbulence measurement in nonuniform open-channel flow using acoustic doppler velocimeter (adv). *Journal of Engineering Mechanics*, 127(3):219–232.
- Song, T. and Graf, W. (1994). Non-uniform open channel flow over a rough bed. *Journal of Hydroscience and Hydraulic Engineering*, 12(1):125.
- Stelling, G. S. and Booij, N. (1999). *Computational modeling flow and transport*. Delft University of Technology. Lecture Notes.
- Tromp, M. (2004). *The influence that fluid accelerations have on the threshold of motion*. M.Sc. thesis, Delft University of Technology.

- Tsujimoto, T., Saito, A., and Nitta, K. (1990). Open-channel flow with spatial acceleration or deceleration. *KHL Prog. Rep., Hydr. Lab., Kanazawa University, Kanazawa, Japan.*
- Uijtewaal, W. (2005). *Turbulence in hydraulics*. Delft University of Technology. Lecture Notes.
- Uittenbogaard, R., Hoffmans, G., and Akkerman, G. (1998). Turbulence schematization for stone stability assessment. Technical Report Q2395.30, WL|Delft Hydraulics.
- Van der Meer, J. W. (1988). *Rock slopes and gravel beaches under wave attack*. Ph.D. thesis, WL|Delft Hydraulics.
- Van der Meer, J. W. (1993). Conceptual design of rubble mound breakwaters. Technical Report 483, WL|Delft Hydraulics.
- Van der Meer, J. W. and Pilarczyk, K. (1986). Dynamic stability of rock slopes and gravel beaches. In *The 20th International Conference on Coastal Engineering*, Taipei.
- Van Maren, D. S. (2004). *Morphodynamics of a cyclic prograding delta: the Red river, Vietnam*. Ph.D. thesis, Utrecht University.
- Van Rijn, L. C. (1984). Sediment transport, Part I: bed load transport. *Journal of Hydraulic Engineering, ASCE*, 110(10):1431–1456.
- Van Rijn, L. C. (1993). *Principles of sediment transport in rivers, estuaries and coastal seas*. Aqua Publications, Amsterdam.
- Van Rijn, L. C. (1994). *Principles of fluid flow and surface waves in rivers, estuaries, seas, and oceans*. Aqua Publications, Amsterdam.
- Wang, S. and Shen, H. W. (1985). Incipient motion and riprap design. *Journal of Hydraulic Engineering*, 111(3):520–538.
- Watters, G. and Rao, M. (1971). Hydrodynamic effects of seepage on bed particles. *Journal of the Hydraulics Division, Proceedings of ASCE*, 97(HY3):421–439.
- White, C. (1940). Equilibrium of grains on bed of stream. *Proceedings of the Royal Society of London, Series A*, 174:322–334.
- Wiberg, P. and Smith, D. (1987). Calculations of the critical shear stress for motion of uniform and heterogeneous sediments. *Water Resources Research*, 23(8):1471–1480.
- Wilcox, D. C. (1994). *Turbulence modeling for CFD*. DCW Industries.

- WL|Delft Hydraulics (1972). Systematisch onderzoek naar twee- en driedimensionale ontgrondingen. Technical report, WL|Delft Hydraulics. In Dutch.
- Xingkui, W. and Fontijn, H. L. (1993). Experimental study of the hydrodynamic forces on a bed element in an open channel with a backward-facing step. *Journal of Fluids and Structures*, 7(3):299–318.
- Yakhot, V., Orszag, S., Thangam, S., Gatski, T., and Speziale, C. (1992). Development of turbulence models for shear flows by a double expansion technique. *Physics of Fluids A*, 4(7):1510–1520.



# Appendix A

## Stones

### A.1 Artificial stones

The artificial stones used in the present experiments were made of a combination of epoxy resin ( $\rho_s \approx 1500 \text{ kg/m}^3$  *Sneldrogende Houtreparatie* in Dutch, available from [www.alabastine.nl](http://www.alabastine.nl)), fine sand ( $\rho_s \approx 2700 \text{ kg/m}^3$ ) and polyfit ( $\rho_s \approx 1000 \text{ kg/m}^3$ ). With a different ratio of the three components, it is possible to make artificial stones with the density ranging from approximately 1100 to 2500  $\text{kg/m}^3$ . The epoxy resin consists of two separate pasty components. When these two components are mixed to each others (and with sand or/and polyfit), the new material becomes hard after approximately 30 minutes. The time before that line time is suitable to model the new mixed material into the shapes of natural stones. This was done by putting the new (soft) material into rubber molds which are hollow containers with particular shapes of natural stones. When the material hardens it takes the shape of the container, i.e., the shapes of natural stones.

The rubber molds were made of silicon rubber. The silicon rubber consists of a pasty component and a liquid. When they are mixed to each other, the new material becomes a rubber after 24 hours. To make the rubber molds, i.e., to copy the shape and size of natural stones, temporary rectangular wooden molds were used and natural stones were placed at the bottom of the wooden molds. The mixed material of the silicon rubber was then poured on the wooden molds. After 24 hours the rubber molds became dry and were taken out of the wooden molds. All the natural stones were then removed from the rubber molds and the molds were ready to be used.

About 2000 artificial stones were made and used in the experiments. These artificial stones are the copies of approximately 100 samples taken from the natural stones used to construct the flume bottom. Because the flow condition varies along the flume and for the testing purpose, different stone densities are required. These are,

- Type 1: Blue, green and yellow stones with the same density ( $\rho_s = 1341 \text{ kg/m}^3$ ). The process of making these stones are identical except the paint color. These stones are placed as uniformly colored strips along the expansion.
- Type 2 & 3: Pink ( $\rho_s = 1384 \text{ kg/m}^3$ ) and [light] orange ( $\rho_s = 1320 \text{ kg/m}^3$ ) stones. These stones with different densities are placed under the same flow condition (i.e., before the expansion, in the straight part of the flume) and therefore can also be used to check for the influence of stone density on the overall test results.
- Type 4: [Heavy] orange stones ( $\rho_s = 1971 \text{ kg/m}^3$ ). Though these stones have the same color and similar in shape and size with the stones of type 3, their density is much higher. These stones and the flow condition in series 3MR are specially designed to check for the influence of stone density on the overall results. These are the only artificial stones used in series 3MR.

For each stone type, about fifty stones are randomly picked up for weighing. These data are used to determine stone parameters such as the density, the nominal diameter and the stone gradation curve. For the detailed information on these measurements the reader is referred to [Hoan \(2007\)](#).

## A.2 Stone gradation

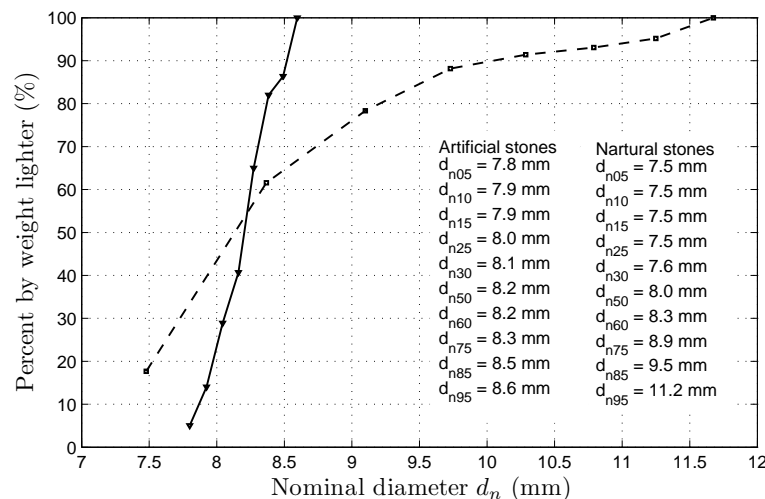


Figure A.1: The grading curves of artificial (line) and natural (dash) stones.

# Appendix B

## Data

### B.1 Introduction

In this appendix, the velocity and turbulence data measured from the experiment are given and compared with the computation. Based on the measured data of the velocity, the turbulence and the stone entrainment the following governing variables were determined:

- The shear velocity  $u_*$ ;
- The Shields stability parameter  $\Psi_s$ ;
- The Jongeling et al. stability parameter  $\Psi_{WL}$ ;
- The Hofland stability parameter  $\Psi_{Lm}$ ;
- The newly-proposed stability parameter  $\Psi_{u-\sigma(u)}$ ;
- The dimensionless entrainment rate  $\Phi_E$ .

The shear velocity was calculated based on the measured Reynolds shear stress distribution as discussed in Chapter 4. The shear velocity data was then used to determine the Shields stability parameter as expressed in Eq. (2.26). The data<sup>1</sup> of  $u$  and  $k$  were used to calculate the stability parameters of Jongeling et al (Eq.(2.27) with  $\alpha = 3.5$ ) and Hofland ( Eq. (2.28) with  $\alpha = 3.0$ ). The data of  $u$  and  $\sigma(u)$  were used to calculate the newly-developed stability parameter [Eq. (5.7)].

For the very detailed presentation of the measured data, the reader is referred to Hoan (2007).

### B.2 Velocity and turbulence data

---

<sup>1</sup>The turbulent kinetic energy  $k$  was determined as discussed in Section 3.6

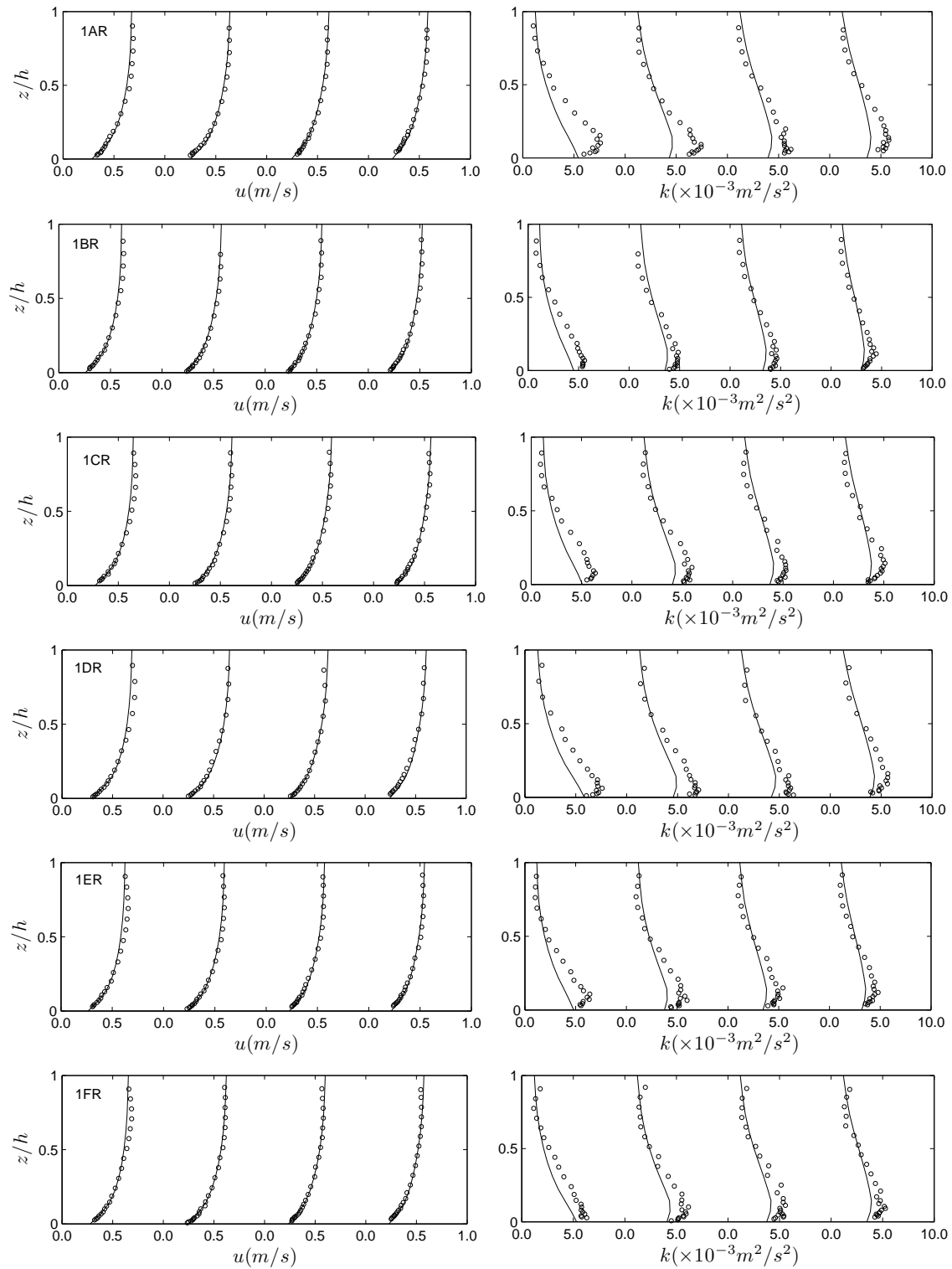


Figure B.1: Calculations (lines) and measurements (circles) of streamwise velocity ( $u$ ) and turbulence intensity ( $k$ ). From top to bottom: flow condition 1AR, 1BR, 1CR, 1DR, 1ER and 1FR. The results at profile 1 to 4 are plotted from left to right.

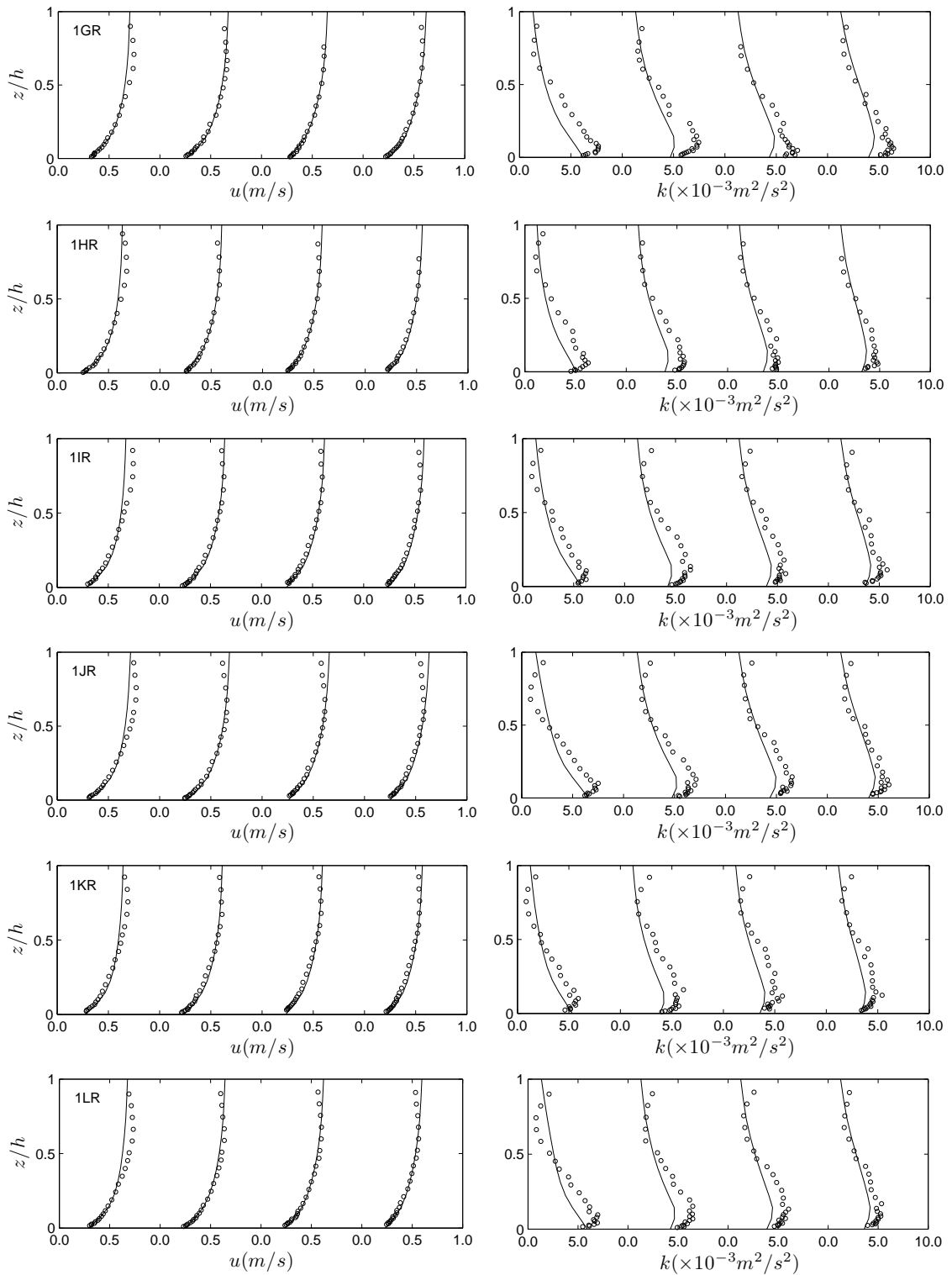


Figure B.2: Calculations (lines) and measurements (circles) of streamwise velocity ( $u$ ) and turbulence intensity ( $k$ ). From top to bottom: flow condition 1GR, 1HR, 1IR, 1JR, 1KR and 1LR. The results at profile 1 to 4 are plotted from left to right.

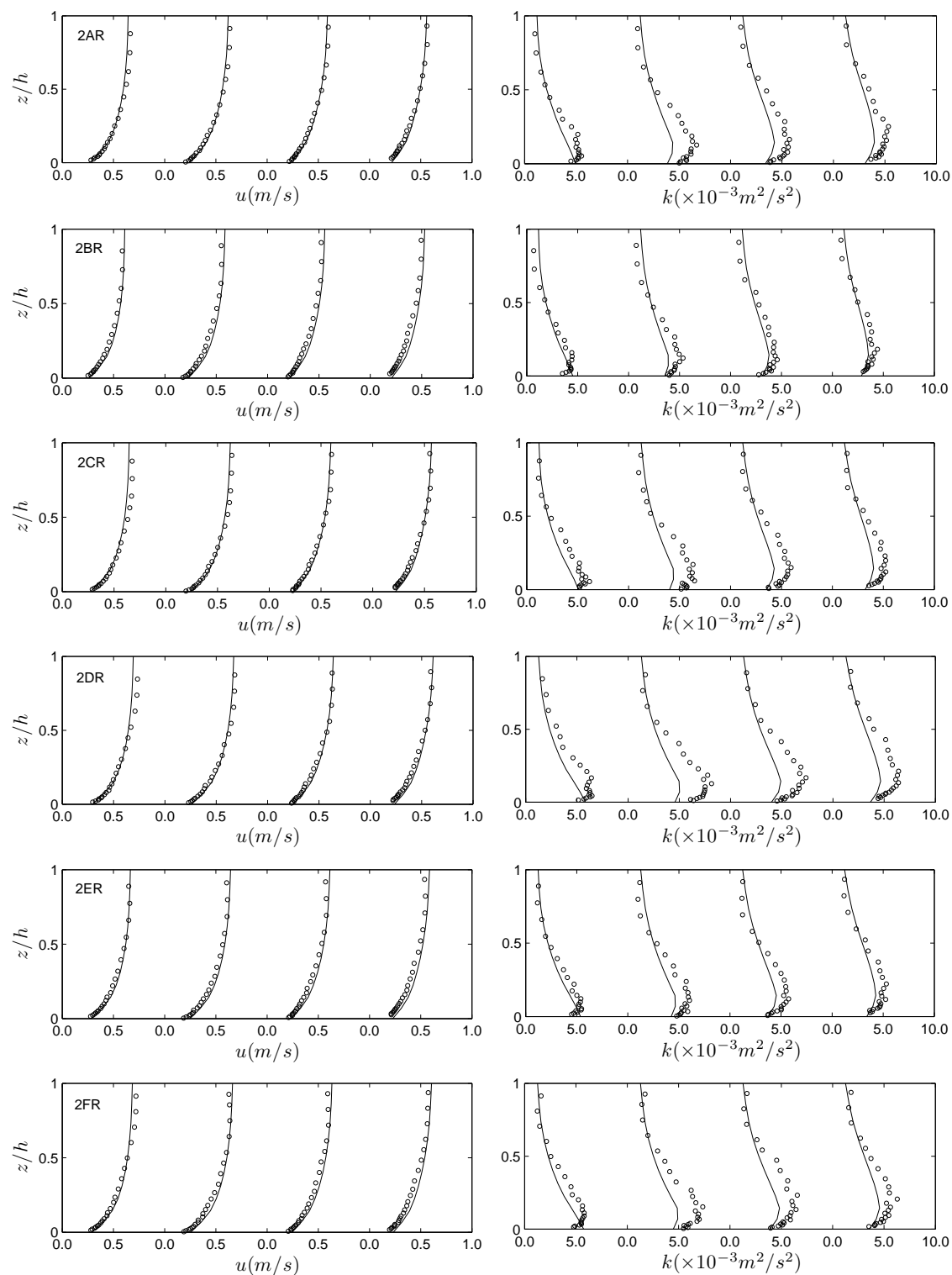


Figure B.3: Calculations (lines) and measurements (circles) of streamwise velocity ( $u$ ) and turbulence intensity ( $k$ ). From top to bottom: flow condition 2AR, 2BR, 2CR, 2DR, 2ER and 2FR. The results at profile 1 to 4 are plotted from left to right.

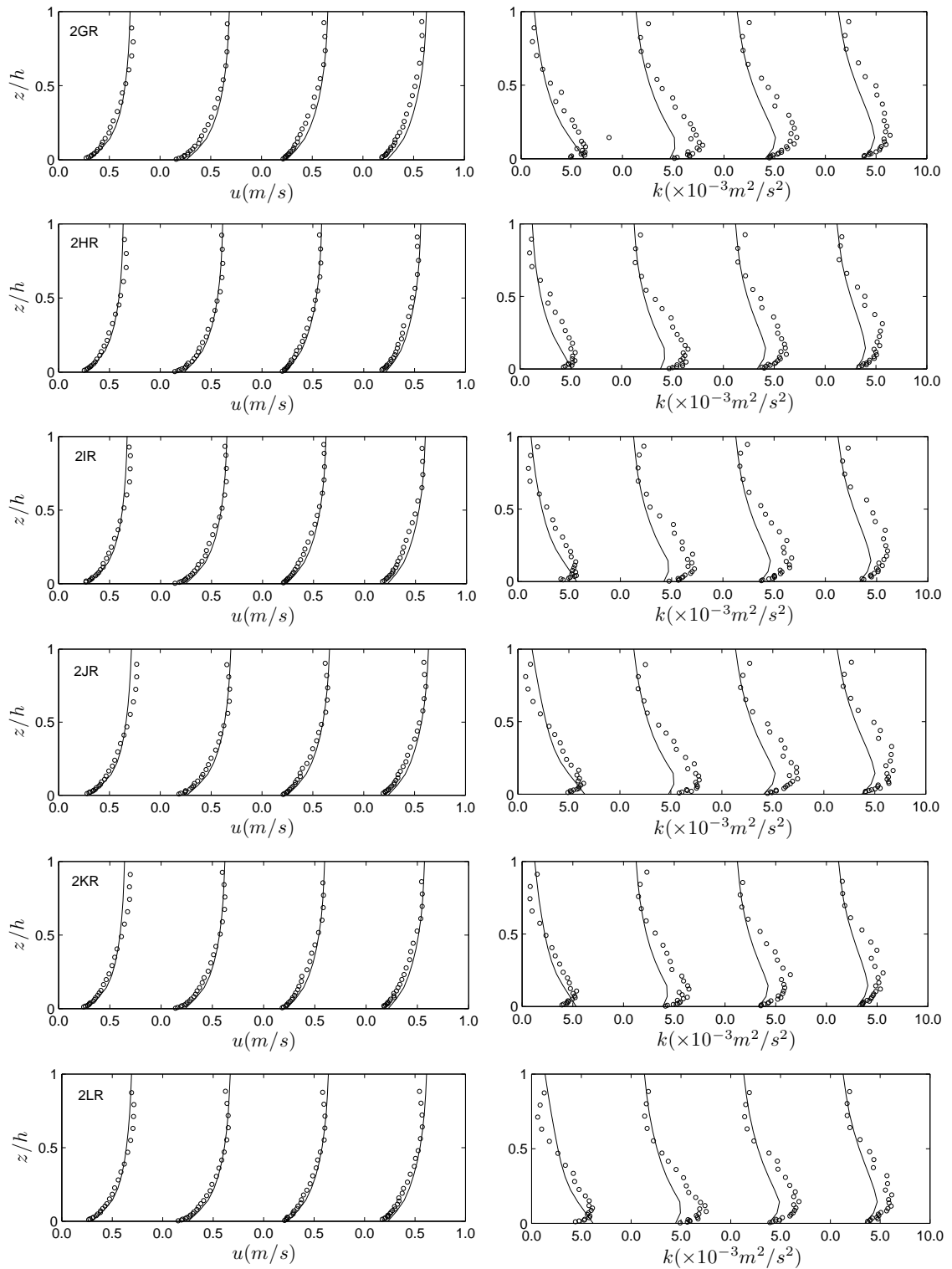


Figure B.4: Calculations (lines) and measurements (circles) of streamwise velocity ( $u$ ) and turbulence intensity ( $k$ ). From top to bottom: flow condition 2GR, 2HR, 2IR, 2JR, 2KR and 2LR. The results at profile 1 to 4 are plotted from left to right.

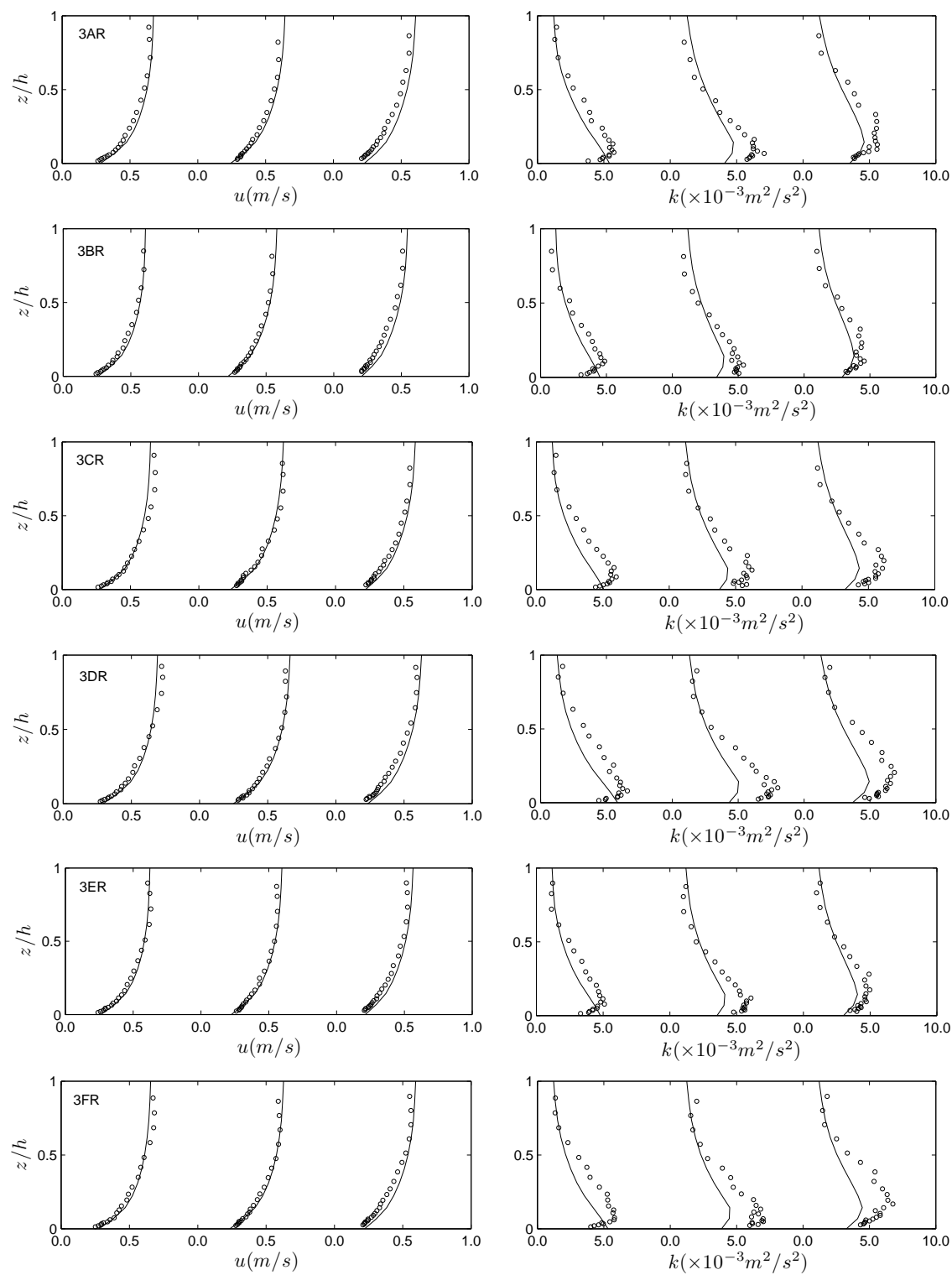


Figure B.5: Calculations (lines) and measurements (circles) of streamwise velocity ( $u$ ) and turbulence intensity ( $k$ ). From top to bottom: flow condition 3AR, 3BR, 3CR, 3DR, 3ER and 3FR. The results at profile 1 to 3 are plotted from left to right.



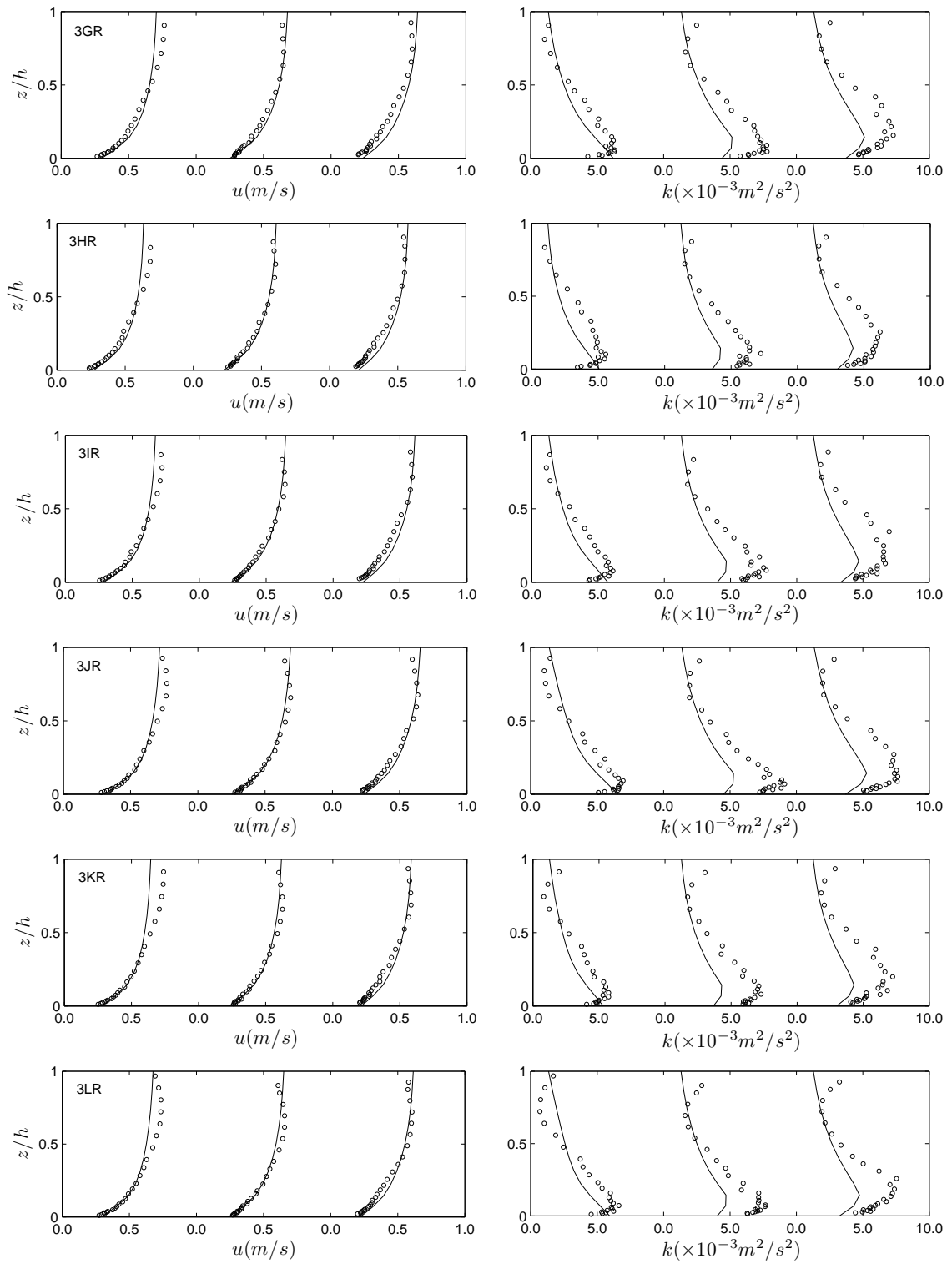


Figure B.6: Calculations (lines) and measurements (circles) of streamwise velocity ( $u$ ) and turbulence intensity ( $k$ ). From top to bottom: flow condition 3GR, 3HR, 3IR, 3JR, 3KR and 3LR. The results at profile 1 to 3 are plotted from left to right.

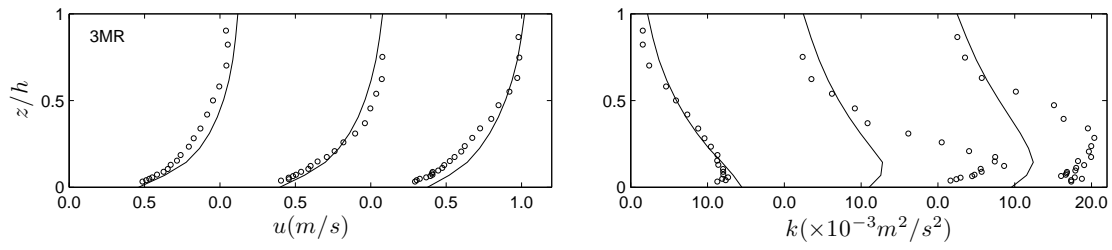


Figure B.7: Calculations (lines) and measurements (circles) of streamwise velocity ( $u$ ) and turbulence intensity ( $k$ ) of flow condition 3MR. The results at profile 1 to 3 are plotted from left to right.

### B.3 Governing variables

Table B.1: Summary of measured governing variables (set-up 1,  $\alpha = 3^0$ ).

	Q	h	Re	Fr	u*	$\Psi_S$	$\Psi_{WL}$	$\Psi_{Lm}$	$\Psi_{u-\sigma}$	$\Phi_E$
	[l/s]	[cm]	[10 <sup>4</sup> ]	[-]	[m/s]	[-]	[-]	[-]	[-]	[-]
Profile 1 ( $\Delta = 0.384$ )										
1AR	22.0	11.7	6.2	0.50	0.056	0.102	20.04	2.44	13.42	7.353E-07
1BR	20.0	12.0	5.7	0.44	0.046	0.068	16.05	1.96	10.88	2.505E-07
1CR	23.0	13.0	6.5	0.45	0.051	0.086	18.10	2.21	12.26	4.248E-07
1DR	26.5	13.9	7.5	0.47	0.053	0.090	20.38	2.49	14.14	1.084E-06
1ER	24.0	13.9	6.8	0.42	0.048	0.076	16.95	2.10	11.57	3.486E-07
1FR	27.0	15.0	7.6	0.43	0.049	0.079	17.92	2.21	12.57	4.357E-07
1GR	31.0	15.7	8.8	0.46	0.053	0.091	21.01	2.61	14.75	9.858E-07
1HR	28.0	15.8	7.9	0.41	0.048	0.075	16.83	2.09	11.86	5.120E-07
1IR	31.5	17.0	8.9	0.41	0.049	0.077	17.68	2.18	13.05	3.050E-07
1JR	35.5	17.9	10.0	0.43	0.054	0.093	20.49	2.56	14.69	8.115E-07
1KR	32.0	18.0	9.1	0.38	0.049	0.077	16.05	2.01	11.66	2.396E-07
1LR	35.5	19.0	10.0	0.39	0.052	0.087	19.27	2.47	13.74	5.446E-07
Profile 2 ( $\Delta = 0.341$ )										
1AR	22.0	12.1	5.5	0.42	0.052	0.100	18.94	2.34	12.90	1.485E-06
1BR	20.0	12.1	5.0	0.39	0.043	0.069	15.60	1.93	10.75	3.005E-07
1CR	23.0	13.0	5.7	0.40	0.051	0.094	18.02	2.24	12.16	6.300E-07
1DR	26.5	14.3	6.6	0.40	0.052	0.100	19.19	2.35	13.40	1.208E-06
1ER	24.0	13.9	6.0	0.37	0.047	0.081	16.51	2.06	11.20	3.468E-07
1FR	27.0	14.8	6.7	0.38	0.047	0.082	17.67	2.21	12.15	4.566E-07
1GR	31.0	16.1	7.7	0.39	0.056	0.113	20.38	2.58	14.16	1.179E-06
1HR	28.0	15.9	7.0	0.36	0.048	0.082	16.68	2.11	11.51	5.028E-07
1IR	31.5	17.1	7.9	0.36	0.051	0.096	17.95	2.27	12.85	6.011E-07
1JR	35.5	18.1	8.9	0.37	0.055	0.109	19.95	2.57	14.01	1.266E-06
1KR	32.0	18.1	8.0	0.33	0.050	0.091	16.01	2.03	11.80	2.601E-07
1LR	35.5	19.1	8.9	0.34	0.051	0.095	18.79	2.44	13.29	6.820E-07
Profile 3 ( $\Delta = 0.341$ )										
1AR	22.0	12.1	5.2	0.39	0.050	0.090	18.01	2.16	12.01	1.272E-06
1BR	20.0	12.2	4.7	0.36	0.041	0.063	14.36	1.73	9.75	2.023E-07
1CR	23.0	13.2	5.4	0.36	0.046	0.078	16.10	1.93	10.93	2.774E-07
1DR	26.5	14.5	6.2	0.36	0.050	0.091	17.97	2.22	12.44	4.913E-07
1ER	24.0	14.1	5.6	0.34	0.046	0.077	14.89	1.79	10.23	3.352E-07
1FR	27.0	15.2	6.3	0.35	0.049	0.089	16.39	2.04	11.23	2.601E-07
1GR	31.0	16.2	7.3	0.36	0.053	0.104	18.83	2.35	13.42	1.087E-06
1HR	28.0	16.2	6.6	0.32	0.047	0.080	15.20	1.91	10.55	2.081E-07
1IR	31.5	17.4	7.4	0.33	0.051	0.094	16.10	2.03	11.62	4.393E-07
1JR	35.5	18.3	8.3	0.34	0.055	0.111	18.13	2.27	12.67	4.277E-07
1KR	32.0	18.3	7.5	0.31	0.052	0.101	14.62	1.83	10.74	2.196E-07
1LR	35.5	19.1	8.3	0.32	0.051	0.096	17.03	2.19	11.99	3.179E-07
Profile 4 ( $\Delta = 0.341$ )										
1AR	22.0	12.3	4.9	0.36	0.050	0.091	16.12	1.95	11.03	4.913E-07
1BR	20.0	12.3	4.4	0.33	0.039	0.056	12.80	1.55	8.76	1.561E-07
1CR	23.0	13.3	5.1	0.34	0.046	0.076	14.44	1.79	9.95	2.485E-07
1DR	26.5	14.5	5.9	0.34	0.050	0.089	15.88	1.96	11.26	4.277E-07
1ER	24.0	14.3	5.3	0.32	0.044	0.069	13.55	1.68	9.35	1.329E-07
1FR	27.0	15.3	6.0	0.32	0.045	0.075	14.69	1.83	10.22	1.676E-07
1GR	31.0	16.2	6.9	0.34	0.050	0.090	16.70	2.07	11.59	5.202E-07
1HR	28.0	16.5	6.2	0.30	0.045	0.073	13.28	1.67	9.71	8.091E-08
1IR	31.5	17.8	7.0	0.30	0.045	0.072	14.58	1.84	10.52	1.849E-07
1JR	35.5	18.5	7.8	0.32	0.049	0.088	16.19	2.03	11.39	4.797E-07
1KR	32.0	18.5	7.1	0.29	0.048	0.084	13.29	1.69	9.75	1.156E-07
1LR	35.5	19.3	7.8	0.30	0.047	0.082	15.02	1.92	10.72	2.312E-07

Table B.2: Summary of measured governing variables (set-up 2,  $\alpha = 5^0$ ).

	Q	h	Re	Fr	$u_*$	$\Psi_S$	$\Psi_{WL}$	$\Psi_{Lm}$	$\Psi_{u-\sigma}$	$\Phi_E$
	[l/s]	[cm]	[ $10^4$ ]	[-]	[m/s]	[-]	[-]	[-]	[-]	[-]
Profile 1 ( $\Delta = 0.320$ )										
2AR	22.0	11.6	6.2	0.51	0.046	0.082	20.55	2.56	14.03	1.790E-06
2BR	20.0	12.0	5.7	0.44	0.043	0.072	16.49	2.03	11.22	6.623E-07
2CR	23.0	12.8	6.5	0.46	0.048	0.088	21.57	2.64	14.86	1.366E-06
2DR	26.5	13.8	7.5	0.47	0.051	0.102	23.55	2.96	17.12	1.623E-06
2ER	24.0	13.2	6.8	0.46	0.046	0.083	19.93	2.47	13.88	9.904E-07
2FR	27.0	14.4	7.6	0.45	0.048	0.090	21.35	2.67	15.29	1.092E-06
2GR	31.0	16.0	8.8	0.44	0.051	0.102	22.26	2.90	16.08	1.593E-06
2HR	28.0	15.9	7.9	0.40	0.049	0.092	19.01	2.39	13.63	7.219E-07
2IR	31.5	16.9	8.9	0.41	0.050	0.097	20.56	2.58	14.88	9.188E-07
2JR	35.5	17.5	10.0	0.44	0.051	0.100	22.73	2.89	16.78	1.104E-06
2KR	32.0	17.8	9.1	0.39	0.047	0.085	18.27	2.32	13.60	1.354E-06
2LR	35.5	18.6	10.0	0.41	0.051	0.100	21.48	2.75	15.48	9.725E-07
Profile 1a ( $\Delta = 0.384$ )										
2AR	22.0	11.6	6.2	0.51	0.046	0.068	17.12	2.13	11.69	6.536E-07
2BR	20.0	12.0	5.7	0.44	0.043	0.060	13.75	1.70	9.35	1.743E-07
2CR	23.0	12.8	6.5	0.46	0.048	0.074	17.97	2.20	12.38	5.555E-07
2DR	26.5	13.8	7.5	0.47	0.051	0.085	19.63	2.46	14.27	6.754E-07
2ER	24.0	13.2	6.8	0.46	0.046	0.069	16.61	2.05	11.57	3.268E-07
2FR	27.0	14.4	7.6	0.45	0.048	0.075	17.79	2.22	12.74	5.174E-07
2GR	31.0	16.0	8.8	0.44	0.051	0.085	18.55	2.41	13.40	7.026E-07
2HR	28.0	15.9	7.9	0.40	0.049	0.077	15.84	1.99	11.36	4.030E-07
2IR	31.5	16.9	8.9	0.41	0.050	0.080	17.13	2.15	12.40	4.575E-07
2JR	35.5	17.5	10.0	0.44	0.051	0.083	18.94	2.41	13.98	4.629E-07
2KR	32.0	17.8	9.1	0.39	0.047	0.071	15.22	1.93	11.33	2.832E-07
2LR	35.5	18.6	10.0	0.41	0.051	0.084	17.90	2.29	12.90	5.446E-07
Profile 2 ( $\Delta = 0.341$ )										
2AR	22.0	11.6	5.6	0.46	0.049	0.088	18.07	2.16	12.19	6.473E-07
2BR	20.0	11.9	5.1	0.40	0.046	0.077	14.21	1.74	9.62	2.196E-07
2CR	23.0	12.6	5.8	0.42	0.050	0.091	18.30	2.23	12.42	5.780E-07
2DR	26.5	13.8	6.7	0.42	0.057	0.119	20.96	2.59	14.60	8.091E-07
2ER	24.0	13.2	6.1	0.41	0.050	0.091	17.33	2.15	11.75	5.780E-07
2FR	27.0	14.1	6.9	0.42	0.051	0.096	18.61	2.32	12.89	4.624E-07
2GR	31.0	15.9	7.9	0.40	0.056	0.112	19.23	2.40	13.84	1.133E-06
2HR	28.0	15.8	7.1	0.37	0.051	0.094	16.76	2.08	11.83	4.855E-07
2IR	31.5	16.7	8.0	0.38	0.053	0.104	18.02	2.29	13.00	5.144E-07
2JR	35.5	18.0	9.0	0.38	0.055	0.111	19.99	2.54	14.60	6.936E-07
2KR	32.0	17.9	8.1	0.35	0.049	0.089	16.09	2.03	11.86	3.121E-07
2LR	35.5	18.2	9.0	0.38	0.053	0.101	18.59	2.36	13.32	5.028E-07
Profile 3 ( $\Delta = 0.341$ )										
2AR	22.0	11.6	5.1	0.42	0.048	0.085	16.10	1.89	10.92	4.393E-07
2BR	20.0	11.8	4.7	0.37	0.039	0.056	12.86	1.53	8.75	1.272E-07
2CR	23.0	12.7	5.4	0.38	0.049	0.088	16.22	1.96	11.15	2.601E-07
2DR	26.5	13.7	6.2	0.39	0.053	0.104	18.51	2.25	12.95	5.491E-07
2ER	24.0	13.3	5.6	0.37	0.049	0.087	15.56	1.89	10.66	3.237E-07
2FR	27.0	14.2	6.3	0.38	0.052	0.097	17.03	2.11	11.76	3.294E-07
2GR	31.0	15.9	7.2	0.37	0.054	0.106	17.13	2.11	12.41	5.780E-07
2HR	28.0	15.9	6.5	0.33	0.049	0.089	15.24	1.88	10.84	3.005E-07
2IR	31.5	16.6	7.3	0.35	0.052	0.097	16.22	2.02	11.73	3.121E-07
2JR	35.5	17.9	8.3	0.35	0.056	0.116	18.08	2.27	13.34	4.797E-07
2KR	32.0	17.8	7.5	0.32	0.050	0.091	14.69	1.88	11.04	1.676E-07
2LR	35.5	18.5	8.3	0.34	0.054	0.108	16.97	2.18	12.18	3.872E-07
Profile 4 ( $\Delta = 0.341$ )										
2AR	22.0	11.8	4.7	0.38	0.046	0.079	14.05	1.67	9.70	2.370E-07
2BR	20.0	11.8	4.3	0.34	0.041	0.060	11.30	1.33	7.75	8.669E-08
2CR	23.0	12.9	5.0	0.35	0.047	0.081	14.26	1.72	9.89	2.023E-07
2DR	26.5	13.9	5.7	0.36	0.051	0.096	16.24	1.96	11.49	4.335E-07
2ER	24.0	13.3	5.2	0.34	0.047	0.082	13.69	1.66	9.49	2.081E-07
2FR	27.0	14.3	5.8	0.35	0.049	0.087	14.66	1.80	10.40	2.138E-07
2GR	31.0	16.1	6.7	0.34	0.051	0.096	14.93	1.85	11.00	3.641E-07
2HR	28.0	15.9	6.0	0.31	0.048	0.084	13.25	1.64	9.52	1.618E-07
2IR	31.5	16.8	6.8	0.32	0.049	0.088	14.08	1.75	10.52	1.965E-07
2JR	35.5	18.1	7.6	0.32	0.053	0.102	15.94	2.04	12.03	2.774E-07
2KR	32.0	17.9	6.9	0.29	0.046	0.078	12.73	1.62	9.71	1.734E-07
2LR	35.5	18.6	7.6	0.31	0.051	0.094	14.71	1.91	10.88	2.890E-07

Table B.3: Summary of measured governing variables (set-up 3,  $\alpha = 7^0$ ).

	Q	h	Re	Fr	$u_*$	$\Psi_S$	$\Psi_{WL}$	$\Psi_{Lm}$	$\Psi_{u-\sigma}$	$\Phi_E$
	[l/s]	[cm]	[ $10^4$ ]	[-]	[m/s]	[-]	[-]	[-]	[-]	[-]
Profile 1 ( $\Delta = 0.341$ )										
3AR	22.0	12.1	6.2	0.47	0.048	0.085	19.10	2.31	13.02	6.647E-07
3BR	20.0	12.0	5.7	0.44	0.042	0.065	15.93	1.97	10.94	3.872E-07
3CR	23.0	12.9	6.5	0.45	0.049	0.089	20.16	2.47	13.99	6.589E-07
3DR	26.5	13.8	7.5	0.47	0.050	0.092	21.06	2.56	15.06	1.341E-06
3ER	24.0	14.1	6.8	0.41	0.044	0.071	16.92	2.11	11.90	2.948E-07
3FR	27.0	14.9	7.6	0.43	0.048	0.084	19.10	2.38	13.73	5.259E-07
3GR	31.0	15.7	8.8	0.46	0.049	0.089	20.87	2.60	15.32	1.607E-06
3HR	28.0	15.8	7.9	0.41	0.046	0.079	17.82	2.23	13.44	8.034E-07
3IR	31.5	16.9	8.9	0.41	0.049	0.086	19.76	2.48	14.62	1.144E-06
3JR	35.5	17.5	10.0	0.44	0.050	0.091	23.03	2.90	16.50	2.283E-06
3KR	32.0	17.7	9.1	0.39	0.047	0.080	19.16	2.44	14.28	9.132E-07
3LR	35.5	18.3	10.0	0.41	0.051	0.095	21.30	2.74	14.97	1.485E-06
Profile 1a ( $\Delta = 0.384$ )										
3AR	22.0	12.1	6.2	0.47	0.048	0.075	16.96	2.05	11.56	8.061E-07
3BR	20.0	12.0	5.7	0.44	0.042	0.057	14.15	1.75	9.72	4.793E-07
3CR	23.0	12.9	6.5	0.45	0.049	0.079	17.90	2.19	12.42	7.897E-07
3DR	26.5	13.8	7.5	0.47	0.050	0.081	18.70	2.27	13.38	9.804E-07
3ER	24.0	14.1	6.8	0.41	0.044	0.063	15.03	1.88	10.57	2.723E-07
3FR	27.0	14.9	7.6	0.43	0.048	0.075	16.96	2.11	12.19	8.714E-07
3GR	31.0	15.7	8.8	0.46	0.049	0.079	18.54	2.31	13.60	1.095E-06
3HR	28.0	15.8	7.9	0.41	0.046	0.070	15.83	1.98	11.93	5.501E-07
3IR	31.5	16.9	8.9	0.41	0.049	0.076	17.55	2.20	12.99	8.496E-07
3JR	35.5	17.5	10.0	0.44	0.050	0.081	20.45	2.58	14.66	2.353E-06
3KR	32.0	17.7	9.1	0.39	0.047	0.071	17.01	2.16	12.68	6.971E-07
3LR	35.5	18.3	10.0	0.41	0.051	0.084	18.91	2.44	13.29	7.952E-07
Profile 1b ( $\Delta = 0.320$ )										
3AR	22.0	12.1	6.2	0.47	0.048	0.090	20.36	2.46	13.87	1.223E-06
3BR	20.0	12.0	5.7	0.44	0.042	0.069	16.98	2.10	11.66	6.682E-07
3CR	23.0	12.9	6.5	0.45	0.049	0.095	21.48	2.63	14.91	1.283E-06
3DR	26.5	13.8	7.5	0.47	0.050	0.098	22.45	2.73	16.05	1.605E-06
3ER	24.0	14.1	6.8	0.41	0.044	0.075	18.03	2.25	12.68	5.370E-07
3FR	27.0	14.9	7.6	0.43	0.048	0.090	20.35	2.54	14.63	1.617E-06
3GR	31.0	15.7	8.8	0.46	0.049	0.095	22.24	2.77	16.32	2.160E-06
3HR	28.0	15.8	7.9	0.41	0.046	0.084	18.99	2.38	14.32	1.432E-06
3IR	31.5	16.9	8.9	0.41	0.049	0.092	21.05	2.64	15.58	2.058E-06
3JR	35.5	17.5	10.0	0.44	0.050	0.097	24.54	3.10	17.59	3.472E-06
3KR	32.0	17.7	9.1	0.39	0.047	0.085	20.41	2.60	15.21	1.784E-06
3LR	35.5	18.3	10.0	0.41	0.051	0.101	22.70	2.93	15.95	2.727E-06
Profile 2 ( $\Delta = 0.341$ )										
3AR	22.0	12.6	5.4	0.39	0.050	0.091	16.79	2.01	11.56	2.427E-07
3BR	20.0	12.7	5.0	0.35	0.045	0.074	14.17	1.70	9.70	2.138E-07
3CR	23.0	13.3	5.7	0.38	0.049	0.089	16.57	2.07	11.70	4.393E-07
3DR	26.5	14.4	6.6	0.39	0.053	0.103	18.94	2.32	13.11	7.860E-07
3ER	24.0	14.7	5.9	0.34	0.046	0.076	14.86	1.85	10.25	1.561E-07
3FR	27.0	15.5	6.7	0.36	0.051	0.094	17.00	2.09	11.95	4.970E-07
3GR	31.0	16.4	7.7	0.37	0.054	0.106	18.56	2.33	13.30	6.820E-07
3HR	28.0	16.4	6.9	0.34	0.052	0.097	16.09	2.02	11.58	5.086E-07
3IR	31.5	17.8	7.8	0.34	0.055	0.109	17.64	2.21	13.04	6.011E-07
3JR	35.5	18.0	8.8	0.37	0.056	0.116	20.77	2.65	14.94	1.578E-06
3KR	32.0	18.0	7.9	0.34	0.052	0.098	16.97	2.14	12.42	6.358E-07
3LR	35.5	19.2	8.8	0.34	0.053	0.101	18.33	2.35	13.41	7.051E-07
Profile 3 ( $\Delta = 0.341$ )										
3AR	22.0	12.8	4.8	0.34	0.049	0.086	14.43	1.74	10.14	2.832E-07
3BR	20.0	13.0	4.4	0.30	0.042	0.064	11.84	1.43	8.39	9.247E-08
3CR	23.0	13.4	5.1	0.33	0.050	0.092	14.61	1.83	10.19	3.121E-07
3DR	26.5	14.7	5.8	0.33	0.053	0.103	16.29	1.99	11.54	3.757E-07
3ER	24.0	15.0	5.3	0.29	0.045	0.072	12.79	1.62	8.99	1.387E-07
3FR	27.0	15.6	5.9	0.31	0.051	0.097	14.73	1.82	10.50	2.774E-07
3GR	31.0	16.8	6.8	0.32	0.056	0.113	16.04	2.01	11.74	7.918E-07
3HR	28.0	16.6	6.2	0.29	0.052	0.100	13.79	1.77	10.12	2.890E-07
3IR	31.5	17.5	6.9	0.31	0.054	0.108	15.36	1.95	11.54	5.202E-07
3JR	35.5	18.5	7.8	0.32	0.056	0.115	18.00	2.34	13.15	8.901E-07
3KR	32.0	18.2	7.0	0.29	0.054	0.107	14.76	1.88	10.98	2.312E-07
3LR	35.5	19.5	7.8	0.29	0.056	0.116	15.96	2.09	11.89	3.699E-07



# Appendix C

## Numerical flow modeling

### C.1 Turbulence modeling

#### C.1.1 Mean-flow equations

The flow of an incompressible, viscous Newtonian fluid can be described by a system of flow equations consisting of a continuity equation

$$\frac{\partial u_i}{\partial x_i} = 0 \quad (\text{C.1})$$

and three momentum equations, the so-called Navier Stokes equations

$$\frac{\partial u_i}{\partial t} + u_j \frac{\partial u_i}{\partial x_j} = -\frac{1}{\rho} \frac{\partial p}{\partial x_i} + \nu \frac{\partial^2 u_i}{\partial x_j^2} + f_i \quad (\text{C.2})$$

where  $t$  is time,  $x_i$  are spatial coordinates,  $u_i$  are components of the velocity vector,  $f_i$  are components of an external force per unit mass,  $p$  is the pressure,  $\rho$  is the fluid density and  $\nu$  is the kinematic viscosity. Additional information of this set of flow equations can be found in, for example, [Hinze \(1975\)](#); [Rodi \(1993\)](#). It is in principle possible to solve this set of equations if we know the boundary conditions and the initial conditions. However, solving these equations for general turbulent flows requires a very fine computational time- and space-grid to resolve all the scales present in the turbulence motion. These requirements are still far beyond the capacity of the modern computer in term of storage and computational time.

Engineers are usually not interested in the details of the fluctuating motion, but in the mean flow field. Therefore a statistical approach can be used in which the Navier Stokes equations are simplified by separating the turbulent flow into a mean ( $\bar{u}_i, \bar{p}$ ) and a fluctuating part ( $u'_i, p'$ ) and restricting the analysis to time-averages of the turbulent motion.

$$u_i = \bar{u}_i + u'_i, \quad p = \bar{p} + p', \quad (\text{C.3})$$

This is called *Reynolds decomposition*. The mean quantities are defined as

$$\bar{u}_i = \frac{1}{T} \int_0^T u_i dt, \quad \bar{p} = \frac{1}{T} \int_0^T p dt \quad (\text{C.4})$$

where the averaging time  $T$  must be sufficiently large (compared with the time scale of the turbulent motion) for the average value to approach the real time-independent mean value. Substituting Eq. (C.3) into Eqs. (C.2) and (C.1) and subsequent averaging leads to a system of equations for the mean motion. For brevity, the overbars indicating averaged values will be dropped from  $u_i$ , and  $p$  from here on.

The mean continuity equation is as follows

$$\frac{\partial u_i}{\partial x_i} = 0 \quad (\text{C.5})$$

And the mean momentum equations are

$$\frac{\partial u_i}{\partial t} + u_j \frac{\partial u_i}{\partial x_j} = -\frac{1}{\rho} \frac{\partial p}{\partial x_i} + \nu \frac{\partial^2 u_i}{\partial x_j^2} - \frac{\partial \overline{u'_i u'_j}}{\partial x_j} + f_i \quad (\text{C.6})$$

The  $-\overline{u'_i u'_j}$  terms represent the contribution of the turbulent motion to the mean stress. The turbulent stresses  $-\rho \overline{u'_i u'_j}$  are called the *Reynolds stresses*. The process of averaging has introduced unknown terms representing the transport of mean momentum by turbulent motion. Consequently, this set of equations cannot be solved without additional information. This is known as the *closure problem of turbulence*. It has led to the development of turbulence models, in which the Reynolds stresses are *modeled*.

An extensive review of turbulence models and their application in hydraulics can be found in [Rodi \(1993\)](#). An assessment of possible turbulence modelings that can be used for the design of bed protections is discussed in [Hofland \(2005, chapter 8\)](#). In this research the two-equation  $k - \varepsilon$  model was chosen as it is widely tested and used for hydraulic flow problems. The  $k - \varepsilon$  model employs conservation equations for the rate of turbulent kinetic energy  $k$  and for the rate of energy dissipation  $\varepsilon$ . In the next section, the  $k - \varepsilon$  model will be described in somewhat more detail.

### C.1.2 The two-equation $k - \varepsilon$ model

In the two-equation  $k - \varepsilon$  model, two extra transport equations are introduced to represent the turbulent properties of the flow.

For turbulent kinetic energy:

$$\frac{\partial k}{\partial t} + \frac{\partial}{\partial x_i} (k u_i) = \frac{\partial}{\partial x_i} \left[ \left( \nu + \frac{\nu_t}{\sigma_k} \right) \frac{\partial k}{\partial x_i} \right] + P_k - \varepsilon \quad (\text{C.7})$$



For turbulent dissipation:

$$\frac{\partial \varepsilon}{\partial t} + \frac{\partial}{\partial x_i} (\varepsilon u_i) = \frac{\partial}{\partial x_i} \left[ \left( \nu + \frac{\nu_t}{\sigma_\varepsilon} \right) \frac{\partial \varepsilon}{\partial x_i} \right] + c_{1\varepsilon} \frac{\varepsilon}{k} P_k - c_{2\varepsilon} \frac{\varepsilon^2}{k} \quad (\text{C.8})$$

where  $\varepsilon$  is the turbulent dissipation that determines the scale of the turbulence,  $k$  is the turbulent kinetic energy that determines the energy in the turbulence,  $P_k$  is the production rate of turbulent energy given by:

$$P_k = -\overline{u'_i u'_j} \frac{\partial u_i}{\partial x_j} \quad (\text{C.9})$$

The eddy viscosity is modeled as:

$$\nu_t = c_\mu \frac{k^2}{\varepsilon} \quad (\text{C.10})$$

The model contains some closure constants which are given as follows:

$$c_\mu = 0.09, c_{1\varepsilon} = 1.44, c_{2\varepsilon} = 1.92, \sigma_k = 1.0, \sigma_\varepsilon = 1.3 \quad (\text{C.11})$$

With the use of the constants in Eq. (C.11) we have the standard  $k - \varepsilon$  model. In the standard  $k - \varepsilon$  model the eddy viscosity is determined from a single turbulence length scale, so the calculated turbulent diffusion is that which occurs only at the specified scale. In reality all scales of motion will contribute to the turbulent diffusion. A mathematical technique used to account for the different scales of motion through changes to the production term results in the so-called RNG  $k - \varepsilon$  model (Yakhot et al., 1992). The RNG  $k - \varepsilon$  model is based on Re-Normalisation Group (RNG) analysis of the Navier-Stokes equations, to account for the effects of smaller scales of motion. The transport equations for turbulence generation and dissipation are the same as those for the standard  $k - \varepsilon$  model but the model constants are different and are given as follows (Segal et al., 2000):

$$c_\mu = 0.085, c_{1\varepsilon} = 1.42 - \frac{\eta(1 - \eta/\eta_0)}{1 + \gamma\eta^3}, c_{2\varepsilon} = 1.68, \sigma_k = \sigma_\varepsilon = 0.7179 \quad (\text{C.12})$$

with  $\eta_0 = 4.38$ ,  $\gamma = 0.012$  and  $\eta = Sk/\varepsilon$ .  $S$  is the magnitude of the mean rate of strain, defined as  $S = (2s_{ij}s_{ij})^{1/2}$ .  $s_{ij}$  is the mean rate of strain:

$$s_{ij} = \frac{1}{2} \left( \frac{\partial u_i}{\partial x_j} + \frac{\partial u_j}{\partial x_i} \right) \quad (\text{C.13})$$

## C.2 Deft input files

The turbulent flows through the flume have been simulated using Deft incompressible flow solver. In this section a complete description of the typical Deft input files used in our simulations is presented. Three following file types are used as Deft input files: \*.msh - grid generation, \*.prb - problem description and \*.f - file contains function subroutine USFUNB used to customize the boundary conditions such as inlet velocity and turbulence distributions.

The first stage of an Deft job is to generate a grid. The geometry of the flume set-up leads to the choice of multi block approach. The grid information is described in a text file (\*.msh) with special format that SEPRAN grid generator SEPMESH can understand. In the mesh file, points, curves, surfaces and volumes are defined. The boundaries are also marked so that they can be prescribed in \*.prb file (see Figure 6.1). The content of a typical mesh file (\*.msh) is described in Section C.2.1.

The next stage of a Deft job is to specify the physical, mathematical and solution parameters of the problems. This includes for example the specification of the viscosity, the density, the boundary conditions, the turbulence model. These are presented and discussed in Section C.2.2. The description of the sequence of a Deft session is presented in Section C.2.3.

### C.2.1 Mesh description

The 37 flow conditions (see Table 6.1) that were modeled requires 37 different mesh files. The following input file 1ar.msh for SEPMESH was used to generate the grid for flow condition 1AR. To make it easy to use for other flow conditions, the main dimensions of the model set-up are defined in the mesh file as constants and can be changed to proper values for each simulation. The plot command at the end of the file is used to generate the graphic output files. These files are used to visually check the grid generation.

```
* 3D mesh for an open-channel with gradual expansion
* The constants below are applied for all flow conditions
* in set-up 1 except the water depth h
* Dimensions are in meters.
constants
  reals
    x1 = 7.6      # start of the expansion
    x2 = 10.5    # end of the expansion
    x3 = 11.5    # flume length
    y1 = 0.075   # distance between inside and outside walls
    y2 = 0.25    # half of the flume width
    h  = 0.12    # water depth
```

```

integers
  nx1 = 130  # the number of cells in the first straight
             # part of the flume in x-direction (7.6 m)
  nx2 = 100  # the number of cells in the expansion
             # part in x-direction (2.9 m)
  nx3 = 35   # the number of cells in the second straight
             # part of the flume in x-direction (1.0 m)
  ny = 8     # the number of cells in y-direction
  nz = 10    # the number of cells in z-direction
end
mesh3d
  isnas
  points
    p1=(0,$y1,0)
    p2=($x1,$y1,0)
    p3=($x2,0,0)
    p4=($x3,0,0)
    p5=($x3,$y2,0)
    p6=($x2,$y2,0)
    p7=($x1,$y2,0)
    p8=(0,$y2,0)
    p9=(0,$y1,$h)
    p10=($x1,$y1,$h)
    p11=($x2,0,$h)
    p12=($x3,0,$h)
    p13=($x3,$y2,$h)
    p14=($x2,$y2,$h)
    p15=($x1,$y2,$h)
    p16=(0,$y2,$h)
  curves
    c1=line1(p1,p2,nelm=$nx1, ratio = 1, factor = 0.25)
    c2=line1(p2,p3,nelm=$nx2)
    c3=line1(p3,p4,nelm=$nx3)
    c4=line1(p4,p5,nelm=$ny)
    c5=line1(p5,p6,nelm=$nx3)
    c6=line1(p6,p7,nelm=$nx2)
    c7=line1(p7,p8,nelm=$nx1, ratio = 1, factor = 4)
    c8=line1(p8,p1,nelm=$ny)
    c9=line1(p1,p9,nelm=$nz, ratio = 1, factor = 2)
    c10=translate c9(p2,p10)
    c11=translate c9(p3,p11)
    c12=translate c9(p4,p12)
    c13=translate c9(p5,p13)

```

```

c14=translate c9(p6,p14)
c15=translate c9(p7,p15)
c16=translate c9(p8,p16)
c17=translate c8(p7,p2)      # x-y plan at z = 0
c18=line1(p6,p3,nelm=$ny)
c19=translate c1(p9,p10)    # x-y plan at z = h
c20=translate c2(p10,p11)
c21=translate c3(p11,p12)
c22=translate c4(p12,p13)
c23=translate c5(p13,p14)
c24=translate c6(p14,p15)
c25=translate c7(p15,p16)
c26=translate c8(p16,p9)
c27=translate c26(p15,p10)  # x-y plan at z = h
c28=line1(p14,p11,nelm=$ny)
surfaces
s1=rectangle5(c1,-c17,c7,c8)      # flume bottom
s2=rectangle5(c2,-c18,c6,c17)    # flume bottom
s3=rectangle5(c3,c4,c5,c18)     # flume bottom
s4=rectangle5(c1,c10,-c19,-c9)   # flume wall
s5=rectangle5(c2,c11,-c20,-c10)  # flume wall
s6=rectangle5(c3,c12,-c21,-c11)  # flume wall
s7=rectangle5(c4,c13,-c22,-c12)  # outflow
s8=rectangle5(-c7,c15,c25,-c16)  # symetric wall
s9=rectangle5(-c6,c14,c24,-c15)  # symetric wall
s10=rectangle5(-c5,c13,c23,-c14) # symetric wall
s11=rectangle5(-c8,c16,c26,-c9)  # inflow
s12=rectangle5(c19,-c27,c25,c26) # surface
s13=rectangle5(c20,-c28,c24,c27) # surface
s14=rectangle5(c21,c22,c23,c28)  # surface
s15=rectangle5(-c17,c15,c27,-c10)
s16=rectangle5(-c18,c14,c28,-c11)
volumes
v1=brick13(s1,s4,s15,s8,s11,s12)
v2=brick13(s2,s5,s16,s9,s15,s13)
v3=brick13(s3,s6,s7,s10,s16,s14)
plot
end

```

The values of the above constants (i.e.,  $x_1$ ,  $x_2$ ,  $x_3$ ,  $y_1$ ,  $y_2$ ) are applied for all flow conditions in set-up 1 (i.e., 1AR to 1LR). The water depth  $h$  varies from 0.12 m to 0.19 m depending on flow conditions. For the flows in set-up 2 and 3, the following constants are used. Again, the water depth  $h$  varies accordingly.

```

* The constants below are applied for all flow conditions
* in set-up 2 except the water depth h
* Dimensions are in meters.
constants
  reals
    x1 = 8.2    # start of the expansion
    x2 = 9.9    # end of the expansion
    x3 = 11.5   # flume length
    y1 = 0.075  # distance between inside and outside walls
    y2 = 0.25   # half of the flume width
    h  = 0.12   # water depth
  integers
    nx1 = 130   # the number of cells in the first
                # straight part of the flume in x-direction
    nx2 = 60    # the number of cells in the expansion
                # length in x-direction
    nx3 = 40    # the number of cells in the second straight
                # part of the flume in x-direction
    ny  = 8     # the number of cells in y-direction
    nz  = 10    # the number of cells in z-direction
end

```

```

* The constants below are applied for all flow conditions
* in set-up 3 except the water depth h
* Dimensions are in meters.
constants
  reals
    x1 = 8.2    # start of the expansion
    x2 = 9.4    # end of the expansion
    x3 = 11.5   # flume length
    y1 = 0.075  # distance between inside and outside walls
    y2 = 0.25   # half of the flume width
    h  = 0.12   # water depth
  integers
    nx1 = 130   # the number of cells in the first
                # straight part of the flume in x-direction
    nx2 = 45    # the number of cells in the expansion
                # length in x-direction
    nx3 = 50    # the number of cells in the second straight
                # part of the flume in x-direction
    ny  = 8     # the number of cells in y-direction
    nz  = 10    # the number of cells in z-direction
end

```

## C.2.2 Problem description

In Deft incompressible flow solver the problem description is specified in a text file (\*.prb). The Deft pre-processor (ISNASPRE) read this input file and interprets it. The same description is used for all the 37 flow simulations and is listed below. The only difference among various simulations (flow conditions) is the definition of the velocity distribution at the *inlet*. This is treated in a separate \*.f file.

```

*
*3D turbulent flow through an open-channel with gradual expansion
*
turbulence
  model = k_eps
  kappa = 0.4187
  E = 9.793
discretization
  turbulence_equations all
  upwind = first_order
time_integration
  tinit = 0
  tend = 30
  timestep = 0.008
  theta = 1
  rel_stationary_accuracy = 1d-2
boundary_conditions
* bottom
  curve 1 to 3:
    wall_functions = roughness
    roughness = 0.02
* inflow
  curve 11:
    un = func = 1, ut1 = 0, ut2 = 0
    k_dirichlet = 1.5d-3
    eps_dirichlet = 8.624833d-5
* outflow
  curve 7:
    outflow
    k_neumann = 0
    eps_neumann = 0
* side wall
  curve 4 to 6:
    wall_functions = roughness
    roughness = 0.005

```

```

* symmetry
  curve 8 to 10:
    freeslip
    k_neumann = 0
    eps_neumann = 0
* top
  curve 12 to 14:
    freeslip
    k_dirichlet = 9.0d-4
    eps_dirichlet = 8.624833d-5
coefficients
  momentum_equations
    rho = 1d3
    mu = 1d-3
    force3 = 10
multi_block
  subdomain_solution = inaccurate
linear_solver
  momentum_equations
    amount_of_output = 0
    relaccuracy = 1d-3
    maxiter = 1000
  pressure_equations
    amount_of_output = 0
    divaccuracy = 0
    relaccuracy = 1d-4
    startvector = zero
    maxiter = 1000
  turbulence_equations all
    amount_of_output = 0
    relaccuracy = 1d-3
    maxiter = 1000

```

To describe the boundary condition at the inlet, the function subroutine USFUNB is used. The following file 1ar.f is used for the flow condition 1AR. For other flow conditions, the corresponding values of water depth (h) and discharge (Q) are applied.

```

program isnasexe

implicit none

integer nbuffr
parameter( nbuffr = 300000000 )

```

```

integer ibuffr
common ibuffr(nbuffr)

call ishmain( nbuffr )

end

function usfunb ( icoice, x, y, z, t )

c  User written function subroutine. It gives
c  the user the opportunity to define a
c  boundary condition as a function of space
c  and time.

implicit none

double precision usfunb, x, y, z, t
integer icoice

c  x      i    x-coordinate
c  y      i    y-coordinate
c  t      i    actual time
c  icoice i    choice parameter given by the user input
c  usfunb o    computed boundary condition

double precision Q, B, h, u

c  Q      discharge
c  B      channel width
c  h      water depth
c  u      inflow velocity u = u(z)

Q = 22d-3
B = 35d-2
h = 12d-2
u = 3*Q*z*z/(B*h*h*h)

if ( icoice.eq.1 ) then
  usfunb = -u
end if

end

```



### C.2.3 Typical sequence of an Deft session

Once the Deft input files have been created, certain commands must be given to run the simulation. Following are typical commands used to simulate a flow condition, for instance, 1AR.

```
sepmesh 1ar.msh      # grid generation
isnaspre 1ar.prb     # read and interpret problem description
islink 1ar           # submit the function subroutine USFUNB
qsub runisnas        # run the simulation
```



# List of Symbols

## Roman Symbols

$a$	coefficient	-
$A$	area	$\text{m}^2$
$b$	coefficient	-
$B$	width (of flume)	$\text{m}$
$C$	Chezy coefficient	$\sqrt{\text{m}}/\text{s}$
$c_{i\varepsilon}, c_\mu$	closure constants in $k - \varepsilon$ turbulence model ( $i = 1, 2$ )	-
$d$	stone, particle diameter	$\text{m}$
$d_n$	nominal stone diameter ( $\equiv \sqrt[3]{V}$ )	$\text{m}$
$d_{n50}$	median nominal diameter ( $\equiv \sqrt[3]{m_{50}/\rho_s}$ )	$\text{m}$
$d_x$	stone diameter where $x\%$ of the stone mass has a smaller diameter	$\text{m}$
$E$	entrainment rate	-
$E_m$	measured entrainment rate, without correction	-
$E_c$	corrected entrainment rate	-
$f$	weighing function ( $\equiv (1 - z/H)^\beta$ )	-
$F$	flow force	$\text{N}$
$F_1$	friction force	$\text{N}$
$F_2$	resistance force	$\text{N}$
$F_D$	drag force	$\text{N}$
$F_g$	gravitational force	$\text{N}$
$F_L$	lift force	$\text{N}$
$F_{max}$	(estimate of) maximum (extreme) occurring force	$\text{N}$
$Fr$	Froude number ( $\equiv U/\sqrt{gh}$ )	-
$g$	gravitational acceleration	$\text{m}/\text{s}^2$
$h$	water depth	$\text{m}$
$H$	water column height above the bed	$\text{m}$
$k$	turbulence kinetic energy	$\text{m}^2/\text{s}^2$
$K_h$	water depth parameter	-
$k_s$	equivalent roughness	$\text{m}$
$K_s$	slope correction factor	-

$k_{sb}$	bottom roughness	m
$k_{sw}$	side wall roughness	m
$K_T$	turbulence correction factor	-
$K_v$	velocity/turbulence correction factor	-
$l$	stone displacement length	m
$L$	stone strip width	m
$\tilde{L}$	dimensionless strip width ( $\equiv L/\bar{l}$ )	-
$l_m$	mixing length	m
$L_m$	Bakhmetev mixing length	m
$m$	mass	kg
$n$	number of displaced stones	-
$p$	pressure	N/m <sup>2</sup>
$P_k$	production rate of turbulent energy	m <sup>2</sup> /s <sup>3</sup>
$q_s$	bed load transport per $m$ width	m <sup>2</sup> /s
$Q$	discharge	m <sup>3</sup> /s
$R$	hydraulic radius ( $\equiv \omega/\chi$ )	m
$R^2$	coefficient of determination	-
$Re$	Reynolds number ( $\equiv Uh/\nu$ )	-
$Re_*$	particle Reynolds number ( $\equiv u_*d_n/\nu$ )	-
$S$	empirical factor accounts for the way the stones are placed	-
$s_{ij}$	mean rate of strain	s <sup>-1</sup>
$t$	time	s
$T$	period, time-scale or duration	s
$u$	streamwise velocity	m/s
$u_*$	shear velocity ( $\equiv \sqrt{\tau_b/\rho}$ )	m/s
$u_{*c}$	critical shear velocity	m/s
$u_b$	near bed streamwise velocity	m/s
$u_{c,u}$	critical flow velocity in uniform flow	m/s
$u_{c,nu}$	critical flow velocity in non-uniform flow	m/s
$u_{max}$	maximum streamwise velocity	m/s
$U$	cross-sectional average of streamwise velocity	m/s
$v$	transverse velocity	m/s
$V$	volume (of stone)	m <sup>3</sup>
$w$	upward velocity	m/s
$x$	coordinate in direction of flow	m
$y$	transverse coordinate	m
$z$	vertical coordinate	m
$z_0$	roughness length	m

### Greek symbols

$\alpha$	empirical constant (various uses) or expansion angle	- degree
$\beta$	empirical constant (various uses) or Clauser's parameter	- -

$\delta$	boundary layer thickness	m
$\delta_*$	displacement thickness	m
$\Delta$	specific submerged density of stone ( $\equiv \rho_s/\rho - 1$ )	-
$\varepsilon$	turbulence dissipation	-
$\kappa$	Von Karman constant	-
$\nu$	kinematic viscosity	m <sup>2</sup> /s
$\nu_t$	eddy viscosity	m <sup>2</sup> /s
$\Pi$	Coles wake parameter	-
$\rho$	density of water	kg/m <sup>3</sup>
$\rho_s$	density of stone, epoxy resin, polyfit or sand	kg/m <sup>3</sup>
$\sigma_k, \sigma_\varepsilon$	closure constants in $k - \varepsilon$ turbulence model	-
$\tau$	shear stress	N/m <sup>2</sup>
$\tau_b$	bed shear stress	N/m <sup>2</sup>
$\tau_c$	critical bed shear stress	N/m <sup>2</sup>
$\Phi$	transport parameter (bed damage indicator)	-
$\Phi_E$	entrainment parameter (dimensionless entrainment rate)	-
$\Phi_q$	dimensionless bed load transport	-
$\Psi$	stability parameter (ratio of load to strength)	-
$\Psi_c$	critical stability parameter	-
$\Psi_{Lm}$	Hofland stability parameter	-
$\Psi_{u-\sigma[u]}$	stability parameter using $u$ and $\sigma[u]$	-
$\Psi_s$	Shields stability parameter ( $\equiv \tau_b/\Delta g d$ )	-
$\Psi_{s,c}$	critical Shields stability parameter	-
$\Psi_{WL}$	stability parameter developed at WL Delft Hydraulics	-
$\Psi_{WL,c}$	critical value of $\Psi_{WL}$	-
$\omega$	wetted cross-sectional area ( $\equiv B \times h$ )	m <sup>2</sup>
$\chi$	wetted perimeter ( $\equiv B + 2h$ )	m

## Mathematics

$ x $	absolute value of $x$
$\bar{x}$	temporal average of $x$
$\langle x \rangle$	spatial average of $x$
$x'$	fluctuating part of $x$ around $\bar{x}$
$\hat{x}$	predicted value of $x$
$\tilde{x}$	dimensionless form
$\equiv$	defined as
$\propto$	proportional to
$\approx$	approximately equal to
$\frac{D}{Dt}$	material derivative
$\frac{\partial}{\partial \cdot}$	partial derivative
$\int$	integral

$\pm$	plus or minus
$f(x)$	unspecified function of $x$
$\delta x$	relative difference between two values of $x$
$\Delta x$	difference between two values of $x$

## Abbreviations

2D	two-dimensional
3D	three-dimensional
BFS	backward-facing step
EMS	Electro Magnetic velocity Sensor
LDV	Laser Doppler Velocimeter
QSF	quasi-steady forces
RANS	Reynolds-averaged Navier-Stokes
TWP	turbulence wall pressures

# List of Figures

1.1	Graphical presentation of the research methodology and thesis lay-out. . . . .	5
2.1	Turbulence intensity distributions downstream of a sudden expansion after El-Shewey and Joshi (1996). . . . .	13
2.2	Forces acting on particles resting on a bed surface . . . . .	14
2.3	Four mechanical model concepts after Mosselman et al. (2000). . . . .	22
2.4	Original Shields curve (1936). The hatched area shows the critical shear stress as a function of the particle Reynolds number. . . . .	23
2.5	Variation of the dimensionless bed load transport with the Shield stability parameter after Paintal (1971) (large particles only). . . . .	27
2.6	Top: measured $\Phi_E$ versus the measured $\Psi_{WL}$ for a variety of flow conditions. Bottom: measured $\Phi_E$ versus the measured $\Psi_{Lm}$ for the same flow conditions with the tentative curve expressed by Eq. (2.46) (Hofland, 2005). . . . .	28
2.7	A summary of stone stability assessment methods. . . . .	29
3.1	Experimental installation (not to scale). . . . .	34
3.2	The first experimental configuration indicating the placement of uniformly colored artificial stone strips (not to scale). . . . .	35
3.3	Longitudinal sections of the three experimental configurations. . . . .	35
3.4	Distributions of velocity and Reynolds shear stress. . . . .	36
3.5	Horizontal distributions of mean velocity ( $u$ and $v$ ) at the middle cross section of the expansion. The measurement was undertaken for flow condition B (top panel) and L (bottom panel). . . . .	37
3.6	The relative errors ( $\delta$ ) of 2-minute (square), 5-minute (plus) and 10-minute (dot) sub-signals to the 30-minute signal. The measurements were carried out at profile 1 under flow condition 1FR. . . . .	44
4.1	Typical velocity profiles. . . . .	54
4.2	Distributions of eddy viscosity and mixing length (set-up 1). . . . .	56
4.3	Distributions of eddy viscosity and mixing length (set-up 2). . . . .	57
4.4	Distributions of eddy viscosity and mixing length (set-up 3). . . . .	58
4.5	Turbulence intensity distributions (set-up 1). . . . .	60

4.6	Turbulence intensity distributions (set-up 2). . . . .	61
4.7	Turbulence intensity distributions (set-up 3). . . . .	62
4.8	Reynolds shear stress distributions. . . . .	64
5.1	The distributions of key parameters used to formulate the new stability parameter. From left to right: extreme force distribution (a), weighting function (b) and weighting average of the extreme forces (c). . . . .	69
5.2	Sensitivity analysis of $\alpha$ , $\beta$ and $H$ . . . . .	70
5.3	Vertical distributions of key parameters in Eq. (5.7). . . . .	71
5.4	Measured $\Psi_{u-\sigma[u]}$ versus measured $\Phi_E$ . . . . .	71
5.5	Measured $\Psi_s$ versus measured $\Phi_E$ . . . . .	73
5.6	Measured $\Psi_{WL}$ (with $\alpha = 6$ ) versus measured $\Phi_E$ . . . . .	74
5.7	Sensitivity analysis of $\alpha$ in Eqs. (2.27) and (2.28). . . . .	74
5.8	Measured $\Psi_{WL}$ (with $\alpha = 3.5$ ) versus measured $\Phi_E$ . . . . .	75
5.9	Measured $\Psi_{Lm}$ (with $\alpha = 6$ ) versus measured $\Phi_E$ . . . . .	76
5.10	Measured $\Psi_{Lm}$ (with $\alpha = 3$ ) versus measured $\Phi_E$ . . . . .	77
5.11	Typical distributions of the key parameters according to Eqs. (2.26), (2.27), (2.28) and (5.7). . . . .	78
5.12	Sensitivity analysis of the velocity and turbulence to the bed damage. The $\alpha$ values of 3.5, 3 and 3 are used in Eqs. (2.27), (2.28) and (5.7), respectively. . . . .	79
5.13	Data comparison. The $\alpha$ value of 6 was used for both $\Psi_{WL}$ (top) and $\Psi_{Lm}$ (bottom). The comparison was made for the measured entrainment data, i.e. $\Phi_E \equiv \Phi_{Em}$ . . . . .	82
5.14	Data comparison. The $\alpha$ value of 6 was used for both $\Psi_{WL}$ (top) and $\Psi_{Lm}$ (bottom). The comparison was made for the corrected entrainment data, i.e. $\Phi_E \equiv \Phi_{Ec}$ . . . . .	83
6.1	Definition region of the model set-up. . . . .	90
6.2	Grid refinement test (velocity and turbulence). . . . .	90
6.3	Profiles of calculated (lines) and measured (circles) flow parameters over the flume with flow condition 1AR. . . . .	93
6.4	Comparison between the standard $k - \varepsilon$ and RNG $k - \varepsilon$ model. . . . .	95
6.5	Comparison of calculations (lines) and measurements (circles). From top to bottom: flow condition 1BR, 2BR, 3BR, 1LR, 2LR and 3LR. The results at profile 1 to 4 are plotted from left to right. . . . .	96
6.6	Vertical distributions of key parameters in Eqs. (2.27) and (2.28). The turbulence magnification factor $\alpha = 3.5$ was used. Left: flow condition 2BR. Right: flow condition 2IR. . . . .	98
6.7	Comparison of measured and calculated stability parameters. . . . .	98



6.8	Comparison of measured and calculated bed damage ( $\Phi_E$ ). The calculated bed damage was determined using Eq. (6.6) [left] and Eq. (6.7) [right]. . . . .	99
A.1	The grading curves of artificial (line) and natural (dash) stones. . . . .	116
B.1	Calculations (lines) and measurements (circles) of streamwise velocity (u) and turbulence intensity (k). From top to bottom: flow condition 1AR, 1BR, 1CR, 1DR, 1ER and 1FR. The results at profile 1 to 4 are plotted from left to right. . . . .	118
B.2	Calculations (lines) and measurements (circles) of streamwise velocity (u) and turbulence intensity (k). From top to bottom: flow condition 1GR, 1HR, 1IR, 1JR, 1KR and 1LR. The results at profile 1 to 4 are plotted from left to right. . . . .	119
B.3	Calculations (lines) and measurements (circles) of streamwise velocity (u) and turbulence intensity (k). From top to bottom: flow condition 2AR, 2BR, 2CR, 2DR, 2ER and 2FR. The results at profile 1 to 4 are plotted from left to right. . . . .	120
B.4	Calculations (lines) and measurements (circles) of streamwise velocity (u) and turbulence intensity (k). From top to bottom: flow condition 2GR, 2HR, 2IR, 2JR, 2KR and 2LR. The results at profile 1 to 4 are plotted from left to right. . . . .	121
B.5	Calculations (lines) and measurements (circles) of streamwise velocity (u) and turbulence intensity (k). From top to bottom: flow condition 3AR, 3BR, 3CR, 3DR, 3ER and 3FR. The results at profile 1 to 3 are plotted from left to right. . . . .	122
B.6	Calculations (lines) and measurements (circles) of streamwise velocity (u) and turbulence intensity (k). From top to bottom: flow condition 3GR, 3HR, 3IR, 3JR, 3KR and 3LR. The results at profile 1 to 3 are plotted from left to right. . . . .	123
B.7	Calculations (lines) and measurements (circles) of streamwise velocity (u) and turbulence intensity (k) of flow condition 3MR. The results at profile 1 to 3 are plotted from left to right. . . . .	124



# List of Tables

2.1	List of dominant governing variables. . . . .	16
3.1	The main characteristics of stones used in the experiments. . . . .	39
3.2	A possible set of hydraulic conditions. . . . .	40
3.3	Summary of hydraulic conditions measured from the experiments. . . . .	42
3.4	Summary of measurements and equipments used in the experiment. . . . .	43
4.1	Summary of measured and calculated flow parameters (set-up 1). . . . .	50
4.2	Summary of measured and calculated flow parameters (set-up 2). . . . .	51
4.3	Summary of measured and calculated flow parameters (set-up 3). . . . .	52
4.4	The empirical constants $\alpha$ and $\beta$ determined from the present data. . . . .	59
5.1	Coefficient of determination for different data sets. . . . .	72
6.1	The flow conditions that are to be modeled. . . . .	88
6.2	Grid refinement test for set-up 2. . . . .	89
6.3	Grid refinement for the three flume set-ups. . . . .	91
B.1	Summary of measured governing variables (set-up 1, $\alpha = 3^0$ ). . . . .	125
B.2	Summary of measured governing variables (set-up 2, $\alpha = 5^0$ ). . . . .	126
B.3	Summary of measured governing variables (set-up 3, $\alpha = 7^0$ ). . . . .	127



# Acknowledgements

This thesis would have not been realized without the support and contributions of many people. Therefore, I would like to thank all of them, including those I may have forgotten to mention here.

First of all, I would like to thank all the members of my guidance committee, Marcel Stive, Rob Booij, Bas Hofland, and Henk Jan Verhagen, for their thoughtful guidance and encouragement during this study. Thank you for allowing me freedom in doing my research. This is especially true when you want to switch the research focus in the middle of the second year of your Ph.D. study as I did. I especially want to thank Rob Booij and Bas Hofland, my daily supervisors, for the good guidance and incisive advice. Thank you very much for sharing your great knowledge of "Rock & Roll" and for always reviewing my manuscripts. I thank Henk Jan Verhagen for recommending me to follow this research topic from the days I was still in Vietnam and for his active supervision during all stages of this research. And I thank Marcel Stive for being my great promotor. Your constructive criticism and comments, especially at the early stage of writing this thesis, have motivated me to improve my writing. Thank you very much for your help, support and for correcting my thesis.

I would like to thank all the staff members of the Laboratory of Fluid Mechanics of Delft University of Technology for their support during my one-year period working in the lab. I would have been lost during the measurements without Wim Uijttewaal and Sander de Vree. Your guidance, enthusiasm, valuable advice and assistance are much appreciated. Jaap van Duin and Ben Lemmers are thanked for setting up the experiments. The artificial stones would have not been made without the help of Arie den Toom. Thank you very much.

I thank Marcel Zijlema for his valuable advice and assistance in the flow simulations using Deft incompressible flow solver. I would have not been able to perform the simulations without you. Many thanks go to Rosh Ranasinghe for his time and effort in reviewing chapter 3 and 5 of this thesis.

I would like to thank all the members of my promotion committee for spending time and effort to review this thesis and provide me with insightful remarks.

I would like to thank all the staff members of CICAT, especially Veronique van der Varst and Paul Althuis, for their support and help. My four years in Delft would have been much more difficult without your assistance.

This research was funded by the Ministry of Education and Training of Vietnam, CICAT and the Hydraulic Engineering Department of Delft University of Technology. This financial support is gratefully acknowledged. Also the financial support from the Lamminga Foundation to return Delft for the defense of this thesis is much appreciated.

I thank all the members of the Hydraulic Engineering Department, especially Kees den Heijer, Tomohiro Suzuki, Fred Vaes and my Vietnamese colleagues, for creating a wonderful working atmosphere. I feel lucky to have fun roommates like Kees den Heijer and Nghiem Tien Lam, who could always understand all those Vietnamese-style jokes. Thank you for the joyful atmosphere and exchange of remarks and thoughts. Kees, thank you for taking care of all the formalities while I was in Vietnam and for translating the summary into Dutch. Many thanks also go to Mark Voorendt, Chantal van Woggelum, Inge van Rooij and Adeeba Ramdjan for all their help and support.

Special thanks go to all my Vietnamese friends for making my four-year stay in Delft very pleasant. I will not forget the football matches every Saturday, and the exercises (and jokes) at the gym with Nguyen Dai Viet. I was lucky enough to stay in the same nice house in Delft for the last four years thanks to brother Vu Ngoc Pi and Nguyen Tien Hung. I will never forget the nice time we had.

I would like to thank my colleagues at the Port and Waterway Engineering Department, Hanoi University of Civil Engineering (HUCE) for their support. I especially want to thank Prof.dr. Luong Phuong Hau for his guidance, support and encouragement since the days I joined HUCE as a lecturer. I have learned a lot more than hydraulic engineering from you. Ass.prof.dr. Pham Van Giap is thanked for recommending me to study hydraulic engineering. And I thank Ms. Dao Tang Kiem for helping me to apply for the Ph.D. position at Delft University of Technology.

A nature word of thanks goes to my parents. Their love, support and trust have encouraged me to pursue my personal objectives. I would like to thank my brother Nguyen Thuan and my sister in-law Nguyen Minh Quy for taking care of our parents and for being my great brother and sister. A sincere appreciation to my parents in-law for their love, support and for taking care of my little family while I was away. I could not have focused on the study without their help and support. I also want to take this opportunity to thank my uncle Phung Xuan Minh and my aunt Nguyen Thi Nham who have cared about me and have always supported me. Thank you very much for your support and trust.

Last, but certainly not least, I would like to express my deepest gratitude to my beloved wife Hai Ly, who has unconditionally supported me. It would have been impossible to reach this day without your love, support, motivation and patience. Thank you for being my wonderful wife. Together with our daughter Tra My, you fill my life with happiness and inspiration every day.

# Curriculum Vitae

[Nguyen Thanh Hoan](#) was born on 24 September 1976 in Nam Dinh, Vietnam. He obtained his high school diploma from Le Hong Phong (Nam Dinh) secondary school in 1994. During the period at secondary school he won a third prize of the National Talent Competition on Physics Subject (thi hoc sinh gioi quoc gia mon Vat Ly, 1993). In 1994 Hoan started his university in Hanoi University of Civil Engineering (HUCE), where he obtained BSc degree, with distinction (one of the three of the university that year), in hydraulic engineering in March 1999. During the period at university he won two third prizes of the National Student Olympic Competition - a prime annual academic event amongst technical universities in Vietnam - on Theoretical Mechanics Subject (1996) and on Structural Mechanics Subject (1997, this one without the first and second prizes). Shortly after graduation, in June 1999 he was employed as an assistant lecturer at the Faculty of Hydraulic Engineering, HUCE while continuing his master study at the Faculty of Postgraduates, HUCE. He obtained his Master degree in 2002 on a thesis entitled "Application of physical model in investigating river revolution". In July 2004, he started his Ph.D. study at the Department of Hydraulic Engineering, the Faculty of Civil Engineering and Geosciences, Delft University of Technology which led to this thesis. Currently Hoan works as a lecturer at the Department of Ports and Waterway Engineering, Hanoi University of Civil Engineering.







## **Propositions**

Pertaining to the thesis

### **Stone Stability under Non-uniform Flow**

by

Nguyen Thanh Hoan

Delft, 3 November 2008

1. Assessing the hydraulic loads exerted on the stones on a bed and the associated stability of the stones are central in stone stability research.
2. Although near-bed velocities cause the main forces on bed material, flow parameters at different depths can be used to represent the hydraulic loads exerted on the bed. (Hofland, 2005 and this thesis)  
Hofland, B. (2005). Rock & roll: turbulence-induced damage to granular bed protections. Ph.D. thesis, Delft University of Technology.
3. A combination of velocity and turbulence distributions should be used to quantify the hydraulic loads exerted on the stones on a bed. (this thesis)
4. The popular stability threshold concept should be used with care; it may yield inconsistent and unreliable design criteria. The stability transport concept may overcome this.
5. With the availability of the newly-developed stone transport formulae and more reliable turbulence models, the bed damage level can be more accurately computed for arbitrary flow conditions. (this thesis)
6. Beneath a good formula for bed processes is a good physical bedding.
7. Doing a Ph.D. study abroad may be very stressful but also very enjoyable.
8. For a starting Ph.D. student, a lack of background knowledge on the subject may be an advantage.
9. A good scientist and a good flume are necessary but not sufficient conditions to perform a good experiment.
10. Strongly economically developing countries such as Vietnam, need to develop a home-base for scientific research.

These propositions are considered opposable and defensible, and as such have been approved by the supervisor, Prof.dr.ir. M.J.F. Stive

## **Stellingen**

Behorende bij het proefschrift

### **Steenstabiliteit onder Niet-uniforme Strooming**

van

Nguyen Thanh Hoan

Delft, 3 november 2008

1. Bepaling van de hydraulische belastingen op de stenen op de bodem en de daaraan gerelateerde stabiliteit van de stenen staan centraal in steenstabiliteitsonderzoek.
2. Hoewel de stroomsnelheden nabij de bodem de belangrijkste krachten op het bodem-materiaal veroorzaken, kunnen stromingsparameters op verschillende diepten gebruikt worden om de hydraulische krachten op de bodem te representeren. (Hofland, 2005 en dit proefschrift)  
Hofland, B. (2005). Rock & roll: turbulence-induced damage to granular bed protections. Ph.D. thesis, Delft University of Technology.
3. Een combinatie van stroomsnelheid en turbulentieverdelingen zou gebruikt moeten worden om de hydraulische belastingen op de stenen op een bodem te kwantificeren. (dit proefschrift)
4. Voorzichtigheid is geboden bij gebruik van het populaire concept voor de drempelwaarde van de stabiliteit; het kan leiden tot inconsistente en onbetrouwbare ontwerpcriteria. Het stabiliteitstransport concept kan hierin uitkomst bieden.
5. Met de beschikbaarheid van de nieuw-ontwikkelde steentransportformules en betrouwbaardere turbulentiemodellen kan het bodemschadeniveau preciezer worden berekend voor willekeurige stromingscondities. (dit proefschrift)
6. Aan een goede formule voor bodemprocessen moet een goede fysische bedding ten grondslag liggen.
7. Een promotieonderzoek in het buitenland doen, kan leiden tot veel stress, maar ook veel plezier.
8. Een gebrek aan achtergrondkennis over het onderwerp kan een voordeel zijn voor een beginnende promovendus.
9. Een goede wetenschapper en een goede goot zijn noodzakelijk maar niet voldoende om een goed experiment uit te kunnen voeren.
10. Sterk economisch ontwikkelende landen zoals Vietnam, hebben een thuisbasis voor wetenschappelijk onderzoek nodig.

Deze stellingen worden oponeerbaar en verdedigbaar geacht en zijn als zodanig goedgekeurd door de promotor, Prof.dr.ir. M.J.F. Stive